GÉP

A GÉPIPARI TUDOMÁNYOS EGYESÜLET MŰSZAKI FOLYÓIRATA

2020/3-4.

Nemzeti Kulturális Alap

116 oldal
LXXI. évfolyam

Mély, alkalmazott tudást hozunk bármely iparágba

Általános ipar

Nyersanyag feldolgozás

Egészségügy és analitika

Gépi automatizálás

Az Emerson-ról

Az 1890-ben alapított Emerson, melynek székhelye St. Louisban, Missouriban (USA) található, globális technológiai és gépészeti vállalat, amely innovatív megoldásokat kínál az ipari, kereskedelmi és lakossági piacok számára.

A vállalat két, egymást kiegészítő platformon működik, amelyek az Automation Solutions és a Commercial & Residential Solutions.

Fluid control és Pneumatika: Iparági szakértelem és alkalmazott megoldások

Egyre több ügyfélmegoldáshoz van szükség fluidtechnikai és pneumatikai termékekre. Az Emerson ennek megfelelően innovatív, megbízható és gyors megoldásokat kínál a fejlődő fluid automatizálási piac számára.

Iparágvezető termékeink - ASCO™, AVENTICS™, TESCOM™ és TopWorx™ márkáinktól - kis energiafogyasztásúak, alacsony hőmérsékleten működőképesek és minden globális engedéllyel rendelkeznek így támogatva ügyfeleinket hatékonyságuk maximalizálásában és teljesítményük mérhető növelésében.

EMERSON™

GÉP

A GÉPIPARI TUDOMÁNYOS EGYESÜLET

műszaki, vállalkozási, befektetési, értékesítési, kutatás-fejlesztési, piaci információs folyóirata

TISZTELT OLVASÓ!

2020. május 07-én került sor a negyedik nemzetközi Agria Conference on Innovative Pneumatic Vehicles - ACIPV 2020 konferenciára, ez évben a kialakult világjárvány miatt jövőbe mutató, online formában.

A Konferenciát 2017-ben a Nemzetközi AVENTICS Pneumobile Verseny kapcsán végzett számottevő tudományos munka hívta életre, kezdeti célja az volt, hogy teret adjon a járműépítési projektekbe bekapcsolódó oktatók, PhD és egyetemi hallgatók tudástranszferjének. Mára azonban a Konferencia tematikája kibővült, vezérléstechnikai, autóipari publikációknak is helyet kínál.

Az ACIPV Konferenciasorozat az üzleti és akadémiai világ találkozásával jött létre, melyben az akadémiai feladatokat az Óbudai Egyetem Mechatronikai és Járműtechnikai Intézete vállalta magára, míg a házigazda szerepét az AVENTICS márkát képviselő Emerson tölti be. Nagy örömünkre szolgál, hogy védnökeink között tudhatjuk az Innovációs és Technológiai Minisztériumot is, támogatásukat köszönjük.

Ez évben huszonkét előadást hallgathattak meg az érdeklődők a Konferencián, amelyek szakcikk változatát a Gép folyóirat jelen számában közöljük.

Jó olvasást kívánunk!

Gödri István
ügyvezető igazgató
Emerson Automation Fluid Control and Pneumatics a Konferencia alapítója

Prof.Dr. Pokorádi László
egyetemi tanár
Óbudai Egyetem, Mechatronikai és Járműtechnikai Intézet, igazgató a Konferencia alapító elnöke

A szerkesztésért felelős: Vesza József. A szerkesztőség címe: 3534 Miskolc, Szervezet utca 67.
Telefon/fax: 06-46/379-530, 06-30/9-450-270 • e-mail: mail@gepujsag.hu
Kiadja a Gépipari Tudományos Egyesület, 1147 Budapest, Czobor u. 68., Levélcím: 1371 Bp. Pf.: 433.
Telefon: 06-1/202-0656, fax: 06-1/202-0252, e-mail: a.gaby@gteportal.eu, internet: www.gteportal.eu
A GÉP folyóirat internetcíme: http://www.gepujsag.hu
Kereskedelmi és Hitelbank: 10200830-32310236-00000000

Felelős kiadó: Dr. Igaz Jenő ügyvezető igazgató.
Gazdász Nyomda Kft. 3534 Miskolc, Szervezet u. 67. Telefon: 06-46/379-530 • e-mail: gazdasz@chello.hu

Előfizetésben terjeszti a Magyar Posta Zrt. • Postacím: 1900 Budapest
Előfizetésben megrendelhető az ország bármely postáján, a hírlapot kézbesítőknél, www.posta.hu WEBSHOP-ban (https://eshop.posta.hu/storefront/), e-mailen a hirlapelofizetes@posta.hu címen, telefonon 06-1-767-8262 számon, levélben a MP Zrt. 1900 Budapest címen. Külföldre és külföldön előfizethető a Magyar Posta Zrt.-nél: www.posta.hu WEBSHOP-ban (https://eshop.posta.hu/storefront/), 1900 Budapest, 06-1-767-8262, hirlapelofizetes@posta.hu

Egy szám ára: 1260 Ft. Dupla szám ára: 2520 Ft.

INDEX: 25 343 ISSN 0016-8572

A megjelent cikkek lektoráltak.
A kiadvány a Nemzeti Kulturális Alap támogatásával jelenik meg.

TARTALOM

A PNEUMOBIL VERSENYEKHEZ KAPCSOLÓDÓ JÁRMŰMODELLEZÉSEK

VEHICLE MODELLING RELATED TO PNEUMOBILE COMPETITIONS

Tamás Szakács, PhD 1081 Budapest, Népszínház u..8 +3616665406 szakacs.tamas@bgk.uni-obuda.hu

ABSTRACT. In 2020 will the XIII. Emerson's International AVENTICS Pneumobile Competition be organized. Since 2010 most of car their system designs are based on any kind of modelling, and simulation. Parallel to that, the number of articles related to pneumatic vehicles is increased.
This article is summarizing the most relevant models and methods have been created during the decade.

1. INTRODUCTION

Since 2017 University of Óbuda is organizing the ACIPV conferences related to the Pneumobile competitions. Most of the articles are dealing with pneumatic components, system, or vehicle modelling. There are also research articles published outside the frame of ACIPV, and there are authors working on pneumatic vehicle drive not related to Pneumobile competition as well. There is an increasing number of researches relating to alternative vehicle protrution. In most of the cases alternative protrution means electric-, or hybrid electric drive, but there is an increasing attention paid on other alternatives, like compressed air vehicles (CAVs). The development of such vehicles also requires modelling and simulation. As the requirements are increasing, so do the expectations from the models created.

The list of the articles is far not complete! There are many other articles publicised in this area, and there are thesis works, student scientific conference papers too

The models used for pneumatically driven vehicles can be grouped in different groups:

The depth of modelling:

- concept,
- component,
- network of components,
- subsysems, and
- the entire vehicle.

The concept publications are not modelling the physical details of the vehicle, but they are laying the base of the pneumatic drive in respect of feasibility, economical, and environmental aspects down.[1], [12] In some cases, the optimisation of single components is required, as in case of optimisation of a directional control valve [3]. There is a need for modelling network of components, like cooperation between the valves, piston, puffer tank etc. There are many articles dealing with complete pneumatic systems from the tank till piston force, and motion [11]; [7], etc. The entire vehicle modelling describes the complete vehicle including pneumatic engine, protrution, control, and vehicle dynamics. [8]

Methods used by the design:

- Worksheets,
- analytical system description and modelling
- block modelling.

Worksheets are simple charts, usually created in Excel in order to support vehicle performance evaluation, and help construction decision making. The best example for that is the modell created by Sziki and his team [9] Analytical system description describes the equation of the complete system, usually in matrix equation, transfer functions, and state-space equations. Block modelling use the method of creating interchangeable individual function blocks, and creating the network of components in a block modelling environment, usually in Matlab/Simulink®

2. PUBLICATIONS RELATED TO PNEUMOBILE MODELLINGS

In this chapter the publications will be organized by their occurance.

2.1 ACIPV related articles

1st Agria Conference on Innovative Pneumatic Vehicles – ACIPV 2017

- Compressed Air, as an Alternative Fuel István Tibor TÓTH [12]

2nd Agria Conference on Innovative Pneumatic Vehicles ACIPV 2018

- Optimized Valve System for a Pneumatic Motor M. Madissoo, K. Türk [3]
- Adaptive control based air expansion range extension of pneumatic vehicles Zoltán Márton; Dénes Fodor [13]

– Analysis of the Rolling Resistance of Pneumobiles for Vehicle Dynamic Modelling Purpose Bence Márk Szeszák, György Juhász, GusztávÁron Sziki, Rita Nagy-Kondor, Tamás Sádor Sütő [9]
– Pneumatic modelling of a pneumobile Tamás Szakács [7]

3th Agria Conference on Innovative Pneumatic Vehicles – ACIPV 2019

– Adaptive Pneumatic Suspension Using Linear Quadratic Control Demeter László, FORGÓ Zoltán (Sapientia EMTE Erdélyi Magyar Tudományegyetem) 11-17
– Designing the Suspension of the Airrari Pneumobile Gábor Horváth, István Péter Szabó [14]
– Modelling and Validation of a Pneumobil Tamas Szakacs [8]
– Autonomous Possibilities of a Pneumatic Driven Vehicle Pintér Péter. Kurucz János [15]

2.2 Articles outer ACIPV

– Air Consumption Analysis in Compressed Air Powered Vehicles Uszynski, S., Ambroziak, L., Kondratiuk, M., Kulesza, Z. [11]
– Síki, G. Á. – Juhász, Gy. – Nagyné Kondor, R. – Juhász, B. (2014). Computer program for the calculation of the performance parameters of pneumobiles, [9]
– The Pneumatic Hybrid Vehicle A New Concept for Fuel Consumption Reduction. Sasa Trajkovic [10],
– Compressed Air Vehicles Drive-Cycle Analysis of Vehicle Performance, Environmental Impacts, and Economic Costs, Andrew Papson, Felix Creutzig, and Lee Schipper, [1]
– Pneumatic Vehicle, Research and Design, Mihai Simon [5]

2.3 Evaluations of the Methods and Results

Trajkovic, in his doctoral thesis concludes ”The pneumatic hybrid vehicle (PHV) concept is a low-cost alternative to the more established electric hybrid. The PHV concept comprises no additional propulsion source and a pressure tank as an energy storage device. The main idea with the pneumatic hybrid is to use the ICE in order to compress atmospheric air and store it in a pressure tank when decelerating the vehicle. [10]

Compressed Air Vehicles Drive-Cycle Analysis of Vehicle Performance, Environmental Impacts, and Economic Costs by Andrew Papson, Felix Creutzig, and Lee Schipper [1]

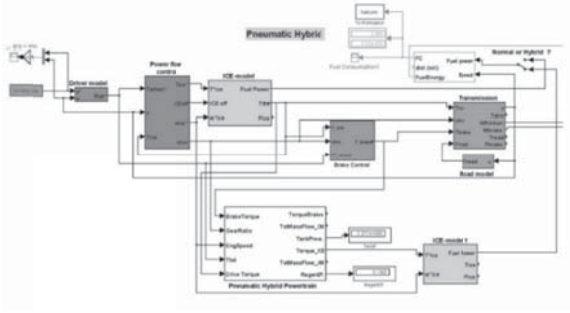

Fig. 1. A PHV Bus model [10]

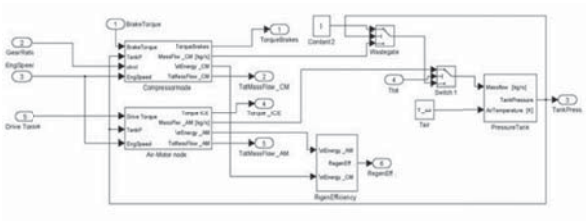

Fig. 2. The pneumatic hybrid specific subsystem [10]

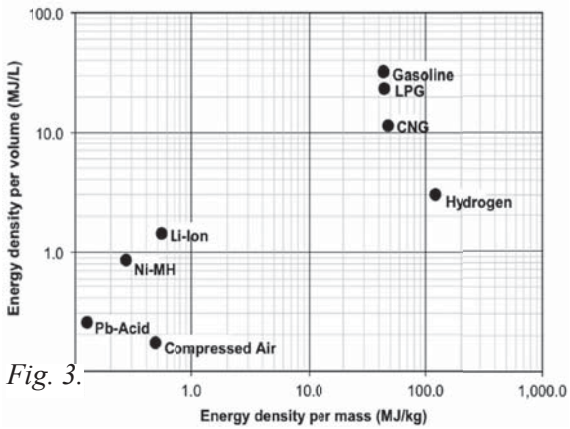

Fig. 3.

Fig. 3 specific energy density in the function of energy density per mass, and per volume [1]

Fig. 3 shows the specific energy density of different energy storages in the function of energy density per mass, and per volume. Their evaluation is: “Even at high pressures, compressed air carries much less energy than other transportation energy sources, including liquid and gaseous fuels as well as rechargeable batteries. Compressed air holds only 0.5% of the energy in gasoline and 1.5% of the energy of gaseous compressed natural gas (CNG). Similarly, the energy density of compressed air is poor compared with the types of rechargeable batteries available for vehicle use: lead acid (Pb–acid), nickel cadmium (NiCd), nickel metal hydride (NiMH), and lithium ion (Li-ion). Although batteries are significantly heavier than

compressed air and hold less energy by mass, they still outperform in terms of volume, with compressed air holding 12% of the energy of Li-ion batteries." [1]

The article assumes the compressed air is at 300bar pressure, and rates the specific energy density of compressed air to 0.35 MJ/kg.
According to other calculations the air itself at 300bar has 0.48 MJ/kg, in 10l industrial bottle (m_b=17 kg) is 0,08MJ/kg. Storing the gas in composite 10l bottle increases the value to 0.213 MJ/kg, and increasing the size from 10 liters to 80 liters increasing the energy density back to the range of Li-Ion batteries. [6]

	Compressed Air Vehicle	Urban Gasoline Vehicle	Urban Electric Vehicle
Fuel type	Compressed air	Gasoline	Electric battery
Fuel economy	38 mpg-e	32 mpg	163 mpg-e
Urban range	29 mi	408 mi	127 mi
Fuel cost ($/mi)	0.21	0.09	0.05

Fig. 4 Performance Characteristics of CAVs vs. Gasoline an EVs [1]

Taking the MDI CityFlowAIR [4] vehicle for basis, the authors published the following: "The drive-cycle simulation used here requires few parameters to calculate energy consumption. The CAV is modelled with the following parameters based on specifications from the vehicle manufacturer: a vehicle with mass of 1,200 kg, a compressed air tank with 300l volume and 300-bar maximum pressure, and a pneumatic motor power with 19 kW (25 hp) maximum power" [1], Fig. 4 shows the result of the calculations
Fig. 5 shows the result of the article. The state of the art in 2010 shows carbon intensity of CAVs, Gasoline vehicles, and EVs

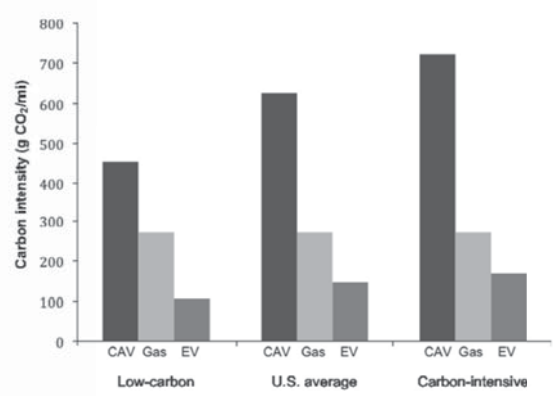

Fig. 5. Comparison of vehicle carbon intensity across electricity generation scenarios [1]

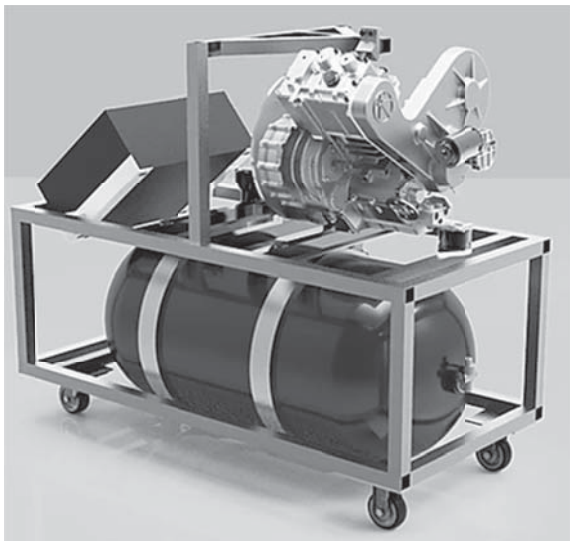

Fig. 6 MDI Air Power Unit [4]

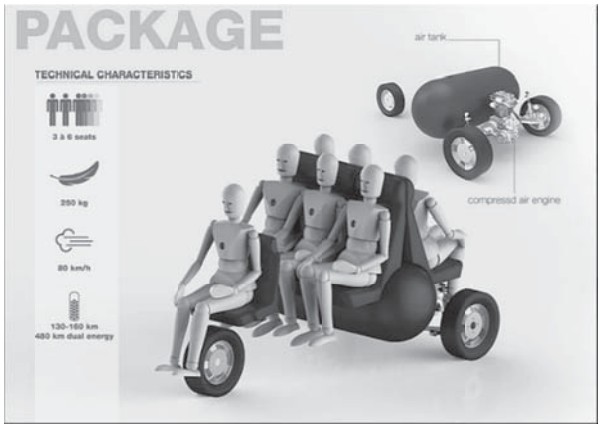

Fig. 7 MDI Air Tuktuk. [4]

The article has been edited in 2010. A decade later the manufacturer provides new different types of vehicles with extended range, and scale. [4]. Fig. 6 shows an air power unit from MDI, and Fig. 7 shows a personal car for 7 persons

An analytical model in Excel has been created by Áron Gusztáv [9]. "The presented computer program is capable of calculating the performance parameters of pneumobiles from the technical parameters of their machine parts."

"The presented computer program is capable of the calculation of the performance parameters of pneumobiles from their other technical parameters.

One of them is done by Uszynski, S., Ambroziak, L., Kondratiuk, M., Kulesza, Z, and have published as "Air Consumption Analysis in Compressed Air Powered Vehicles" [11], the other is "Pneumatic modelling of a pneumobil", and "Modelling and validation of a pneumobil" [7],[8]. The motivation for both is the Pneumo-

bile competition. Both authors are based their concept on describing the pneumatic system of the vehicle based on gas chambers, and pressures building up caused by gas mass flows between chambers.

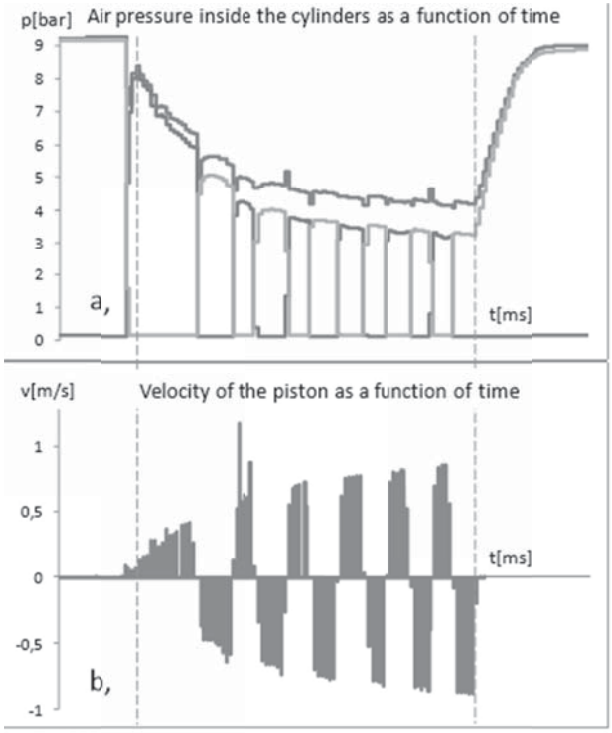

Fig. 8. Air pressure inside the cylinder and flowing out of the tank (a) velocity of the piston (b) as the function of the running time of the pneumobil [9].

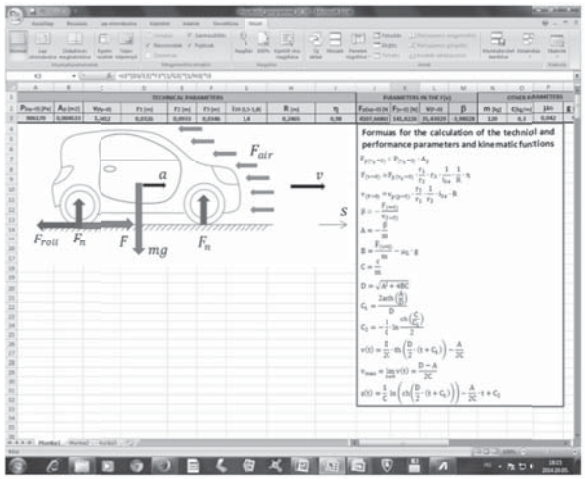

Fig. 9. The Excel program (columns A- M). [9].

Reached speed and covered distance within a given period of time and also the top speed of the vehicles can be calculated. Moreover, the optimal values of the technical parameters (such as the optimal gear ratio in the chain drive and in the internal gear hub) can be determined indirectly".

There is a couple of research publication building up the pneumatic system of a Pneumobile vehicle from function blocks. Two models have been developed in the same time, independent from each-other.

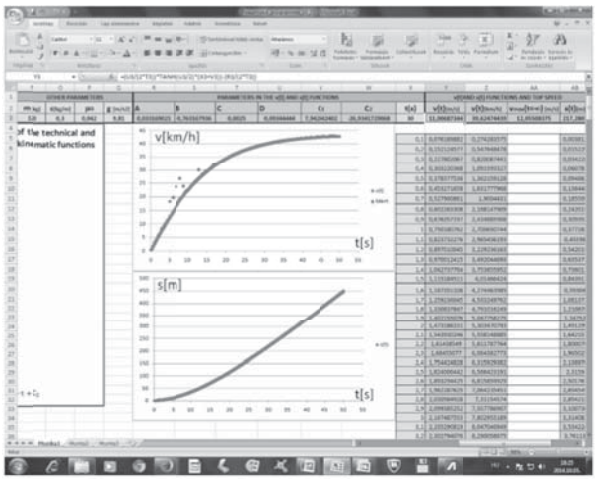

Fig. 10. The Excel program (columns N-AB). [9].

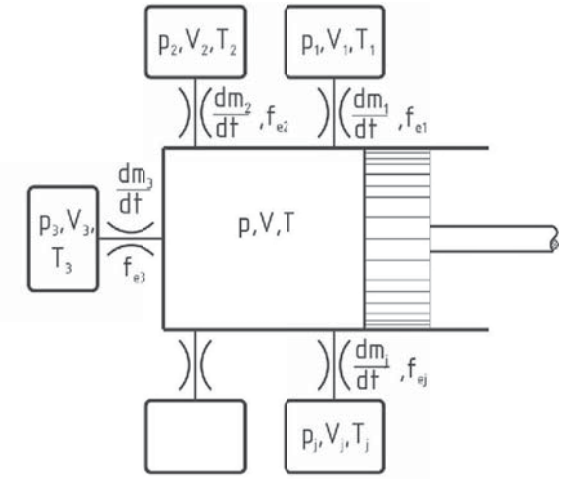

Fig. 11. Variable volume chamber in connection with other chambers [11]

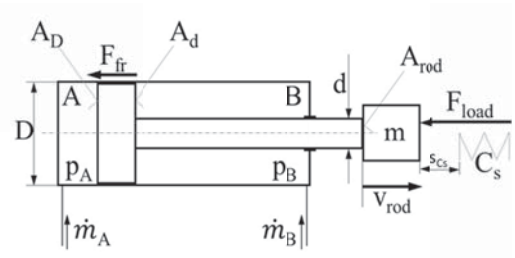

Fig. 12. The dual chamber piston by Szakács

$$F = p_1 \cdot A - p_2 \cdot A_2 - F_{fr} - p_0(A - A_2) - F_{load} \quad (1)$$

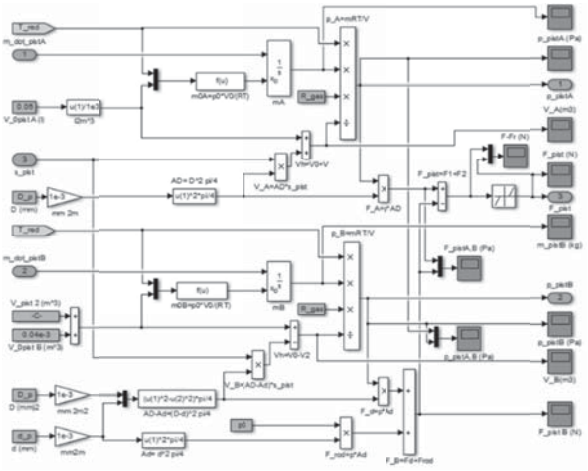

Fig. 13. The dual-chamber piston model in MatlabSimulink® [8]

Validation measurements carried out in order to gain information about piston chamber pressures. And piston speed during a straight run, on a measuring track.

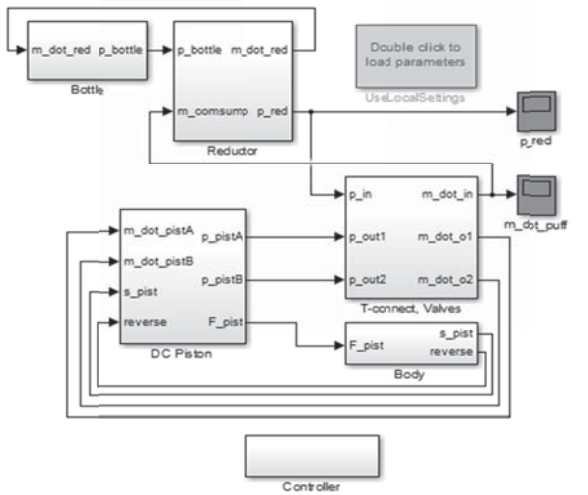

Fig. 14..The pneumatic system model [8]

A car setting of 8 bars system pressure, and 30% expansion mode has been selected [2]. The chamber pressures and piston position were recorded. The results are shown on Fig. 16

Having the same parameters set on the model, there was a simulation run. the simulation results of the two channel pressures are shown in Fig. 17

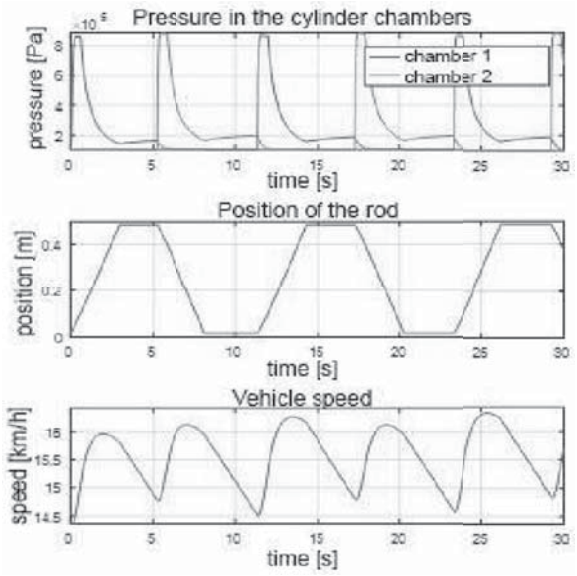

Fig. 15. Pressure in the piston chambers, change of position and vehicle speed in case 20 % of the actuator piston feed/pull-out [11]

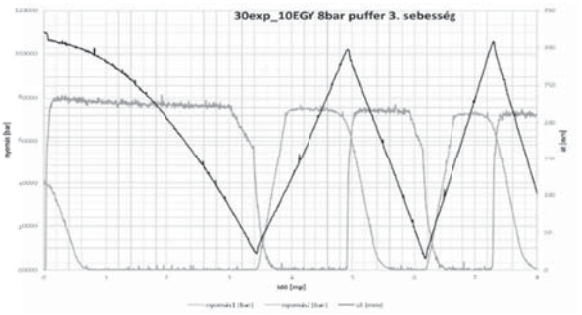

Fig. 16..Measuring results [2] [7]

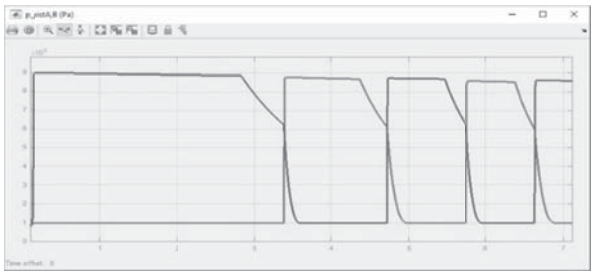

Fig. 17..Simulated piston chamber pressures [8]

3. CONCLUSIONS

The different research groups are developing their own models. Each groups are using their own modelling method, but sometimes these are very similar to each other. The ACIPV conferences are the most active events for researchers working in the area of pneumatically driven vehicle to share their results.

There are research groups working on the field of CAV modellings, and development outside

the Pneumobile competition. There are such vehicles available in the market in Europe, India, and China.

4. OUTLOOK, RECOMMENDATIONS

The market potential of CAVs are currently low, but there is a potential in the area. The currently independently working research teams are already cooperating in the field of Pneumobile vehicle developments, but further increase of cooperation is expected. A formation of a consortium is recommended. A SWOT analysis of compressed air drive is still missing, and the published researches did not involve yet vehicle informatic system in the modelling, or it has not published yet. The stronger publicity of the research results are also recommended to connect the groups working within, and outside Pneumobile competition.

ACKNOWLEDGEMENT

The research presented in this paper was carried out as part of the EFOP-3.6.2-16-2017-00016 project in the framework of the New Széchenyi Plan. The completion of this project is funded by the European Union and co-financed by the European Social Fund.

REFERENCES

[1] Andrew Papson, Felix Creutzig, and Lee Schipper: Compressed Air Vehicles Drive-Cycle Analysis of Vehicle Performance, Environmental Impacts, and Economic Costs Transportation Research Record: Journal of the Transportation Research Board,No. 2191,Transportation Research Board of the National Academies, Washington,D.C., 2010, pp. 67–74.DOI: 10.3141/2191-09

[2] Heisz P. Engineering and optimizing a controller for the PowAir Team's Pneumobile (Vezérlés tervezése és optimalizálása a PowAir csapat pneumobiljához) Thesis work Department of Mechanical, and Safety Engineering, Óbuda University, (2017)

[3] Madissoo, M., Türk, K.: Optimized Valve System for a Pneumatic Motor (Estonian University of Life Sciences, Institute of Technology) 5-11

[4] MDI GREEN'AIR Vos courtes distances au grand air https://www.mdi.lu/projets)

[5] Simon, Mihai: Pneumatic Vehicle, Research and Design, 10th International Conference Interdisciplinarity in Engineering, INTER-ENG 2016,

[6] Szakács, Tamás: Pneumatikus járműhajtás múltja, jövője (Pneumatic vehicle protrution past, and future) In: Péter, Tamás (szerk.) IFFK 2017 : XI. Innováció és fenntartható felszíni közlekedés, Budapest, Hungary: Magyar Mérnökakadémia (MMA), (2017) pp. 176-180.

[7] Szakács, Tamás: Pneumatic modelling of a pneumobil In: Pokorádi, László (editor.) Proceedings of the 2nd Agria Conference on Innovative Pneumatic Vehicles ACIPV 2018 Eger, Hungary: Óbudai Egyetem, (2018) pp.25-30.

[8] Szakács, Tamás: Modelling and Validation of a Pneumobil In: Pokorádi László: Proceedings of the 3th Agria Conference on Innovative Pneumatic Vehicles – ACIPV 2019 Eger, Hungary (2019) pp. 31-35.

[9] Síki, G. Á., Juhász, Gy., Nagyné Kondor, R., Juhász, B. (2014). Computer program for the calculation of the performance parameters of pneumobiles, Proceedings of the International Scientific Conference on Advances in Mechanical Engineering.

[1] Trajkovic, Sasa: The Pneumatic Hybrid Vehicle A New Concept for Fuel Consumption Reduction Doctoral Thesis Division of Combustion Engines Department of Energy Sciences Faculty of Engineering Lund .

[11] Uszynski, S., Ambroziak, L., Kondratiuk, M., Kulesza, Z.: Air Consumption Analysis in Compressed Air Powered Vehicles, 2018 23rd International Conference on Methods and Models in Automation and Robotics, MMAR 2018 pp. 837-842.

[12] Tóth, István Tibor: Different Compressed Air, as an Alternative Fuel, 1st Agria Conference on Innovative Pneumatic Vehicles ACIPV 2017 pp. 17-19.

[13] Adaptive control based air expansion range extension of pneumatic vehicles Zoltán Márton; Dénes Fodor (University of Pannonia, Faculty) 12-16

[14]Designing the Suspension of the Airrari Pneumobile Gábor Horváth, István Péter Szabó (University of Szeged Faculty of Engineering) 19-25

[15] Autonomous Possibilities of a Pneumatic Driven Vehicle Pintér Péter. Kurucz János (University of Óbuda, BGK MEI) (53-56)

SPECIÁLIS SEBESSÉGVÁLTÓ TERVEZÉSE

DESIGN OF SPECIAL GEARBOX

Dr. Bihari János, associate professor, Filepkó Máté, BSc student, Szőnyi Szabolcs, alumni
University of Miskolc, Institute of Machine and Product Design

ABSTRACT
In general, it is specifically significant to design the units of the Pneumobile race vehicles according to the competition's principles. It could mean that we do the dimensioning of the parts for a short lifetime in order to save mass, but also to implement everyday solutions particularly for the needs of the competition to minimize costs. Nevertheless, a present-day Pneumobile is always a small moving test lab, where the students can try out such own ideas which help to improve their professional development. This paper presents the design and dimensioning of such a gearbox, which was created for a Pneumobile. This gearbox belongs to the orbital gear-drive systems. This kind of solution is almost only used in toys nowadays, but it will be clearly seen that this is suitable for this usage as well. As compared to the well-known applications there is a fundamental difference that we want to switch the gearbox under load without a disengaging clutch or stopping the motor. While connecting the gears, the load of the teeth can be increased to the multiples of the nominal load, which has to be handled and taken into account by dimensioning. For this reason, we present in this paper the basic construction and operation of the gearbox as well as those factors that we considered during the design and dimensioning. Currently we are testing the second version of the gearbox, thus we share the gained experiences from the first version as well.

Definitions:
Pneumobile: a vehicle, which transforms the energy of the pressurized gases with the help of pneumatic parts into kinetic energy [1].

1.INTRODUCTION

Pneumobiles at the University of Miskolc

The teams of the University of Miskolc are being taken part in the Pneumobile competitions since 2008. One team is typically at work for 3-4 years. In their first year, the teams usually aim to build functionally working vehicles, but later they develop these Pneumobiles in several way. [2], [3], [4].
For the second or third year, a Pneumobile is a moving test lab, where the students try out their own different ideas.

2. REQUIREMENTS FOR A GEARBOX OF A PNEUMOBILE

The need of a gearbox in the Pneumobiles are not certainly necessary thanks to the design and operation of the motors. However, it could be an advantage by deeper analyzing of the processes in the cylinders, if the transmission ratio can be modified during operation. In addition to these, the competition firstly provides the professional development of the students. From this aspect, designing any kind of mechanical unit can be beneficial.

In this paper, we present the design of a given Pneumobile's gearbox, therefore the requirements are valid for this vehicle.

- The maximum RPM of the given vehicle's driven shaft is 342 1/min, the torque on the driven shaft is 42 Nm.
- The gearbox must have two forward gears.
- One of the gear's transmission ratio must be underdrive, the other must be overdrive. Their proportion must be at least 2.
- The gearbox must have a neutral.
- Connection of the gears during the operation of the motor without a clutch is an expectation.
- The parts of the gearbox must be manufactured on general machining tools.
- For cost effective reasons, straight-toothed gears with the module of 1, 1.5, 2 or 3mm must be used.

Based the above written requirements, the design of an orbital gearbox seemed reasonable.

3. THE OPERATION OF THE GEARBOX

Fundamentally, this sort of a gearbox is built up by four pinions with the same number of teeth and two other toothed gears with differ-

ent number of teeth from the before mentioned pinions and from each other as well. The operation principle of the gearbox is based on a rotatable bearing seated console (central unit), between the continuously rotating drive- and driven-shafts. Thus, in the console the reciprocal of the transmission ratio can be generated without using additional parts (Figure 1.).

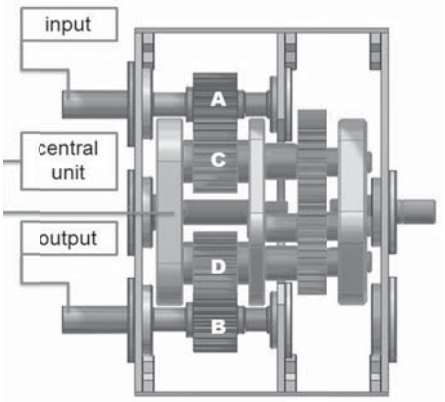

Figure 1: The Structure of the Gearbox

The geometrical design of the toothed-gears were done according to the DIN 3960 standard. The toothing of the gears are straight outside and pressure angle is 20°.

The module and number of teeth, so the dimensions and the centre distance of the gears were determined by cost effectiveness and simplicity. It means that the available bearing sizes on the market in a given budget and the necessary parts for the installation define how big the centre distances could be. Based on the centre distances, the size of module was chosen for the possibly biggest in a way that addendum modification is not needed. While defining the number of teeth it was considered that the contact ratio factor must be above 1,2. The minimum lifetime of the gears and bearings was specified as 5 operating hours. By determination of the lubrication factor, the opened gearbox and lubricated operation were taken into account.

On the grounds of the figures 2 and 3 it is easy to understand the operation of gearbox. On the drive- and driven-shafts one identical piece of pinion (Fig. 1: A and B) with 20 number of teeth are placed. A same pinion (C in the Fig. 1.) with 20 number of teeth on the central unit is connected to the pinion of the drive-shaft in the 1st gear, which turns on a common shaft with a toothed gear with X number of teeth. This toothed gear with X number of teeth is connected a toothed gear with Y number of teeth. The toothed gear with Y number of teeth is placed on a common shaft with a pinion (Figure 1: D) with 20 number of teeth, which is connected to the pinion with 20 number of teeth of the driven-shaft. In this state the transmission ratio of the gearbox is X:Y. If the central unit if turned by 90°, there is no connection between the drive- and driven-shaft. This is the neutral of the gearbox. If the central unit is turned by 90° again, the drive- and driven are connected again. This is the 2nd gear of the gearbox, where the transmission ratio is Y:X. In case of a further turn by 90° neutral comes again (Figure 2. and 3.).

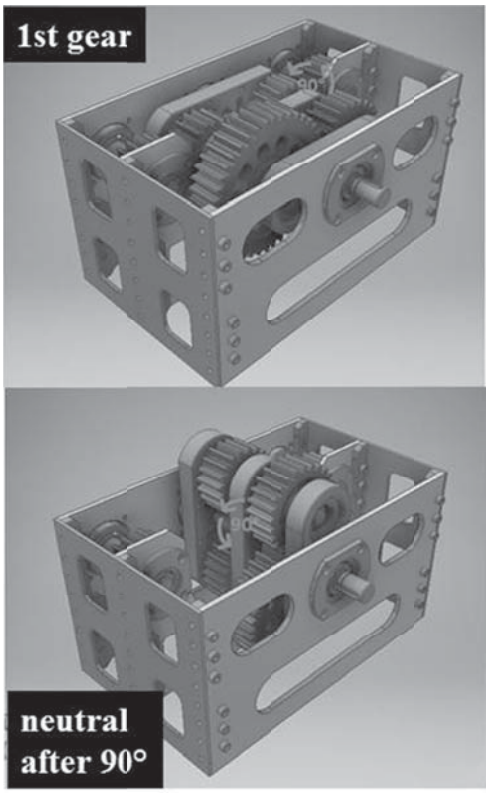

Figure 2: The 1st Gear and Neutral

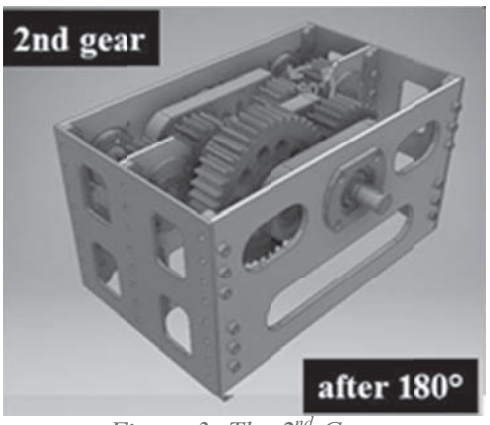

Figure 3: The 2nd Gear

The turning motion can be realized by many mechanisms, but automation can be done simply as well. We have chosen the manual coupling. Coupling of the gears can be adjusted easily to the needs of the driver. A coupling can be worked out, when an actuating arm needs to be moved in opposite direction or another one, which needs to be moved only in one direction and the arm returns to its initial position between the gears.

In our solution for setting and adjusting certain positions a Geneva drive is provided. This can guarantee the necessary discreet angular displacement for the right connection of the pinions and the fixing of the central unit in connected gears in the same time (Figure 4).

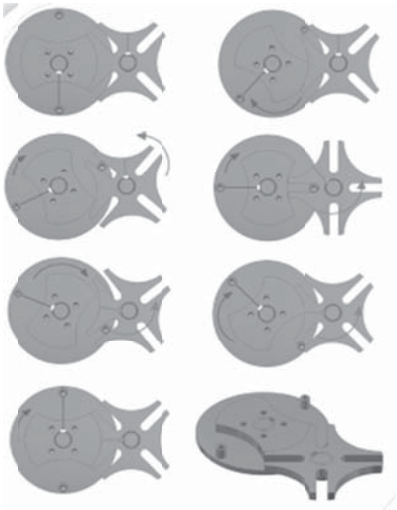

Figure 4: The Operation of a Geneva Drive

There is one additional positive advantage of the Geneva drive that all of the drive's parts can be simply manufactured on lathe and milling cutter, so we can make the drive easily.

4. SPECIAL DIMENSIONING PRINCIPALS OF THE GEAR-DRIVES

The control of the strength calculation of the toothed gears and pinions were done according to the DIN 3990. Since their geometrical dimensions are basically determined by other parameters of the gearbox, the toothed gears and pinions are significantly bigger than the given loads and the expected lifetime would require. The strength calculation were done according to the DIN 3990:1987 B [11]. The material of the toothed gears and pinions is 16MnCr5 and the surface treatment is nitridation, because its costs are favorable. The value of the K_A operating factor was chosen for 1.75, because the drive is under brusty loads while connection the gears and the direction change of the cylinder. By the calculation the parameters of the grease was fit for the UNIGEAR LA02 grease. Based on the calculations, the pinions of the drive- and driven shafts (A and B) and the pinions of the central unit (C and D) are used the most. Their safety factor of the tooth root strength is 3.06 and the safety factor of the flank pressure is 2.08. This last value may seem small, but the maximum value of the motor's torque loads teeth only for a short time because of the operating characteristics of the motor. The load is much smaller approximately in 90 percent of the operation.

After all we experienced during the race that the teeth were significantly damaged on all of the four pinions (A,B,C and D).

Firstly the root cause was searched in the failure of the surface treatment, but was found in the specialty of the gearbox's design. The central unit of the first gearbox can be seen on the Figure 5. It means that the A and B pinions turn in the opposite direction as the C and D pinions (Figure 1.). This has the results while coupling that the central unit wants to turn out from the connection and it makes the turnover harder, so the coupling process is uncertain. The teeth are loaded with huge dynamic impacts depending on velocity of the vehicle and the RPM of the motor. This fact was taken into consideration with value of the K_A factor, but we have chosen 1.75, because these loads act for a short period.

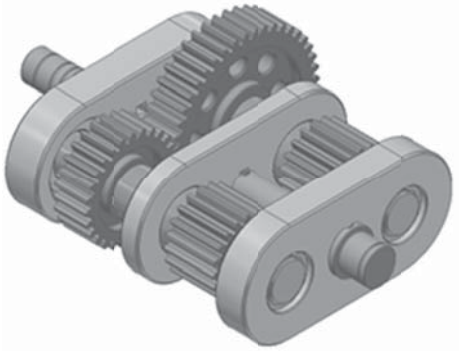

Figure 5: The First Design of the Central Unit

For the redesign of the gearbox the right values of the parameters had to be defined, so the root causes of the failure had to be revealed.

5. ROOT CAUSES OF THE FAILURE

The calculations were done only for the states of the connected gears of the gearbox. According to the experiments, it was determined that

the coupling process takes place for at least 1 second. During this time the pinions rotate 5.7 turns. In these moments the center distance changes and the contact ratio factor is smaller than the nominal. As a first step, we have searched that point where value of the contact ratio factor is already not zero.

This could be easily done by a graphic method (Figures 6 – 9). This state takes place when the center distance of the A and C or A and D pinions are 44mm. The contact ratio factor is 0.033 at this time (Figure 6).

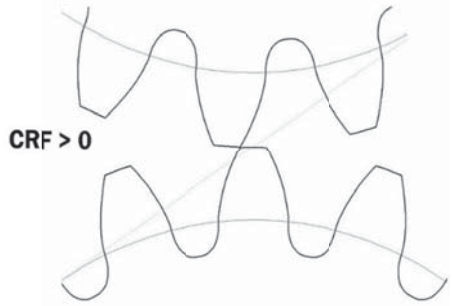

Figure 6: Modelling of the Effect of Centre Distance on the Contact Ratio Factor A_w: 44mm.

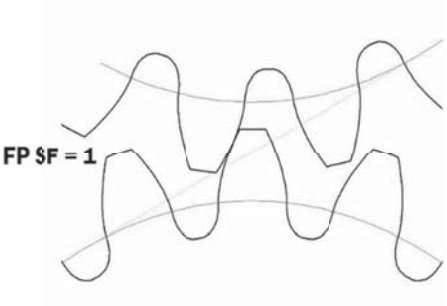

Figure 7: Modelling of the Effect of Centre Distance on the Contact Ratio Factor A_w: 42,38mm.

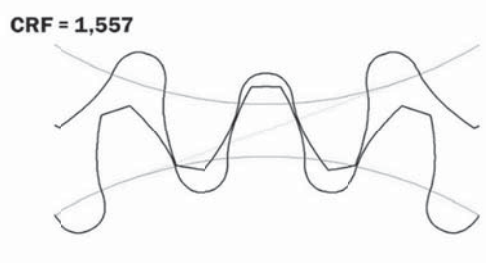

Figure 9: Modelling of the Effect of Centre Distance on the Contact Ratio Factor A_w: 40mm.

In this way a range can be defined where a certain point has to be found when the safety factor of the flank pressure is 1. At such points the center distance is 42.38mm and the contact ratio factor is 0.625 (Figure 7).

The next wanted point is that when the contact ratio factor is 1. For this point belongs 41.05mm of center distance (Figure 8).

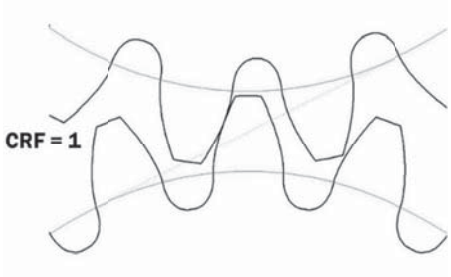

Figure 8: Modelling of the Effect of Centre Distance on the Contact Ratio factor A_w: 41,05mm.

The Figure 9 shows the state of full connection. The contact ratio factor is 1,557.

It means that the pinions rotate ca. 4 turns while coupling besides the contact ratio factor of 1, the safety factor of the flank pressure is under 1 during more than the one third of the coupling time. The contact ratio factor under 1 means itself as well that the operation factor was chosen wrongly. The period of time when the surface of the teeth is under huge flank pressure was underestimated.

Besides this we did not consider in the lubrication factor that one part of the grease does not stay on the surface of the teeth and dust sticks into the grease because of the open design, so the lubrication factor is not true for the whole expected lifetime.

6. THE POSSIBLE SOLUTIONS

For the problem of the flank pressure among industrial circumstances a material with bigger strength and more resistant surface would be a good answer, which can be provided e.g. by case-hardening. This solution could not be chosen because of the costs.

Increasing the connecting surfaces is also a good solution. We did not want to modify the bearing seats and the frame of the gearbox, because this would have gone with significant costs.

The safety of the coupling had to be increased. This was important from the aspect of decreasing the coupling time and from the aspect of the usage as well. The most practical solution for these was to modify the direction of rotation of the toothed gears in the central unit.

6.1 Considered other parameters at redesign

The lubrication had to be re-evaluated, the value of the lubrication factor was modified. The new value was set according to the research experiences from the field of the open gear drives operated without lubrication in the Institute of Machine and Product Design at the University of Miskolc [6], [7].

The central unit moves a bit during operation because of the manufacturing inaccuracy of the Geneva drive, therefore the center distance is not constant. These limits were measured and the most unfavorable state was taken into account at the calculations.

7. THE SOLUTIONS

We investigated how the direction of rotation at the toothed gears in the central unit could be modified. The best solution was to implement additional pinions.

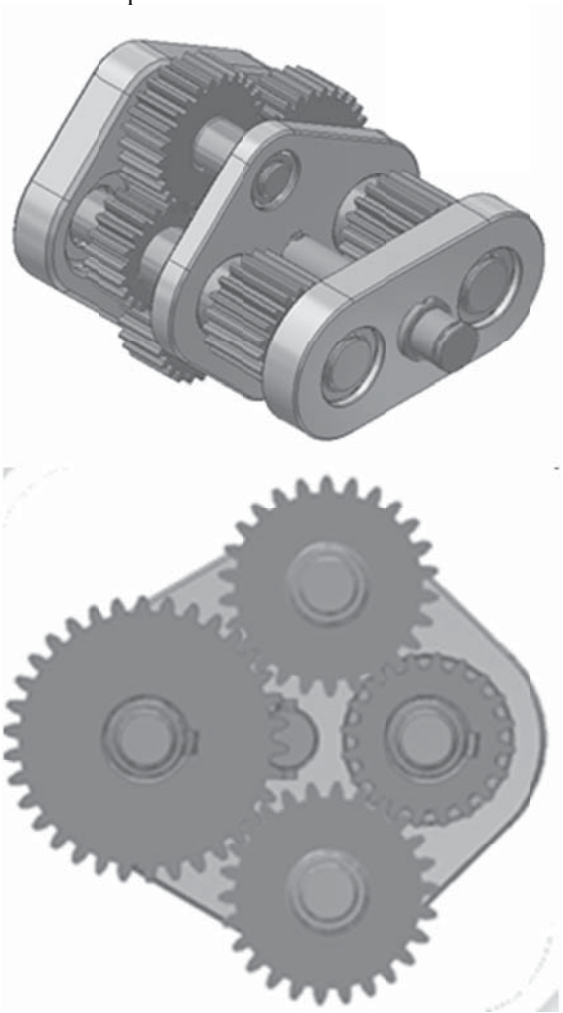

Figure 10: The Modified Central Unit

As shown in the Figure 13, the pinions are now rotating in the same direction.

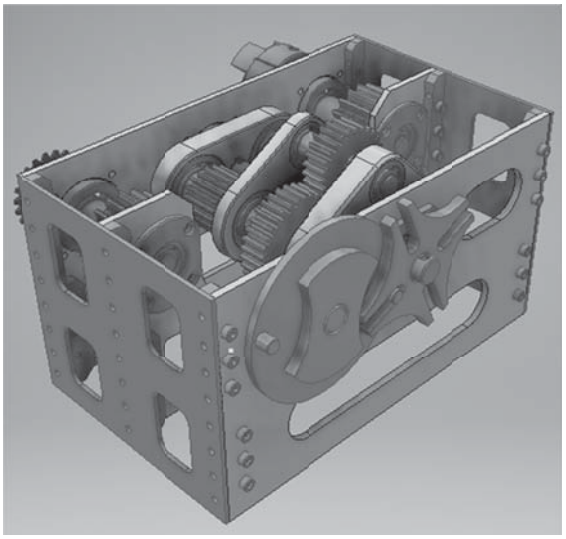

Figure 11: The New Central Unit Fits in the Old Housing

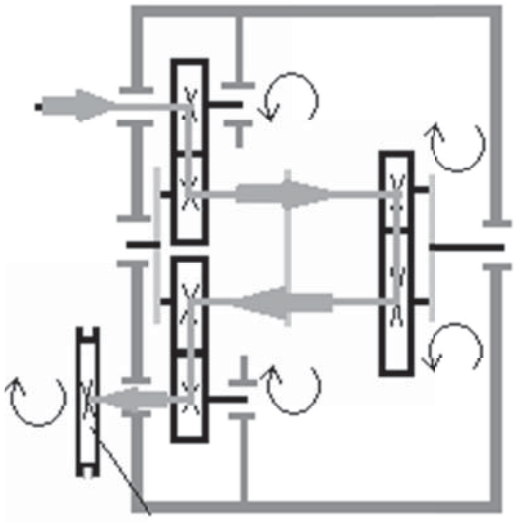

Figure 12: Kinematic Sketch of the Old Design

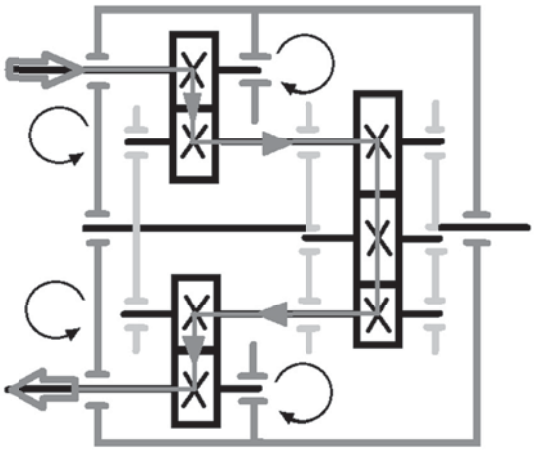

Figure 13: kinematic sketch of the new design

Thereafter, we examined that how big module and face width are necessary with the new parameters in order to have a sufficient flank pressure at least in 70 percent of the coupling time.

For this calculation, the value of the lubrication factor was chosen for 0.4 and the value of the K_A operating factor was increased to 2.25. From the available modules with fair prices the 3mm was chosen and after investigating the available space we increased the face width to 30mm.

In this manner, we got 6.72 for the safety factor of the flank pressure, which does not decrease to a critical value neither in case of a very small contact ratio factor.

This fact, that the centre distance is not constant means also, that it does not makes sense to specify an ISO 1328 accuracy grade 5 for the pinions, the accuracy grade 8 may be sufficient [8], [9]. This means significantly less cost, which allows the pinions to be manufactured of hardened BC3 steel.

8. SUMMARY

Penumobile competitions are perfect opportunities to test ideas of students in the field, they can push their boundaries. One of those boundaries is the design of complete working gearboxes. Our gearbox is working fine now, has reached its calculated lifespan without any signs of gear damage.

The contact ratio factor is one of the most important parameters of all gear drives. Most standards recommend that its value be higher than 1,15. But there are cases, when this cannot be achieved. Is the contact ratio factor below 1, high dynamic loads affect the teeth. There are not recommendations for such cases neither in the standard DIN 3990 nor in the standard ISO 3663 [10]. The low contact ratio can be taken into account by the factor K_A, but it certainly has its limitations. Our gearbox is a simple problem in this world because of its short lifespan, and because the contact ratio factor is only for a short time below 1, but managing low contact ratio is a major problem in many applications.

ACKNOWLEDGMENTS

This paper could not have been completed without the enthusiastic and persistent people who work from year to year for the success of the Pneumobile competitions and the AICPV.

Thank you very much for all of you.

The scientific work behind this paper was organized by the Association for the Development of Innovative Ultralight Vehicles[3].

LITERATURE

[1] https://en.pneumobil.hu/pneumobile_2020/announcement_and_rules/announcement_and_prizing_2020, download date: 20.02. 2020

[2] Bihari János, PEUMOBILE COMPETITION AND EDUCATION. (2012) ADVANCED ENGINEERING 1846-5900 2 1 125-134

[3] Kelemen László, A pneumobil verseny 10 éve a Miskolci Egyetemen. (2017) GÉP 0016-8572 68. 4. 21-24

[4] László Kelemen. 10 Years of Pneumobile Competition at the University of Miskolc. (2018) Vehicle and Automotive Engineering 2 pp. 526-5330

[5] DIN 3960 : 1987-03 Begriffe und Bestimmungsgrößen für Stirnräder (Zylinderräder) und Stirnradpaare (Zylinderradpaare) mit Evolventenverzahnung (1987), Deutsche Institut für Normung

[6] F. Sarka. The use of the linear sliding wear theory for open gear drives that works without lubrication (2019), Solutions for Sustainable Development pp. 1-5

[7] J. Bihari. The effect of the gear wear for the contact ratio (2019), Solutions for Sustainable Development pp. 20-24

[8] ISO 1328-1:1995 Cylindrical gears. ISO system of accuracy. Part 1: Definitions and allowable values of deviations relevant to corresponding flanks of gear teeth

[9] ISO 1328-1:2013 Cylindrical gears. ISO system of flank tolerance classification. Part 1: Definitions and allowable values of deviations relevant to flanks of gear teeth

[10] ISO 6336-1:2019 Calculation of load capacity of spur and helical gears — Part 1: Basic principles, introduction and general influence factors

[11] DIN 3990-1 1987 Edition, December 1987 Calculation of load capacity of cylindrical gears; introduction and general influence factors

[3] Innovatív Ultrakönnyű Járművek Fejlesztéséért Egyesület, Miskolc, e-mail: machbj@uni-miskolc.hu, kksalieri@gmail.com.

KORMÁNYMECHANIZMUS TERVEZÉSE KÖNNYŰSZERKEZETES JÁRMŰHÖZ

STEERING MECHANISM DESIGN FOR LIGHTWEIGHT VEHICLE

Zoltán PUSZTAI, Péter KŐRÖS***
**Széchenyi István University Research Center of Vehicle Industry, Győr, Hungary, pusztai.zoltan@ga.sze.hu*
***Széchenyi István University Research Center of Vehicle Industry, Győr, Hungary,* korosp@ga.sze.hu

ABSTRACT
In this paper the main design concepts and calculations of an alternative steering mechanism are presented, which are dedicated for purpose-made lightweight vehicles. Losses are generated during steering as the tires are not rolling perfectly in curves, what are caused by lateral sliding. The widely used Ackerman steering geometry has its specific error. In order to avoid Ackermann error, the design of an alternative steering mechanism was carried out. This mechanism aims to keep both steered wheels at ideal turning angles. This cannot be achieved using the common rack and pinion steering, therefore a mechanism was designed based on our optimal spiral path method. The advantages of this steering besides eliminating Ackerman error, is that the mechanism is able to self-locking. This mechanism is ideal base for autonomous application as the system doesn't require energy to hold the turning angle, it just consumes energy when the angle is changed. This article covers the main theoretical concept, design fundamentals, FEM simulations and calculations.

1. INTRODUCTION

The alternative vehicle development has great tradition in the Széchenyi István University in Győr. The electric vehicle development team – SZEnergy Team – has been participating in Shell Eco-marathon (SEM) since 2008, which is the world largest energy efficiency competition.

Figure 1. SZEmission, the most recent SEM race car of SZEnergy Team 2019

The participating vehicles have different propulsion system compared to pneumatic vehicles, but still has a lot in common. Our development goals are to reduce the vehicle mechanical, aerodynamical and electrical losses. In this article we're presenting special steering mechanism design, which is also applicable in autonomous driving challanges as well. The most recent battery electric vehicle of the SZEnergy Team can be seen in figure 1.

2. GEOMETRY FUNDAMENTALS

One of the most crucial sub-components of these special vehicles is the steering system. The steering geometry design largely influences the vehicle dynamics. Ideal Ackerman geometry could be defined as a state, when the tire's rotational axes are perfectly intersecting the center of the turn. [1]

This ideal geometry can be defined based on the given vehicle data. The SZEmission parameters are shown in table 1.

Table 1. – SZEmission vehicle data

Wheelbase (L)	1300 mm
Front track	1000 mm
Rear track	800 mm
Drag link radius (Ls)	19,5 mm
Kingpin distance (b)	961 mm
Minimal turning radius (rho)	5676 mm

These vehicle data were directly acquired from the 3D CAD models of the car. The abbreviations can be found in figure 2., which clearly shows the main principle of Ackerman steering geometry. Based on the presented kinematics scheme the following equations can be established. The outer wheel angle can be calculated from the vehicle data as follows [2].

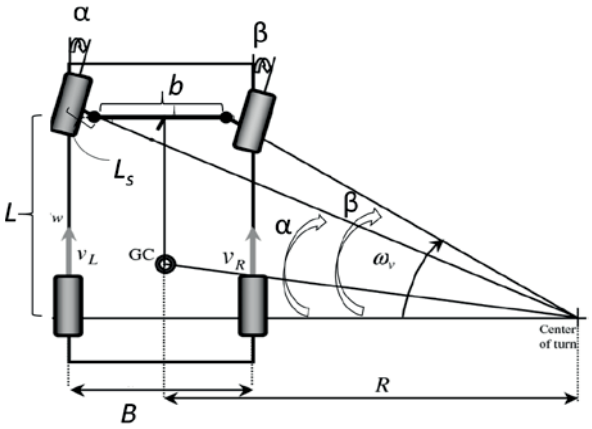

Figure 2. Ackerman steering geometry [2]

$$tg\alpha = \frac{L}{R + \frac{b}{2}} \quad (1)$$

The inner wheel angle can be determined similarly as the outer.

$$tg\beta = \frac{L}{R - \frac{b}{2}} \quad (2)$$

The radius of curve depends on the wheelbase and steering angle.

$$R = \frac{L}{tg\alpha} \quad (3)$$

The vehicle's turning ability relates to the smallest turning radius, which can be defined as the outer front wheel's center distance from the curves center. The following equation describes the minimal turning radius, marked as *rho*.

$$rho = \sqrt{(R + \frac{b}{2})^2 + L^2} + l_s \quad (4)$$

(4)

In case of Ackerman steering geometry, the inner and outer wheels are in different angle position. The inner wheel angle *(β)* is always greater than the outer wheel angle *(α)*, when we're observing normal Ackerman geometry. SZEmission's optimal wheel angles depending on the actual turning radius can be seen in figure 3.

Figure 3. Characteristics of SZEmission's wheel angle

There are methods when the wheels are turned by computer controlled actuators to their ideal position. These steer-by-wire methods have no direct physical connection between the steering wheel and the rotating wheel, that's why safety issues arise related to those systems.

Based on SEM regulations, we have to design a physically connected steering system, which has the lowest possible backlash and closest to ideal Ackerman geometry in our operating range. The situation become more complex if we examine the parts deformation under operating loads and variable suspension geometry design with different loadings. In this article we're designing unique steering mechanism, which is using optimal spiral path calculated from vehicle data with our method to guide the wheels according to ideal Ackerman geometry. The calculations were carried out using simplified rigid suspension kinematic model. [2]

3. OPTIMAL SPIRAL PATH METHOD

In order to apply the method, first we have to create the movement function of steering shaft position compared to the rotation of the knuckle. The function's directional correlation is shown in the figure 4.

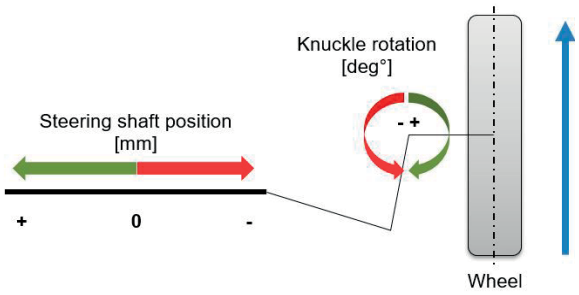

Figure 4. Directional correlation in our movement function

Further on, we also used the previously presented vehicle data table with adding other geometric data such as base radius of our spiral geometry. From CAD models we have to acquire the appropriate data pairs of the ideal Ackerman angle and the translational position change of our steering shaft.

Table 2. – Abbreviation for optimal spiral path calculation

Base radius for spiral path	r_{base}
Steering shaft position – x direction	x_{shaft}
Optimal wheel angle	λ

The value of base radius depends on the steering torque, drag link radius and the expected turning radius. Due to the modification of the

base radius value we can achieve different force ratios in the steering mechanism. The listed parameters and their abbreviations can be seen in table 2.

The optimal spiral path x and y coordinates can be determined by applying the following geometry transformation.

$$x = (r_{base} + x_{shaft}) * \cos(\lambda) \quad (5)$$

$$y = (r_{base} + x_{shaft}) * \sin(\lambda) \quad (6)$$

This x and y coordinates exactly describe the optimal spiral path. The rotating spiral path guides the steering shaft translational movement which keeps the angles of the steered wheels in the position when their rotational axis perfectly intersect the center of the turning radius, achieving the ideal Ackerman geometry. Due to this mechanism we can notice remarkable decrease in the suspension losses, particularly in curves. The spiral path x and y coordinates are illustrated in figure 5. The points are connected with spline interpolation and the base radius is also shown in the figure.

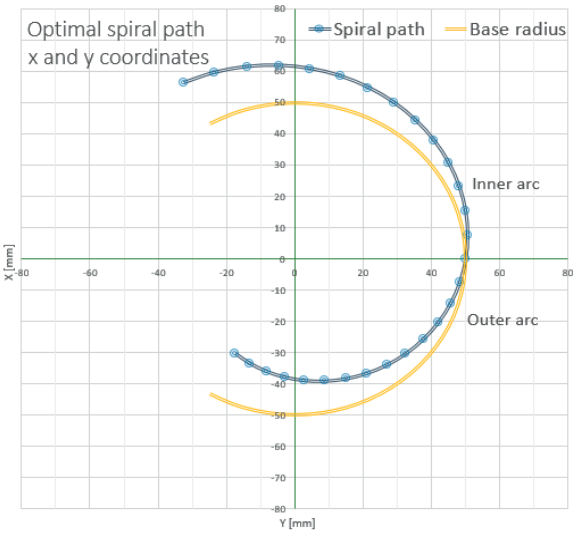

Figure 5. Spiral path x-y coordinates

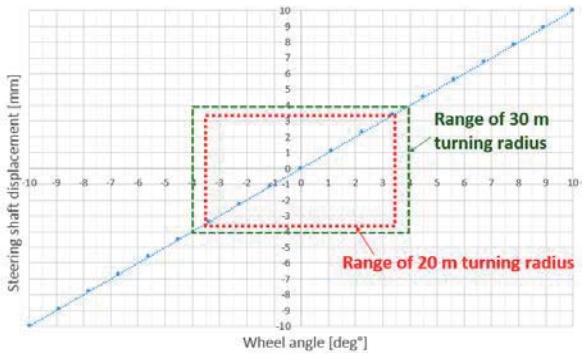

Figure 6. Relation between steering shaft displacement and wheel angle

The relation between the shaft displacement and the wheel angle is almost perfectly linear as it is shown in the figure 6.

Based on the calculations we graphically display two rectangles in figure 6. These rectangles shows the range of 20 m turning radius and 30 m turning radius from inside to outside respectively. These are the most commonly measured turning radius values in a SEM race track.

It's noticeable that the steering system mostly needs to cover only 4 mm shaft displacement in its operating conditions.

4. STEERING MECHANISM DESIGN IN CAD ENVIRONMENT

CAD design implementation immediately started after the calculations of the optimal spiral path were carried out. The most important part is the spiral disk. This part was design in two different concepts.

In one hand, the spiral path equation is drawn in CAD with using spline tools and this curve is offset with given width. On two sides of resulted spline there are urethane molded bearings, which are connected to the steering rods. In this case the spiral guides the rods through rolling bearings.

On the other hand, the disk can be designed with doubling the extruded curve to create a hollow between the curves. The inside of the hollow could guide a properly fitted shaft. In both case the rotation of the spiral disk is transformed into the steering rods translation movement. The main difference between these options is the way of friction and the clearance between the parts, which could easily cause undesired backlash in the whole system.

The spiral disk and its shaft has to be supported by bearings from both side. We designed a framed construction, which connects the bearing housings. The frame and the housings are fitted with positioning pins to keep the shaft in its designed place.

The steering rods are connected to the spiral disk through adjustable arms. The rods are made from hard anodized square sectioned aluminum bar. The steering rods are supported and mounted by plastics crossbars. The whole construction is placed in U-profile aluminum frame, which unites parts and increases the system rigidity. The figure 7. shows the CAD assembly of the designed spiral path steering.

SZEnergy Team is making great effort in autonomous driving development, that's why an autonomous steering extension was designed to the presented steering system, illustrated in figure

8. The steering is driven by a DC motor through timing belt connection. The motor controller gets position information from linear sensor placed on the steering rod. The autonomous extension is separate unit, so it could easily attached to the steering system.

Figure 7. CAD assembly of the steering system

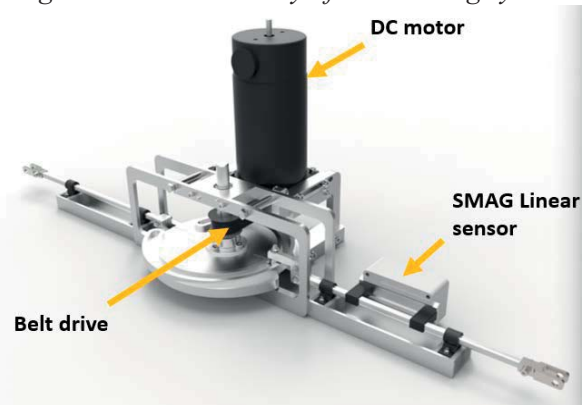

Figure 8. Autonomous steering system

5. STATIC STRUCTURAL AND RIGID BODY DYNAMICS SIMULATION IN ANSYS

The CAD design process was supported by plenty of FEM simulations. Traditional static mechanical simulations were made to determine the different dimensions of the presented parts. Main goal was to specify the width of the contacted spiral disk. In case of static simulation we have to regulate the system's degree of freedom (DOF) with constrains and apply loads to the system. We made simulation cases with different sample loads as we had no exact data about the occurring loads. The load cases with different CAD data were matched. The results of these cases were compared to each other to determine the trends.

We used the available basic ANSYS material models such as aluminum and structural steel. Tetrahedron meshing with local mesh tools in the main contact area was chosen. We tried to make mildly detailed mesh to check the models with reasonable accuracy.

Some simulation input were received from CAD design such as the geometry data of the bearings. These commercial products have exact size limitation, so we have to adjust our parts dimension to them. We targeted to find dimensions, which give the part near the same strength as the bearings. It means that we didn't examined exact numeric results just compared the different simulation cases. One of the static structural simulations isoline results can be seen in figure 9.

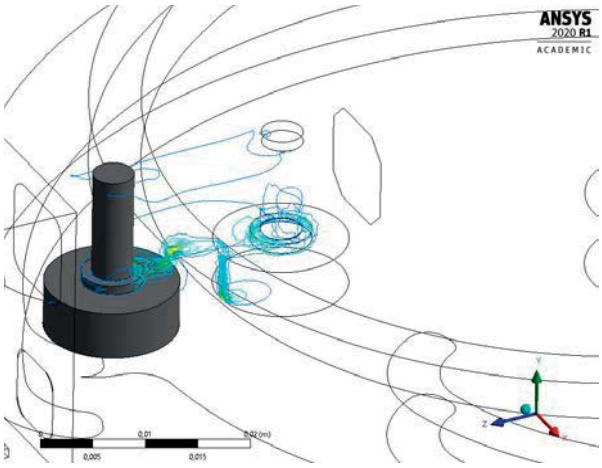

Figure 9. Static structure isoline result

Evaluating the simulation results we agreed on 5 mm spiral curve width, which satisfy both mechanical and manufacturing demands. The manufactured and pre-assembled spiral disk can be seen in figure 10.

Figure 10. Pre-assembled spiral disk

Rigid body dynamics module of ANSYS was also used to receive approximate data of the system movement characteristics. Firstly, we had to modify the simulation constrains and adjust the system's DOF to create a periodically repeated movement. The main simulation constrains and joints are illustrated with the simplified model in figure 11.

The sample spring load is similarly determined as in the static structural module as the exact loads are unknown yet. The spring load connects the fixed knuckle (simplified as a rectangular body) to the steering rod. The steering

rod can move translationally in the supports. The polymer crossbars are also fixed to the ground. No separation contact is applied between the roller bearing's cylindrical surface and the designed spiral path surface, the figure 12 shows that in details.

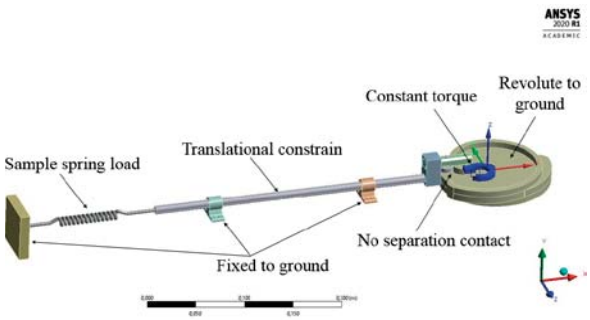

Figure 11. Constrains and joints in ANSYS Rigid Dynamics module

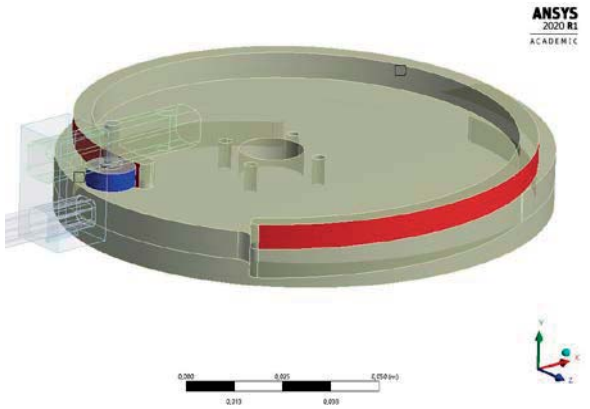

Figure 12. No separation contact on the spiral path

The spiral disk is able to revolute around its local Z axis. This revolute joint is driven with constant torque. The rotation is limited from 0° to 315°, it's the physical limit of the spiral path. The movement starts from the maximum distance from the knuckle. The spring is unloaded at the beginning. The rotating disk moves the steering rod only in the global X direction, the rod compress the spring which generates reaction force in the knuckle. When the angle limit of the spiral disk is reached, reversed rotation starts to take the simulation back to the initial condition. The simulation runs periodically. Joint and position probes were queried to get the movement, velocity (angular and translational) and force results. The comparison of the translational and angular velocity is illustrated in figure 13.

The rotational and translational performance can be also calculated from the queried simulation results as it is shown in figure 14.

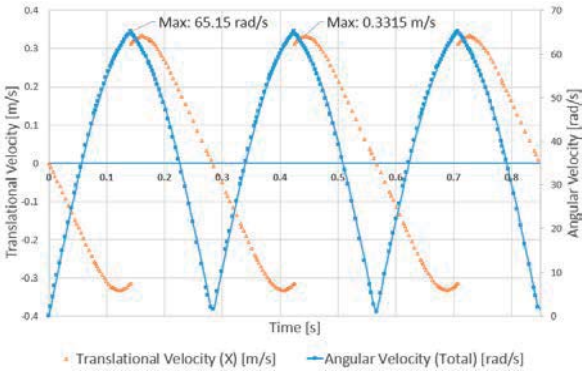

Figure 13. Translational and angular velocity results from ANSYS Rigid dynamics

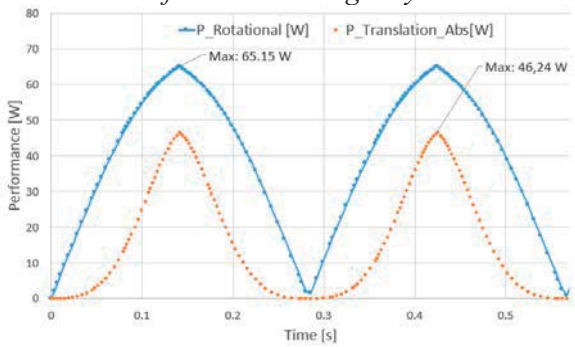

Figure 14. Performance results from ANSYS Rigid dynamics

5. SUMMARY

Special steering mechanism concept based on the calculation of the optimal spiral path was presented in this paper. This spiral path creates unique curves depend on different suspension characteristics. The curves follow the ideal Ackerman angle in every position, which extensively reduce the suspension losses. The main design and simulation principles of the steering systems were also presented.

6. ACKNOWLEDGEMENT

The research presented in this paper was carried out as part of the "Autonomous Vehicle Systems Research related to the Autonomous Vehicle Proving Ground of Zalaegerszeg (EFOP-3.6.2-16-2017-00002)" project in the framework of the New Széchenyi Plan. The completion of this project is funded by the European Union and co-financed by the European Social Fund.

6. BIBLIOGRAPHY

[1] N.W. Troupe.: Optimization of Steering Geometry For Ultra-High-Mileage Vehicles, The Pennsylvania State University, 2011.

[2] K. Hartani, Y. Miloud, A. Miloudi.: Electric Vehicle Stability with Rear Electronic Differential Traction, EFEEA'10 International Symposium on Environment Friendly Energies in Electrical Applications, Ghardaïa, Algeria, 2-4 November 2010.

GERJESZTŐ HATÁSOK HENGERES FERDE FOGÚ FOGASKERÉK KAPCSOLÓDÁSBAN

EXCITER EFFECTS IN CYLINDRIC HELICAL GEAR MESHING

Drágár Zsuzsa, Dr. Kamondi László PhD
Institute of Machine and Product Design, University of Miskolc

ABSTRACT
Automotive industry needs more and more quiet and vibration free drive systems. Cylindric helical gear pairs are suited to complete such claims of a power train, if the sources of vibration excitation can be reduced. The source of the vibration excitation is the contacting field, whose shape and dimension besides the characteristics depending on the direction of rotation can be influenced effectively. This article presents eventuality that reducing of vibration exciting in meshing is how can be forwarded by contacting field modification and tooth shape symmetry ending, and how can it be achieved.

1. INTRODUCTION

Function of energetic systems which have toothed element pairs, without intermediary elements decreases several cases in the past decades. These systems however couldn't loose its importance. One reason is the correct, and continually more correct, transmission of energy components (load and motion). Those dynamic systems, among the power trains in automotive industry, which contain gear contact, have to meet increasingly difficult expectations. Expectations can be traced back to vibration and acoustic effects. Drive systems take an important role in the function of systems (products), it can be expected to be unrecognizable, unidentifiable. A household appliance has to assimilate itself to that acoustic environment where it is used. It mustn't be loud, mustn't cause unhealthy vibration. These expectations be valid for other applications, e.g. underwater vehicles should not be recognised. This article presents some problems, which originate from meshing of cylindric external toothed helical gear pairs (see later CEH).

2. INFLUENTIAL PARAMETERS IN MESHING

Meshing problems of gear pairs, within CEH, have always appeared in different form during the technical development [1, 2]. It is caused by:

- qualitative improvement of the material properties, reliability of its documentation,
- increasing improvement of the tooth surface structure mapping,
- improvement of design operations' accuracy, appearing of alternative calculation methods,
- appearing of environmental influence,
- possibility of hiding some applications

Assignment of design is to solve and eliminate raised problems. Designer can effect on three tasks:

- installation ambiance of gear pair,
- meshing field and it's characteristics with the help of teeth geometry,
- expected accuracy of manufacture.

The installation environment of gear pair with deformation (angular motion / banking and torsion) caused by loading influence, locates the spatial position of the gear bodies. This change has an influence on the characteristic of load distribution in the meshing field (the distribution of load develops on the line of contacting teeth), in addition on extent of load distribution among the lines. Figure 1. shows derivation of the meshing field. Characteristics of load distribution can be seen on Figure 2.

3. CHARACTERISTICS OF THE GEAR PAIR MESHING

Meshing of the helical gear pairs (CEH) has several advantages in the meshing process [1, 2]. It is typical for the meshing process:

- fluctuation of the contact ratio is smaller between the entering and the leaving gear pairs,
- bending stiffness of the tooth rises because of the helix angle,
- total length of the contacting components becomes more equable, but it changes during meshing (Figure 3.).

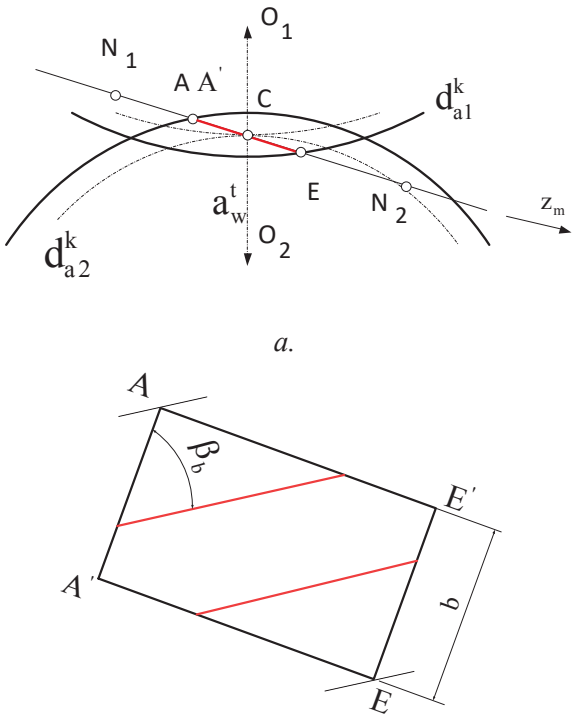

a.

b.

Figure 1. Derivation of the meshing field

This contradiction of meshing originates from that width of the meshing field (b), specified by the common tooth width, determines current total contacting apex distance and its character (ΣL).

$$\Sigma L = f(\sum L_i(dz), b) \qquad (1)$$

Above reasons can't be considered complete, because meshing has other characteristics, which are determined by the accuracy of manufacturing as well.

The load distribution cases shown in Figure 2, with the refinement of the manufacturing technology and the surface modifications made on the tooth, result in a situation whereby the load distribution on the tooth pairs becomes uniform over the contacting component.

It can also mean that the result of the load transmitted by the tooth pair can be placed in the middle of the component length and the load can be proportional to the component length [3].

Several researches deal with developing of the drive systems. Numerous conclusions are drawn from investigation of the meshing field. Typical for these are the follows:

- The torsional vibration excitation from the meshing can be stopped, if the axial contact ratio (overlap: ε_β) is set to an integer. Then the total length of the component is permanent throughout the whole meshing process [2].
- In the meshing process strength analytical studies have begun to deviate from the integer axial contact ratio. The tooth width has to be set that the fractional part of the axial pitch provides the additional tooth width [4].
- Japanese researchers have found, on the basis of purely experimental results, that no integer axial contact ratio should be sought [5].

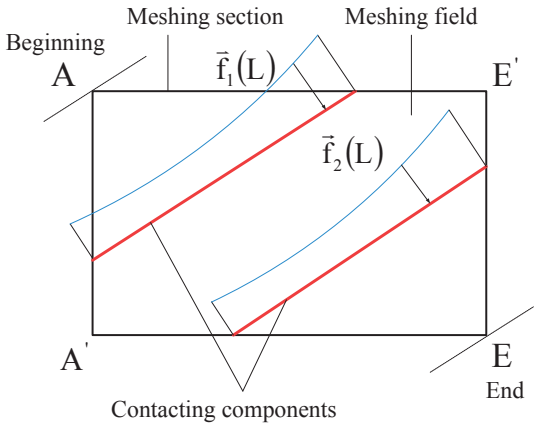

a.

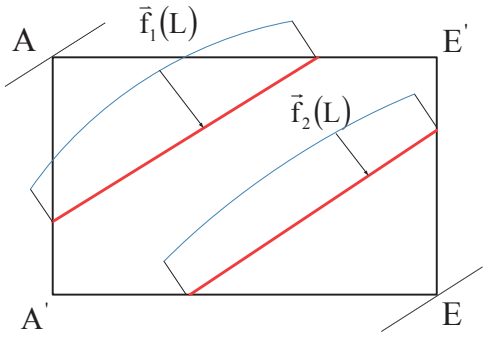

b.

Figure 2. Characteristics of load distribution in the meshing field

4. INFLUENCING OF THE MESHING CHARACTERISTICS

The size and shape of the meshing field is a challenge because the designer should answer why and how to choose the common tooth width. If it is appropriate, why the shape of meshing filed deviates from the rectangular shape.

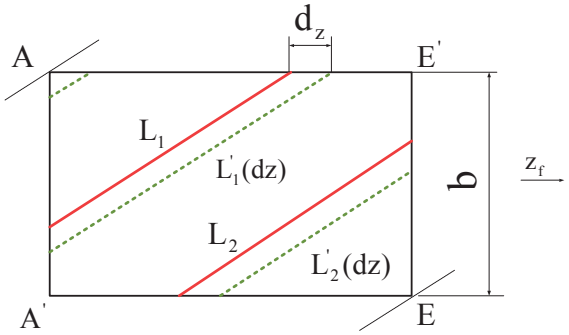

Figure 3. The length change of the contacting components

4.1. Effect of meshing field size

In the meshing field, the total length of the contacting components varies as the period of the base pitch of the meshing in the transverse plane. This change varies with the current common tooth width. The tooth width can always be written as the integer multiple of the axial pitch (p_x) and the sum of its fractional units (db)

$$b = k \cdot p_x + i \cdot p_x = (k + i) \cdot p_x, \; db = i \cdot p_x \quad (2)$$

where k = 1, 2, … n (integer) and i is any value from 0 to 1.

The literature has contradicted the results of research in choosing the value of i. Previous research and theoretical ideas have suggested that for i = 0, the value of the resulting contact length is constant [1, 2], because the change of the torsional stiffness is zero. Others inferred from measurement results [5] but did not theoretically justify their results. Another line of research concluded that it is theoretically possible to deduce from the real tooth stiffness change that i = 0 cannot be justified [4]. The purely experimental and theoretical approaches have gone beyond the previous one, but their results have not reinforced each other.

The direction of the research, which started from the exploration of the source of vibration excitation [6], concluded that the result of the experimental research can be well approached and theoretically supported if we choose (db) determined by the value of i such that the value of the given contact ratio (ε_γ) must be an integer. The basis of this research was the examination of the displacement of the resulting tooth force on the contacting components in the meshing field. The result of the research found that the range of motion of the resultant of the tooth forces can be minimized, but not reduced to zero. Research has proven to be a wise choice of common tooth width, makes the acoustic recognition of a drive difficult.

4.2. Changing the shape and effect of the meshing field

The change of shape of the meshing field was based on the fact that the shape can influence the total length of the instantaneous contacting components throughout the meshing phase. Changing the shape of the contacting field is possible by modifying the meridian curve of the head cylinders. This possibility is also important because, in the case of gears with asymmetrical tooth shape, a change in the direction of rotation results in different meshing field parameters [7].

There are two ways to modify the contacting field:

- modifying the meridian of the head cylinders to map the meshing field,
- modifying the meshing field freely and generating head cylinder meridians from it.

The goal of both methods is to reduce the tooth force moving that generates the vibration excitation in the contact to an absolute minimum instead of a local minimum.

Without changing the meshing field, it will take the shape of Figure 4. Changing the direction of rotation and changing the base cylinders also changes the size of the contacting field [7]. Changing the meridian of the head cylinder changes the shape of the meshing field as shown in Figure 5. Changing the direction of rotation in the drive changes the size of the modified field [8], distorting its shape only. It can be seen from the figure that the contact ratio is slightly reduced due to the theoretical meshing length (H), the sum of the theoretical instantaneous meshing component length (L_i) is also reduced, but the substantial change is observed in the decrease of the L_i fluctuation over time. The trajectory of the resultant tooth forces formed on the meshing members can be effectively influenced within a period of meshing.

This type of modification of the meshing field affects both the torsional excitation of the meshing and the radial and axial excitation of the bearings. The study of this effect is becoming more and more important for toothed pairs as the precision becomes more important.

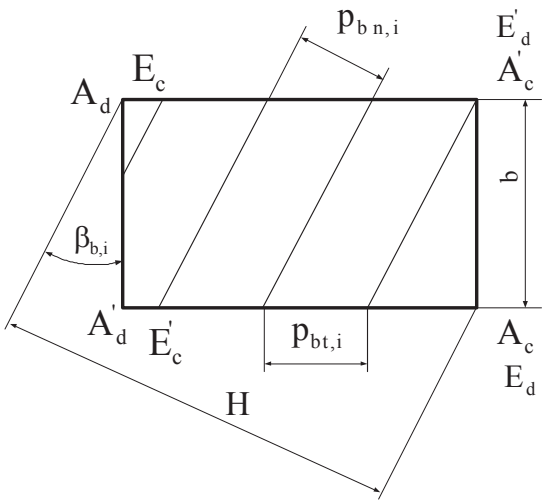

Figure 4. Regular meshing field

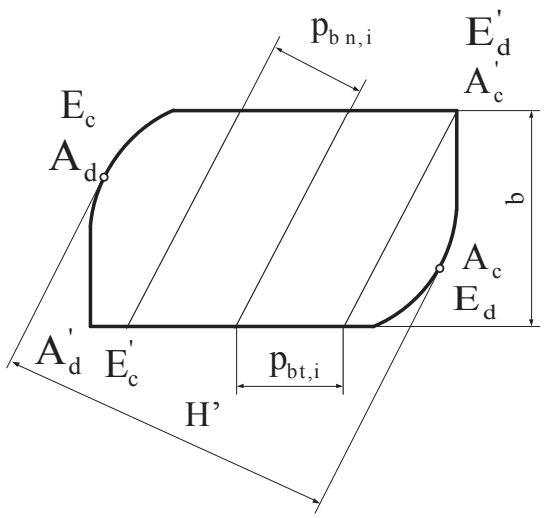

Figure 5. Modified general meshing field

In this case, we should consider what solution we recommend to the designer. These are the following:

- defining a regular rectangular contacting field with excitation at the local minimum,
- modifying the meshing field with one of the two recommended methods to minimize (absolute minimum) the excitatory effect.

5. SUMMARY

The aim of the article is to draw the attention of gear developers to the specific requirements of a drive system that they can follow during the development and design phase. We have presented a suggestion regarding the acoustic recognition of the drive chains. We have presented a research process that will show the way to a solution. We have raised some questions that induce further research.

ACKNOWLEDGEMENT

The described article was carried out as part of the EFOP-3.6.1-16-2016-00011 "Younger and Renewing University – Innovative Knowledge City – Institutional development of the University of Miskolc aiming at intelligent specialization" project implemented in the framework of the Széchenyi 2020 program. The realization of this project is supported by the European Union, co-financed by the European Social Fund.

LITERATURE

[1] Niemann, G.: Maschinenelemente II. Springer Verlag. Berlin/Göttingen/ Heidelberg. 1961

[2] Erney, Gy.: Fogaskerekek. Műszaki Könyvkiadó. Budapest, 1983.

[3] Linke, H. - Gajevski, G.: Breiten lastverteilung unter besonderer Berücksichtigung der Breiben balligkeit bei Verzhnungen. Maschinenbau-technik. Berlin. 32 (1983) 10. p. 445-449.

[4] Ajrapetov, E. L., Genkin, M. D.: Kolebanija mechanizmov sz zubcsatümi peredacsami. Izdatelsztvo Nauka. Moszkva. 1977.

[5] Fukuma, H., Aida, T.: Fundamental research on Gear Noise and Vibration. Bulletin of the JSME. 17 (1974) 113. p. 1502-1512.

[6] Kamondi, L.: Verallgemeinerung der Bestimmung der Überdeckungszahl für dem Fall einer schrägverzahnten Stirnräderpaares mit korrigiertem Evolventenprofil. Publications of the Technical University for Heavy Indusrty. Series C (Machinery). 40/1984/ 2-4. pp: 123/133.

[7] Drágár, Zs., Kamondi, L.: Determination of general tool basic profile for gears using analytical geometry, pp. 105-108, ISSN 2068-1267, XX. International Conference on Mechanical Engineering, OGÉT 2012, April 2012, Romania, Cluj (in Hungarian).

[8] Kamondi, L., Drágár, Zs.: The role of the tooth shape in powertrains containing gears, pp. 232/235, ISS 2068-1267, XXVI. International Conference on Mechanical Engineering, April 26-29, 2018. România, Targu Mures (in Hungarian).

PROSZTETIKUS KEZEK ÁLTAL KIFEJTETT ERŐ A KORMÁNYKEREKEKRE

FORCES APPLIED ON STEERING WHEELS BY PROSTHETIC HANDS

Kmetz Barbara, MSc gépészmérnök hallgató, Jálics Károly, címzetes egyetemi docens

ABSTRACT
Artificially made limbs have almost reached human's force limits, sometimes they even exceed them. These prosthetics make life easier for a lot of people, for example many prostheses are suitable to drive cars. With the right forces applied by an artificial hand a person can drive a car with even two missing limbs. This article deals with estimating connections between prosthetic hand's force and driving force.

1. BEVEZETÉS

Manapság a gyors prototípusgyártás már sokak számára elérhető gyártómódszer, számos amatőr vásárol magának otthonra is hobbygépeket. Az egész világon széles körben elterjedt a 3D nyomtatás. Mára már prosztetikus végtagokat is nyomtatnak az emberek. A cikk megvizsgálja, hogy ezeknek a prosztetikus végtagoknak mekkora erőt kellene kifejteniük a kormányzáshoz, illetve összehasonlítja kormányerőt az izmok erejével izomjelek formájában.

2. ELEKTROMIOGRÁFIA SZENZOR (EMG)

Az elektromiográfia szenzorok egyre jelentősebbek a gépészeti, biomechanikai és klinikai területeken. Napjainkban már készítenek rehabilitációs készülékeket, prosztetikus végtagokat, illetve robotokat is elektromiográfia vezérléssel. Az elektromiográfia, röviden EMG az izom elektromos jeleinek detektálására, feldolgozására és elemzésére használatos.

Az elektromiográfia szenzor összegyűjti az izom jeleit, amelyek az idegrendszer irányításával keletkeznek izomösszehúzódás alatt. A jel az izom fiziológiai és anatómiai tulajdonságait mutatja. Tulajdonképpen az EMG jel az izom motorikus egységeinek az elektromos aktivitása. Kétféle elektromiográfiáról beszélünk. Az egyik a felületi EMG, a másik pedig az intramuszkuláris EMG, amely azt jelenti, hogy az adott izomba az ideg lefutása mentén két elektródát helyeznek fel, két különböző pontra. Jelen esetben azonban az előbb említett felületi EMG-vel foglalkozunk, mivel számunkra ez elérhető. A felületi elektromiográfia jóval egyszerűbben kivitelezhető eljárás, ezzel szemben sokkal pontatlanabb is lesz és csak közelítő értékeket fog adni az izom erősségéről.

1.ábra. Elektromiográfia szenzor

Az elektromiográf jelek leghasznosabban elektrofiziológiai jelekként hasznosíthatók az orvoslásban és a műszaki alkalmazások területén. Az emberi test izmai működésének megismeréséhez egyszerűen elvégezhető eljárása a felületi EMG. A biológiai elektromos jeleket lehet gyűjteni minden olyan testrészről, amelyek mozgatásakor elektromos jeleket hoznak létre a motoros egységek által. A jel alapjában véve egy bizonyos időlefolyás alatt értelmezett jel, emellett amplitudóval, frekvenciával és periódussal rendelkezik. Az EMG jel, egy olyan fiziológiai jel, amely az izom elektromos jelét méri összehúzódást, neuromuszkuláris aktivitást mutatva. Az izmok működtetése mindig idegi alapon történik, az idegrendszer felelős érte. Láthatjuk, hogy az elektromiográfia egy rendkívül összetett elemzési módszer, amely számos fiziológiai és anatómiai adottságtól függ. Jelenleg a legnagyobb igény a szenzor használatára az orvosi diagnosztikában és az egészségügyi, mechatronikai mérnökök (művégtag fejlesztők) között van.

3. KORMÁNYKERÉK MEGENGEDETT EREJÉNEK MEGHATÁROZÁSA

A kormányberendezés erejének meghatározására külön szabvány van felállítva. A szabvány egy mérési módszert határoz meg az erő megállapításához.

A kormány úgy is működhet, hogy a vezető erején kívül, kiegészítő erő van igénybe véve, amely lehet erőrásegítő kormányberendezés vagy szervó kormány. A legtöbb jármű szervó kormánnyal rendelkezik, amely a motor járó állapotában segíti a kormányzást. A kormányt lehet csak külső erővel is működtetni, ilyen például a hidraulikus gépkormány. Ezen vezérléssel működő járműveknek álló (nem járó) helyzetben is üzemszerűen működőképesnek kell lennie.

A kormányszerkezetet olyanra kell tervezni, hogy üzemzavara jelentkezésekor a kormányzás vezérlése és a kormányzott kerekek erőátvitele (mechanikus meghibásodást nem számítva) a gépjárművet kormányozni lehessen. Az így keletkező erők meghatározását szigorú, leírások alapján lehet elvégezni.

A vizsgálat véghezviteléhez a következő feltételeknek kell teljesülnie:

- A rendelet 5.2 pontja szerint kell végrehajtani a mérést
- Az eljárás lényege, hogy a járművel egy 50 méter sugárral rendelkező kanyarban kell haladni tangenciális irányban
- A haladási sebesség legtöbb esetben 40 km/h vagy 50 km/h kell, hogy legyen
- Figyelembe kell venni a jármű fajtáját a sebesség megállapításához (M1, M2, M3 jelű járműveknek 50km/h-val kell haladniuk, a N1, N2, N3 jelű járműveknek 40km/h sebességgel vagy a jármű legnagyobb tervezési sebességével, ha az kevesebb a feltüntetett sebességeknél)
- A megfelelő tapadást kell biztosítani, emellett pedig a tesztfelületnek vízszintesnek kell lennie
- A vizsgálat előtt a gumikerekek nyomása ellenőrizendő és beállítandó az adott megfelelő értékre.

„A kormányzáshoz szükséges erőkifejtés mérése során a 0,2 másodpercnél rövidebb ideig ható erőket nem kell figyelembe venni.”

Ezen feltételek és kikötések teljesülése mellett a kormánykeréken a kormányzáshoz szükséges kerületi erő nem haladhatja meg a 150 N-t.

4. EGY ISMERT ELJÁRÁS TANULMÁNYOZÁSA

Sajnos nem született még megfelelő eljárás, számítás az elektromiográfia szenzor által kibocsájtott jel és az erő közötti kapcsolat meghatározására. Közelítő kísérletezésekből is csak néhány angol irodalmat lehet találni, ezek közül a legtöbb nem érhető el az olvasók számára. Szerencsére sikerült találni egy leírást egy közelítő számításról és kísérletről. Az izomjelek technikai, anatómiai és fiziológiai adottságai miatt rendkívül nehéz feladat párhuzamot felállítani az izomjelek és az erő között. A kutatók az izmok számos biológiai és neuro-fiziológiai tulajdonságát kutatták az elmúlt évtizedekben, hogy meghatározzák az előbb említett kapcsolatot, azonban pontos meghatározás az ismert adatok alapján még a mai napig nem született. A kapcsolat megfejtése magában azonban nem elegendő megoldás a protézisek használatára autóvezetés közben.

A napjainkban használt művégtagokra még mindig azt kell, hogy mondjuk, hogy a flexibilitásuk és a funkcionális használhatóságuk nagyban korlátozott, nem is beszélve a finommotorikus mozgáselemekről. Lényegében két nagy nehézség megoldására lenne szükség, az egyik a protézisek mechanikai designja, amelynek biztosítani kellene a megfelelő mozgástartományt. A másik probléma egy komplexebb elektronikának a kifejlesztése, amely képes a mechanikailag is fejlettebb művégtag kezelésére.

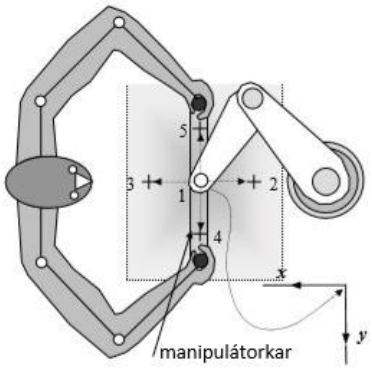

2.ábra. A kísérlet váza

A leírásban az egyszerű erő-jel kapcsolatot vizsgálták, az EMG szenzort a különböző izomokra rögzítve. A kísérlethez egy kétkarú manipulátort használtak, így mindkét karból tudtak egy egységes jelet rögzíteni. A manipulátort 0,75 méter távolságban helyezték el a kényelmes mozgathatóság érdekében. A kísér-

lethez két, 25 és 35 év közötti egészséges jobbkezes alanyt használtak. Az alanyoknak a meghatározott pozícióban kellett helyet foglalnia és a kart elfordítania meghatározott ideig. A kart egy adott séma szerint kellett mozgatni, a sémát három különböző részre lehetett osztani. Az első a kezdő fázis, amelyet 2 másodpercig kellett tartani, a második a megtartó fázis, amit 4 másodpercig kellett megtartani, végül a visszaállító fázis, amelye szintén két másodpercig tartott. A kísérletet tízszer ismételték meg és a kapott erőket, izomjeleket összegyűjtötték és kiértékelték. A kísérlethez használt EMG szenzor erősítőbe, négy csatornán keresztül érkezett a jel, ennek hála négyizom erejét tudták rögzíteni. A négy izom a bicepsz, a tricepsz, a pectoriális és a trapéz izom volt. Azért ezen izmokat vizsgálták, mert ezeket az izmokat használja az ember legjelentősebben kormányzáskor. Nagyon fontos az elektródák pontos elhelyezése az izmok közepén, hiszen így kapható a legpontosabb jel. A még jobb eredmények érdekében egy speciális gélt használtak a szenzorok rögzítésekor a zavaró jelek jobb szűrése érdekében. A kiértékelések alapján különböző összefüggéseket állapítottak meg, amelyekkel közelítő értékeket lehet számítani a jel és az erő között. A kísérlet konklúziója szerint képesek kimutatni a kapcsolatot maximum 15% hibalehetőség mellet, amely nagyon szép teljesítmény, de távol áll a közel pontosnak mondható számítási módszerektől. Ezen kísérletet, és egyéb leírásokat tanulmányozva szerettük volna megpróbálni kimutatni az erő és az izomjelek kapcsolatát egy másfajta módszer alapján. A tanulmány első fázisairól szólnak a következő fejezetek.

5. EGY LEHETSÉGES KÍSÉRLETI ELJÁRÁS

A tanulmányozásokat olvasva kirajzolódott egy másfajta megközelítési módszer tesztelése. Saját ötlet alapján a 3. pontban meghatározottak alapján erő mérését kíséreltük meg EMG szenzor jelek párhuzamos felvétele közben. A kísérlet három autó használatával lett elvégezve, megfelelő mennyiségű különböző mérés alapján. A kísérlet helye: Miskolc, Auchan parkoló területe. Mindhárom jármű az M1 (személyautó) kategóriába tartozik, ami azt jelenti, hogy 50km/h sebességgel kellett haladni a járművekkel. A három autó a különböző adottságaik és karakterisztikájuk miatt lett kiválasztva. Az első számú autó egy Renault Clio, szervó kormányos, két kerék meghajtású, kézi váltós, 800kg tömegű személyautó. A második számú autó egy Toyota Rav4, egy városi crossover terepjáró négy kerék meghajtással, szervó kormánnyal és automata váltóval, a jármű össztömege 1,9 tonna. A harmadik számú személyautó egy Audi A4 allroad quattro, szervó kormányos, szintén négy kerék meghajtású (saját szabályozás, és arányosítás alapján használva a kerekeket szükség esetén) 1,5 tonna össztömegű jármű. Kísérlet előtt a járművek megfelelő tapadása és a gumikerekek előírt nyomása ellenőrzésre került. Az előírások szerinti feltételeknek eleget téve ment végbe a kísérlet. A kísérlet helyszínére indulás előtt készített kép látható a 3. ábrán.

3.ábra. Kísérlet előtt szenzorok a karon rögzítve

Az erők mérése rugós erőmérővel történt álló és haladó helyzetekben, mivel az autók szervója már a motor beindítása után is segíti a kormányzást, nem szükséges elindulni a járművel. A kísérlet elvégzése közbeni biztonsági megfontolásokból adódóan az adatokat segítő személyek rögzítették. Az erő mérése többször lett elvégezve, szám szerint minden egyes eshetőségre tíz mérés lett végezve. A tíz különböző mérés átlagolva lett, majd a mért erők táblázatban lettek rögzítve.

A kísérlet másik része az izomjelek rögzítése volt. Sajnos nem volt lehetőség a legdrágább, legfejlettebb elektromiográfia szenzorok beszerzésére, egy egyszerűbb, kísérletezés szempontjából megfelelő készülék volt használva a teszthez. A korábbiakban már be lett mutatva, hogy mi is ez a szenzor és hogyan működik. A kísérlet pontosságának érdekében utánaolvastam, hogy milyen izmokat célszerű használni és hogyan kell az elektródákat elhelyezni. A kar izmai kifejezetten alkalmasak a jelek felvételére, ugyanis itt nagy és fejlett iz-

mok tapadnak a csontokra. Minél tónusosabbak egy ember izmai, annál erősebb jelet tud a területről felvenni az elektróda. A karon a tricepsz és a bicepsz rendkívül erősek, ezért kiválók a tappancsok rögzítésére, én azonban az alkar izmait választottam, mert ez közelebb esik távolságban az esetünkben tekintett hiányzó végtagrészhez, valószínűleg ezen a területen kell majd rögzíteni a művégtag használókon is az elektródákat. Az elektróda három ágát különböző színekkel jelölték meg. A piros színű elektróda kerül az izom testére, a zöld elektróda kerül az izomcsoport végére, a sárga elektródát pedig csont közelében helyezem el a megfelelő földelés céljából. Ezután egy mikroszámítógép segítségével a jelek felvételre kerülnek és a számítógép kijelzőjén láthatók lesznek. A felvett jelek és rögzített erők összehasonlítása után a következő táblázat készült.

1. táblázat-Kísérlet mért eredményei

Autó sorszám	Mért érték[kg] [N]	EMG jel
1. szervó álló	2 kg~20 N	160
1. szervó járó	1,5 kg~15 N	120
2. szervó álló	1,9~19 N	150
2. szervó járó	0,9~9 N	70
3. szervó álló	1,2~12 N	100
3. szervó járó	0,8 kg~8 N	60

Az 1. táblázat csak az átlagolt értékeket prezentálja mivel az egész táblázat beszúrására nincsen mód. A mért értékek alapján levonható következtetés, hogy a jel és az erő viszonyára nem lehet egy teljesen lineáris skálát felállítani. Az értékek alapján párhuzam vonható az adatok közé. A párhuzam pontosabb megállapításához diszkrét Fourier transzformációk további tanulmányozása szükséges. A kutatás következő fázisaiban kerül majd sor ezen képletek pontos leírására.

6. AZ EMG SZENZOR ZAVARÓ TÉNYEZŐI

A szenzor két legjelentősebb befolyásoló tényezőjét szeretném említeni, ami torzítja a mérés hitelességét. Az egyik a jel-zaj arány. A szenzor zajt is felvesz a jel felvétele közben. A jel több réteg szöveten keresztül jut el a jelfelvevő elektródához, ezért nem csak veszít a jel erősségéből, hanem továbbítás közben különböző zavaró zajokat is összeszed. Jelenleg a zajt olyan elektromos jelekként definiáljuk, amelyeket nem szeretnénk, hogy részei legyenek a végső felvett jelnek. A másik probléma a jel disztorziója. Bármilyen frekvencia komponens relatív hozzájárulása megváltoztathatja az EMG jeleket. Ezen zavaró tényezőkkel kell számolni a jelfelvétel közben.

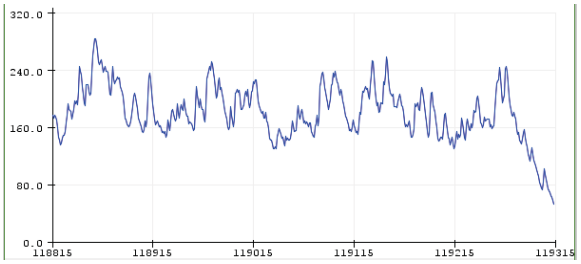

4.ábra. Szenzor jel zavarói

7. ÖSSZEFOGLALÁS

A kutatás célja egy módszer kifejlesztése volt, amellyel lehet kormányerőt mérni, illetve izomjeleket felvenni és rögzíteni. A kutatás további fázisaiban pontos képletek kerülnek meghatározásra diszkrét Fourier transzformációk felhasználásával.

8. FELHASZNÁLT IRODALOM

[1] 6/1990. (IV. 12.) KöHÉM rendelet a közúti járművek forgalomba helyezésének és forgalomban tartásának műszaki feltételeiről
[2] Yunus Ziya Arslan, Mehmet Arif Adli, Aydin Akan: Investigation of the relationship between EMG signals and the forces applied to human arms, 2005
[3] Yahui Liu, Xuewu Ji, Hayama Ryouhei, Mizuno Takahiro: Function of shoulder muscles of driver in vehicle steering maneuver
[4] Kmetz Barbara: Kéz művégtag fejlesztése, szakdolgozat, Miskolc, 2018

A TAKARÁS ÉS AZ ALAPÁRAMLÁS SEBESSÉGÉNEK HATÁSA EGY AXIÁLIS HŰTŐVENTILÁTOR ÜZEMÉRE

CFD ANALYSES OF EXTERNAL DISTURBANCES ON FLUID FLOW IN AND AROUND AN AXIAL COOLING FAN

Bolló Betti[*]*, Dorogi Dániel*[**]*, Fodor Béla*[***]
**egyetemi docens, **doktorandusz, ***tanszéki mérnök*
Miskolci Egyetem Energetikai és Vegyipari Gépészeti Intézet, Áramlás- és Hőtechnikai Gépek Tanszék

ABSTRACT
In this study the effect external disturbances on the pressure difference between the suction and pressure sides of the impeller of an axial fan, and aerodynamic forces acting on the blades are investigated by the means of CFD computations using the commercial software package, ANSYS Fluent. Two distinct external disturbances are applied, namely free stream velocity U (varied between 0 and 72 km/h) and covering plates arranged symmetrically and asymmetrically on the suction side of the fan.

1. BEVEZETÉS

Egy axiális kialakítású ventilátor numerikus modellezése nem egyszerű feladat, de a rendelkezésre álló kereskedelemben kapható szoftvercsomagok segítségével megoldható.

Az axiális hűtőventilátor működését számos kutató vizsgálta mind kísérleti, mind numerikus módszerekkel. E tanulmányok elsősorban a ventilátor által keltett zajra, a kimeneti áramlás egyenletességére és az elválasztó zónák elemzésére koncentrálnak. Park és Lee [1] hibrid megközelítést alkalmazva vizsgálták a szélessávú zaj forrását egy autóipari hűtőventilátornál. A ventilátor által generált zaj kiszámításához nagy számítási tartományra volt szükség, ezért a vizsgált geometriát egy 5,2 millió sejtből álló hibrid hálóval osztották fel. A turbulens áramlás számításához a k-ω SST turbulencia modellt alkalmaztak, a zaj meghatározásához Ffowcs Williams és Hawkings [2] általánosított akusztikai módszerét használták. A számítás gyorsítására Park és Lee [1] először időben állandó modellt alkalmaztak, és miután a reziduális hibák a konvergenciakritérium értékéhez csökkentek, akkor tértek át időtől függő számításra. A számítási eredményeiket összehasonlították a mérésnél kapott értékekkel, és jó egyezést találtak.

Lallier-Daniels et al. [3] a hűtőventilátor modul akusztikus tulajdonságait vizsgálták Lattice-Boltzmann módszer alkalmazásával. A CFD számítások eredményei jó egyezést mutatottak a ventilátor elé helyezett mikrofonnal kapott mérési eredményekkel. Ambdekar et al. [4] az ANSYS Fluent kereskedelmi szoftvercsomag segítségével a hűtőventilátor áramlási struktúráit elemezték. Megvizsgálták a ventilátoron belüli sebesség- és nyomásmezőket, a kimeneti áramlás egyenletességét és a zajterhelést.

Ye et al. [5] a lapátvégen elhelyezett horony aerodinamikai hatását vizsgálta ANSYS Fluent szoftverrel segítségével. Azt tapasztalták, hogy a horonyszélesség növelésével a ventilátor nyomásnövekménye, illetve tengelyteljesítménye csökkenő, ugyanakkor hatásfoka növekvő tendenciát mutat. Azonban megállapították azt is, hogy a barázdált lapátoknak zajkeltő hatása is van.

Jelen cikkben egy axiális hűtőventilátor körüli háromdimenziós áramlást vizsgálunk a kereskedelmi ANSYS Fluent CFD szoftvercsomag segítségével. Az axiális ventilátort először egyenletes áramlásba helyeztük (U=0 és 72 km/h), és a sebesség hatásait elemeztük. Ezután a ventilátor szívóoldala elé szimmetrikus és aszimmetrikus takarásokat helyeztünk és megvizsgáltuk különböző megfúvási sebességeknél (U=0, 36 és 72 km/h) a járókerék lapátjaira ható erőt Ezen aszimmetrikus erőhatások későbbi mechanikai elemzések kiinduló adatai leszek a járókerék rezgésanalízise számára.
A vizsgált elrendezés egy U sebességgel haladó jármű hűtőventilátorának modellezése amikor a ventilátor előtt, a beépítéséből adódóan az áramlást letakaró szerkezeti elemek vannak.

2. SZÁMÍTÁSI MÓDSZER

A számításokat az Ansys Fluent programcsomaggal végeztük el, ami a véges térfogatok módszerét alkalmazza. Egy áramlási csatornába helyezett axiális hűtőventilátor által létrehozott áramlást

modelleztük, amikor a csatornában egy alapáramlás is jelen van. Háromdimenziós, nem összenyomható, newtoni folyadékáramot egy. A szakirodalom alapján [4-6] a turbulens áramlás számítására a standard k-ε turbulencia modellt alkalmaztuk. A vizsgálatok során a ventilátorban és a gép körül lejátszódó folyamatokat időben állandósult módszer segítségével vizsgáltuk, ahol a járókerék forgó mozgását az MRF ('Moving Reference Frame') technika segítségével modelleztük. A járókerék fordulatszámát mindvégig n=2500 min^{-1} állandó értéken tartottuk.

A kutatás korábbi szakaszában [7], ahol a ventilátor körüli áramlási viszonyok vizsgálatával foglalkoztunk, problémák merültek fel. Egyrészt az elkészült geometrián a hálózás elemszáma 58 millió volt, ezért a számítás sokáig tartott és a fájlok kezelése is nehézségekbe ütközött. Másrészt a ventilátort rögzítő keretet nem vettük figyelembe. Ezért jelen tanulmányban új geometriát készítettünk, ahol már a ventilátor rögzítő keretét is megrajzoltuk. A vizsgált csatornaszakasz hosszát korábbi tapasztalataink alapján 1,5 m-re választottuk, magassága és szélessége pedig 0,8×1,2 m. A csatorna közepére helyeztük el az axiális ventilátort. A számítási tartomány vázlatos rajza az 1. ábrán látható.

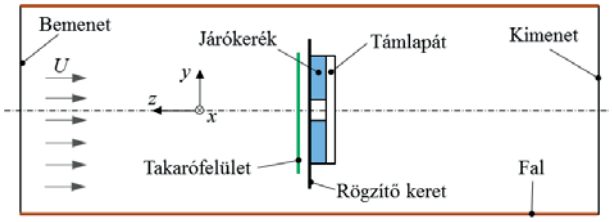

1. ábra A számítási tartomány kialakítása

A ventilátor szívóoldalára egy 13 felületből álló takarólemezt raktunk, amelyeket a számítások során aktív, illetve inaktív falfelületként definiáltunk. Az aktív felület azt jelenti, hogy fal, ellenkező esetben (inaktív) a levegő keresztüláramlik rajta (interior). A bemeneten az egyenletes áramlást a szabad áramlás U sebességének megadásával írjuk elő. A folyadéknyomáshoz és a kimeneti keresztmetszet sebességkomponenseihez Neumann típusú határfeltételeket használtunk.

A hálózás során a geometriai teret feldaraboltuk és a ventilátor előtti és utáni teret hexagonális elemekkel hálóztuk be, míg a járókerék, támlapát és a takarófelület közvetlen közelében sűrűbb elemszámú tetragonális hálót hoztunk létre. A 2. ábra a ventilátor közvetlen közelében lévő térrészben lévő hálókialakítást mutatja.

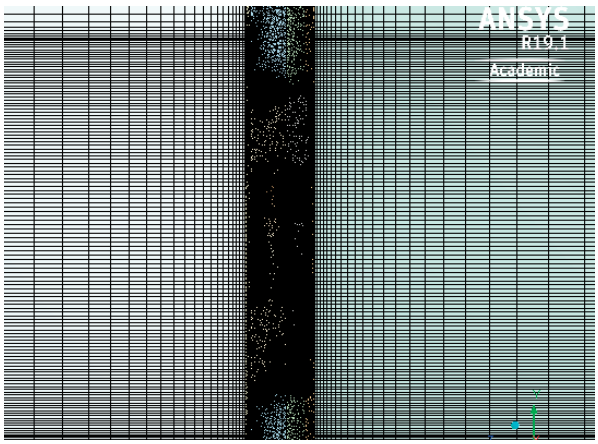

2. ábra A ventilátor közvetlen közelében lévő térrészen lévő háló

Kétféle hálókialakítást készítettünk, egy ritkább ~21 millió, és egy finomabb hálózást ~28 millió elemszámmal. Az előző tanulmányban [7] ismertetett mérési értékekkel összehasonlítva azt tapasztaltuk, hogy a ritkább háló esetén számított értékek is jó egyezést mutatnak a méréssel, ezért a további számításokat a ritka hálón végeztük el.

3. SZÁMÍTÁSI EREDMÉNYEK

A numerikus számításaink során az alapáramlás U sebességének és a ventilátor szívóoldalára helyezett takarófelület hatásainak vizsgálatával foglalkoztunk. A takarás mértékét az ε fajlagos takarási paraméterrel adjuk meg, ami azt jelenti, hogy takarás nélküli esetben ε=0. A járókerék fordulatszámát mindvégig n=2500 min^{-1} állandó értéken tartottuk, míg az alapáramlás sebességét U=0, 36 és 72 km/h értékekre választottuk. A számítások során a ventilátorlapátokra ható aerodinamikai erő három komponensét (F_x, F_y és F_z) és a járókerék nyomáseloszlását vizsgáltuk.

A 3. ábra az abszolút nyomáseloszlást mutatja a ventilátor szívóoldalán takarás nélküli (ε =0) esetben, illetve 50%-os takarásnál (ε=0,5) aszimmetrikus és szimmetrikus esetben három különböző megfúvási sebesség esetén. Az ábrára berajzoltuk a takarófelületek elhelyezkedését is. Mindhárom esetben megfigyelhető, hogy U növelésével a ventilátort terhelő nyomása növekvő tendenciát mutat. Aszimmetrikus takarás estén a takarófelület mögött elhelyezkedő lapátokon átlagosan kisebb nyomások vannak, mint a szabadon lévő lapátokon.

A 3. ábrán jól látható, hogy ventilátor szívóoldalán szimmetrikusan elhelyezett takarófelület aszimmetrikus terhelést okoz. A takarófelület a 2, 3, 5 és 6-ossal jelölt lapátok egy részét takarja ki.

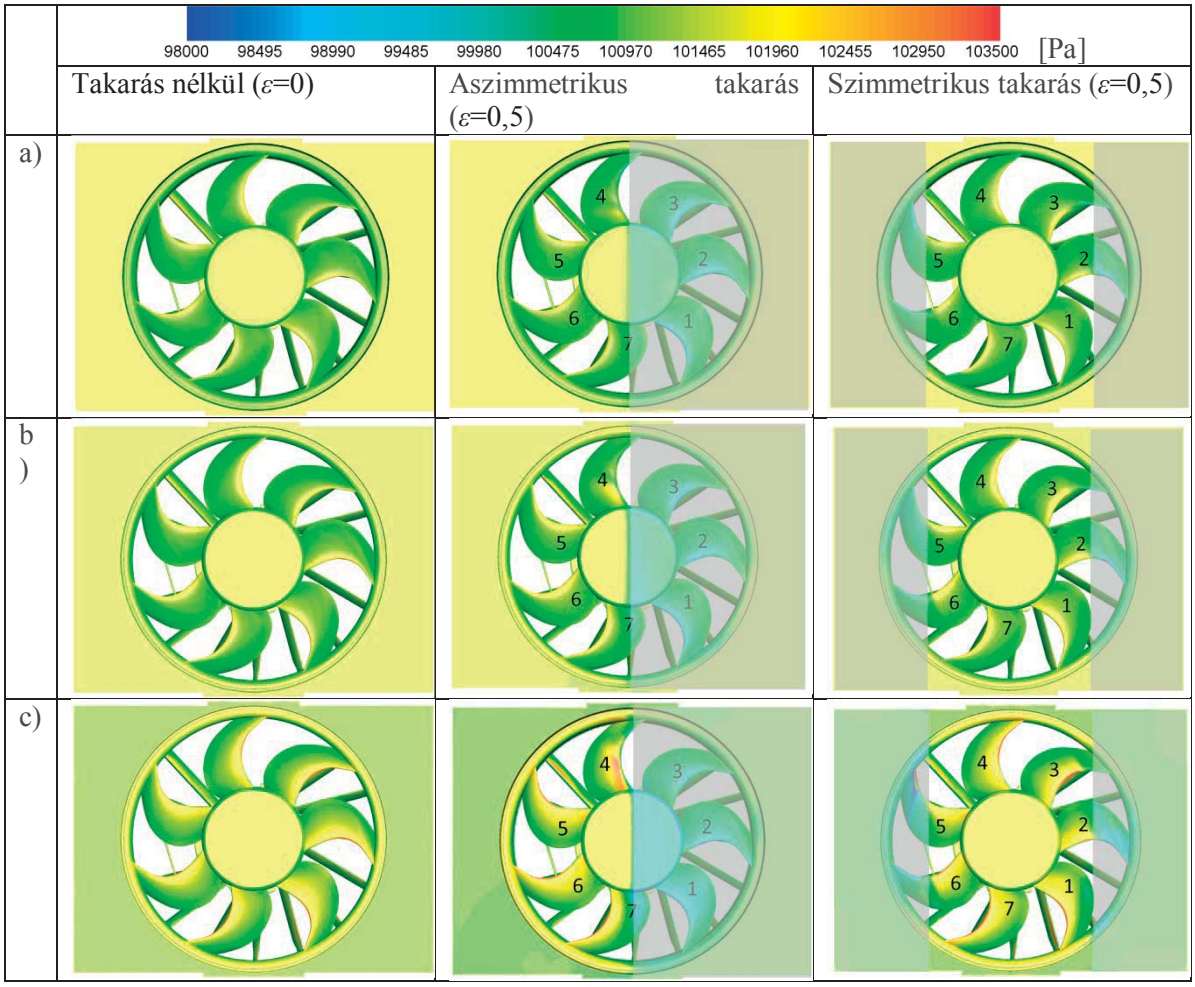

3. ábra A járókerék lapátokra ható Fz erőkomponens

A kitakart lapátrészeken a nyomóoldalon a nyomás lecsökken, míg a szívott oldalon megnő a nyomásérték, ez főként U=72 km/h sebességnél jelentős.

Megvizsgáltuk a ventilátor nyomó- (p_{ny}) és szívóoldalán (p_{sz}) lévő abszolút átlagnyomások különbségét ($\Delta p=p_{ny}-p_{sz}$). A ventilátor által létrehozott nyomásnövekményt a 4. ábra mutatja különböző sebességértékeknél. Azt tapasztaltuk, hogy U=0 km/h esetén a szívóoldalon lévő nyomás kisebb, mint a nyomóoldalon lévő abszolút nyomásérték, amely a ventilátor alapműködése esetén természetes.Az alapáramlás sebességét növelve, U=36 és 72 km/h esetén $p_{sz} > p_{ny}$ tapasztalható takarás nélküli esetben, tehát a ventilátor nyomásnövekménye negatív. Ez azt jelenti, hogy a ventilátor $U\geq$36km/h esetén ellenállástestként viselkedik. Ennek oka, hogy a nagy szélsebesség miatti levegőáram nem tud a ventilátoron áthaladni, a levegő feltorlódik a ventilátor előtt. Ez esetben a ventilátort a szél is hajtja, „szélturbina” üzemhez hasonló állapot alakul ki. Ez a jelenség takarás esetén csak U=72 km/h értéknél figyelhető meg.

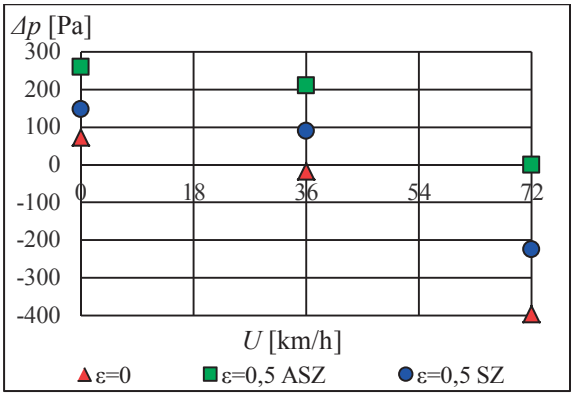

4. ábra A ventilátor Δp nyomásnövekménye takarás nélkül és fél takarással

A 4. ábrán az is megfigyelhető, hogy ε növelésével a nyomásnövekmény növekvő tendenciát mutat mindhárom U sebességérték esetén. Az ábrából az is látszik, hogy az aszimmetrikus takarás sokkal nagyobb nyomásnövekményt okoz, mint a szimmetrikus takarás.

A számításaink alapján megállapítottuk, hogy a ventilátorra ható aerodinamikai erő növekszik az alapáramlás sebességének növekedésével.

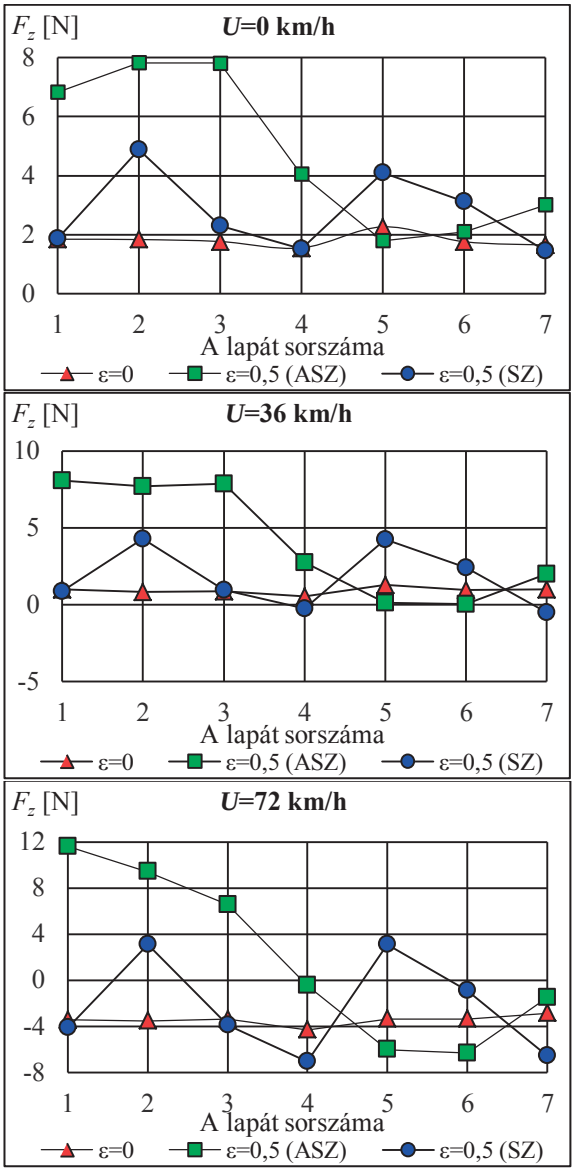

5. ábra A járókerék lapátokra ható F_z erőkomponens különböző megfúvási sebességeknél és takarásoknál

A lapátokra ható erő vizsgálatánál azt tapasztaltuk, hogy az F_x és az F_y komponensek lehetnek pozitív és negatív értékűek is, azaz az erő a járókerék forgásirányával vagy azzal ellentétesen hat. Jelentős eltérés ezekben a komponensekben U=72 km/h esetén van, de nagyságát tekintve 2-3-szorosára növekszik a letakart lapátokon a takarás nélküli esethez képest. Az axiális irányú erőnek (F_z) van a legjelentősebb hatása, ezért jelen cikkben ezt részletezzük. Az 5. ábra az F_z erőkomponens értékét mutatja takarás nélküli, aszimmetrikus és szimmetrikus féltakarásnál különböző áramlási sebességeknél. Az F_z előjele az alapáramlási sebesség növelésével változáson megy keresztül: U=0 és 35 km/h értékeknél $F_z > 0$ takarás nélküli és aszimmetrikus esetben, tehát az axiális erő a főáramlás irányával megegyező irányú. Ezzel szemben U=70 km/h-nál az F_z a főáram irányával ellentétes irányba mutat takarás nélküli esetben, takarásnál viszont ismét pozitív értékű lesz. Jelentős hatása az aszimmetrikus takarásnál (1., 2. és 3. lapátnál) tapasztalható, itt az F_z erőkomponens értéke 3-4-szeresére nő a takarás nélküli esethez képest U=0 km/h esetén, míg U=36 km/h sebességnél ez elérheti a nyolcszorosát is. A sebességet tovább növelve az F_z abszolút értéke csak 2-3-szorosára növekszik meg. Szimmetrikus takarásnál (2, 3, 5 és 6 lapát) is megnő F_z erőkomponens abszolút értéke, de nem olyan jelentősen, mint aszimmetrikus takarásnál. Ennek valószínű oka az, hogy a lapátoknak csak egy részét takarja ki, nem az egészet, mint aszimmetrikus féltakarás esetén.

4. ÖSSZEFOGLALÁS

A vizsgálataink kimutatták, hogy amennyiben egy axiális ventilátort alapáramlásba helyezünk, akkor e szélsebességnek a ventilátor működésére és a lapátjaira ható erőre, az előállított nyomáskülönbségre jelentős hatása van. További fontos eredmény, hogy amennyiben a szabad áramlás útját takaróelemekkel megváltoztatjuk, akkor a lapátozást érzékelhető aszimmetrikus terhelés éri, amely hatással van a ventilátor rezgésjellemzőire is. ACFD szimulációból kapott eredmények így fontos kiinduló adatai lehetnek részletes numerikus mechanikai elemzéseknek.

5. KÖSZÖNETNYILVÁNÍTÁS

A kutatás az Európai Unió és a Magyar Kormány támogatásával, az Európai Regionális Fejlesztési Alap társfinanszírozásával valósult meg az „E-mobility Miskolcról: Hűtővíz keringető szivattyú és motorhűtő ventilátor továbbfejlesztése az elektromos járművekben elvárt magasabb minőségi követelmények figyelembevételével” című GINOP-2.2.1-15-2017-00090 azonosítószámú projekt keretében.

6. IRODALOM

[1] PARK M.-J., LEE D.-J.: Sources of broadband noise of an automotive cooling fan. *Applied Acoustics* Vol. 118 (2017), pp. 66–75.

[2] FFOWCS WILLIAMS J.E., HAWKINGS D.L.: Sound generation by turbulence and surfaces in arbitrary motion. *Philosophical Transactions of the Royal Society of London.*

Series A, Mathematical and Physical Sciences Vol. 264 (1969), pp. 321–342.

[3] LALLIER-DANIELS D., PIELLARD M., COUTTY B., MOREAU S.: Aeroacoustic study of an axial engine cooling module using lattice-Boltzmann simulations and the Ffowcs Williams and Hawkings' analogy. *European Journal of Mechanics B/Fluids* Vol. 61 (2017), pp. 244–254.

[4] AMBDEKAR T.C., BARVE, S.B., KOTHAVALE B.S., DHOKANE N.T.: Design and analysis of engine cooling fan. *International Journal of Current Engineering and Technology* Vol. 3 (2014), pp. 114-118.

[5] YE X., LI P., LI C., DING X.: Numerical investigation of blade tip grooving effect on performance and dynamics of an axial flow fan. *Energy* Vol. 82 (2015), pp. 556–569.

[6] ZHANG L., JIN Y., JIN Y.: Effect of Tip Flange on Tip Leakage Flow of Small Axial Flow Fans. *Journal of Thermal Science* Vol. 23 (2014), pp. 45–52.

[7] DOROGI D., BOLLÓ B., SZABÓ SZ.: Effects of external disturbances on the performance of an axial cooling fan. *Review of Faculty of Engineering Analecta Technica Szegedinensia*, Vol. 13 (2019), pp. 48-55.

PNEUMATIKUS HENGEREK VIZUÁLIS TERMIKUS SZIMULÁCIÓJA LABVIEW HASZNÁLATÁVAL

VISUAL SIMULATION OF THERMODYNAMIC EFFICIENCY OF PNEUMATIC CYLINDER USING LABVIEW

Arturs Rugajs, Janis Rudzitis, Maris Gailis, Juris Kreicbergs
**Riga Technical University; **Latvia University of Life Sciences and Technologies*

ABSTRACT
Performance of pneumatically driven vehicle depends on multiple factors, and efficiency of energy to work conversion in the pneumatic cylinder is one of them. This paper describes thermodynamic model of pneumatic cylinder. Equations that define cylinder's geometric properties, gas supply control parameters and energy conversion are presented. *MATLAB* scripts are included. *LabVIEW* user interface is presented, which allows altering of geometric and control parameters of the pneumatic cylinder in real time. The results of the simulation can be presented graphically and numerically.

1. INTRODUCTION

Linear pneumatic actuators are significant part of industrial machinery, that provide fast acting and relatively low cost solutions to automation tasks [1]. Improvement of pneumatic system efficiency is a topical research subject. Selection of the right dimensions of pneumatic cylinders and control valves for the given task are emphasized and discussed in previous work [2–4].

Loses in the control and supply circuit are important, especially in the large industrial installations. Efficiency of the pneumatic control valve and its improvement were presented in the work of Estonian researchers [5].

In a typical application of pneumatic cylinder, at the end of the expansion cycle gas is released to the surroundings. Energy recovery from the released gas is explored by various researchers. Luo *et al*. propose application of rotating compressors to convert gas energy to electrical energy. They experimentally achieved energy efficacy improvement up to 18.1% using scroll-type compressor and DC generator [6].

Letai *et al*. presented design of pneumatic motor that uses four sequentially working paired cylinders, where at the end of expansion cycle under constant gas supply, smaller cylinder transfers gas to the larger cylinder where the gas expands. The energy efficiency improvement was not fully described in the paper [7].

Industrial application of the pneumatic systems has been around for a significant time and some design principles and traditional assumptions has been settled in [1,3]. *Emerson Electric Co* and its division *AVENTICS Hungary Kft* has been organising Pneumatic Vehicle competition in Eger, Hungary since 2008, which promotes out-of-the-box thinking on pneumatic actuator and control system application and design [8]. Unusual area of application demands for lightweight, compact and highly effective solutions. Use of dry, clean nitrogen gas allows control strategies that include high ratio of gas expansion, as the risk of water ice accumulation in the pneumatic system is reduced, comparing to use of compressed air.

Simon presented results of theoretical and experimental work, describing performance and efficiency of pneumatically driven vehicle. The level of detail of presented mathematical model is limited [9,10]. Szakacs developed and presented computer model of entire pneumatic system of pneumatic vehicle. Although the model appears to be highly sophisticated, governing equations, the results and wider conclusions were not included [11].

There is a lack of practical models that explain impact of geometric and control parameters on efficiency of pneumatic cylinder. Mathematical model, computer code and user interface of thermodynamically based model of pneumatic double acting cylinder has been developed. Computer codes for practical implementation using relatively popular commercial software *MATLAB* are presented.

2. MATERIALS AND METHODS

Gas energy conversion to mechanical work in double action pneumatic cylinder is modelled, excluding turbulence effects, friction and heat exchange. Pneumatic diagram of the proposed system is shown in Fig. 1.

Only process in the cylinder is modelled. Assumption is made that process in the cylinder is quasistatic, and calculations are performed by discrete steps. Theoretical pressure – volume diagram of the working cycle of the pneumatic cylinder is presented in Fig. 2. According to the model, gas is supplied at constant pressure up to the specific point in the piston travel, which is marked with index *3*. The gas supply is cut at the specific point to ensure that desired pressure is reached at the end of expansion, at the point marked as index *4*.

where *sgc* – specific gas consumption, g·kJ^{-1}.

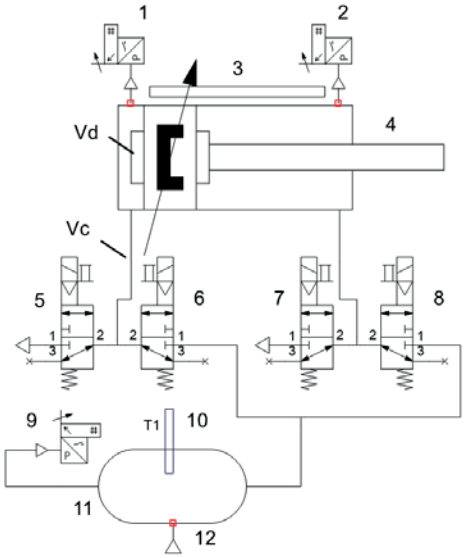

Figure 1. Diagram of the simulated pneumatic circuit

1, 2, 9 – pressure sensors; 3 – piston position sensor; 4 – pneumatic cylinder; 5, 7 – exhaust valves; 6, 8 – inlet valves; 10 – temperature sensor; 11 – gas buffer; 12 – gas inlet, V_d – cylinder displacement volume; V_c – volume of supply pipe, control valve and cylinder cushioning volume

Energy conversion efficiency is the ratio of work done to energy supplied:

$$ece = \frac{W_w - W_e}{E} = \frac{W_w - W_e}{U_{1\_2} + H_{2\_3}} \qquad (1)$$

where W_w – gas work on the piston, J; W_e – piston work on the gas at expulsion side, J; E – energy, J; U – internal energy, J; H – enthalpy, J.

Specific gas consumption is the ratio of gas mass supplied in the cycle to work done:

$$sgc = \frac{m_{1\_2} + m_{2\_3}}{W_w - W_e} \qquad (2)$$

Indexes (for instance U_{1_2}) in this and further equations correspond to the indexes presented in Fig. 2.

Supplied energy depends on type of gas, amount of gas and its temperature. Internal energy of the gas stored in the supply pipe and control valve (in the volume V_c) is calculated [12]:

$$U = c_v \cdot m \cdot T \qquad (3)$$

where c_v – specific heat capacity at constant volume, J kg^{-1} K^{-1}; m – mass of gas, kg; T – temperature, K.

When gas is supplied in constant pressure process, additional work on surroundings is performed, which is accounted in the enthalpy. Enthalpy of the gas in the displacement volume of pneumatic cylinder working side [12]:

$$H = c_p \cdot m \cdot T \qquad (4)$$

where c_p – specific heat capacity at constant pressure, J kg^{-1} K^{-1}.

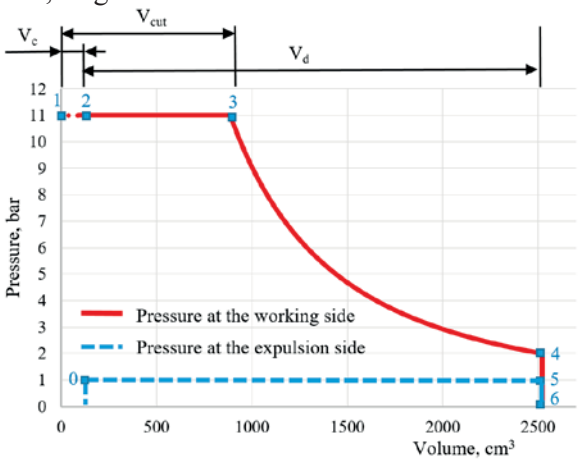

Figure 2. Pressure – volume diagram of the simulated pneumatic circuit. The numbers at the marked points represent index in the equations

V_d – cylinder displacement volume; V_c – volume of supply pipe, control valve and cylinder cushioning volume; V_{cut} – volume at which the gas supply is stopped

Mass of the gas in the supply pipe and control valve, and separately in cylinder up to the point where the gas supply is cut (index *3* in Fig. 2), is calculated according to ideal gas law [12]:

$$m = \frac{P \cdot V}{R \cdot T} \quad (5)$$

where P – pressure, Pa; V – volume, m^3; R – specific gas constant, J kg^{-1} K^{-1}.

Area of the piston at the top side is calculated[1]:

$$A_w = \frac{\pi \cdot B^2}{4} \quad (6)$$

where B – cylinder bore, m.

Area of the piston at the rod side is calculated[1]:

$$A_e = \frac{\pi \cdot (B^2 - b^2)}{4} \quad (7)$$

where b – rod diameter, m.

Cylinder volume at any piston position is calculated [13]:

$$V_i = V_c + A \cdot s_i \quad (8)$$

where i – calculation step; V_c – total volume of supply pipe, control valve and cylinder cushioning volume, m^3; A – area of piston, m^2; s – instantaneous piston position, m.

Volume V_{cut}, at which the gas supply is stopped to ensure desired gas pressure at the end of expansion on the working side, is calculated:

$$V_{cut} = \left(\frac{P_4 (V_c + V_d)^\gamma}{P_1} \right)^{\frac{1}{\gamma}} \quad (9)$$

where γ – ratio of heat capacities, ($\gamma = c_p/c_v$).

Ratio of heat capacities for nitrogen (N_2) at the temperature range, that is typical for pneumatic cylinder, is approximately γ = 1.4. The authors analysed the experimentally obtained data, and found that due to heat exchange between the gas and cylinder walls, apparent value is approximately γ = 1.16.

Changes in the pressure during gas expansion are calculated:

$$dP_{i+1} = \frac{\gamma \cdot P_i \cdot dV_{i+1}}{V_i} \quad (10)$$

where dV – change in cylinder volume, m^3.

Changes in cylinder volume dV are calculated by simple numeric differentiation. Pressure at the working side of the cylinder during expansion is then calculated by numerical integration:

$$P_w = P_3 + \int_{P3}^{P4} dP_i \quad . \quad (11)$$

Pressure at the beginning on the expulsion side is close to the final pressure of the working side from the previous cycle, as the working and expulsion sides switch between cycles. Then expulsion side pressure reduces and eventually reaches value that is close to surrounding pressure. The pressure changes can be modelled using relations of pressure and volume in the isentropic process [14]:

$$P_{e\,i+1} = \frac{P_{e\,i} \cdot V_i^k}{V_{i+1}^k} \quad (12)$$

where k – constant; P_e – pressure at the expulsion side, Pa.

To imitate conditions of gas expansion at the expulsion side, value of constant can be set at approximately k=0.2...0.5 Limits to the pressure drop should be included in the model code, to keep expulsion side pressure above ambient pressure.

Work on the both sides of the piston is equal to the area under pressure – volume curve. It is calculated using following equation [13]:

$$W = \int_{V2}^{V4} P \cdot dV \quad (13)$$

The work on both piston sides is calculated using trapezoidal numerical integration and subtracted to find total work.

Instantaneous force on the piston rod is calculated using following equation:

$$F_i = A_w \cdot P_{w\,i} - A_e \cdot P_{e\,i} \quad (14)$$

where P_w – pressure at the working side, Pa.

The equations are implemented in the *MATLAB* code. The code can also be used in the open-source software environment, such as *Octave*. User interface is realised in *LabVIEW*, deploying *MATLAB* code in the *MathScript* module. Two instances of the simulation run continuously. For the separation of the workspace each instance of the main script and its functions are named distinctly. In that way two design and control scenarios can be compared simultaneously.

3. RESULTS

The user interface of computer simulation is shown in Figs 3 and 4. Several parameters are available for the user to control.

Geometrical parameters:

- Piston stroke;
- Cylinder bore;
- Length of supply pipe.

Gas parameters:

- Initial temperature;
- Initial pressure;

- Pressure at the end of expansion.
- Pressure difference at the end of expansion and beginning of expulsion;
- Isentropic constant at the expulsion side.

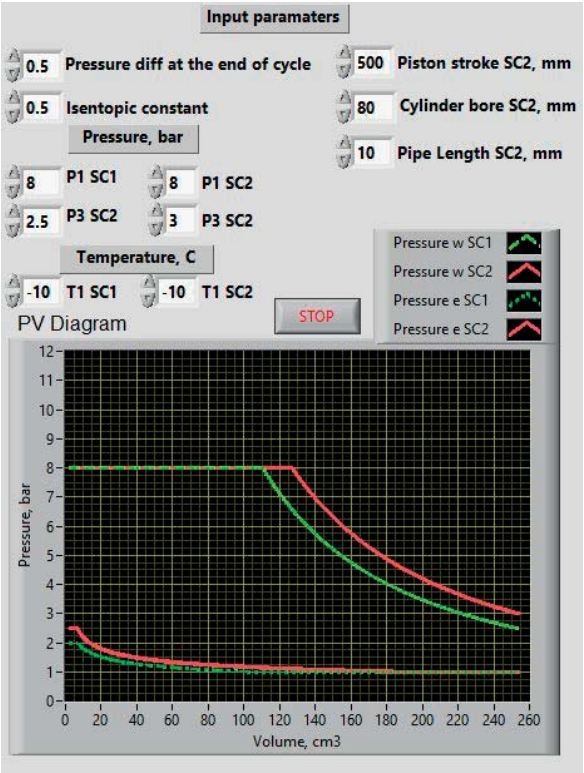

Figure 3. User interface of the model for entering of input parameters and observing pressure – volume diagram

Performance parameters are then calculated for two scenarios and displayed to the user:

- Pressure – volume diagram;
- Force – volume diagram;
- Specific gas consumption (*sgc*);
- Energy conversion efficiency (*ece*);
- Relative difference in *sgc* of two scenarios.

MATLAB code of the model is presented in the appendix of this paper. The analysis of the impact of various geometric and control parameters on the efficiency of pneumatic cylinder will be presented and discussed in the future work of the authors.

4. CONCLUSIONS

Developed code can be used in *MATLAB* or compatible open-source software environment *Octave*. User interface and continuous execution of two instances of the simulation are realised in *LabVIEW*. Effect of pneumatic cylinder bore, piston stroke and gas supply pipe volume on its work, force and energy conversion efficiency can be evaluated. Further, impact of gas temperature and cycle pressure parameters on pneumatic cylinder performance can be investigated. In the future development of this model, heat exchange, turbulence effects and also dynamics of moving parts should be accounted.

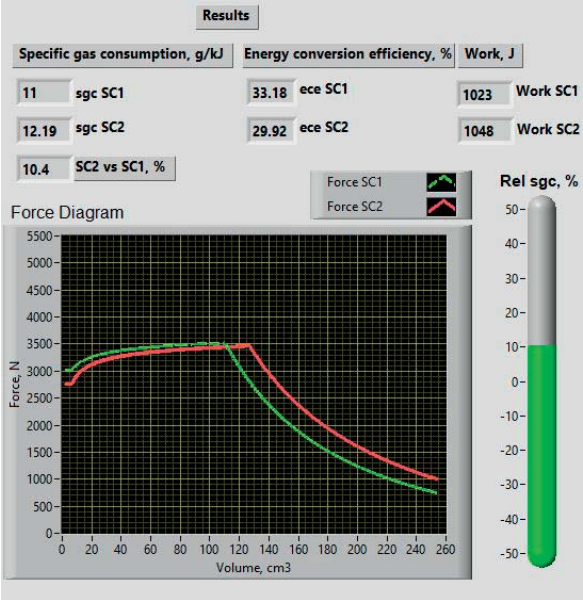

Figure 4. User interface of the model. Force – volume diagram and calculated efficiency parameters are shown

5. REFERENCES

[1] HARRIS, P., O'DONNELL, G.E., WHELAN, T.: Leveraging Technology for a Sustainable World: Energy Efficiency in Pneumatic Production Systems: State of the Art and Future Directions, Springer 2012, ISBN 978-3-642-29069-5

[2] DOLL, M., NEUMANN, R., SAWODNY, O.: Dimensioning of pneumatic cylinders for motion tasks, *Int. J. Fluid Power*, Vol 16, No 1, (2015) pp. 11–24, doi:10.1080/14399776.2015.1012437.

[3] CAMBELL, S., *Guidelines for Selecting Pneumatic Cylinders*, https://www.machinedesign.com/mechanical-motion-systems/pneumatics/article/21831605/guidelines-for-selecting-pneumatic-cylinders, 2018.

[4] RAKOVA, E., WEBER, J.: Process Simulation of Energy Behaviour of Pneumatic Drives, *Procedia Eng.* Vol 106, (2015), pp. 149–157, doi:10.1016/j.proeng.2015.06.018.

[5] MADISSOO, M., TÜRK, K.: Optimized Valve System for a Pneumatic Motor, *Proceedings of 2nd Agria Conference on Innovative Pneumatic Vehicles – ACIPV 2018*, Eger, 2018.
[6] LUO, X., WANG, J., SUN, H., DERBY, J.W., MANGAN, S.J.: Study of a New Strategy for Pneumatic Actuator System Energy Efficiency Improvement via the Scroll Expander Technology, *IEEE/ASME Trans. Mechatronics*, Vol. 18, No 5, (2013), pp. 1508–1518. doi:10.1109/TMECH.2012.2203920.
[7] LÉTAI, L.S., POP, O., BUZGUTA, P., AND CANALAS, F.:PLC controlled racing vehicle with pneumatic engine, *Proceedings of 1st Agria Conference on Innovative Pneumatic Vehicles – ACIPV 2017*, Eger, 2017
[8] Aventics Hungary Kft: *Pneumobil 2020 Competition rules*, Eger, 2019.
[9] SIMON, M.: Pneumatic Vehicle, Research and Design, *Procedia Eng.*, Vol. 181, (2017), pp. 200–205, doi:10.1016/j.proeng.2017.02.370.
[10] SIMON, M.: Alternative Energy Driven Pneumatic Vehicle, *Procedia Eng.,* Vol. 181, (2017), pp. 725–730, doi:10.1016/j.proeng.2017.02.455.
[11] SZAKACS, T.: Modelling and Validation of a Pneumobil, *3th Agria Conference on Innovative Pneumatic Vehicles*, Eger, 2019.
[12] SERWAY, R. A., KIRKPATRICK, L.D.: *Physics for Scientists and Engineers with Modern Physics*, 9th ed., Brooks Cole 2014, ISBN 978-1337553292.
[13] HEYWOOD, J. B.: *Internal Combustion Engine Fundamentals*, McGrawHill, 2018, ISBN 978-1-260-11610-6.
[14] KADAMBI, V.: *An Introduction to Energy Conversion*, Volume 2,Wiley Eastern Private Limited, 1974, ISBN 0-470-50926-0.

APPENDIX

MATALB script consists of main part and three user-defined functions.

Main script

```
clear
T1=20+273.15; %Initial temperature, K
Pr=0.5; %Pressure difference at the end and beginning of the cycle
k=0.20; % Isentropic constant
P1=11; %Initial pressure, bar
P3=2; % Final pressure, bar
s=0.5; %Stroke m
B=0.08; %Bore, m
Lp=0.1; %Length of pipe, m
%calling external function to perform the calculation
[ece, Volume, Pressure_w, Work, sgc, Pressure_e, Force]= energy (T1, Pr, P1, P3, B, s, Lp, k);
```

Function ‘energy’

```
function [ece, VFi, Pressure_w, Work, Vd, sgc, Pressure_e, Force]=energy ( T1,Pr, P1, P3, B, s, Lp, k)
P1kPa=P1*100; %kPa
P1Pa=P1kPa*1000; %Pa
P3Pa=P3*10^5; %Pa
MolarMass=28.01348;%g/mol
Ru=8.314; %J/molK
Ri=Ru/(MolarMass/1000); %J/kgK
CalcSteps=1000;
Dp=16/1000; %diameter of supply pipe, m
%calling function to calculate volume
[ VFi,dVFi,Vd, Vc, A] = volume ( B, s, CalcSteps , Lp, Dp);
Smm=s*1000;
Smm_vect=linspace(0,Smm,CalcSteps);
cv=745.6739; %J/kgK
cp=cv+Ri; %J/kgK
Gamma=cp/cv; Vmax=Vd+Vc;
Vcut=((P3Pa*Vmax^Gamma)/P1Pa)^(1/Gamma);
CutOff_mm=round((((Vcut-Vc)*4)/(pi*B^2))*1000);
CutOff_CalcStep=min(find(Smm_vect>
CutOff_mm));%, 'first');
% Reallocation of vector size
P(1:CalcSteps)=P1kPa.*1000;
Pbar(1:CalcSteps)=P1kPa.*10^(-2);
Po1(1:CalcSteps)=Pr;
Po(1:CalcSteps)=Pr;
VFi(1:CalcSteps)=VFi;
dp(1:CalcSteps)= P1kPa*10^3;
Scut=CutOff_CalcStep;
mVc=(P1kPa*1000*Vc)/(Ri*T1); %kg
mVSupply=(P1kPa*1000*(Vcut-Vc))/(Ri*T1); %kg
UVc=mVc*T1*cv; %J
H=mVSupply*T1*cp; %J
USupply=UVc+H; %J
for ii=1:20
    Po1(ii)=P3-Pr;
    Po(ii)=Po1(ii);
end
for ii=20:(CalcSteps)
nn=ii-1;
Po1(ii)=Po(nn)*VFi(nn)^(k)/VFi(ii)^k;
Po(ii)=Po1(nn);
 if Po(ii)<1
    Po(ii)=1;
end
end
for ii=Scut:(CalcSteps-1)
Smm(ii+1)=Smm_vect(ii+1);
dp(ii+1)=((Gamma/VFi(ii))*P(ii)*dVFi(ii+1))*(-1);
P(ii+1)=P(ii)+dp(ii+1);
Pbar(ii+1)=P(ii)*10^(-5);
end
Pressure_e=Pbar;
Pressure_o=Po;
%calling function to calculate work
[Work_w ] = work (Pressure_w, dVFi);
[Work_e ] = work (Pressure_e, dVFi);
ece=(( Work_w - Work_e)/USupply)*100; %%
sgc=((mVSupply+mVc)*10^6)/( Work_w - Work_e);
% g/kJ
Work= Work_w - Work_e; %J
Force=A*Pressure*10^5-A*Pressure_o*10^5; %N
```

Function ‘volume’

```
function [ VFi,dVFi,Vd, Vc, A] = volume ( B, s, s_mm, Lp, Dp )
A=pi*(B/2)^2;
Vpipe=((pi*Dp^2)/4)*Lp; % Volume of supply pipe
Vc=Vpipe;
Vd=((pi*B^2)/4)*s; % Volume of displacement
S_travel=linspace(0.00,s,s_mm);
VFi=Vc+Ak*S_travel;
VFim=VFi([2:(s_mm) 1:1]);
dVFi=VFim - VFi;
```

Function ‘work’

```
function [W] = work ( Pressure, dVFi,)
P_Pa=Pressure*10^5;
PdV_Pa=P_Pa.*dVFi;
W=(trapz(PdV_Pa)); %work, J
```

JÁRMŰ HŰTŐVENTILLÁTORÁT TERHELŐ VÍZPERMET MENNYISÉGÉNEK MEGHATÁROZÁSA KÜLÖNBÖZŐ ERŐSSÉGŰ ESŐK ÉS JÁRMŰ HALADÁSI SEBESSÉGEK ESETÉN

DETERMINING THE QUANTITY OF WATER SPRAY ON THE VEHICLE COOLING FAN FOR DIFFERENT RAIN STRENGTHS AND VEHICLE DRIVING SPEEDS

Szabó Szilárd egyetemi tanár, Miskolci Egyetem, Energetikai és Vegyiperi gépészeti Intézet, Áramlás- és Hőtechnikai Gépek Intézeti Tanszék

ABSTRACT

Engine cooling fans in vehicles are exposed to various effects, including the effects of precipitation drops, the effects of wind, and the effects of ambient temperature. The impact of these factors on fan operation must be known to ensure that the cooling system can perform its duty under any circumstances. In the present study, the amount of precipitation hitting the cooling fan of a vehicle running in rainy weather is to be determined. This is necessary to clarify the boundary conditions for later laboratory and numerical investigations. Based on the literature on precipitation drops and on meteorological data, the amount of water spray hitting the cooling fan is determined in case of different precipitation drop sizes and different operating speeds.

1. BEVEZETÉS

A járművekben, tipikusan a jármű orr-részében a motortér elején a hűtőrács mögött helyezik el a motorhűtő berendezés ventilátorát. A cél az, hogy a menetszél kényszerkonvekciós folyamaton keresztül minél jelentősebb hűtőhatást fejtsen ki a hűtő radiátorban áramló hűtőközegre. A radiátor a ventilátor előtt, vagy a ventilátor után helyezkedik el. Ezen túl további számtalan variáció lehetséges a gépjármű homlokfala, hűtőmaszkja kialakításának tekintetében. Ezért alapesetként azt vizsgáljuk, hogy a ventilátor járókerekére akadálymentesen érkezik az esővel terhelt menetszél. Ez a menetszélből adódó hatás a különböző beépítés esetén adódó valós hatás felső becslésének tekinthető. Jelen esetben a menetszél víztartalmának meghatározásával foglalkozunk. A kapott mennyiségek például numerikus szimuláció esetén peremfeltételként alkalmazhatók, amikor a szimuláció már a konkrét beépítési helyzetet is figyelembe veszi.

2. JELÖLÉSEK

2.1. Jelölések

d_d esőcsepp átmérője,
D_f ventilátor járókerék átmérője,
v_d esőcsepp esési sebessége,
ρ_d esőcsepp sűrűsége,
T_a a levegő hőmérséklete,
υ_a a levegő kinematikai viszkozitása T_a hőmérsékleten,
ρ_a a levegő sűrűsége T_a hőmérsékleten,
Re Reynolds-szám,
C ellenállástényező,
H esési magasság,
g nehézségi gyorsulás,
Q menetszél térfogatárama,
v_c a jármű haladási sebessége,
t idő,
$X\left[\frac{\text{mm}}{\text{h}}\right]$ az eső fajlagos mennyisége,
Q_r a ventilátort érő esőpermet térfogatárama,
$\dot{m}_r$ a ventilátort érő esőpermet tömegárama.

2.2. Indexek

a levegő (air),
c jármű (car),
d esőcsepp (drop),
f ventilátor (fan),
r eső (rain).

3. ESŐ TÍPUSAI ÉS ERŐSSÉGE

A folyadék halmazállapotú csapadék mennyisége jelentős mértékben változik időben és térben. Ezen belül a folyadékcseppek mérete is jelentős eltérést mutathat. Vizsgálatainkat $T_a = 20°\text{C}$ hőfokú nyugvó levegőben ($\rho_a = 1{,}205\ \text{kg/m}^3$, $\upsilon_a = 15{,}273 \cdot 10^{-6}\ \text{m}^2/\text{s}$) végezzük, a gravitáció hatására függőlegesen hulló eső esetén. A szakirodalom általában

4 különböző erősségű esőt különböztet meg. Ezek határait, a bennük hulló esőcseppek esési sebességét és a cseppméreteket igyekeztek meghatározni. Az 1. táblázatban néhány fellelhető adatsort foglaltunk össze. A táblázatban szerepelnek az időegységre jutó eső mennyiségei (X), a cseppméretek (d_d) és a cseppek esési sebességei (v_d). A táblázat utolsó 3 oszlopában pedig ezek alapján jellemző közepes értékeket tüntettünk fel. A továbbiakban ezekkel fogunk számolni. Fontos megjegyezni, hogy a közepes értékek közelítésnek tekinthetők, hisz például egy adott eső esetén a cseppméretek nagysága és a különböző méretű cseppek aránya is igen különböző lehet.

1. táblázat Eső típusok és jellemzőik

[1]	[2]	[3]			[4]		**közepes**		
X	X	X	d_d	v_d	X	d_d	X	d_d	v_d
$\left[\frac{\text{mm}}{\text{h}}\right]$	$\left[\frac{\text{mm}}{\text{h}}\right]$	$\left[\frac{\text{mm}}{\text{h}}\right]$	[mm]	[m/s]	$\left[\frac{\text{mm}}{\text{h}}\right]$	[mm]	$\left[\frac{\text{mm}}{\text{h}}\right]$	[mm]	[m/s]
0÷2	0÷2,5	1,01	0,5÷2	2,06÷6,49	-	<0,5	**1**	**1**	**3,93**
2÷10	2,6÷7,6	6,35	1,0÷2,6	4,03÷7,57	1-4	>0,5	**6,35**	**1,8**	**6,10**
10÷50	7,6-	25,4	1,2÷4,0	4,64÷8,83	1-100	max 6÷8	**25,4**	**2,6**	**7,56**
>50							**80**	**5**	**9,11**

4. AZ ESŐCSEPPEK ESÉSI SEBESSÉGEINEK MEGHATÁROZÁSA

Az esőcseppek esési sebességeinek számítással való meghatározásához az irodalomban különböző méretű és sűrűségű gömbszemcsékre vonatkozó összefüggéseket alkalmazzuk. A számos közelítő eljárás közül mi a 2. táblázatban szereplőkkel számoltunk. Ezek mindegyike a cseppre ható erőhatások alapján levezetett (1) összefüggést alkalmazza, amely:

$$v_d = \sqrt{\frac{4}{3} \cdot \left(\frac{\rho_d}{\rho_a} - 1\right) \cdot \frac{d_d \cdot g}{C}}. \tag{1}$$

A különbség az eljárások között a C ellenállástényező és a

$$Re = \frac{v_d \cdot d_d}{v_a} \tag{2}$$

kifejezés szerinti Reynolds-szám közötti összefüggésekben van [7,8]. E kapcsolatokat öt különböző közelítés alapján a 2. táblázatban foglaljuk össze [8]. A táblázatban feltüntettük a kifejezések érvényességi tartományát is.

Az (1) összefüggés és a 2. táblázat implicit összefüggései alapján meghatároztuk az esési sebességeket $d_d = 0{,}1 \div 1{,}87\ \text{mm}$ cseppátmérő mellett. A 2. táblázatban szereplő összefüggések ugyanis

2. táblázat Az ellenállástényezők összefüggései különböző szerzők szerint [8]

Szerző	ellenállástényező	érvényességi tartomány
Allen	$C \cong \frac{10}{\sqrt{Re}}$	$30 < Re < 300$
Oseen	$C = \frac{24}{Re} \cdot \left(1 + \frac{3}{16} \cdot Re\right)$	$0{,}1 < Re < 10$
Dellavalle	$C = 0{,}4 + \frac{40}{Re}$	$2 < Re < 500$
Schiller-Neumann	$C = \frac{24}{Re} \cdot (1 + 0{,}15 \cdot Re^{0{,}678})$	$0{,}5 < Re < 800$
Langmuir-Blodgett	$C = \frac{24}{Re} \cdot (1 + 0{,}197 \cdot Re^{0{,}63} + 0{,}0026 \cdot Re^{1{,}38})$	$1 < Re < 100$

a Reynolds szám határ miatt nem érvényesek nagyobb méretű részecske esési sebességének számítására. A 3. táblázatban a számítások eredményeit foglaltuk össze. A táblázat utolsó oszlopában a különböző közelítésekkel kapott értékek átlagait tüntettük fel.

A szakirodalomban többen foglalkoztak az esőcseppek esési sebességének kísérleti úton való meghatározásával [5, 6]. Ezek közül alapműnek számít Gunn és Kinzer [6] tanulmánya. Ők $d_d = 0{,}1 \div 5{,}8\ \text{mm}$ cseppátmérő tartományon végeztek méréseket. Eredményeik alapján készítet-

tük az 1. ábrát, amelyből kiindulva a cseppátmérő d_d [mm] és a v_d [m/s] esési sebesség között az alábbi (3) közelítő összefüggést találtuk:

$$v_d = 0{,}0466 \cdot d_d^3 - 0{,}8061 \cdot d_d^2 + 4{,}687 \cdot d_d \,. \qquad (3)$$

3. táblázat Esőcseppek esési sebességei

d [mm]	v_d [m/s]					
	Allen	Oseen	Dellavalle	Schiller-Neumann	Langmuir-Blodgett	átlag
0,10	-	0,230	-	0,245	0,234	0,236
0,20	0,850	0,519	0,653	0,700	0,652	0,675
0,30	1,275	-	1,275	1,162	1,060	1,193
0,40	-	-	1,895	1,600	1,426	1,640
0,50	-	-	2,455	2,014	1,750	2,073
0,75	-	-	3,600	2,968	-	3,284
1,00	-	-	4,494	3,841	-	4,167
1,25	-	-	5,237	4,659	-	4,948
1,50	-	-	-	5,437	-	5,437
1,75	-	-	-	6,198	-	6,198
1,85	-	-	-	6,475	-	6,475
1,87	-	-	-	6,532	-	6,532

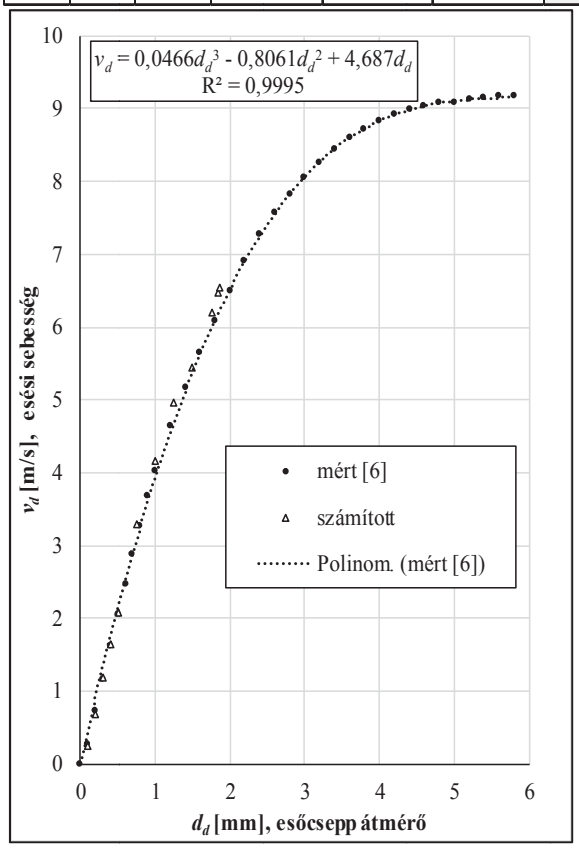

1. ábra Az esőcseppek esési sebessége

Megemlítjük, hogy Beard [9] is adott 3 cseppátmérő tartományra egy-egy polinomiális összefüggést. Az 1. ábrában feltüntettük az általunk számolt, a 3. táblázatban feltüntetett eredményeket is. Jól látható, hogy a számítások kellő pontossággal, de némi felülbecsléssel követik a mérések eredményeit.

4. A HŰTŐVENTILÁTORT ÉRŐ ESŐPERMET MENNYISÉGE

Feltételezve, hogy adott típusú eső esetén az esőcseppek mérete azonos, vagy másképpen fogalmazva közepes szemcse mérettel számolva meghatározzuk a hűtőventilátorra jutó vízmennyiséget.

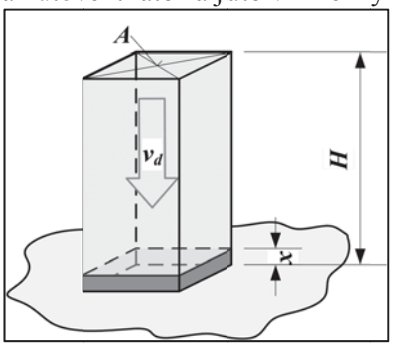

2. ábra Az esőcseppek a légtérben

A Földfelszín A nagyságú felületére t idő alatt hulló eső eső x rétegvastagsága $x = X \cdot t$ (2. ábra). A v_d esési sebességgel érkező esőcseppek ezen idő alatt $H = v_d \cdot t$ magasságú utat tettek meg. Ez azt jelenti, hogy egy A nagyságú terület felett az esőcseppek egy $V = H \cdot A = v_d \cdot t \cdot A$ térfogatban oszlottak el, miközben e térfogatban az esőcseppek össztérfogata $V_r = x \cdot A = X \cdot t \cdot A$ volt. Ebből következően egységnyi levegő térfogatban az esőcseppek k_r részaránya:

$$k_r = \frac{V_r}{V} = \frac{X}{v_d}. \qquad (4)$$

E vízarányú térben v_c sebességgel közlekedő jármű elején függőlegesen elhelyezkedő A_f járókerék felülettel rendelkező hűtőventilátor időegység alatt $Q = v_c \cdot A_f$ légtérfogattal (menetszél) találkozik, mint az a 3. ábrán látható. Ebből a ventilátort érő esővíz térfogatárama

$$Q_r = k_r \cdot Q = \frac{X}{v_d} \cdot v_c \cdot A_f = \frac{v_c}{v_d} \cdot X \cdot A_f, \qquad (5)$$

tömegárama pedig:

$$\dot{m}_r = \rho_d \cdot Q_r = \rho_d \cdot \frac{v_c}{v_d} \cdot X \cdot A_f. \qquad (6)$$

A (5) és (6) összefüggésekből látható, hogy a ventilátort érő vízmennyiség egyenesen arányos a jármű haladási v_c sebességével és a ventilátor járókerekének A_f felületével. Mivel az 1. táblázat utolsó három oszlopa szerint mind az X esőmennyiség, mind pedig a v_d esési sebesség (ez utóbbi éppen a (3) összefüggés szerint) kapcsolatban áll a

d_d cseppmérettel, így ezek nem függetlenek egymástól. Eredőként az X esőmennyiséggel párhuzamosan nővő v_d esési sebesség ellenére a $k_r = X/v_d$ részarány, és így a ventilátort érő Q_r vízmennyiség a vizsgált X tartományon fokozatosan nő, ahogy az a 3. ábrán látható. A növekedés közel lineáris, de például $v_c = 100$ km/h járműsebesség esetén jobb, 99,95%-os közelítést ad a

$$Q_r = -0{,}00133 \cdot X^2 + 0{,}5760 \cdot X, \quad Q_r[\mathrm{l/h}],\ ha\ X[\mathrm{mm/h}] \tag{7}$$

négyzetes összefüggés.

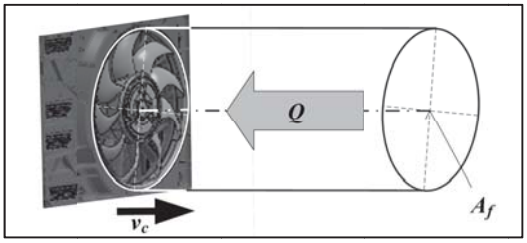

3. ábra A ventilátort érő menetszél

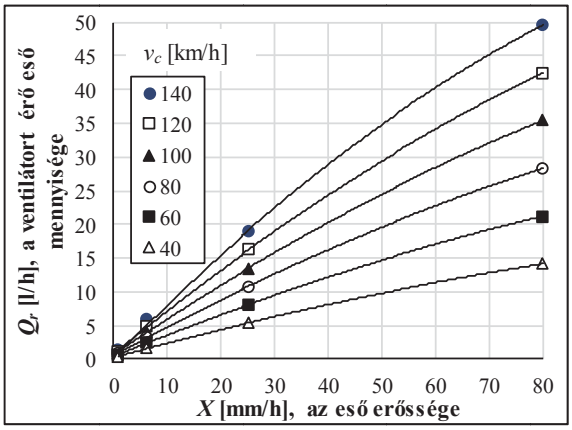

4. ábra A ventilátort érő esővíz mennyisége az esőerősség függvényében

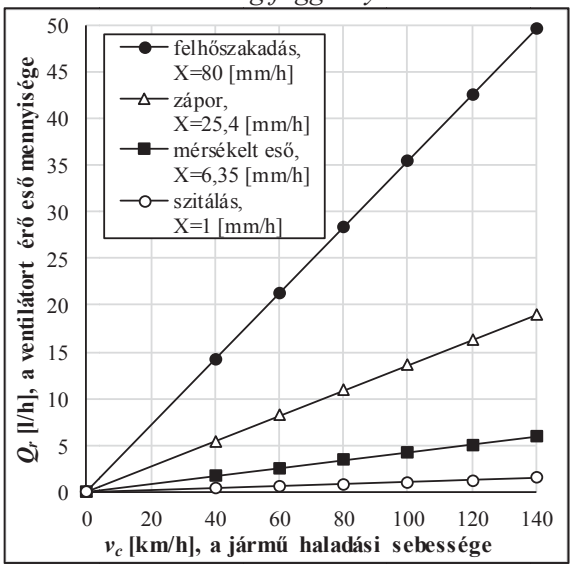

5. ábra A ventilátort érő esővíz mennyisége a jármű haladási sebességének függvényében

Másik fontos diagramot kapunk (lásd 5. ábrát), ha az (5) kifejezés segítségével ábrázoljuk a négy jellegzetes esőtípus esetén az átlagos esőmennyiség (és cseppméret), mint paraméter függvényében (lásd az 1. táblázat utolsó három oszlopa) a ventilátort érő esővíz térfogatáramát a jármű különböző haladási sebessége esetén. A 4. és 5. ábrákon ismertetett mennyiségi adatok felhasználásával lehetőség van a ventilátorra ható vízmennyiség hatásának (mint peremfeltételnek) elemzésére numerikus módszerekkel. Kísérleti vizsgálatok esetén a szükséges vízmennyiség biztosításához jelentenek kiinduló adatokat.

5. KÖSZÖNETNYILVÁNÍTÁS

A kutatás az Európai Unió és a Magyar Kormány támogatásával, az Európai Regionális Fejlesztési Alap társfinanszírozásával valósult meg az „E-mobility Miskolcról: Hűtővíz keringető szivattyú és motorhűtő ventilátor továbbfejlesztése az elektromos járművekben elvárt magasabb minőségi követelmények figyelembevételével” című GINOP-2.2.1-15-2017-00090 azonosítószámú projekt keretében.

6. IRODALOM

[1] National Meteorological Library, and Archive, Fact sheet No. 3 – *Water in the atmosphere*, http://www.spilve.lv/library/meteo/Water.pdf

[2] Glossary of Meteorology. Rain, American Meteorological Society, http://glossary.ametsoc.org/wiki/Rain

[3] http://www.shorstmeyer.com/wxfaqs/float/rdtable.html

[4] https://hu.wikipedia.org/wiki/Csapadék

[5] A. F. Spilhaus: *Raindrop Size, Shape, and Falling Speed*, Journal of Meteorology, Volume 5, 1948, pp. 108-110.

[6] R. Gunn and G. D. Kinzer: *The terminal velocity of fall for water droplets in stagnant air*, Journal of Meteorology, Volume 6, 1949, pp. 243-248.

[7] S. Yuu and Y. Ohtani: *Particle Motion in Fluid*, Powder Technology Handbook, Third Edition, Chapter 2.3, CRC Press, Taylor & Francis Group, 2006, pp. 125-132.

[8] Dr. Koncz István: *Portalanítás és Porlevválasztás*, Műszaki Könyvkiadó, Budapest, 1982. 236

[9] K. V. Beard: *Terminal Velocity and Shape of cloud and Precipitation Drops Aloft*, Journal of the atmospheric Sciences, volume 33, 1976, pp. 851-864

SOROS GERJESZTÉSŰ EGYENÁRAMÚ MOTOR DINAMIKUS TESZTMÉRÉSEI ÉS SZIMULÁCIÓJA

DYNAMIC TEST MEASUREMENTS AND SIMULATION ON A SERIES WOUND DC MOTOR

Attila Szántó, András Szántó, Gusztáv Áron Sziki PhD, Éva Ádámkó, György Juhász PhD

ABSTRACT
This paper presents the experimental study and simulation of the series wound DC motor of a prototype racing car designed and constructed at the Faculty of Engineering, University of Debrecen. During the measurements, different loads were applied on the motor shaft, and the motor was spun up from rest. During spinning up the intensity of current flowing through the motor and the angular speed of the rotor were measured. After that simulation was performed with the same parameters applied. This allowed us comparing the measured and simulated values.

1. INTRODUCTION

The Faculty of Engineering, University of Debrecen has had more than a decade of tradition in the development and construction of various alternative (electric, pneumatic) powered vehicles [1, 2, 3, 4, 5, 6], with which student teams take part in various national and international competitions. These include the MVM Energy Race, the Shell ECO Marathon, and the Pneumobil races [7, 8].

In order to achieve more effective racing, we have been developing a vehicle dynamics model and a simulation program based on it for several years [9, 10]. This program calculates the vehicle dynamic functions of a vehicle from its technical data and also calculates the loads on each vehicle component (e.g. axle loads) during vehicle movement. Using the program and supplementing it with an optimization procedure, the optimal vehicle parameters (e.g. optimum gear ratio in the drive train) can be calculated for a given driving dynamics aim (racing task). The application of these technical parameters to the vehicle significantly increases the chances of successful racing.

2. SIMULATION PROGRAM

The vehicle dynamics model and the simulation program based on it are capable of generating, the dynamic functions of a vehicle moving on a linear track. Complemented by an optimization process, the program can be used indirectly to determine the optimal vehicle parameters for a given driving dynamics aim.

In addition to the usual driving dynamics functions (acceleration, velocity and position-time functions), the program is able to calculate the time dependence of the tangential and normal forces on the wheels and the loads on the front and back axles. It also calculates the intensity of current flowing through the motor, the voltage on the motor, and the angular speed and torque of the motor versus time.

The program takes into account almost all the factors that influence the vehicle's motion. These include electromagnetic and dynamic motor characteristics (electric resistance and self- and mutual inductance of windings, bearing and brush resistance torque on the motor shaft), rolling and air resistance, moment of inertia of the rotating machine parts, vehicle's centre of gravity and the coefficient of friction between the wheels and the ground as a function of tyre slip [11, 12, 13, 14].

The program can be used to determine the optimal technical parameters (e.g. the gear ratio in the chain drive) for a given vehicle dynamics aim (e.g. completing the race in the shortest possible time). As the program is based on a general vehicle dynamics model, it can be used to design, simulate the motion and optimize the technical data any of our racing cars [15, 16].

For modular development and greater clarity, the main vehicle components are organized into separate blocks, which are:

- front wheels;
- rear wheels;
- vehicle body;
- motor;
- powertrain.

The block diagram of the vehicle dynamics simulation program is shown in Figure 1.

The forces between the "vehicle body" and "front and back wheels" (vertical and horizontal axle loads) are calculated in the "vehicle body" and the "front and rear wheel" blocks. In addition, the "rear wheel" block is used to calculate vehicle

velocity, acceleration, and motor load (M_{terh}). Since the motor load is provided by the vehicle itself, the motor simulation block also uses the output data computed by the "vehicle body" block. The calculated loading torque is finally read by the "motor block" which calculates the motor angular speed and then, from the angular speed, loading torque, $L_a(I)$, $L_g(I)$, $L_{ga}(I)$, $M_{ell}(\omega)$ characteristics, R_a, R_g resistances and supply voltage ($U_{TÁP}$) it calculates the motor torque applied on the vehicle (M_{motor}). From the motor angular speed (knowing the gear ratio), the "powertrain block" calculates the angular speed of the rear wheels. The cycle ends by feedback, the rear wheel angular speed is connected back to the "rear wheel block" and the torque of the motor (M_{motor}) back to the "vehicle body" block. By running the cycle several times, the program generates the vehicle dynamics functions specific to the motor and vehicle. To perform the calculations, the motor and vehicle technical data (input parameters) described above are required. A detailed list of input parameters required to run the program can be found in reference [9].

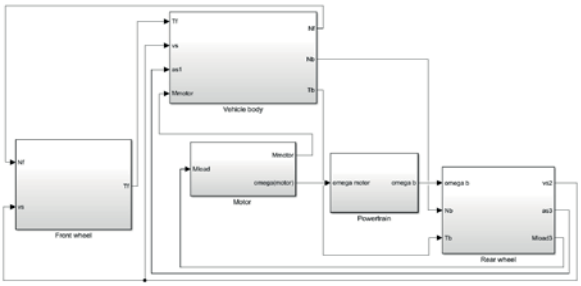

Figure 1. Block diagram of the vehicle dynamic simulation program

From the input parameters, the simulation program generates the following vehicle dynamic functions as a function of time [17]:

- the intensity of current flowing through the motor;
- motor torque on the vehicle;
- acceleration, velocity and distance travelled by the vehicle;
- tangential and normal forces exerted by the road on the vehicle wheels;
- tangential and normal axle loads;
- rolling and bearing resistance torques;
- air resistance force;
- tyre slip.

Based on the dynamics functions that can be generated by the program, we can determine the optimal vehicle parameters.

A key part of the simulation program is the "motor simulation block", which performs the simulation of the electric motor [18, 19, 20, 21, 22]. This requires an accurate knowledge of the technical characteristics of the motor (electric resistance and dynamic inductances of windings, brush voltage, bearing and brush resistance torques). To determine these characteristics and data experimentally, we have developed (and are still developing) a measuring system for testing electric motors.

3. APPLIED MEASURING SYSTEM AND EXPERIMENTAL METHOD

A schematic drawing of the measuring system used is shown in Figure 2.

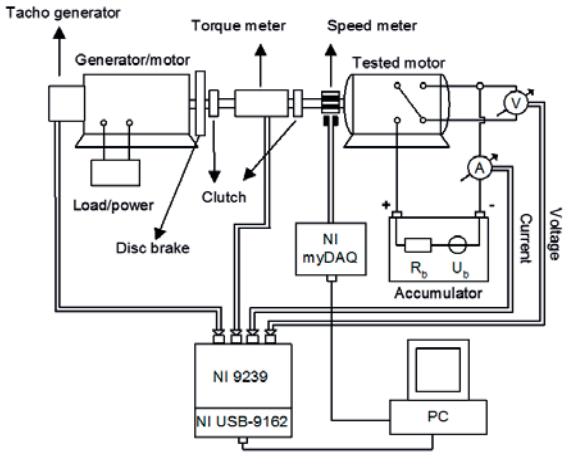

Figure 2. Schematic drawing of the measuring system

In Figure 2 the motor under test is connected to a generator (which is used to change the load on the motor) through a torque meter (rotary shaft torque meter type 7934, marketed by Kaliber Instrumentation and Measurement Ltd.). The motor rpm, torque, and intensity of current flowing through it are converted into voltage signals and measured using a NI 9239 data acquisition card that is connected to a computer using an NI USB-9162 USB adapter. The rpm can be measured either by a tachogenerator or by an optical tachometer.

Test measurements were also performed to test the accuracy of the simulation program and measured motor characteristics. Previously, test measurements were performed on a fixed rotor motor (locked rotor tests [17, 22]). In these measurements the measured values were in good agreement with the simulated ones. In the current dynamic test measurements, the motor is spun up from rest. Power is provided by a 12 [V], 60 [Ah] car battery. During spinning up the intensity of current flowing through the motor and the angular

speed of the rotor are measured versus time. First, the unloaded motor was tested, and then, the measurement was repeated, applying discs (Figure 3) of different moments of inertia on the shaft of the motor.

Figure 3. Steel discs used for measurements

The moment of inertia of the discs in Figure 3 and the ribbed sleeve mounted on the motor shaft are shown in Table 1.

Table 1. Moments of inertia of the discs and ribbed sleeve used for the measurements

Disc	Moment of inertia [kg·m^2]
Small disc	0.00151
Big disc	0.0688
Ribbed sleeve	0.000157

Then, in the simulation program, the input parameter values (battery voltage, moment of inertia of the discs, etc.) used for measurement were set and the simulation was run. The measured and simulated values were then compared.

4. MEASUREMENT RESULTS

Figures 4 and 5 show the rpm and current intensity versus time measured during the motor was spinning up from rest. First, the motor was spun up without load, and then the measurement was repeated, with discs of various moments of inertia mounted on the motor shaft (1 small disc, 2 small discs, and finally 1 large disc).

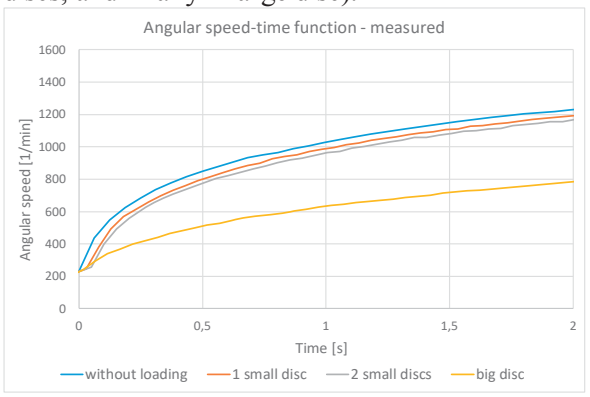

Figure 4. Measured rpm-time functions

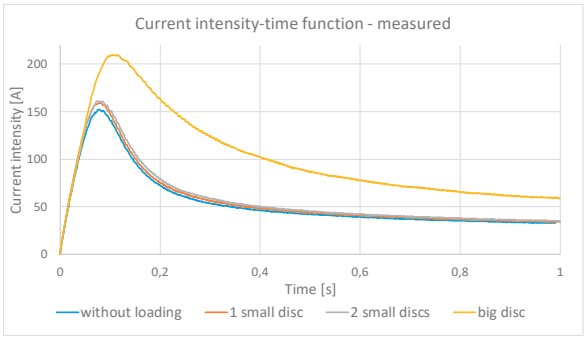

Figure 5. Measured current intensity-time functions

It can be seen from the diagrams that as the load increases, the motor spins up to a lower rpm during the same period of time, whereas the reverse is true for the current: increasing the load results in a higher current at the same time.

5. SIMULATED RESULTS

The previously measured characteristics [22] and other parameter values used for the recent measurements were set in the simulation program as input parameters and the simulation was run. Figures 6 and 7 show the simulated rpm- and current intensity-time functions applying different loads on the motor shaft.

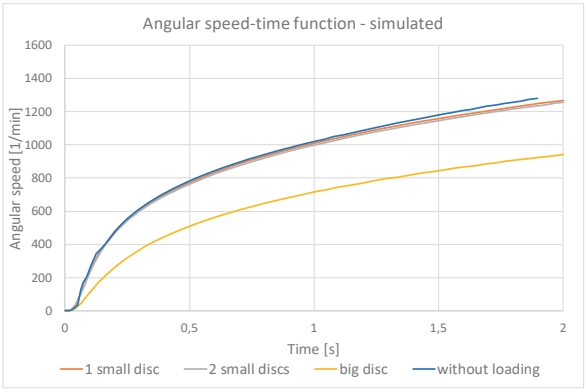

Figure 6. Simulated rpm-time functions

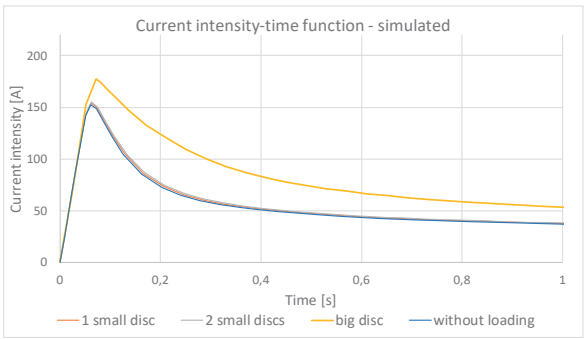

Figure 7. Simulated current intensity-time functions

6. COMPARISON OF MEASURED AND SIMULATED VALUES CONCLUSIONS

Figures 8 and 9 show the relationship between the measured and simulated current intensity- and rpm-time functions in case of an unloaded motor.

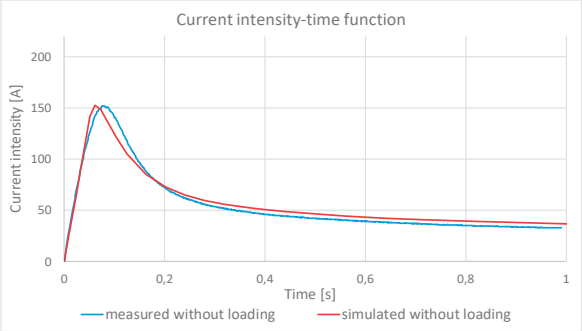

Figure 8. Measured and simulated current intensity-time functions

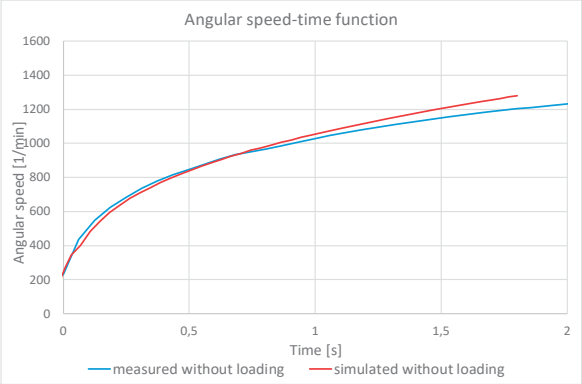

Figure 9. Measured and simulated rpm-time functions

When the loading moment of inertia on the rotor has a low value (unloaded motor or 1 or 2 small discs applied on the motor shaft), the measured and simulated values show good agreement. However, at higher loading moments of inertia the difference is already significant. The reason for this is unknown, and we are planning new test measurements using the new, more advanced torque meter to clarify it.

7. SUMMARY

During the presented research work we performed dynamic test measurements on a series wound DC motor, then simulated it applying the same input parameter values. We used our own simulation program that was developed in Matlab/Simulink environment previously.

On the basis of the results it can be concluded that the measured and simulated values are in a good agreement under unloaded conditions and also, when the loading moment of inertia is small. However, at higher loadings on the motor shaft the difference is already significant. The reason for this is not known yet, and we are planning new test measurements using a new, more advanced torque meter to clarify the difference. Furthermore, we plan to use other types of motor models in the simulation program in the near future, and to compare the simulation results obtained with different models.

8. ACKNOWLEDGEMENT

"The research was financed by the Thematic Excellence Programme of the Ministry for Innovation and Technology in Hungary (ED_18-1-2019-0028), within the framework of the (Automotive Industry) thematic programme of the University of Debrecen."

9. REFERENCES

[1] GÁBORA András, SZÍKI Gusztáv Áron, SZÁNTÓ Attila, VARGA Tamás Antal, MAGYARI Attila, BALÁZS Dávid: Prototype battery electric car development for Shell-ECO-Marathon® competition. Proceedings of the XXII International Conference of Young Engineers, Kolozsvár (2017), 167-170.

[2] JUHÁSZ György: A pneumobil versenyek és az oktatás - a felkészülés tanári szemmel, Debreceni műszaki közlemények. - 10: 1 (2011), p. 35-40. ISSN: 1587-9801

[3] Szakács T.: Modelling and Validation of a Pneumobil. In: Pokorádi, László (szerk.) Proceedings of the 3th Agria Conference on Innovative Pneumatic Vehicles – ACIPV 2019 Eger, Magyarország : Óbudai Egyetem Mechatronikai és Járműtechnikai Intézet, (2019) pp. 31-35. , 5 p.

[4] Pokorádi L., Szakács T.: Graph Modelling of Pneumatic Vehicle Control System. In: Pokorádi, László (szerk.) Proceedings of the 3th Agria Conference on Innovative Pneumatic Vehicles – ACIPV 2019 Eger, Magyarország : Óbudai Egyetem Mechatronikai és Járműtechnikai Intézet, (2019) pp. 43-51. , 9 p.

[5] Szakács T.: Pneumatic modelling of a pneumobil. In: Pokorádi, László (szerk.) Proceedings of the 2nd Agria Conference on Innovative Pneumatic Vehicles ACIPV 2018 Eger, Magyarország : Óbudai Egyetem, (2018) pp. 25-30. , 6 p.

[6] ZÖLDY Máté, Dr. EMŐD István, TÖLGYESI Zoltán: Alternatív járműhajtások – Maróti Könyvkereskedés és Könyvkiadó Kft. (2006) ISBN 9639005738

[7] Shell-ECO-Marathon® competition, http://www.shell.com/energy-and-innovation/shell-ecomarathon.html download: 2020. 03. 20.

[8] Aventics pneumobil competition In: https://en.pneumobil.hu/news download:

2020. 03. 20.
[9] SZÁNTÓ Attila: Elektromos hajtású tanszéki versenyautó járműdinamikai modellezése, TDK dolgozat (2015), Debreceni Egyetem Műszaki Kar.
[10] Matlab 2014b, The MathWorks, Inc, Natick, Massachusetts, United States.
[11] Hans B. PACEJKA, Igo BESSELINK: Tire and Vehicle Dynamics (Third edition) – Published by Elseiver Ltd. (2012) ISBN 978-0-08-097016-5.
[12] Jörsen REIMPELL, Jürgen W. BETZLER, BÁRI Gergő, HANKOVSZKI Zoltán, KÁDÁR Lehel, LÉVAI Zoltán, NAGYSZOKOLYAI Iván: Gépjármű futóművek I. (2012) ISBN 978-963-279-606-2
[13] Bernd HEISSING, Metin ERSOY: Chassic Handbook (2011) ISBN 978-3-8348-0994-0
[14] SZIKI Gusztáv Áron, HAJDU Sándor, SZÁNTÓ Attila: Vehicle Dynamics Modelling of an Electric Driven Race Car, International Scientific Conference on Advances in Mechanical Engineering proceedings (2015) Debrecen, Hungary.
[15] Erdősné SÉLLEY Csilla, GYURECZ György, JANIK József, KÖRTÉLYESI Gábor: Mérnöki optimalizáció, 2012, Typotex kiadó, ISBN 978-963-279-538-6
[16] SZÁNTÓ Attila: Járműdinamikai szimuláció és optimalizáció Matlab és LabVIEW környezetben, TDK dolgozat (2017), Debreceni Egyetem Műszaki Kar.
[17] SZÁNTÓ Attila: Soros gerjesztésű DC motor modellezése a járműdinamikai szimulációs programunkban, TDK dolgozat (2016), Debreceni Egyetem Műszaki Kar.
[18] Miralem HADŽISELIMOVIĆ, Matic BLAZNIK, Bojan ŠTUMBERGER, Ivan ZAGRADIŠNIK: Magnetically Nonlinear Dynamic Model of a Series Wound DC Motor, PRZEGLĄD ELEKTROTECHNICZNY (Electrical Review), ISSN 0033-2097, R. 87 NR 12b/2011
[19] SZÁNTÓ Attila, Dr. SZÍKI Gusztáv Áron, HAJDU Sándor: Soros gerjesztésű egyenáramú motorral hajtott versenyautó dinamikai modellezése, Műszaki tudomány az Észak-Kelet Magyarországi régióban 2016, szerk. Bodzás Sándor, Debreceni Akadémiai Bizottság Műszaki Szakbizottsága, Debrecen, 406-414, 2016.
[20] SZIKI Gusztáv Áron, SARVAJCZ Kornél, SZÁNTÓ Attila: Dynamic simulation of a series wound DC motor applying the Control Design and Simulation Module of LabVIEW, International Scientific Conference on Advances in Mechanical Engineering proceedings (2017) Debrecen, Hungary.
[21] SZÁNTÓ Attila, Dr. SZÍKI Gusztáv Áron, Dr. HAJDU Sándor, GÁBORA András (2017): Simulation of a series wound DC motor in MATLAB environment, Proceedings of the XXII International Conference of Young Engineers, Kolozsvár (2017), 367-370.
[22] SZIKI Gusztáv Áron; SARVAJCZ Kornél; KISS János; GÁL Tibor; SZÁNTÓ Attila; GÁBORA András; HUSI Géza: Experimental investigation of a series wound dc motor for modeling purpose in electric vehicles and mechatronics systems. In: MEASUREMENT (ISSN: 0263-2241) 109: pp. 111-118. (2017) IF: 1.742

ELEKTROMOS JÁRMŰVEK ALKALMAZÁSAI

OPPORTUNITIES OF ELECTRIC VEHICLES

Dr. Péter Bencs[1], Dr. Katalin Voith[2], associate professor[1], senior research fellow[2]
[1,2]Department of Fluid and Heat Engineering, University of Miskolc, HU-3515, Miskolc, Miskolc-Egyetemváros

ABSTRACT: Nowadays, the number of vehicles with minimum emissions that meet environmental requirements is increasing. In this paper, we present a comprehensive technological study and comparison of clean electric vehicles. This paper addresses this issue and summarizes current and future strategies. Environmental guidelines and policy incentives are constantly increasing the number of electric vehicles and the rapid development of technology.

1. INTRODUCTION

The literature review clearly shows that the conditions for the introduction of electric vehicles (EV) need to be examined on a country-specific basis. A good example is European countries that are heavily relying on renewable energies, such as France or Norway. Countries like Germany, the United Kingdom, and the US should focus on significantly reducing greenhouse gas emissions from electricity generation [1]. The tendency to purchase electric vehicles is influenced by several factors, such as price, driving experience and availability of the necessary infrastructure. During the investigation, special attention is paid to environmental awareness among the customers of electric vehicles. These analyze aid policy makers and researchers to introduce and encourage the utilization of new technologies.

2. ENVIRONMENTAL EFFECTS

Vehicle manufacturers need electric vehicles at fleet level to comply with ever-changing regulations. At EU level, Regulation 2019/631 sets the new directions and expected emission standards that vehicle manufacturers must follow [2]. Currently reducing emissions of internal combustion engines is stressed, however, this is no longer adequate. It is important to emphasize that each vehicle manufacturer should examine the emission limit value for its entire vehicle fleet. Nowadays, this has brought about changes that seem to be narrowing the category of mini-cars in the manufacturers' fleet. The reason for this change is multi-directional compliance with environmental norms and commercial demands.

Table 1. summarizes literature data, which reflect the targets set by different manufacturers (in terms of adverse environmental emissions) well [2]. Compliance with the 95 gCO_2 / km benchmark will be introduced internationally by vehicle manufacturers (fleet level) in 2021.

Table 1. CO_2 emission target [gCO_2 / km]

Manufacturer	2020	2030
BMW (incl. Mini)	102	64
Daimler	102	64
Fiat	92	58
Ford	95	60
Hyundai Kia	95	59
PSA	90	56
Renault-Nissan	91	57
Toyota	92	58
Volkswagen Group	95	60
Volvo	107	67

The conclusion can be drawn from the table data that it is essential to increase the fleet level of electric vehicles in the future in order to meet the expected targets at fleet level. Electric vehicles in the fleet produce 0 gCO_2 / km and thus have a positive impact on the fleet average.

The primary limiting adverse emission parameter of car manufacturers is compliance with the CO_2 standard. Examining several air quality parameters from a health perspective may be important for further investigations. With the continuous reduction of emissions, NO_x and PM_{10} particulates remain a problem in the automotive industry [3]. Today, air particle filters are the solution for PM_{10} emissions of vehicles. Auto-ignition diesel vehicles produce much higher levels of NO_x than petrol vehicles. Since the introduction of the Euro 6 directive series in 2014, only new diesel vehicles equipped with a

NO_x-trap or SCR (Selective Catalytic Reduction) can be placed on the market.

For NO_x, Fig. 1 clearly shows that transport causes the highest emissions. Fig. 2 shows the composition of the sources of PM_{10} particulate emission. Commercial, institutional and household sectors contribute the most to PM_{10} emissions. The introduction and distribution of electric vehicles are essential to reduce environmental impacts (emissions).

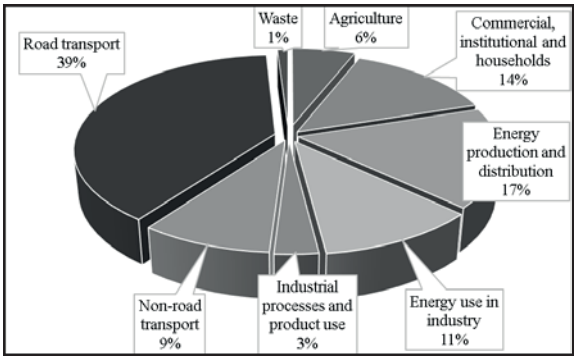

Fig. 1. Sectoral composition of NO_x emissions [3].

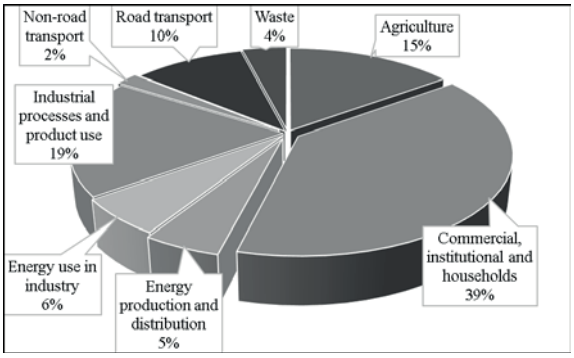

Fig. 2. Sectoral composition of PM_{10} emissions [3].

The measurements and compliance of the previously described adverse environmental emissions do not include further vehicle related emissions. PM_{10} particulate emissions are greatly contributed by brake dust from vehicle braking systems.

Today, the Euro 5 and 6 directive series typically feature higher particle emissions from the road and the tires and in the form of break-dust than directly from exhaust gasses.

Fig. 3 shows the origin of various PM_{10} particles within the toxic emission in Germany.

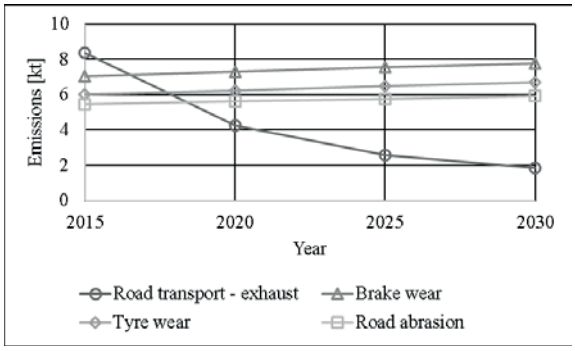

Fig. 3. PM_{10} particulate emission composition in road transport [4].

3. SELECTION PRINCIPLES

While studying environmental impacts and parameters, it is necessary to examine the consumer's choice principles. With this knowledge, we can estimate future trends and processes.

Fig. 4 shows the decision framework [5]. Consumer decisions greatly influences the future growth of the number of electric vehicles. The decision framework illustrates the decision-making processes and decision-making principles among internal combustion engines (ICE), hybrid vehicles (HEV) and electric vehicles (BEV).

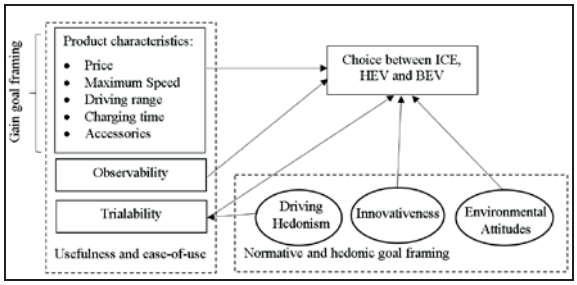

Fig. 4. Decision Framework [5].

The design of the decision framework is based on the Rogers Innovation Model (Diffusion of Innovations – DIM) [5]. There are two types of application motivation in making a decision: product characteristics and individual attitudes and attributes. The model also takes the utility and ease of use of the product into account, and it also considers the acceptance of innovation as essential. If a particular innovation is only available on the market, its usefulness and ease of use cannot be reliably evaluated. Instead, potential consumers judge the product on the basis of expected properties, feasibility and observations.

The application of the decision framework also requires the development of a discrete test

model. During the discrete investigation, vehicle profiles that are currently available in the market, and profiles that will be available in the future may be taken into account. A detailed evaluation procedure is described below [5]. During the evaluation, the following three options were developed:

- ICE – internal combustion engine.
- HEV – hybrid system (consisting of internal combustion engine and electric battery). The battery is charged while driving.
- BEV – fully electric vehicle with rechargeable battery. Charging can be done while driving (recharging) and from an external charging source.

Table 2. Attributes and attribute levels employed in the design [5].

Attribute	ICE	HEV	BEV
Price (in thousand €)	2 levels: 33.5, 40	2 levels: 36.5, 40.5	3 levels: 36.5, 44.5, 54
Accessories standard	3 levels: standard, upgraded luxury	3 levels: standard, upgraded luxury	3 levels: standard, upgraded luxury
Maximum speed (km/h)	2 levels: 180, 210	2 levels: 180, 210	3 levels: 135, 175, 210
Driving range in km	660	990	3 levels: 150, 175, 200
Charging/ fueling time	5 min	3 min	3 levels: 4h, 6h, 8h
Number of people you know who drive that car	Many	3 levels: no one, few, more than 10	3 levels: no one, few, more than 10

Parameter tests in Table 2. must also comply with applicable laws and regulations in the particular country. Car pricing does not take the country's tax policy (incentives for electric vehicles) into account. Based on the primary results, it can be concluded that hybrid and electric vehicles will be competitors in the future. In the case of electric vehicles, it must be kept in mind that consumers are also changing their basic vehicle usage patterns. As a result of the model tests, the use of fully electric vehicles is not expected in the near future. Hybrid drive systems are a compromise for consumers switching from internal combustion engines.

4. ELECTRIC VEHICLES

It is important to mention the LCA (Life Cycle Assessment) when inspecting electric vehicles. It is a widely used method in the automotive industry, which, with the right basic knowledge, can bring significant decision benefits to both manufacturers and society.

Fig. 5 shows the energy mix expected in the EU between 2015 and 2050 [6].

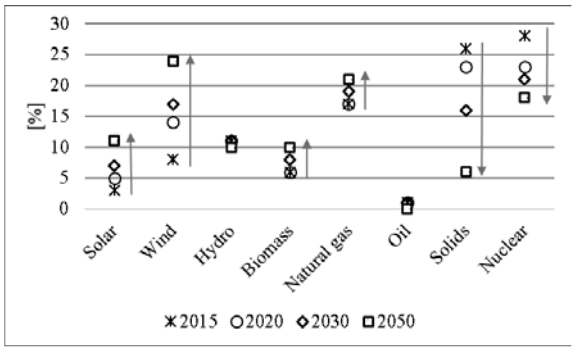

Fig. 5. EU 2015-2050 energy mix [6].

The figure shows that renewable energy will play a greater role in energy production over the projected period. At EU level, the contribution of solid fuels and nuclear energy to energy production is planned to decline. The future growth tendency of electric vehicles is analyzed in the light of this basic information and current legal principles.

There are several studies in the literature examining where electric vehicles stand based on their CO_2 emissions in a life-cycle [7, 8]. The aim is to identify large differences between diesel and electric vehicles. It is only possible to determine exact results when analyzing the parameters presented in the previous chapters together. When testing diesel vehicles, the primary consideration is the application of emission standards and test methods in accordance with these laws. In the case of electric vehicles, the main considerations are the battery capacity and the ratio of renewable energies in the production of electricity in connection with LCA [7, 8].

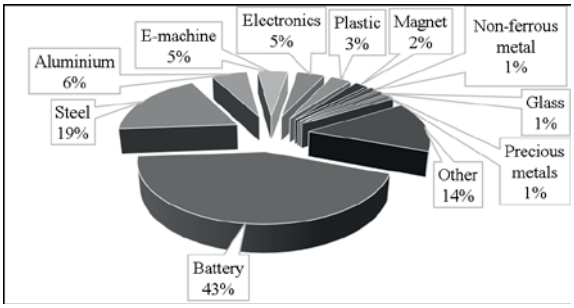

Fig. 6. Pollutant emissions from VW electric vehicle production [8].

It is important to note in the LCA that, in case of electric vehicles, most of the carbon dioxide is released during production.

Fig. 6 clearly shows that the highest adverse environmental emission in the production of electric vehicles is due to the production of the battery. During production, the reduction of toxic emissions can be achieved by increasing the renewable energy content of the energy mix used.

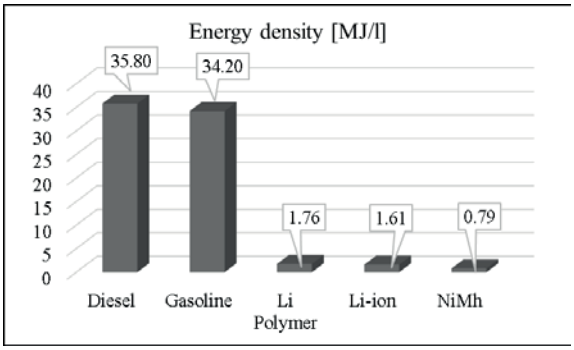

Fig. 7. Energy densities of energy media [9].

We have to keep the special needs of installing and using batteries in mind. Primarily due to their energy density, as shown in Fig. 7, their installation size can cause problems during design [9]. In addition to size, it also represents a significant weight increase for vehicles. When designing vehicles, they are trying to make the most of this feature, so there are new ways to adjust the vehicle's center of gravity by repositioning the battery packs. The battery pack is interchangeable with many manufacturers to maintain the long-term use of the vehicle. Manufacturers are also trying to utilize the high rigidity of battery packs when designing the vehicle body structure [9].

Batteries are constantly being developed, and there are many directions in professional scientific journals. There is great potential for silicon-carbon hybrid composite anodes (cheap and high performance), while commercially available lithium-ion batteries use graphite anodes [10].

When using batteries, it is important to consider that a cycle consists of a discharging and a recharging process. The definition used for general characterization of batteries is the number of cycles. The cycle can consist of a given charge level, a charge to another level. As the number of cycles increases, the battery capacity drops. A property of a charged battery is its capacity, which supplies a certain amount of electrical energy (Ah) at a given current for a given period of time. Nowadays, managing rechargeable batteries is a problem that remains unresolved, as a result of which heavy-duty equipment is simply landfilled. However, there is a practical, economical and environmentally friendly solution: recycling batteries. The most common way to do this is to use it in industrial energy storage devices that help to stabilize the electricity grid [11].

Table 3. Cost of electricity storage [12]

Type	Unit cost [€/kWh]	Investment cost [€]
VW e-up! Li-ion battery	1.09	27 000
Toyota Prius NiMH battery	2.07	10 845
Gyrodrive HP MK4 flywheel	0.12	58 450
Goldisthal power plant Pumped Hydro	0.001	623 000 000

Based on the research detailed above, energy storage is a major issue in the distribution of electric vehicles. The cost of energy storage is an important consideration when optimizing the price of electric vehicles. The use of renewable energies can reduce their emissions. We have also seen examples of the recycling of batteries from electric vehicles. Looking at several lines of research, it can be stated that the development of appropriate energy storage methods is a question of the future. Hydroelectric power stations are currently well suited for increasing the stability of electricity networks. An energy storage method used today is flywheel energy storage.

Table 3. shows four energy storage methods and their unit costs [12]. It is clear from the table that the unit cost of energy storage is the highest when using electric vehicles. Evidence shows that reservoirs are still the most efficient systems, but have the highest investment costs [13].

5. SUMMARY

In this study, we have summarized the factors influencing the future growth tendency of electric vehicles. The effect of standards that limit toxic emissions has a positive effect on the production of electric vehicles. It is clear that manufacturers will increase the proportion of electric vehicles in their fleet due to lower emission standards. In addition to the much-used CO_2 limits, other pollutants need to be taken into account as well. Other pollutants include, for example, NO_x, which is primarily related to road transport and transportation, shipping. The research methods required for the social acceptance of electric vehicles were also presented in this study. The inspection method will help decision makers and electric vehicle manufacturers alike. Today, hybrid vehicles are the primary competitor for electric vehicles. We also discussed the challenges and issues encountered in the production of electric vehicles in detail. LCA research shows that electric vehicles are constantly improving their image (they produce less adverse environmental emissions than internal combustion engine vehicles). Further development of energy storage is essential for further development and increasing production.

6. ACKNOWLEDGMENTS

The research was supported by the EFOP-3.6.1-16-00011 "Younger and Renewing University – Innovative Knowledge City – institutional development of the University of Miskolc aiming at intelligent specialization" project implemented in the framework of the Széchenyi 2020 program. The realization of these two projects is supported by the European Union, co-financed by the European Social Fund.

7. REFERENCES

[1] KUMAR, Rajeev Ranjan; KUMAR, Alok. Adoption of electric vehicle: a literature review and prospects for sustainability. Journal of Cleaner Production, 2019, 119911.

[2] FRITZ, Markus; PLÖTZ, Patrick; FUNKE, Simon A. The impact of ambitious fuel economy standards on the market uptake of electric vehicles and specific CO2 emissions. Energy Policy, 2019, 135: 111006.

[3] EEA Report Air quality in Europe — 2018 report.

[4] HASCOET, Matthieu; ADAMCZAK, Loïc. At source brake dust collection system. Results in Engineering, 2020, 5: 100083.

[5] TCHETCHIK, Anat, et al. The joint effects of driving hedonism and trialability on the choice between internal combustion engine, hybrid, and electric vehicles. Technological Forecasting and Social Change, 2020, 151: 119815.

[6] BURCHART-KOROL, Dorota, et al. Life cycle impact assessment of electric vehicle battery charging in European Union countries. Journal of Cleaner Production, 2020, 120476.

[7] BUCHAL, Christoph; KARL, Hans-Dieter; SINN, Hans-Werner. Kohlemotoren, Windmotoren und Dieselmotoren: Was zeigt die CO2-Bilanz?. ifo Schnelldienst, 2019, 72.08: 40-54.

[8] Volkswagen Aktiengesellschaft Electric Vehicles with Lowest CO_2 Emissions, 2019.

[9] NÁDASI, Réka; TÓTH, Csaba; BALOG, Péter. Towards the inductive on-road charging system for electric buses: Inspection of the Hungarian electric mobility fleet. Transportation Research Procedia, 2019, 41: 380-394.

[10] Kwon, H. J., Hwang, J.-Y., Shin, H.-J., Jeong, M.-G., Chung, K. Y., Sun, Y.-K., & Jung, H.-G. (2019). Nano/Microstructured Silicon–Carbon Hybrid Composite Particles Fabricated with Corn Starch Biowaste as Anode Materials for Li-Ion Batteries. Nano Letters, 20(1), 625–635.

[11] OMRANI, Mahyar Mirzaei; JANNESARI, Hamid. Economic and environmental assessment of reusing electric vehicle lithium-ion batteries for load leveling in the residential, industrial and photovoltaic power plants sectors. Renewable and Sustainable Energy Reviews, 2019, 116: 109413.

[12] Dr. Barna Hanula: Sustainable-sustainability LCA. LCA Center, 2019. – presentation.

[13] GUEZGOUZ, Mohammed, et al. Optimal hybrid pumped hydro-battery storage scheme for off-grid renewable energy systems. Energy Conversion and Management, 2019, 199: 112046.

VVVF HAJTÁSVEZÉRLÉSŰ NAPENERGIÁVAL HAJTOTT ELEKTROMOS AUTÓ

SOLAR POWERED ELECTRIC CAR WITH VVVF DRIVE CONTROL

István Bodnár Ph.D., Rafael Ruben Boros, Dávid Matusz-Kalász

ABSTRACT
The popularity of electric vehicles has been expanding rapidly due to the subsidies and are worldwide used What if, solar panel help us to drive the car? The World Solar Challenge is exemplary. In Australia directly solar powered cars can across the continent during a 3000 km long race. Let's use this technology! Our goal is to create a theoretical model of an electric car, which can directly use solar energy or restore it. We would like to use a three-phase induction motor to drive the electric car. The motor is control by variable voltage frequency drive (VVFD). The solar panel string supplies the inverters DC link.

1. INTRODUCTION

Nowadays energy hunger favours the accelerated expansion of renewables. Of the renewable energy sources, solar electric power generation is one of the least located option. Since the solar panels generate direct current, it is an obvious solution to place them on top of vehicles and connect them to a 12 VDC system. Although solar panels are not suitable for running an electric car in its entirety, however they can provide power to the control circuits or provide a slight increase in range. Over the past decade, many vehicle manufacturers have experimented with solar cars, with greater or lesser success.

The solar panels are always used to charge the vehicle battery pack. For some cars, the charge only works when stationary. Basically, electric cars run on tens of kW electric motors, on the other hand, only a few hundred watts of solar power capacity can be placed on them. It follows that solar panels alone are not enough to charge and operate the vehicle. For this reason, the importance of solar cars lies primarily in the daily commuting of the urban population. If the distance travelled per day is considered and how much energy the solar panels produce daily in unclouded, sunny days, then the difference between consumption and production is less perceptible. It should not be overlooked that most cars are usually used by one person at a time, so it is unnecessary to produce large and powerful solar cars. It would be practical to design these vehicles for daily, low-power commuting, rather than for a family car. It is worth researching in this direction and developing cheaper solar cars.

2. INDUCTION MOTORS

AC induction motors are the most common motors used in industrial motion control systems, as well as in main powered home appliances. Simple and rugged design, low-cost, low maintenance and direct connection to an AC power source are the main advantages of AC induction motors. Various types of AC induction motors are available in the market. Different motors are suitable for different applications. Although AC induction motors are easier to design than DC motors, the speed and the torque control in various types of AC induction motors require a greater understanding of the design and the characteristics of these motors [1].

Like most motors, an AC induction motor has a fixed outer portion, called the stator and a rotor that spins inside with a carefully engineered air gap between the two. Virtually all electrical motors use magnetic field rotation to spin their rotors. A three-phase AC induction motor is the only type where the rotating magnetic field is created naturally in the stator because of the nature of the supply. DC motors depend either on mechanical or electronic commutation to create rotating magnetic fields. A single-phase AC induction motor depends on extra electrical components to produce this rotating magnetic field. Two sets of electromagnets are formed inside any motor. In an AC induction motor, one set of electromagnets is formed in the stator because of the AC supply connected to the stator windings. The alternating nature of the supply voltage induces an Electromagnetic Force (EMF) in the rotor (just like the voltage is induced in the transformer secondary) as per Lenz's law, thus generating another set of electromagnets; hence the name – induction motor. Interaction between the magnetic field of these electromagnets generates twisting force or torque. As a result, the motor rotates in the direction of the resultant torque [1].

2.1. Stator

The stator is made up of several thin laminations of aluminium or cast iron. They are punched and clamped together to form a hollow cylinder (stator core) with slots. Coils of insulated wires are inserted into these slots. Each grouping of coils, together with the core it surrounds, forms an electromagnet (a pair of poles) on the application of AC supply. The number of poles of an AC induction motor depends on the internal connection of the stator windings. The stator windings are connected directly to the power source. Internally they are connected in such a way, that on applying AC supply, a rotating magnetic field is created [1].

2.2. Rotor

The rotor is made up of several thin steel laminations with evenly spaced bars, which are made up of aluminium or copper, along the periphery. In the most popular type of rotor (squirrel cage rotor), these bars are connected at ends mechanically and electrically using rings. Almost 90% of induction motors have squirrel cage rotors. This is because the squirrel cage rotor has a simple and rugged construction. The rotor consists of a cylindrical laminated core with axially placed parallel slots for carrying the conductors. Each slot carries a copper, aluminium, or alloy bar. These rotor bars are permanently short-circuited at both ends by means of the end rings. This total assembly resembles the look of a squirrel cage, which gives the rotor its name [1].

The rotor is mounted on the shaft using bearings on each end; one end of the shaft is normally kept longer than the other for driving the load. Some motors may have an accessory shaft on the non-driving end for mounting speed or position sensing devices. Between the stator and the rotor, there exists an air gap, through which due to induction, the energy is transferred from the stator to the rotor. The generated torque forces the rotor and then the load to rotate. Regardless of the type of rotor used, the principle employed for rotation remains the same [1].

2.3. Application

The use of induction motors in electric cars is subservient because of their low maintenance requirements. This is due to the fact, that induction motors do not contain carbon brushes and slip ring, in contrast with synchronous and DC motors. Therefore, only the bearings should be maintained. The induction motor has good starting torque, which gives good acceleration in cars.

2.4. Speed of an Induction Motor

The magnetic field created in the stator rotates at synchronous speed (*equation 1*). Where: f_1 the supply frequency, p the number of pole pairs [1].

$$n_0 = \frac{f_1 \cdot 60}{p} \tag{1}$$

The magnetic field produced in the rotor because of the induced voltage is alternating in nature. To reduce the relative speed, with respect to the stator, the rotor starts running in the same direction as that of the stator flux and tries to catch up with the rotating flux. However, in practice, the rotor never succeeds in "catching up" to the stator field. The rotor runs slower than the speed of the stator field. This speed is called the Base Speed (n). The difference between n_0 and n is called the slip. The slip varies with the load. An increase in load will cause the rotor to slow down or increase slip. A decrease in load will cause the rotor to speed up or decrease slip. The slip is expressed as a percentage and can be determined with the following formula (*equation 2*) [1, 8]:

$$s\,[\%] = \frac{n_0 - n}{n_0} \cdot 100 \tag{2}$$

3. SPEED OF CONTROL

The best way to control the rotor speed is to change the f_1 supply frequency. Variable frequency drives can vary the frequency stepless from 0 Hz to a few hundred Hz. The variable frequency drive is an electronic device which has three main part inside: rectifier, DC link with filter capacitor and inverter. The input and output can be one or three-phase AC voltage. For high power usages, a three-phase motor is recommended which requires a three-phase inverter. The inverter makes AC voltages from DC voltage where the frequency can vary. If the inverter's input is constant voltage, we called it VVFD (Variable Voltage Frequency Drive). The rectifier and the filter capacitor make the constant voltage at the inverter's input.

3.1. Voltage control

The torque will be constant only if the flux is constant as well (*equation 3*). U_{i1} means the induced voltage in the stator, Φ_{max} is the flux amplitude, N_1 is the number of turns, ξ_1 is the winding factor. If we do not reduce the voltage at low frequency, the stator iron core is saturated. So, the frequency and the voltage must also be changed together [8].

$$\Phi_{max} = \frac{U_{i1}}{4{,}44 \cdot f_1 \cdot N_1 \cdot \xi_1} \tag{3}$$

3.2. V/f control

The variable-voltage/variable-frequency (VVVF) drive powered induction motors have several control engineering problems. For optimal utilization of the drive, the slip-frequency should not be bigger than the pull-up slip-frequency.

Current overload must also be eliminated, the slip must remain below the nominal slip. Therefore, it is expedient to measure the slip and, on this basis to control the frequency of the VVVF drive, so that a specific adjustable slip frequency is not exceeded. In addition, it must be ensured that the motor is always supplied with the correct frequency-proportional voltage. This is necessary, on the one hand, to ensure that the machine flux does not exceed the nominal value, on the other hand, to achieve the nominal flux, apply the motor torque with the lowest possible current and reach the nominal torque at any speed. This condition can be achieved by controlling the voltage directly in proportion to the frequency [2].

Figure 1 shows two sections [3]. n the first section, the frequency and the voltage are increased proportionally to the limit frequency, then the flux and the torque are constant. Once the nominal voltage has been reached, the voltage applied to the motor terminals can no longer be increased, but the frequency can.

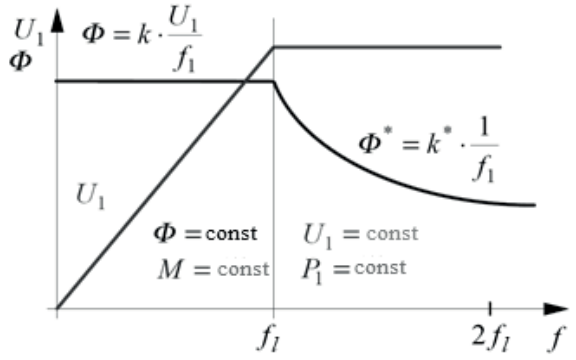

Figure 1. Voltage and flux variations as a function of frequency

This has the disadvantage that the flux is reduced, so that the motor torque and the engine power do not increase further. In the second section we talk about field weakening, not to be confused with that of DC machines. In this case, the field weakens due to constraints, and is not intentionally weakened.

4. POWER ELECTRONICS IN ELECTRIC CARS

In electric cars, the input DC comes from the battery for the inverter. DC/DC converter is needed because the battery voltage is different from the motor voltage. If we charge the battery with solar panel, one more DC/DC converter is required. These converters reduce efficiency due to power dissipations.

In many electric cars, the three-phase inverter consists of IGBT switches. These high power IGBT modules contain driver circuits as well. The modules are mounted on a heatsink.

5. THREE-PHASE INVERTER

A power inverter is an electrical device that converts direct current (DC) to alternating current (AC). The frequency of the generated AC voltage is arbitrary.

Simple control is when modulation of the control voltage is not applied. By simple control neither sine current nor sine voltage can be realized at the output. If a pulsating torque on the motor shaft is not tolerated, a simple controlled inverter is not advisable.

Six IGBT semiconductor switches are connected to the intermediate DC circuit. The alternating voltage is realized by switching these, which forms a three-phase network. The phase is offset from the others by 120°. During one period, one of the IGBT elements is switched off or on six times. An IGBT can take part in driving till 180°. The structure of the inverter is shown in Figure 2, where the induction motor is connected to the output.

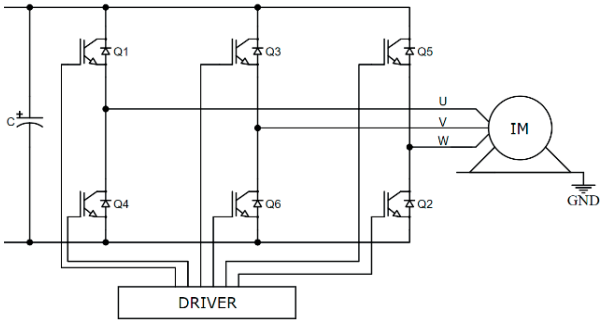

Figure 2. Three-phase inverter

The phase voltages generated on the star-connected power supply are shown in Figure 3. In the case of electric cars, simple control is not allowed because the torque will be pulsating, the car will not accelerate smoothly. The smoothest torque is created by sinusoidal current and flux.

Since IGBT switches are only controlled by rectangular signals, Sine Pulse Width Modulation (SPWM) must be used. This method results that the fundamental frequency of the control signal will be sinusoidal. Therefore, the basic harmonic of the current includes the sine as well as overtones due to the switching frequency. The amplitude of the overtones can be greatly reduced by an LC low-pass filter. The IGBT Gate-Emitter capacity has the following control volt-

age in case SPWM control (Figure 4), switching frequency is 7,3 kHz.

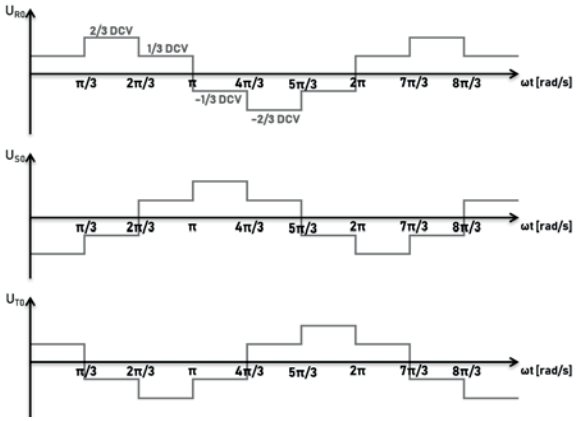

Figure 3. The three-phase voltage

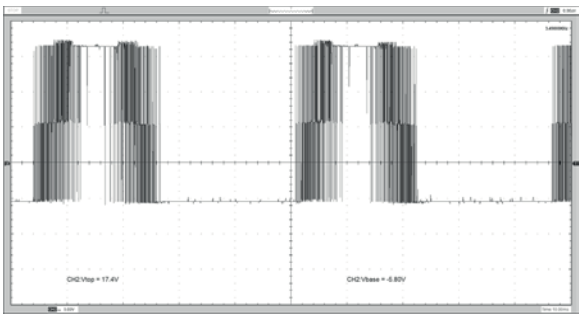

Figure 4. IGBT driver voltage

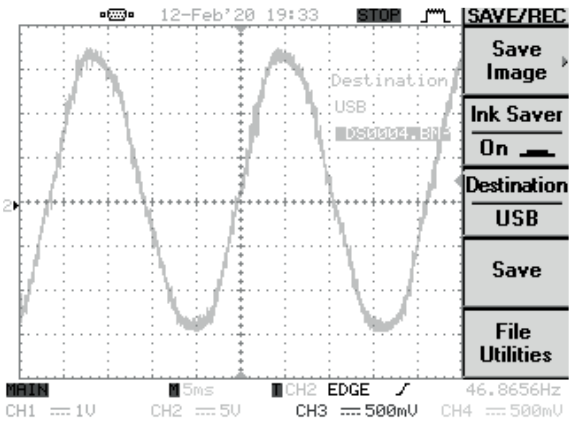

Figure 5. Phase current

If a low pass filter on the inverter output is used, the current of Figure 5 is obtained on one of the motor coils. Of course, THD is not 0% even so, but the amount of overtone content is greatly reduced. During the measurement, the DC/DC converter stably provided a DC voltage powered by the solar cell string.

6. TYPE OF SOLAR CELLS

The solar cell is an electrical device that converts the energy of light directly into electricity, its operational background is the photovoltaic effect. They are more and more popular year after year and their residential and industrial usage is constantly increasing.

As a result of their development, their efficiency is increasing, while their production cost is constantly decreasing. Depending on the type, the efficiency of the solar panel can reach 22%. Under laboratory conditions, efficiency of 30% also has already been achieved. The vast majority of currently used solar cells are based on silicon semiconductors, but there is ongoing research into the development of new technologies to further maximize existing efficiency [4].

The major types of currently applied solar cells:

- amorphous
- polycrystalline
- monocrystalline
- organic.

Nowadays amorphous solar cells are faded into the background, among other things, due to their low efficiency (5 – 8%). In the case of amorphous silicon solar cells, the silicon atoms are less ordered, and atoms are less attached to neighbours, like in the crystalline version. One of the advantages of amorphous silicon solar cells is that they are cheaper to produce than crystalline silicon cells, have thinner layers, thus they can be placed in rigid or flexible frames [5, 7]. They absorb more light, so their power decreases lesser in low-light, cloudy conditions than crystalline types. Among their disadvantages are the lower efficiency, and the degradation of efficiency by aging. The reason for this is the lower stability of amorphous silicon [6].

The use of polycrystalline solar cells is the most common among residential users. This is due to the fact, that they have the most favourable cost per produced energy. Price plays a very important role in the development of silicon based crystalline solar cells. The production of monocrystals is very expensive due to the technology. This led to the development of polycrystalline solar cells. The bottom line of the production of polycrystals, that the electronic grade silicon base material is melted and poured into a graphite crucible and crystallized under controlled cooling. Crystallization starts at several focal points and the solidified material becomes polycrystalline [6, 7].

Their efficiency can reach 18%, and this value is less dependent on the age of the solar panel. Manufacturers generally warrant staying the loss of efficiency within the 20% limit for 25 years [5, 7]. Crystalline solar cells can be easily recognized by their cellular structure, which cells

are galvanically coupled to one another and their combined power supplies the electricity of a solar module.

Monocrystalline solar cells produce the highest efficiency. However, their manufacturing technology is very expensive, so their popularity in the residential usage is less significant than the polycrystalline type. Crystalline silicon solar cells, and generally most semiconductor devices are made on a crystalline semiconductor chip, also known as a wafer. Their efficiency can reach 22% [5].

Organic solar panels are the youngest type of solar panels. Their development began in the last decade and has developed significantly during this time. As thin-film technologies, organic cells can be used to coat different surfaces like glass, metal, plastic, or can be print by using 3D printers. Another advantage of organic technology is that it is less sensitive to the angle of incidence of light, thus they are ideal for the not exactly southern orientation. They are also excellent for colouring and patterning. The most important promise, that they will be produced very cheaply, large surfaces will be coated with them, however this could not be proved in practice in the absence of large-scale production [7]. Organic solar panels are now seen as a major, untapped, environmentally friendly possibility for large energy and oil companies. Carbon-based organic polymer solar cells still operate at very low efficiency (<4%), however they were able to achieve 6% efficiency under laboratory conditions. Another disadvantage, that their production is relatively expensive compared to silicon based solar cells. In addition to the high price, there is another problem to be solved, which is their short lifetime. While conventional, crystalline and thin-film solar cells are sold with a 20- to 25-year performance guarantee, organic solar cells operate for 3 to 5 years based on current tests.

In fact, organic solar technology can be divided into two main groups:

- semiconducting organic polymers,
- dye-sensitised cells (DSC) [7].

Solar panels are manufactured in a variety of sizes. There are many categories ranging from the very small cell of a few mm^2 to the module of 1.6 m^2. The solar modules are made up of small cells, usually 100 cm^2 cells connected in series and parallel. While unit price per power in case of a 100 W monocrystalline solar cell is ~602 Ft/W, a polycrystalline solar cell with the same performance is only ~484 Ft/W. Because of this difference in value for money, polycrystalline solar panels are the best choice to use in solar cars. In addition, the dimensions of the solar panel can be selected depending on the location. It is advisable to install fewer but larger solar panels on the roof or engine hood.

Table 1. The parameters of the most commonly used monocrystalline solar cells

Power [W]	Operating voltage [V]	Dimensions [mm]
5	12	220x250x18
10	12	370x250x18
20	12	500x350x25
25	12	500x350x25
30	12	520x510x28
40	12	530x520x28
50	12	630x545x35
80	12	1080x545x35
100	12	1205x545x35
140	12	1480x680x35

Table 2. The parameters of the most commonly used polycrystalline solar cells

Power [W]	Operating voltage [V]	Dimensions [mm]
10	12	245x415x17
20	12	345x535x25
30	12	356x798x30
50	12	655x668x30
80	12	674x950x35
85	12	674x951x35
100	12	674x1131x35
130	12	674x1482x35
140	12	680x1479x35
150	12	674x1482x35
200	12	992x1488x35
250	24	992x1650x40
260	24	992x1640x40
270	24	992x1640x40

Table 2 contains the parameters of the most commonly used solar cells. 10 W polycrystalline solar panel (in uppermost row of Table 2) can generate only ~98 W of electricity per square meter (since the solar panel has a surface of ~ 0.1 m^2), while its value for money is ~895 Ft/W. On the other hand, the capacity per unit surface area of a 270 W solar panel (in undermost row of Table 2) is ~165 W/m^2, while its value for money is ~284 Ft/W. (The used values for money and values per unit surface area are informative average values given the large number of manufacturers and distributors.)

7. CONCLUSIONS

The source of our inspiration was the World Solar Challenge. However, these cars are one-man vehicles and not particularly suitable for daily use. Several companies and universities are already working to resolve this issue. Build a family car powered by solar panels.

Solar powered prototype is currently being developed by the Lightyear company and the German start-up Sono Motors. The Lightyear One is a large hatchback, with 5 m^2 of solar panels. The company Lightyear claims that the car can add 50–65 km of range per day during summer. It seats five adults and luggage.

The Sono Sion (Sono Motors) is an announced solar powered, electric car. The drive will be a three-phase induction motor with a power of 120 kilowatts (161 hp). The top speed of 140 kilometres per hour should be possible. The total area of photovoltaic modules is 7.5 m^2. The daily range gained in Central Europe is at a maximum of 34 kilometres a day under favourable conditions and on average over a whole year about 10 kilometres a day. The production of both vehicles is scheduled to start in 2021.

An induction motor can operate by being powered exclusively by the solar cell string through the DC / DC converter and inverter. The current is sinusoidal, so little torque pulsation occurs on the motor shaft. The solar panel on top of cars can run the motor only at very low power. Therefore, it is best, if only the battery is charged continuously by it. Another option is to supply the auxiliary circuit of the inverter, independently of the battery, from a solar panel. The auxiliary circuit may cover the control power of the IGBTs from the solar panel. IGBT modules require high control power in pulsed mode due to their Gate-Emitter capacity.

Consider an average-sized electric car with a consumption of 200 Wh/km and a roof area of 4 m^2. Ideally 350 W solar capacity can be placed on a surface of this size. On an average summer day, we can expect 3.5 kWh of electricity. This means that our car would ideally be able to cover 17.5 km with electricity from solar panels. Of course, this requires that the roof of the car (where the solar panels are located) is constantly shining by the sun. Annually, this small solar power plant can produce maximally 950-1000 kWh/year of electricity, which is enough to cover 4750-5000 km/year. The annual average is 13 km per day. It should not be overlooked, that the battery pack and electronic devices, charge controllers, and electric motor controllers have efficiency-reducing effect, which can reduce these theoretical distances.

8. ACKNOWLEDGMENT

"The described article was carried out as part of the EFOP-3.6.1-16-2016-00011 "Younger and Renewing University – Innovative Knowledge City – institutional development of the University of Miskolc aiming at intelligent specialisation" project implemented in the framework of the Szechenyi 2020 program. The realization of this project is supported by the European Union, co-financed by the European Social Fund."

9. REFERENCIES

[1] Parekh R.: AC Induction Motor Fundamentals (AN887), Microchip Technology Inc., 2003, p. 24.

[2] Kosmodamianskii A. S., Vorob'ev V. I., Pugachev A. A.: Scalar Control Systems for a Traction Induction Motor. Russian Electrical Engineering, 2016, Vol. 87, No. 9, pp. 518–524.

[3] Bilal A., Nishant, G.: Scalar (V/f) Control of 3-Phase Induction Motors, Texas Instruments, 2013, p. 25.

[4] Juhász Á., Láng I., Blaskovics GY., Mika J., Szépszó G., Horányi A., Dobi I., Nagy Z.: Megújuló Energiák. Sprinter Kiadói Csoport, Budapest, 2009.

[5] Ferenczi Ö.: Áramtermelés nap- és szélenergiából. Budapest, 2007.

[6] Nemcsics Á.: A napelem és fejlesztési perspektívái, Budapest, 2001.

[7] Dr. Bodnár I.: Napelem működésének alapjai, a napelemes villamosenergia-termelés elmélete és gyakorlati megvalósítása. Miskolci Egyetem, 2019. p. 108. ISBN 978-615-00-4566-5.

[8] Retter Gy.: Az egységes villamosgép elmélet. 1970. p. 243.

KÜLÖNBÖZŐ AUTÓIPARI CSAPÁGYAK ELEKTROMÁGNESES KOMPATIBILITÁSI HATÁSAI

ELECTROMAGNETIC COMPATIBILITY EFFECTS OF DIFFERENT BEARINGS IN AUTOMOTIVE INDUSTRY

István Bodnár Ph.D., Rafael Ruben Boros, Dániel Erdősy

ABSTRACT
The effects of different bearings on EMC might be an uncommon idea, but in electric motors, it can be the source of unwanted electromagnetic radiation. This article is about a BLDC motor, where only with different type of bearings we could achieve decreasing of radiated electromagnetic waves. As this motor is part of a cooling fan for automobiles, we should consider other automotive applications. BLDC motors are widely used in modern vehicles, due to several advantages, but EMC might be their biggest issue in some applications if they are not properly designed.

1. INTRODUCTION

As a part of a bigger project, we were analysing an automotive cooling fan module. For us, EMC of the driving motor was in spotlight, but we should have work and consult with colleges with other specialization in order to achieve the best results. In this article a brief summary is about BLDC motors in general to learn about its working principle, then another short section is about EMC and finally our measurement method and results are written, we made on the mentioned driving motor.

2. BLDC MOTORS

BLDC motors are a type of synchronous motor. This means the magnetic field generated by the stator and the magnetic field generated by the rotor rotate at the same frequency. BLDC motors do not produce “slip” that is normally seen in induction motors. BLDC motors come in single-phase, 2-phase and 3-phase configurations. Corresponding to its type, the stator has the same number of windings. Out of these, 3-phase motors are the most popular and widely used [1].

A brushless motor is constructed with a permanent magnet rotor and wire wound stator poles. Electric energy is converted to mechanical energy by the magnetic attractive forces between the permanent magnet rotor and the rotating magnetic field induced in the wound stator poles. *Figure 1.* shows a simplified illustration of BLDC motor construction.

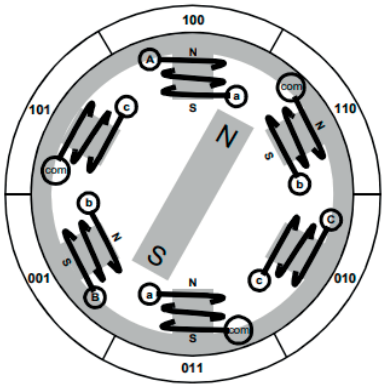

Figure 1. Simplified BLDC motor construction [2]

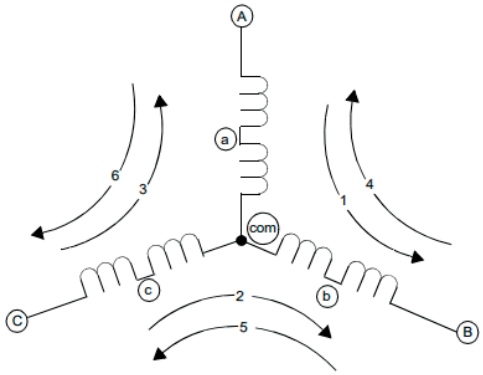

Figure 2 Three-phase windings with terminals [2]

Most BLDC motors have a three-phase winding topology with star connection. A motor with this topology is driven by energizing two phases at a time. The three-phase winding is feed by a three-phase inverter and the electronic commutation is implemented also by the inverter. *Figure 2.* shows the three-phase windings in star connection and the terminal names which are corresponding to *Figure 1.* Three-phase

motors are better than two-phase design, because the rotating magnetic field is much more symmetrical. The three-phase windings make less EMC noise.

The rotor is made of permanent magnet and can vary from two to eight pole pairs with alternate North (N) and South (S) poles. Based on the required magnetic field density in the rotor, the proper magnetic material is chosen to make the rotor. Ferrite magnets are traditionally used to make permanent magnets. As technology advances, rare earth alloy magnets are gaining popularity. The ferrite magnets are less expensive, but they have the disadvantage of low flux density for a given volume. In contrast, the alloy material has high magnetic density per volume and enables the rotor to be compressed further for the same torque. Also, these alloy magnets improve the size-to-weight ratio and give higher torque for the same size motor using ferrite magnets. Neodymium (Nd), Samarium Cobalt (SmCo) and the alloy of Neodymium, Ferrite and Boron (NdFeB) are some examples of rare earth alloy magnets. Continuous research is going on to improve the flux density to compress the rotor further.

Unlike a brushed DC motor, the commutation of a BLDC motor is controlled electronically. To rotate the BLDC motor, the stator windings should be energized in a sequence. It is important to know the rotor position in order to understand which winding will be energized following the energizing sequence. Rotor position is sensed using Hall effect sensors embedded into the stator.

Most BLDC motors have three Hall sensors embedded into the stator on the non-driving end of the motor. Whenever magnetic poles of the rotor pass near the Hall sensors, they give a high or low signal, indicating the N or S pole is passing near the sensors. Based on the combination of these three Hall sensor signals, the exact sequence of commutation can be determined.

The Hall sensors increase the price of the motor. The sensors can leave, if we measure the motors back EMF. When a BLDC motor rotates, each winding generates a voltage known as back Electromotive Force or back EMF, which opposes the main voltage supplied to the windings according to Lenz's Law. The polarity of this back EMF is in the opposite direction of the energizing voltage.

2.1. The analysed BLDC motors

The motors of our project (*Figure 3.* shows) compliance the required emission rates, but in stricter conditions, for example in electric vehicles electromagnetic (EM) radiation of them should be reduced.

It has two phase winding, which is not the best choice if EMC is important. Next to the winding, the rotor has permanent magnets, 5 of them which can cause not some mechanical but also magnetic issues, because they are not so close to each other and the magnetic flux lines are not evenly distributed inside the rotor. The control electronics are on the back side, on a baseplate, which is also used for mounting the motor onto the whole fan assembly. The controlling here works with back EMF, so our motor doesn't contain Hall sensors [3].

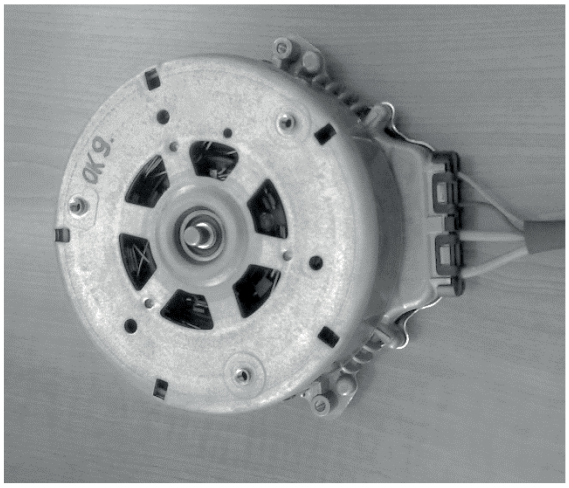

Figure 3 The driver BLDC motor of the cooling fan module

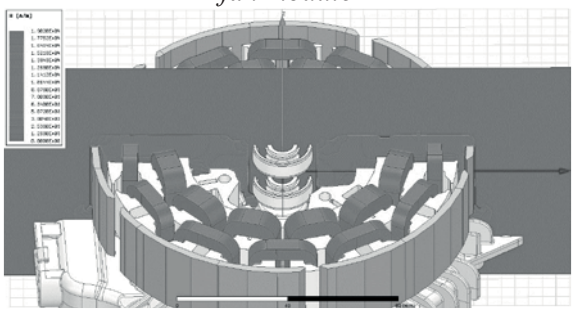

Figure 4 3D FEM analyses on the BLDC motor

It needs 12 V DC power and a simple 100 Hz PWM signal with 15-90% duty cycle to set the RPM. The rotor is connected to the shaft of the stator with a simple ball bearing. Before we have made modification plans, we had had to carefully analyse the source of the radiated electromagnetic waves. We also made 3D FEM

analyses of the motor (*Figure 4.* shows), so we could learn more about the electromagnetic fields and how they change if we modify the motor.

Next to changing other parameters and parts, we made a choice to try other type of bearings. Different types of bearings have different electric conductivity, which is important for us, because of the shape of the rotor. The metal part of the rotor may work like an EM shielding, but if it is not properly connected, it causes other, unwanted problems. Charges can amass on the metal surface which, like a capacitor, can discharge in short periods, causing high frequency EM waves. The precision of the bearings influences the air gap between the rotor and stator, and magnetic flux could "escape" the motor, causing low frequency magnetics problem [4].

3. SHORTLY ABOUT EMC

Every electronic device radiates electromagnetic waves. Some of them might malfunction from a higher level of other devices radiation. These two properties are called electromagnetic compatibility or EMC. Emission rates, EM immunity and the different measurement methods are restricted by local and international standards. In automotive industry CISPR 25, CISPR 12 and ISO 11452-2 are the most important restrictions [5, 11, 12]. Engineers must make their plans, factories must produce devices, EMC laboratories must measure in a way, just like the restrictions say.

All kind of electric motors have different EMC problems. It depends on the size, the required voltage type, having brushes or not, how speed controlling work, how the stator and rotor produce the magnetic field, what materials are used in the construction and so on. We had a BLDC motor, which type has major advantages. The main reason it is used more frequently nowadays, the lack of brushes and wide variety of size and power, but it needs an electrical commutation, which can have EMC problems.

4. MEASURING TECHNIQUES AND RESULTS

We made the comparison measurements with the following settings and methods.

Evaluation method:

- Radial and axial measurements
- Horizontal and vertical antenna polarity
- The distance between the EUT (Engine Under Test) and the antenna is exactly 30 cm
- Duty cycle of the controlling PWM signal: 0%, 25%, 50%, 70%, 90%
- Measurement frequency range: 100-1500 kHz
- Evaluated frequency range: 900-1100 kHz
- 4 distinct frequency have been chosen to evaluate the amplitude: 900 kHz, 966,667 kHz, 1033,33 kHz, 1100 kHz
- In the examined frequencies RMS (Root Mean Square) value of the amplitude is calculated (1)
- We calculated the ratio between the RMS values of the original EUT and the modified EUT. It's marked with "H". If H<1, then the modification made an improvement, if H is about 1, there were no improvement and if H>1, that means the modified version performed worse.

$$RMS = \sqrt{\frac{1}{N} \cdot \sum_{i=1}^{N} x_i^2} \qquad (1)$$

where *RMS* is Root Mean Square, N is the number of samples, i is the index number, x_i is the i-th value of x.

We made 24 different measurements on each EUT (4 different antenna arrangement and in one arrangement 6 different RPM). We created a specific excel sheet in order to do the mathematical calculations. We used only the data required for our evaluation method, because the measurement makes almost 15000 data points per EUT.

EMC measurements require precise measurement methods and equipment, showed on *Figure 5.*

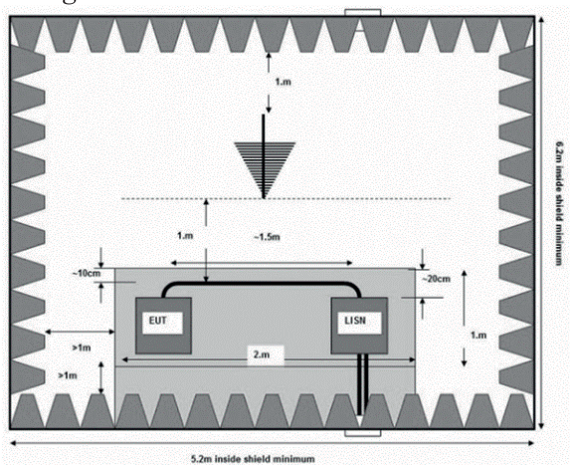

Figure 5.: Proper automotive EMC test method according to CISPR 25 [9, 10]

Our measurements were made in our EMC laboratory. This lab is owned by the University of Miskolc, Institute of Physics and Electrical Engineering, Department of Electrical and Electronic Engineering. It is in building A3, on the basement floor. This lab is not an accredited, proper EMC laboratory, but it has a good electromagnetic shielding, and we made our best to build the required test conditions. It must be mentioned that the later detailed measuring data is only for reference, it can't be used for qualification purposes. At earlier stages we used an old PMM 7000 emission precompliance system, but the lack of the suitable antenna and software support, we decide to use a more modern device [6].

We used a handheld spectrum analyser FSH-8 from Rohde & Schwarz for the measurements and a computer to collect the data with. The antenna was a HE300HF antenna. Its frequency range is from 9 kHz to 20 MHz [7, 11]. Other test equipment was an oscilloscope (to set the control PWM signal precisely), a simple analog PWM signal generator, a car battery (for supply DC power for EUT). The EUT was mounted with wooden blocks on a metal plate covered wooden table. The covering plate was grounded. We made an extra grounding pole into our lab to increase the grounding properties in order to achieve higher shielding factors [8]. One of the measurement arrangements is showed on *Figure 6.*

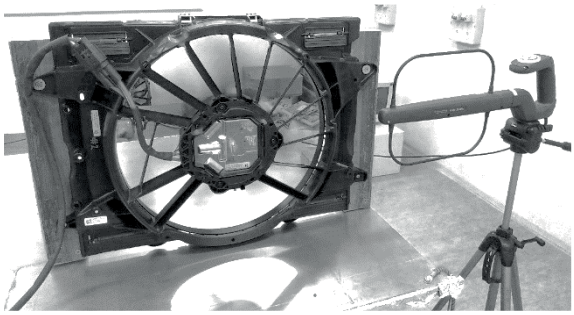

Figure 6.: Cooling fan module (EUT) under measurement

The results of our measurements lead to the fact, that in the radial direction modules produce less electromagnetic radiation in the full examined frequency range. Due to this fact, we used the axial directional data when comparing different modifications and modules. We made another simplification, not to use the horizontal data, because vertical radiation was much more intense at all modules.

(We made all the measurements, but at the final evaluation we used only the limited data). According to the usage of these modules, important PWM duty cycles are 25%, 70% and 90%, so we could ignore more data. All these considerations result in a massive decrease of evaluated data points. From the 15000 collected data, we only had to analyse 270. The settings of the spectrum analyser are in *Table 1.*

Table 1.: Applied settings on FSH8

Settings	Value
Middle Frequency	800 000 Hz
Frequency offset	0 Hz
RF dampening	manual
RF dampening	0 dB
Preamp	ON
RF input	50 Ohm
RBW	10 000 Hz
VBW	100 000 Hz
Sweep time	200 ms
Type of measurement	Average
Detection method	RMS
Primary transducer	HE300A-HF
Number of averages	10

The original module contains ball bearings. Modifications were used to test different bearing types (3 different types from the original).

Name of the analysed samples:

- **A0, B0, C0 samples**: these were original products, each of them has been modified after the measurement.
- **A1 sample**: modified with higher grade precision bearing
- **B1 sample**: modified with needle roller bearing
- **C1 sample**: modified with angled bearing

*Table 2.: Normalized amplitude of electromagnetic emission of **A0 sample***

[dBµV/m]	PWM		
Frequency [Hz]	**25%**	**70%**	**90%**
900 000,00	8,591	15,425	2,379
966 666,67	7,675	16,324	2,503
1 033 333,33	8,201	16,601	1,482
1 100 000,00	7,307	17,121	1,603
RMS	6,800	15,361	1,934

*Table 3.: Normalized amplitude of electromagnetic emission of **A1 sample***

[dBµV/m]	PWM		
Frequency [Hz]	**25%**	**70%**	**90%**
900 000,00	7,646	11,736	1,412
966 666,67	6,385	14,747	1,399
1 033 333,33	7,515	15,966	2,429
1 100 000,00	8,442	14,285	2,424
RMS	7,322	13,854	2,104

Table 4.: Emission ratio between the original (A0) and modified (A1) modules

Ratio	PWM		
Frequency [Hz]	**25%**	**70%**	**90%**
900 000,00	0,890	0,761	0,594
966 666,67	0,832	0,903	0,559
1 033 333,33	0,916	0,962	1,638
1 100 000,00	1,155	0,834	1,512
RMS	1,077	0,902	1,088

*Table 5.: Normalized amplitude of electromagnetic emission of **B0 sample***

[dBµV/m]	PWM		
Frequency [Hz]	**25%**	**70%**	**90%**
900 000,00	8,724	13,492	2,908
966 666,67	9,385	16,785	3,656
1 033 333,33	9,887	14,304	3,551
1 100 000,00	7,651	14,322	2,617
RMS	7,516	14,094	3,176

*Table 6.: Normalized amplitude of electromagnetic emission of **B1 sample***

[dBµV/m]	PWM		
Frequency [Hz]	**25%**	**70%**	**90%**
900 000,00	6,719	15,894	2,554
966 666,67	8,294	13,124	3,081
1 033 333,33	8,893	13,520	2,056
1 100 000,00	7,195	14,925	2,674
RMS	6,912	13,016	2,567

Table 7.: Emission ratio between the original (B0) and modified (B1) modules

Ratio	PWM		
Frequency [Hz]	**25%**	**70%**	**90%**
900 000,00	0,7702	1,1780	0,8782
966 666,67	0,8838	0,7819	0,8428
1 033 333,33	0,8995	0,9452	0,5791
1 100 000,00	0,9404	1,0421	1,0219
RMS	0,9196	0,9235	0,8083

*Table 8.: Normalized amplitude of electromagnetic emission of **C0 sample***

[dBµV/m]	PWM		
Frequency [Hz]	**25%**	**70%**	**90%**
900 000,00	9,207	14,327	2,628
966 666,67	8,609	15,133	3,042
1 033 333,33	10,352	15,261	3,098
1 100 000,00	9,767	15,297	3,793
RMS	8,110	13,553	3,006

*Table 9.: Normalized amplitude of electromagnetic emission of **C1 sample***

[dBµV/m]	PWM		
Frequency [Hz]	**25%**	**70%**	**90%**
900 000,00	6,129	11,317	2,078
966 666,67	5,949	13,888	5,345
1 033 333,33	6,704	14,889	2,029
1 100 000,00	6,684	13,062	2,086
RMS	5,740	12,282	2,687

Table 10. Emission ratio between the original (C0) and modified (C1) modules

Ratio	PWM		
Frequency [Hz]	**25%**	**70%**	**90%**
900 000,00	0,6657	0,7899	0,7908
966 666,67	0,6910	0,9177	1,7570
1 033 333,33	0,6476	0,9757	0,6547
1 100 000,00	0,6843	0,8539	0,5499
RMS	0,7077	0,9062	0,8938

With the acquired data we could calculate an approximated measurement error and determine the linear and RMS value of changes. *Table 11.* shows that measurement error was less than 2% at all measured modules, furthermore negative percentage means that underestimation is common.

Table 11.: Results of the evaluation method

	„A”	**„B”**	**„C”**
Approximated error percentages	-1,036%	-0,653%	-1,947%
Linear value of changes	-4,37%	-9,83%	-17,66%
RMS value of changes	-7,46%	-8,74%	-15,68%

From linear and RMS changes, RMS values are more representative due to our evaluation method mentioned before. Signs in these rows shows the direction of change, so a negative sign means improvement. The results show

that C1 sample performed the best, so the angled bearings have the best EM emission levels.

Higher grade precision bearings in A1 sample worked well, because it produced a better dynamical balancing, which affect the EM radiation. Airgap between stator and rotor can change less due to the better balancing, so magnetic force lines scatter less. Needle roller bearing and angled bearing can decrease not only the dynamic balance, but also improve conductivity between the stator and rotor.

This reduces the shock-like electrical pulses between the two parts, which significantly reduces the pulsing EM emission. As a result, time-based emissions are also reduced.

5. SUMMARY

The goal of the whole project is to reduce the EM emission rates of this automotive cooling fan module. The driving BLDC motor have minor EMC problems and this article was about only one part, the ball bearings. We tried different type of bearings and as a result we can say that it is possible to reduce electromagnetic noise by changing the bearings in this motor.

6. ACKNOWLEDGMENTS

"The described article/presentation/study was carried out as part of the EFOP-3.6.1-16-2016-00011 "Younger and Renewing University – Innovative Knowledge City – institutional development of the University of Miskolc aiming at intelligent specialization" project implemented in the framework of the Széchenyi 2020 program. The realization of this project is supported by the European Union, co-financed by the European Social Fund."

"This research was supported by the European Union and the Hungarian State, co-financed by the European Regional Development Fund in the framework of the GINOP-2.2.1-15-2017-00090 project, titled „E-mobility from Miskolc: Improvement of Coolant Pump and Engine Cooling Fan Taking into Account the Higher Quality Requirements in Electric Vehicles"."

7. LITERATURE

[1] Yedamale P.: Brushless DC (BLDC) Motor Fundamentals (AN885), Microchip Technology Inc., 2003, p. 20

[2] Ward Brown, Brushless DC Motor Control Made Easy (AN857), Microchip Technology Inc., 2011, p. 48

[3] Rejtő F.: EMC alapok. Magyar Elektrotechnikai Egyesület, Budapest, 2006. p. 260.

[4] Iványi A.: Hysteresis models in electromagnetic computation. Budapest, 2007.

[5] Automotive EMC Testing: CISPR 25, ISO 11452-2 and Equivalent Standards

[6] Szűcs L.: RF zavarkibocsátás és zavarérzékenység mérés. Mérési segédlet, Budapesti Műszaki és Gazdaságtudományi Egyetem, 2002. p. 13.

[7] EMCO: Antenna Catalog. Austin, Texas, USA, 2000.

[8] Varga A.: Grundlage des Elektrosmogs in Bildern. Verlag Umwelt + Medizin, Heidelberg, 2002. p. 155.

[9] ISO-11452 Road vehicles — Component test methods for electrical disturbances from narrowband radiated electromagnetic energy — Part 2: Absorber-lined shielded enclosure Second Edition 2011-11-01

[10] CISPR 16-1-4 Specification for radio disturbance and immunity measurement apparatus and methods Part 1-4 radio disturbance and immunity measuring apparatus – Antennas and test sites for radiated disturbance measurements. 3rd Ed. IEC Geneva, Switzerland 2010.

[11] Bruns C., Leuchtmann P., Vahldieck R.: Analysis of a 1-18GHz Broadband Double-Ridge Antenna, IEEE Transactions of Electromagnetic Compatibility, Vol 45, No. 1, 2003. pp.55-60.

[12] Rodriguez V.: New Broadband EMC double-ridge guide horn antenna. RF Design. May 2004, pp. 44-50.

TERMÉKFEJLESZTÉSI FOLYAMAT ELEMZÉSE ÉS ÉRTÉKELÉSE

ANALYSIS AND ASSESSMENT OF THE PRODUCT DEVELOPMENT PROCESS

Soltész László, Berényi László**, Kamondi László****
** PhD student, István Sályi Doctoral School, University of Miskolc*
*** PhD, associate professor, Institute of Management Science, University of Miskolc*
**** PhD, honorary professor, Institute of Machine and Product Design, University of Miskolc*

KIVONAT
Új termék kifejlesztése az innovációval foglalkozó vállalatok egyik legnehezebb folyamata, ám ez a versenyképesség legfontosabb forrása. Számos megközelítés és módszer létezik innovatív tartalommal ellátott projektek végrehajtására. Ez a cikk elemzi a termékfejlesztési folyamatot a multinacionális ipari környezetben. A kutatás célja a termékfejlesztési folyamat kritikus pontjainak meghatározása a hatékonyság javításának érdekében, a várt eredmények elérése vagy túlteljesítése. Fontos továbbá a termékfejlesztés sikertényezőinek azonosítása, mivel ez lehetővé teszi a fejlesztési tevékenységek hatásának fokozását. A cikk a termékfejlesztés feltételezhető sikerének és akadályozó tényezőinek feltérképezésére összpontosít.

ABSTRACT
Developing a new product is one of the most challenging processes of companies dealing with innovation. However, it is a major source of competitiveness. There are several approaches and methods for delivering innovative content of the projects. This paper analyzes the product development process in a multinational industrial environment. The purpose of the research is to find the critical movements of the product development process with regard to the efforts to improve its efficiency and deliver or over-deliver results that are expected. Moreover, it is also essential to identify the success factors of product development since it allows enhancing the impact of the development actions. The paper focuses on mapping the presumable success and hindering factors of product development.

1. INTRODUCTION

Product innovation and competence of innovation are the key success factors for every modern industrial company. McKinsey Corporation found a clear relationship between innovation activities and business success [1]. Companies must continuously find new and newest ways for creative and cost-efficient solutions to keep their competitiveness. Usually, purchasing and product development departments are working together to manage the changes and to implement cost-savings in running production. Beyond these efforts, a big challenge is maintaining or improving the quality of products. Several perspectives are considered during this process to be successful. This paper presents the interrelation between the departments for managing an environmentally friendly, effective product development project in the sustaining engineering phase to deliver benefits to the company by cooperation.

2. OVERVIEW OF PRODUCT DEVELOPMENT PROCESS

The mainstream approaches to product development come from VDI 2221 and 2222 structure of product development during the analysis of the product development process. In a broader approach, checking the concept of process in a more traditional way, the definition of Deák [2] is applicable (Figure 1), which states that product development delivers an idea to customers.

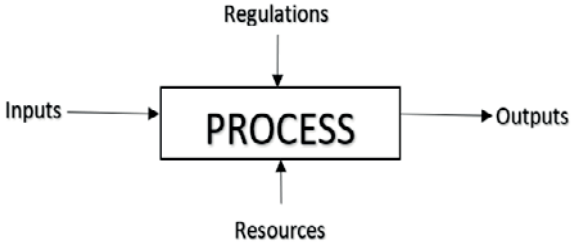

Figure 1. Process and connections [2]

Otherwise, delivering time, cost, quality 'magic triangle' (Figure 2) is usually overweighed in product development departments [3]. Measurement of the performance of product development teams is usually built up for the cost, quality, time triangle. During the regular review of the related indicators, and the introduction of PDCA according to the lean approach, it continuously

will provide a performance increase at the delivery of projects. However, this performance can be presented by delightful and satisfying figures in business overview dashboards, and the line management cannot see a real evaluation of the innovation level of the products.

Figure 2. Product development triangle [5]

3. EMPIRICAL ANALYSIS OF PRODUCT DEVELOPMENT PROJECTS

The next sessions of the paper give an empirical overview of the product development projects based on the experience of the authors.

This analysis emphasizes how industrial companies can handle the cost, quality, and time triangle in practice (Figure 2). A general approach to the process shows that critical points awake in the progress when the importance of these three elements are in focus, but parallel, there are rooms for changes at all three elements.

3.1. Product development triangle: Cost

The most important goal of companies with industrial products is to support their customers to increase their performance [4]. Cost planning is a key element of product development projects already from the start. After accepting the design concept, a predictive cost calculation is prepared by the project manager (with or without the involvement of designers and other interested parties).

During the project acceptance meetings, the cost and payback calculations are in the focus of management. The match of costs, business case calculation, and payback with each other is an essential topic of these meetings. If accepted, the figures are built into budgeted investment plans for the timeline of projects.

A great challenge for the managers of product development projects is keeping the cost plan, and changing it during milestone meetings if necessary. However, the cost calculation in this project phase is only a preliminary one. Most of the management teams of industrial companies want to keep this 'promised' cost plan until the end of the project.

Otherwise, in the finish of the project planning, a time plan must be saved, but different difficulties during the development project with an effect on cost. The planned and achieved figures can become irrelevant to compare with each other, especially in the case of possible turnover losing due to the late step into the market with a new product or technical changes of the product.

3.2. Product development triangle: Time

To introduce a newly developed, innovative product into the market is a necessary condition for successful companies as McKinsey proves that via researches [1]. The success of a company is measured by both the management and the investors/stock market through various financial indicators. If we predict that a product will be successful on the market – according to previous market researches and tests –, the product development schedule becomes a key factor of the product development triangle. In other words, the late of the project (not keeping the original time plan) leads to a delay in the market introduction and causes lost profit.

During the project planning phase, the project manager should focus on administrative details, including time plan and cost calculation. The task of the design engineering team is to deliver verified technical solutions that we can see in Figure 2 as the scope.

Finally, during project planning, the project manager should find a great balance between cost (resource use) and timing. In the right case, product strategy and profitability together can define perfectly or at least the best deliverable and the project timing plan, considering the available resources by the company. Within a product development project, attention, and influence of management to project timing are varying. This attention is quite intensive at the beginning of the project, and it becomes lower during the execution phase. The next peak of attention comes during the verification and implementation phases [6]. In these phases, delays due to non-predicted issues during verification or further necessary design changes cost, especially if a timing dual leads to an extra resource need.

3.3. Product development triangle: Quality

Product scope is specified first, followed by milestones and market research phases. In front-loaded product development projects, the scope and customer requirements are well-defined and carefully researched, as well as verified by different control groups. The main objective of the product design engineers is to fulfill this specification for satisfying future consumers. Parallel delivery of technical specifications and special capability of the company must be considered, like production capabilities, available technologies, raw materials, or cost-effective solutions.

Product quality strictly belongs to product specification, but it is a different topic. Several years ago, high-level quality (according to consumer requirements) was a remarkable advantage in the market and supported the companies to improve their market share, turnover, and profit [8].

Nowadays, market situations with a large number of competitors raise different problems. A high level of quality is just a 'must' but not an advantage. During the execution of the project, there is no way to make any concession of quality, the only way to change timing or cost if any fine-tuning is necessary even lightening of quality level can be an easier way to deliver product development project.

4. INTRODUCTION OF A PRODUCT DEVELOPMENT PROJECT IN PRACTICE

This study shows an industrial product development process. The reason for product development, specification, and requirements of market and company management for the project will be understood in detail. An accurate description of the product and its specifications is not recognizable in this paper due to privacy and disclosure reasons.

4.1 Project definition

Product development targets were in this analyzed project to solve three topics against available product via redesign and modernize product:

- solving delivery disturbances;
- cost-saving;
- reducing dependence from external conditions.

The subject is a new product family of an industrial product that makes regulation, control, and operation function in automation assemblies. The products are combined with electrical and mechanical components converting the electric controller signal to mechanical signals. Two versions of the products were designed with different voltage and power level versions. In both cases, speed is highly important since it influences the working speed of the total system. These are measured in the test laboratory within the company.

4.2 Project targets, specification

The most important goal of companies producing industrial products is to help their customers to increase their performance [4]. That is why the main properties of the new product family were defined at the start of the development process as key factors for customer's performance increase:

- speed;
- environmental efficiency;
  - energy efficiency;
  - stable operation;
  - usage of less packaging (replacing supplier import);
  - design for assembly/automation;
  - cost-savings.

The product operates on a medium scale of input mechanical driving input; however, it is able to operate and control the higher limit value of mechanical input. This means that the product can work on lower level input that is not the same as the input level in the executing system.

The most important market advantage of the product compared to similar products is the short working time, operation speed (Table 1).

Table 1. Speed comparison

Version	Working speed new product [ms]	Working speed average competitors [ms]
Version 1	15	25
Version 2	20	35

4.2 Product design details

The goal of the company is to serve the customers with the required quality and innovative solutions created with the optimal extent of energy investment. Besides, to set an example with the quality of the work on the domestic and national market with our intention to help the Hungarian industry and economy. Therefore, European industrial and automotive standards were satisfied by involving and develop a product. In the year of product development, the company reacted to the actual customer needs high speed, robust design, high level of reliability since the products were popular and were requested in a large quantity by the heavy industries.

In both cases (Version 1 and Version 2),

the manufacturing process happens in our Hungarian factory, and no external supplier is needed anymore. As a result, the manufacturing cost of the products got significantly lower as well as the material flow got more simple. In the case of Version 1 product, the material of the house is black surface treatment metal. Internal parts are also made from light metals, which guarantees the resistance and the long lifetime of the parts against corrosion and the extreme temperature intervals.

The house of Version 2 product is made of glass-fiber reinforced plastic, and the parts are produced of light metals. The lifetime of products is measured in actuating cycles. The guaranteed value is several million cycles for both versions.

Considering the stress tests, a triple safety factor is applied in both versions, which means that for a short period of time, they can bare three times the maximal operating load. As a result of the Version 1 valve development, on maximum operating load, it grants a more stable and more reliable function than before. The usage of the product is relevant because it is used as a control actuator in the high flow-rate systems in heavy industry. A high level of usage comes from the ship and train industry.

4.3. Verification

During the design of the construction and the functional structure of the product, consumer interest was a primary aspect. The product has a wide range of consumers, i.e., the usage has various locations, temperature ranges, and functioning mediums. The product has to stand against climate impacts and disturbing factors, including high temperature, low temperature, vibration, salt-saturated medium.

From a design point, these outer impacts during the functioning of the product have to be considered. Product Version1 and Version 2 also have a lower function range of -50°C, and the higher function range is +85°C. In the case when products work on this low or high temperature, we cannot neglect the importance of the testing phase. In order to guarantee the customers the functioning of these extreme temperature ranges, in the company, there is an officially developed and investigated testing laboratory is in service, where testing engineers are working to create a product with better quality. Even satisfying special non-series needs, they are testing the half-done products, in a simulated, close to real-life circumstances. Therefore, eliminating the errors occurring during function and raising safety. It is to confirm that different tests with one test plan template and one test record sheet example. The record sheet displays the function speed of the running system, using a Product developed.

4.4. Market situation

Regularly, the product is produced for the domestic market in the normal product life-cycle in the ramp-up phase, and after sufficient marketing and manufacturing knowledge is built up, the international market introduction is targeted [7]. Because the predecessor product was available in Europe at the beginning of developing Product, the product family of Product has shown the potential to improve, based on former functions and inner customer feedback. Therefore, we took a commitment to improving them further, as well as to create new ones. The results are the current Version 1 and Version 2 products. The new Product shows improvement in several features (e.g., reliability, speed) contrary to its predecessor. Therefore, the expansion of the market segment is expected by the company both in internal and foreign areas, even where former products were not in a competitive position.

5. RESULTS OF PRODUCT DEVELOPMENT PROJECT

By the analysis of this special Product Development project following weak points of the process were found.

5.1 Database of product design lessons

At every product development case, a mandatory session is to analyze the design of similar products to see design solutions. This requirement also managed by the ISO 9001 standard too. In practice, both the own products and competitors are regularly revised by the designer. All companies are focusing on building up design lesions or best practice databases to provide available design information from the past for new product development projects and especially for design engineers.

However, in every case, these databases are available and available to designers; they usually find it difficult to search in. Design issues are not always clear because past designers are not interested in supporting future research in the database. Another problem comes up if the author of learning in the database is not available for discussion anymore.

These points establish an uncertainty of usage of lessons from previous design works to avoid similar design-related failures in the future.

5.2 IT environment for product development

IT systems for product development are inevitable for successful, efficient delivery of projects. From project management tools, during Product Lifecycle Management (PLM) systems until design lesson databases. Via analysis of projects, some bottlenecks were popping up.

5.2.1. Change management systems

Change Management System is an important tool to provide enough information for production about technical changes in product development. This tool can be combined with the PLM system and MRP (Material Requirements Planning) systems on a professional level. Change management mandatory to use by Sustaining Engineering after product introduction into production when any undocumented changes can cause difficulties in operation systems and/or quality issues. Between milestones of production start and ramp-up phase before design ownership handover by Sustaining Engineering necessity of Engineering Change management is questionable. Product Development project members (product designers) are not entirely familiar with the Engineering Change Management system because, in routine work, they do not have to use. Otherwise, in the case of products already in mass production, the Bill Of Material and other technical documents are released as mandatory to documentation.

6. SUMMARY

Critical points awake in the progress when the importance of these three elements are in focus, but parallel, there are rooms for changes at all three elements. In the right case, product strategy and profitability will define perfect or at least the best deliverable project time plan considering available resources by the company Introduced Product development study has shown that new products took over the position of the predecessor. In several aspects like producibility, economy, energy efficiency, and environmentally friendly solution can overdeliver original product to fulfill the requirement of company management. Customers will be satisfied with stable working in a hard environment in a heavy industry area parallel high speed and quick reaction time. Especially excellent achievement to execute this design work with the focus for manufacturing. This project, according to the required specification, quality, business case, timing point of view, is successful. During the analysis of the project, two critical points were defined, as the efficiency of the lesson database and change management system just before design handover to sustaining engineering from new product development engineers.

7. REFERENCES

[1] MCKINSEY GLOBAL SURV. RESULTS: R&D in the downturn, (2009), pp. 1-7

[2] DEÁK CS.: *Innovációmenedzsment kutatás és gyakorlat*: *Folyamatmenedzsment, folyamatinnováció*, Miskolci Egyetem, Innovációmenedzsment Kooperációs Kutatási Központ, Miskolc, 2007

[3] VIELHABER M., BERGSJÖ D., CATIC A.: Mechatronic Systems Engineering – Theory and Automotive Practice. In: Marjanovic D., Storga M., Pavkovic N., Bojcetic N. (Eds.): DS 60: Proceedings of DESIGN 2010, the 11th International Design Conference, Dubrovnik, Croatia, 2010, pp. 975-984

[4] KÄRKKÄINEN H., PIIPPO P., TUOMINE, M.: Ten tools for customer-driven product development in industrial companies. International *Journal of Production Economics*, Vol. 69, No. 2, (2001), pp. 161-176. https://doi.org/10.1016/S0925-5273(00)00030-X

[5] CACCAMESE A., BRLAGANTITNI D.: Beyond the iron triangle: year zero. Paper presented at PMI® Global Congress EMEA, Marsailles, France. Newtown Square, PA: Project Management Institute, 2012

[6] BITZER M., EIGNER M., LANGLOTZ M.: Management decision support by PLM solutions. In: Bocquet, J. C. (Ed.): DS 42: Proceedings of ICED 2007, the 16th International Conference on Engineering Design, Paris, France, paper DS42_P_462, 2007, ISBN 1 904670 02 4

[7] WORTMANN J. C., MUNSTLAG D. R., TIMMERMAND P. M. J.: *Customer-driven manufacturing*, Chapman & Hall: London, 1997, ISBN 0-412-57030-0

[8] ERDEI J., KÖVESI J., TOPÁR J., TÓTH ZS. E.: *A minőségmenedzsment alapjai*, TYPOTEX Kiadó, Budapest, 2006, ISBN 963 9664 11 1

JÁRMŰ MIKROKAPCSOLÓK GYORSÍTOTT ÉLETTARTAM VIZSGÁLATA

METHODS FOR ACCELERATED LIFE TESTING OF MICRO SWITCHES IN VEHICLES

Vivien Sipkás, PhD student, University of Miskolc, machsv@uni-miskolc.hu
Gabriella Bognár, Prof. Dr., v.bognar.gabriella@uni-miskolc.hu
University of Miskolc, Institute of Machine and Product Design

ABSTRACT
Our aim is to obtain reliable test results for determining the product's life cycle of micro switches. The requirement producing products with high reliability have increased the need for testing of components. Systems generally require system components having predetermined reliability during a determined time. It is difficult to assess reliability with traditional life tests recording only failure times. A relationship between component failure and operational conditions makes it possible to use accelerated models and to predict failure-time distribution. In addition, we use the factorial experiment design method to design the tests. Our goal is to use this to draw conclusions about product life.

1. INTRODUCTION

In everyday life, we often come across micro switches, and this is no different for vehicles. In passenger cars, several functions can be operated with the help of micro switches, such as the index, the hazard warning button and various functions on the dashboard.

The topic of the research is the investigation of accelerated lifetime data of micro switches. The micro switch test bench designed for this purpose can test four products at the same time [4, 5]. The tests reveal the operating conditions under which a higher load than normal load can be applied. The design, operation and testing process of the apparatus have been previously described. In this article we introduce the basics of experimental design methodology and how we can analyse the investigated structural elements using the experimental design methodology.

The constant evolution of the market requires the development of more innovative products than ever, all of which must be performed with ever-increasing technological content and in record time, while improving productivity, product reliability and quality. Nowadays in the industrial practice, traceability is becoming more and more important, as customers demand not only high quality but also its professional proof. There are several experimental design methods for controlling these processes, so many industries are using experimental design methods to test the quality of processes and products. The basics of experimental design were made possible by Ronald Fischer's statistical analyzes. The common methods can be divided into three groups *(Table 1.*) [1-3].

Table 1. Classification of statistical experiment design types

Factorial plans
• Chane factor level one by one
• One factors
• Group factors
• Full factorial
• Partial factorial
• Shainin
• Taguchi
Interface design
• Gauss-Seidel
• **Gradient (Box-Wilson)**
• Simplex
• Method of Stochastic Approaches
Square plans
• Latin square
• Greek - Latin square
• Hiper Greek- Latin square
• Youden square
• Lattice square

Factorial designs allow multiple factors to be examined simultaneously. To reduce the number of attempts, the number of settings tested is usually maximized to two per factor. This value is sufficient to indicate the importance of the factors and, in some cases, to determine the optimum setting range. They are simple and logical to handle and therefore excellent and easy to use in industrial practice. In recent years, the industry has favoured simplified methods such as Shainin and Taguchi factorial methods. The response interface methods are used to model the curve fields and to examine the relationships in detail. The advantage of the methods is that the predefined experimental instructions make it possible to construct a mathematical model of the curve fields. Square designs can be used to

simultaneously analyse a factor with more than two options. However, the number of factors should be limited for ease of use. An analysis of the experiments performed gives information on the importance of the factors [2].

1.1. The steps of the experimental design

The more precisely an experiment is designed, the less effort it takes to execute it and the more reliable the conclusion from the evaluation of the experiment is. It follows that the design phase is most accurate, but great care must also be taken in estimating interactions and in designing the factors to be considered.

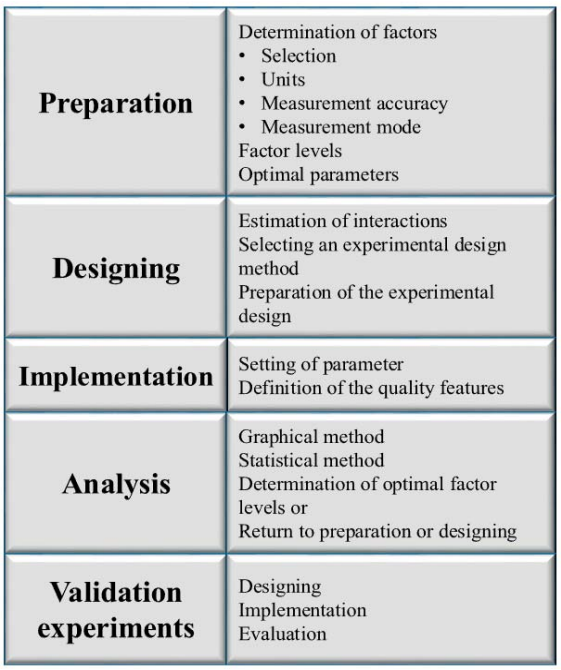

Figure 1. Steps of the experimental design [2]

2. THE TWO LEVELS OF EXPERIMENTAL DESIGN

Based on the type of statistical experiment design, we will choose the Box-Wilson method to apply *(Table 1)*. When using this method, each factor in a series of experiments will be set to one level once and once to another level. Therefore, ch factor will have only two levels. Number of experimental settings that realize all possible level combinations of factor *k* (*k* is the number of factors):

$$N = 2 \cdot k\,, \qquad (1)$$

when designing our experiments, one level of the factors is *+1* and the other level is *-1*. It does not matter whether the lower or upper level is denoted by *+1* or *-1*, respectively. These specified levels will represent specific physical quantities during the tests, such as the amount of a given factor. The experiment should be designed so that each factor appears at the same level as the *+1* level, and the factor combinations appear in the same amount at the *+1* level as the *-1* level. This is shown in the experimental matrix (see *Table 2.)* [1].

2.1. Experimental matrix

The experimental matrix summarizes all possible experimental settings and systematically shows the results of the experiments *(Table 2.)*. The rows in the matrix represent one experiment, that is, it shows the adjustment levels of the factors in one experiment. Each column of the experimental matrix helps calculate the effect of each factor. To fill in the columns of the table, we use the sign rotation method. For the first factor, the signs are rotated individually, for the second factor two, for the third factor four. In the cross-effect columns, we multiply the columns of the factors involved in the cross-effect by determining the signs. The product of two identical signs is always '+' and the product of two different signs is always '-' [1].

Table 2. Experimental matrix

Number of the experimental setup serial (*N*)	x_1	x_2	x_1x_2	Experimental result *(y)*
1	-1	-1	+1	y_1
2	+1	-1	-1	y_2
3	-1	+1	-1	y_3
4	+1	+1	+1	y_4

3. COMPLETE FACTORY EXPERIMENTAL PLAN

Experiments in which all possible combinations of levels of factors are determined is a complete factorial experiment. In this case, such an experiment is called a *2k* experiment for a two level experimental design.

Requirements for the factors:

- be controllable,
- be clear,
- be effective, therefore have a significant effect on the result of the experiment,
- have a known and limited set of values,
- factor levels can be set [1,2].

The x_0 column always contains *+1* value. This column will be needed to evaluate the experiments. The column x_1, x_2, x_1x_2 contains the adjustment values for the single factor, and the column contains the experimental results.

The combined effect of all factors can be described by a linear model as follows based on *Table 4.*

We have only two data in one step in the direction of one factor in the *n*-dimensional experimental space, we can lay a straight line at this *2* points. Therefore, the experimental surface to be determined on the basis of the measurement data.

The combined effect of all factors can be described by a linear model as described above [1].

$$y = b_0 \cdot x_0 + b_1 \cdot x_1 + b_2 \cdot x_2 + \ ... + b_N \cdot x_N (2)$$

In (2), we calculate the coefficients b_i (i=0...N), which are determined by the experiments, that is, the slope of the response function caused by each factor; while b_0 represents the initial value of the experiments. The number of possible effects, including b_0 the linear effects, and all possible interactions, is equal to the number of settings for the full factorial experiment using the next formula:

$$2^N = \sum_{l=1}^{N} \binom{N}{l}, \qquad (3)$$

where N denotes the number of experimental settings that realize all possible level combinations of factors and l is the serial number of effects examined.

Generally, in a full factorial experiment, the order of the highest order interaction is one less than the number of factors. In our case, the number of attempts in the interaction is *4*, the relation (3) is as follows [2]:

$$2^N = \sum_{l=1}^{N} \binom{4}{2} = 2^4 = 16. \qquad (4)$$

3.1. Determination of the factors and factor levels

We determine the factors and the factor levels. The factors significantly influence the processes. Factor levels are values that can be taken up by factors. These factors and factor levels are summarized in *Table 3.*

Table 3. Determining factors and levels

Number of factors (*k*)	Number of levels *(p)*
Factor 1: Micro switch's type	Level 4: *D1, D2, K1, K2*
Factor 2: Switch time (ST)	Level 2: *0.25s; 0.30s*
Factor 3: Relative humidity (RH)	Level 2: *60 %; 80 %*

If all factors can take the same level in an experiment, then the number of all possible factor levels in the experiment is

$$n = p \cdot k, \qquad (5)$$

where n is the number of experiments, p is the number of levels of each factor and k is the number of factors.

In our case the number of levels is *2* and the number of factors is *2*.

According to the formula (4) we should take 16 measurements, because we are testing *4* types of products, but we repeat all *16* type of measurements *10* times, so we will have a total of *160* measurement results.

Generally, a maximum of *15* factors and up to *30* levels are expedient per experiment. There are five basic requirements when designing your experiments.

In our case, the experimental matrix is shown in *Table 2.*, as follows:

Table 4. A 22 type two-factor full experimental matrix

N	Factor (ST) [s]	Factor (RH) [%]	Transformed factors				Exp. result *(y)*
			x_0	x_1	x_2	x_1x_2	
1	0.25	60	+1	-1	-1	+1	y_1
2	0.30	60	+1	+1	-1	-1	y_2
3	0.25	80	+1	-1	+1	-1	y_3
4	0.30	80	+1	+1	+1	+1	y_4
			b_0	b_1	b_2	b_{12}	

4. DETERMINATION OF THE COEFCIENTS b_i

Using the Box-Wilson method, we change the level of each factor at one step in the first set of experiments. Then, we examine which factor has impact on the value of the optimization parameter and we design the next set of experiments based on it. To determine the effect of each factor, it is sufficient to know the slope of the response function for that factor to plan the next step.

Determining the coefficients b_i *in* formula (2) using the experimental matrix is very simple. The signs of each factor are in its own column vector. The column vector of the experimental results y must be scalarly multiplied by the column vector of the given factor and then summed up by the sum of the elements of the column vector. The amount should be divided by the number of items in the column. Mathematically, it can be expressed as follows [1]:

$$b_j = \frac{\sum_{i=1}^{N} x_{ji} \cdot y_i}{N} . \qquad (6)$$

In our case x_{ji} also appears in columns x_0, x_1, x_2 and x_1x_2 as transformed factors as shown in *Tables 2, 4* and *5*. In our case the type *22* experimental matrix is formed as follows *(Table 5)*. Based on equation (6) the coefficients b_0, b_1, b_2 and b_{12} has been determined.

Table 5. Determining factors and levels

i	Factor (ST) [s]	Factor (RH) [%]	Transformed factors				Exp. result *(y)*
			x_0	x_1	x_2	x_1x_2	
1	0.25	60	+1	-1	-1	+1	y_1= 148664
2	0.30	60	+1	+1	-1	-1	y_2= 171711
3	0.25	80	+1	-1	+1	-1	y_3= 100200
4	0.30	80	+1	+1	+1	+1	y_4= 126511
b_0=136711			b_1=12339,5		b_2= -93664		b_{12}=816

To formulate the relationship between the two interacting factors, we may use the product of the two factors. In the case of two factors.

After determining the values of b_i, we can substitute them into relation (2):

$$y = 136711 + 12339{,}5 \cdot x_1 - 93664 \cdot x_2 \ . \quad (7)$$

However, it is not the best solution to approximate the experimental surface with the linear model. This is due to the fact that there is an interaction between the two factors.

$$\hat{y} = b_0 + b_1 \cdot x_1 + b_2 \cdot x_2 + b_{12} \cdot x_1 \cdot x_2 + \cdots. \quad (8)$$

Substituted in the formula (8) the relationship is as follows:

$$\hat{y} = 136711 + 12339{,}5 \cdot x_1 - 93664 \cdot x_2 + 816 \cdot x_1 \cdot x_2. \quad (9)$$

5. MEASUREMENTS AND DATA

In our measurements a total of four types of micro switches denoted by *D1, D2, K1* and *K2* are tested, with two different switching times of *0.30 s* and *0.25 s*, with two relative humidity setting *60 %* and *80 %*.

During the tests, *20* of the *4* types of switches at *0.25 s* and *0.30 s* switching speeds have failed. *Table 6.* illustrates the measurement results.

Table 6. Database with failure cycles

	Type	Switch time	Relative humidity	1	2	3	4
1	D1	0.30	60%	131186	171712	168082	100826
2	D1	0.25	60%	165500	148664	139034	139034
3	D2	0.30	60%	180230	191019	196031	189966
4	D2	0.25	60%	182918	170965	205622	225077
5	K1	0.30	60%	134494	197341	182428	197917
6	K1	0.25	60%	138167	212413	99140	185672
7	K2	0.30	60%	134494	180235	212592	209829
8	K2	0.25	60%	196937	134958	154036	91140

The horizontal axis in *Figure 2* represents the time of the test and the vertical axis show the temperature for a switch, as an example. The blue curve indicates one of the micro switch sample D1 temperature suddenly rises to *206.40 °C*, at this point it goes to failure. The green curve is for *K1*, the red curve is for *D2* and the yellow curve is for *K2*. The *Table 7* summarize the data related to the time-temperature diagram.

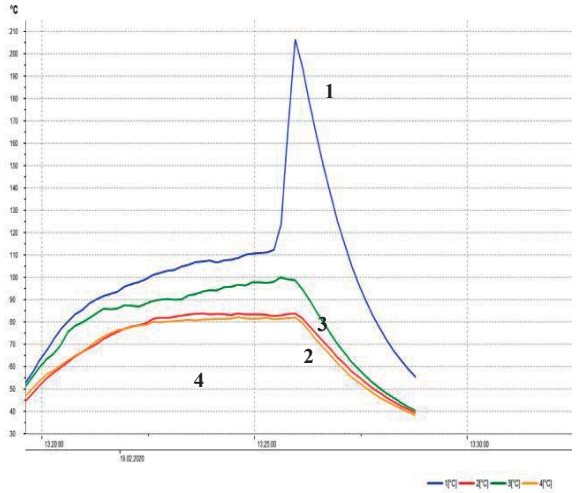

Figure 2. Time-temperature diagram

Figure 3 and *Figure 4* exhibit microscopic images of broken micro switches. The 3D images show the small or large burns on the contacting surfaces of the switches.

Table 7. Details of the time-temperature diagram

Broken switch type:	*D1(blue)*
Failure temperature:	*206.40 °C*
Failure switching cycle:	*100.826 cycle*
Switch time:	*0.25 s*
Relative humidity:	*60 %*

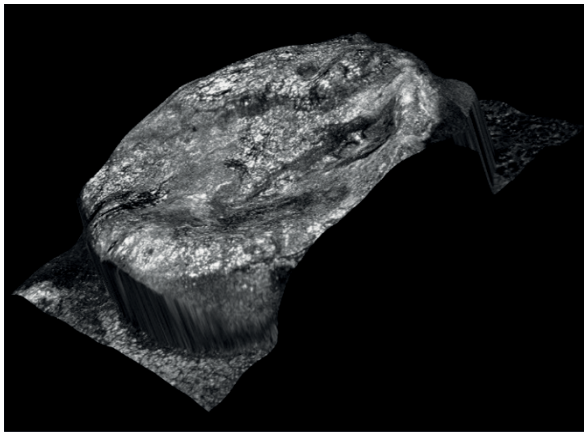

Figure 3. Contacting surface of a micro switch *(Type D1)*

Figure 4. Contacting surface of a micro switch *(Type K2)*

6. EXPERIMENTAL MODEL OF THE RESPONSE FUNCTION

We use a mathematical model of the process to describe the process. The model is the function relation between the optimization parameter y and the factors *ST* and *RH*, the general form of which is the response function φ:

$$y = \varphi(x_1, x_2). \quad (10)$$

To illustrate the relationship between the optimization parameter and the factors, the "black box" likeness is used.

The black box is the process or object under investigation that we want to describe and replace with the mathematical model presented

during experiment and implementation. The black box symbolizes the unknown relationship between the *ST* and *RH* factors acting on it as input and the optimization parameter *y* as output [2].

Figure 5. The "black box"

In the case of two factors, the response function can be represented in space, as illustrated in *Figure 6*. Here, the *ST* and *RH* factors are on the horizontal plane, while the values of the optimization parameter *y* plots the surface of the response function, the highest point of which indicates the desired optimal setting. Now, we see only a small rectangular part of the response function with the number of failure cycles of *171 711* created by setting a switching speed of *ST = 0.30 s* and a relative humidity of *60%*.

The failure rate for the *148 664* cycle was obtained by setting a switching speed of *ST = 0.25 s* and a relative humidity of *60%*. Cycle *126 511* was generated with a switching speed of *0.30 s* and 80% humidity setting, while *100 200* was generated with a switching speed of *0.25 s* and *80%* humidity setting.

Table 8. Determining factors and levels

ST	*RH*	*y*
0.30 s	60 %	171711
0.30 s	80 %	126611
0.25 s	60 %	148664
0.25 s	80 %	100200

Based on the above calculations, we can conclude that the best results are obtained when tested with a switch time of *0.30 s* and humidity setting of *60%* and the worst results is obtained by settings a switch time of *0.25 s* and *80%* humidity.

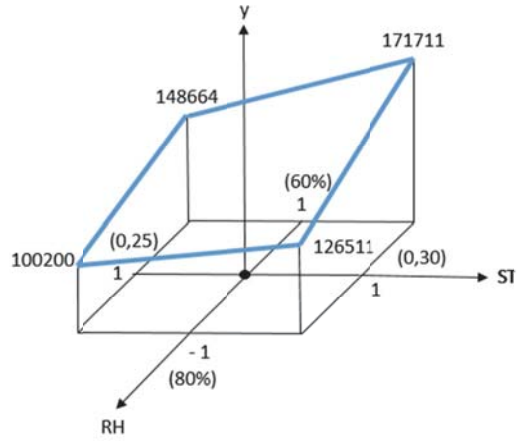

Figure 6. The response function φ for two factors, with the linear model [2]

7.SUMMARY

In this paper the experimental design methods used for testing micro switches are presented. By selecting the Box-Wilson method, we determined all possible level combinations of factors and the number of experimental settings.

The experimental matrix summarizes all possible experimental options and the results of the experiments are plotted. Each column of the experimental matrix provided help in calculating the effect of each factor.

On the base of our experiments we defined the relationship suitable for the calculation of the b_i coefficients using the experimental matrix. It gives us more information on how to estimate the lifetime for these devices. The temperature-time diagram of a test and some 3D microscope images of broken contacting surfaces are illustrated to show the failures of the contact surfaces.

ACKNOWLEDGMENT

The research work described in this paper supported by the ÚNKP-19-3 New National Excellence Program of the Ministry for Innovation and Technology.

REFERENCES

[1] Finszter, F., Aradi P., Czmerk A., Németh Z., Wenzelné Gerőfy K., Halmai A.: *Járműipari tesztelés és jóváhagyás* (Date of download : 21.02.2020)

[2] Johanyák Zs.: *Bevezetés a kísérletmódszertanba*, Kecskeméti Főiskola, Kecskemét, 2002.

[3] Fridrik, L. Csóka, J., Maros, Zs., Orosz, L.: *Faktoriális kísérlettervezés I., Nehézipari műszaki Egyetem, Gépészmérnöki kar,* Miskolc, 1988.

[4] Sipkás Vivien, Vadászné Dr. Bognár Gabriella: *Kerti gépekben alkalmazott mikrokapcsolók élettartam adatainak vizsgálata,* Multidiszciplináris Tudományok, Évf. 9, szám 2, pp. 90-95, https://doi.org/10.35925/j.multi.2019.2.13

[5] Sipkás Vivien, Vadászné Dr. Bognár Gabriella: *Testing accelerated life data of micro switches,* Design of Machines and Structures, A Publication of the University of Miskolc, vol. 9, no.2, pp. 44-50, 2019, ISSN 1785-6892

FORGATTYÚS TENGELY SIKLÓCSAPÁGYAZÁSÁNAK TRIBOLÓGIAI VIZSGÁLATA

TRIBOLOGY TEST OF CRANKSHAFTS' PLAIN BEARING

Papp Szonja, MSc Gépészmérnök hallgató

ABSTRACT
The subject of the presentation is the examination of crankshafts' plain bearing, regarding tribology with the usage of Tribology Simulator. During the examination, we have to define the following: the condition of the lubrication, the properties of the examined bearing, and the parameters of the examination. From the input data the software can predict the operating forces and wear patterns.

1. BEVEZETÉS

Tribológiának nevezzük a kölcsönösen egymásra ható és egymáshoz viszonyítva elmozduló felületek viselkedésének tudományát és technológiáját. A tribológia a szilárd-szilárd, szilárd-folyékony, mozgó szilárd-gáz, folyadék-folyadék és folyadék-gáz határfelületeken lejátszódó jelenségekkel foglalkozik. Tribológiai rendszerek létrejöttekor érintkezési, súrlódási és kopási folyamatok játszódnak le, ezáltal veszteségek alakulnak ki.

2. TRIBOLÓGIAI RENDSZER

A rendszer leírható a fekete doboz módszerrel, melynek során kijelölünk egy rendszerhatárt, vagyis a rendszert elkülönítjük a környezettől. Ezután megállapítjuk a be- és kimenő mennyiségeket, majd ezen mennyiségek közötti összefüggéseket. A rendszer szerkezeti leírásánál fontos a rendszerelemek azonosítása, az elemek közötti kapcsolatok megállapítása, valamint az elemek fontosabb paramétereinek meghatározása. Különböző tulajdonságokkal jellemezhető a rendszer, mint például geometriai- és anyagjellemzők.

Az állandó változás a tribológiai rendszer fontos jellemzője, mivel a keletkező veszteségek megváltoztatják a rendszer viselkedését. Ez az oka annak, hogy nem elegendő a be- és kimenő mennyiségek közötti kapcsolatot vizsgálni. Szükséges a tribológiai hatásokra kialakuló rendszerszerkezet változásainak és azok rendszerműködésre gyakorolt hatásainak a tanulmányozása.

A rendszer részei egymással mozgó kapcsolatban vannak. Fő részei a két egymáshoz viszonyítva elmozduló felület és azok környezete (1. ábra). Az alapanyag, az összetevők kialakítása, a köztes anyagok, a környezeti befolyások és az alkalmazási feltételek határozzák meg a kopás jellegét, lefolyását, illetve a mértékét. [1]

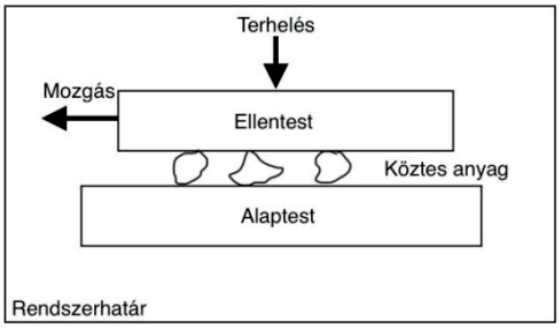

1. ábra. A tribológiai rendszer sematikus ábrája [1]

2.1. Kopás

A felszíni károsodás egyik legjellemzőbb formája a kopás. Kopás alatt az egymással súrlódó kapcsolatban lévő felületek anyagi részecskéinek leválását és ezáltal a felület geometriájának visszafordíthatatlan megváltozását értjük. A kopási folyamatot két csoportba lehet osztani: enyhe és intenzív. Ezt csak azok a vizsgálatok mutatják ki, ahol azt találták, hogy növelve a normál terhelést, vagy térfogati hőmérsékletet, vagy a relatív csúszási sebességet van egy olyan határ, ahol a kopási együttható hirtelen, nem lineáris módon megugrik.

Enyhe kopás tartományában relatíve sima felület keletkezik, a keletkező törmelék-átmérő kisebb, mint 100 nm. Az ilyen kopás miatt nagy kontaktellenállás jön létre.

Ezzel szemben az intenzív kopás tartományában a keletkező felület durva, mélyen barázdált a kiinduló állapothoz képest. Nagy törmelék-átmérő, akár 0,01-es átmérővel. Tiszta fémes kapcsolat a felületek között, így alacsony elekt-

romos kontaktellenállás. Mérnöki szempontból elmondható, hogy míg a enyhe kopás megengedhető, addig az intenzív kopás kerülendő folyamat. Ezért fontos tudni, hol van a két különböző típusú folyamatot elválasztó határ, illetve az üzem során becsülni a kopási együtthatót, ezáltal beazonosítani, hogy az intenzív határtól milyen messze áll folyamat.

A kopási folyamat jellemzésére használható az általános kopásdiagram (2. ábra), mely három egymástól különböző szakaszra bontható [2]:

I bejáratási szakasz: degresszív
II állandósult kopás: kvázi-lineáris
III túlkopás: progresszív

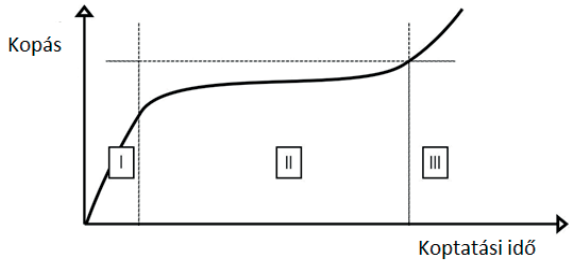

2. ábra. Jellegzetes kopásgörbe [1]

3. FORGATTYÚS TENGELY SZEREPE

A forgattyús tengely fő feladata a forgó mozgás egyenes vonalú alternáló mozgássá alakítása, vagy ennek fordított alkalmazása. Általános felhasználása belsőégésű motorokban történik, amelyeknél a dugattyúk egyenes vonalú mozgását alakítja forgó mozgássá. A tengely különleges kialakítása miatt tengelyirányban nem helyezhető fel csapágy, valamint nagy és váltakozó dinamikus terhelés jön létre működésnél. Ezek alapján olyan csapágyra van szükség, ami egyszerűen beépíthető, vagyis osztható, és nagy a radiális terheléssel szembeni ellenálló képessége (3. ábra). Így a forgattyúkar és forgattyúcsap közé siklócsapágy beépítése szükséges, amely általában bi-metálból vagy tri-metálból készül.

3. ábra. forgattyús tengely felépítése

4. CSAPÁGYAK SZEREPE

A csapágyak olyan gépelemek, amelyek tengelyek, forgó alkatrészek alátámasztásául szolgálnak, úgy, hogy a forgó mozgást minél kisebb ellenállás mellett, minél pontosabb vezetéssel biztosítsák. A csapágyba illeszkedik a tengelycsap. A csapágyaknak általában különböző terhelésekből adódó nagy erőket kell felvenniük, melyek származhatnak a forgó alkatrész súlyából, a kiegyensúlyozatlanságból származó forgó és alternáló tömegerőkből, vagy akár a gép működése folyamán fellépő más hatásokból is.

A csapágyak csoportosítása történhet működési elv és a terhelés iránya szerint. Terhelés iránya alapján megkülönböztetünk:

- axiális (4. ábra);
- radiális (5. ábra);
- axiális és radiális erők felvételére alkalmas csapágyakat.

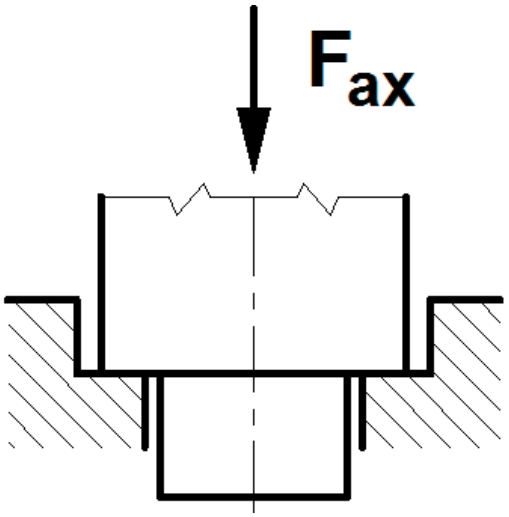

4. ábra. Axiális terhelés

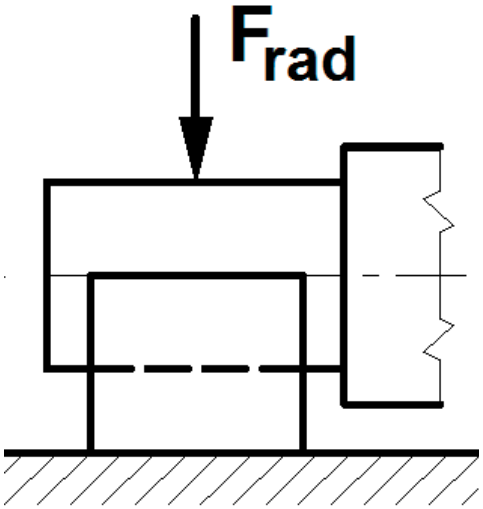

5. ábra Radiális terhelés

Működési elv szerint a csapágyak típusai lehetnek:

- Gördülőcsapágy
- Mágneses elven működő csapágy
- Rugalmas csapágy
- Siklócsapágy

5. SIKLÓCSAPÁGYAK OPTIMÁLIS ANYAGÖSSZETÉTELEI

A siklócsapágyakat olyan anyagokból kell elkészíteni, melyek képesek nagy erőket felvenni, kicsi a súrlódási együtthatójuk, ellenállóak a megemelkedett hőmérséklettel szemben és korrózióállók. Ezen szempontok figyelembevéve kell kiválasztani a megfelelő csapágy anyagot. Felhasználási területtől függően a legkülönfélébb anyagokból választhatunk.

5.1. Bi – material

A bi – material, vagyis két anyagból álló csapágyaknál a külső, nagy terheléseket felvevő felületet fémből, míg a belső, csappal érintkező felületet műanyagból készítik. Az ellenálló külső fém héj képes nagyobb terheléseket is felvenni, míg a kevésbé strapabíró, belső műanyag hüvely kisebb súrlódásának köszönhetően simább járást és kisebb kopást eredményez.

5.2. Fehérfém

Rendkívül előnyös tulajdonságokkal rendelkeznek a lágy, szárazon is jó súrlódási jellemzőkkel bíró fehérfémből készült csapágyperselyek. Ezek a fehérfém perselyek készülhetnek ónból, ólomból vagy akár antimon ötvözetéből.

5.3. Grafit

A grafit szilárd kenőanyagként viselkedik, ebből következtethetően meglehetősen jó választás siklócsapágy anyagának. Vegyítetlen formában akár nedves körülmények melletti használatra is alkalmas.

5.4. Plasztik

Manapság a műanyag csapágyak meglehetősen nagy népszerűségnek örvendenek, mivel nem igényelnek kenőanyagot, nem korrodálódnak, kicsi a tömegük és nem igényelnek karbantartást. Azonban hátrányaik is akadnak. A hőtágulási együttható változása nem lineáris, valamint nagy tartományban mozog, ezért tervezésnél bonyolult vele számolni. A nem rendeltetésszerű használatból adódóan rendkívül gyorsan melegednek.

6. SIKLÓCSAPÁGY KOPÁSANALÍZISE

A siklócsapágyak felületei között felléphet határréteg-súrlódás, vegyes súrlódás, folyadéksúrlódás, de alapvetően folyadék-(hidrodinamikus) súrlódás állapotára tervezik a siklócsapágyakat. Az egyes súrlódási állapotok fellépésének lehetőségét a Stribeck görbe (6. ábra) segítségével lehet megállapítani a jellemző üzemi paraméterekből.

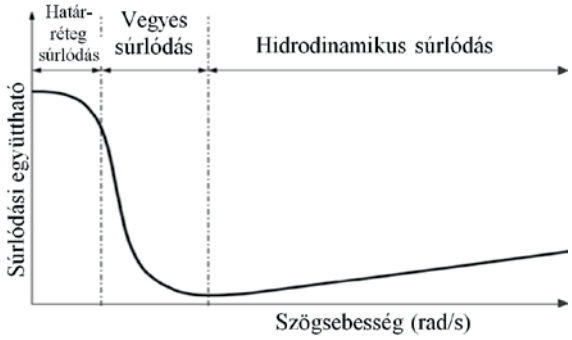

6. ábra. Stribeck görbe

Álló helyzetben a nyugalmi állapotot veszi fel tengely és a kenőanyag a siklócsapágyon belül [4]. Indításkor egy nagyon rövid időtartamra lép fel az indulási állapot. Ebben az állapotban a tengely először gördül a csapágyfalon, ezáltal jut abba a pozícióba, ami a 7. ábrán látható. Ez a mozgás fokozatosan átvált csúszásba, amivel párhuzamosan felépül a hidrodinamikus nyomás, és fokozatosan kezdi a tengely megközelíteni az üzemi állapotot. Az üzemi állapotban megközelíti a rendszer az elaszto-hidrodinamikus kenési állapotot és felveszi az állandósult állapotú pozícióját, amint azt a 7. ábra is mutatja.

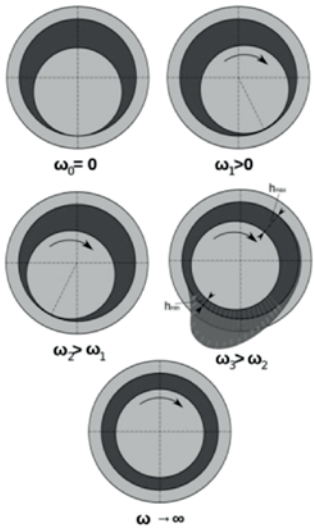

7. ábra. A siklócsapágy jellemző állapotai az életciklusa során.

A leállás során az indulási állapothoz képest egy hosszabb időtartamban a tengely fokozatosan, monoton módon megközelíti a nyugalmi állapotot, és végül elfoglalja az ehhez tartozó pozíciót, amikor a forgása leáll.

7. TRIBOLÓGIAI SZIMULÁCIÓ

A kopás szimulációját a Tribology Simulator nevű szoftver segítségével végeztük el. A szoftver a leggyakrabban előforduló tribológiai érintkezési feladat szimulációjára alkalmas. A szimulátor fő funkciója a vegyes kenési körülmények közt érintkező kontaktfelületek között fellépő súrlódás számítása, amikor a terhelést részben a kenőanyag, részben pedig a közvetlenül érintkező felületek veszik fel. [5]

Az eredmény kiértékelésénél a csapágyban bekövetkezett változásokat vizsgáltuk idő és terhelés függvényében. Mivel egy forgattyús tengely dinamikus terhelése a forgattyúkar és tengely által bezárt szög tekintetében változó, a szimulációt két különböző terhelés mellett futtattuk. Kb 17 kN terhelés lép fel abban az esetben, amikor a dugattyú működésbe lép. Ez a körülfordulásnak csupán rövid részét teszi ki, kb 10°. A működés során az átlag terhelés a tengelyen 5 kN, ezzel a faktorral végeztük a második szimulációt. Az így kapott eredményekből megállapítható, milyen mértékben befolyásolják a csapágy kopását a különböző terhelések.

8. EREDMÉNYEK KIÉRTÉKELÉSE

Az alábbiakban láthatóak az Tribology Simulatorban kapott eredmények összesítései diagram formátumban:

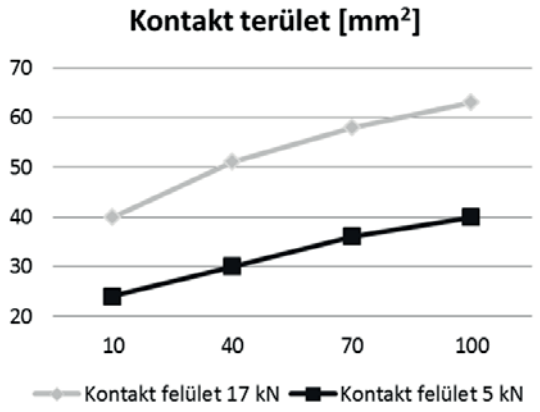

8. ábra Érintkező felület nagysága

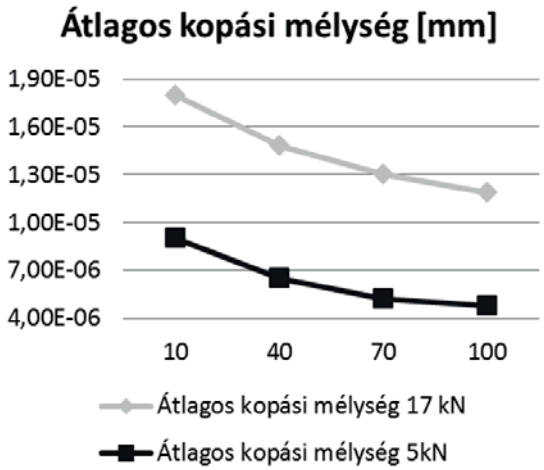

9. ábra Átlagos kopási mélység

Az eredmények alapján látható, hogy nagyobb terhelés esetén a kopási folyamat gyorsul, ezáltal az érintkező terület megnő (8. ábra). A különböző terhelések mellett tesztelt csapágyak felületét fontos vizsgálni a kopás nyomok elemzésével, hogy megbizonyosodjuk arról, hogy a károsodási mechanizmus ugyanaz a különböző terhelések mellett.

9. KÖSZÖNETNYILVÁNÍTÁS

A cikkben ismertetett kutató munka az EFOP-3.6.1-16-2016-00011 jelű „Fiatalodó és Megújuló Egyetem – Innovatív Tudásváros – a Miskolci Egyetem intelligens szakosodást szolgáló intézményi fejlesztése” projekt részeként – a Széchenyi 2020 keretében – az Európai Unió támogatásával, az Európai Szociális Alap társfinanszírozásával valósul meg.

10. IRODALOMJEGYZÉK

[1] Dr. Jenei I., Ladányi G.: Kenésgazdálkodás, 2013.

[2] Dr. Előd A.: Géptervezés I., Budapest, 1994.

[3] BME Járműgyártás és –javítás Tanszék: Károsodás (letöltés ideje: 2019.11.29.)

[4] Mokthar MOA, Howarth RB, Davies PB.: „The behavior of plain hydrodynamic journal bearings during starting and stopping”, ASLE Trans, Vol. 30(3), p.183–90, 1977.

[5] Tribology Simulator User Manual, www.tribonet.org, 2018.

MEGBÍZHATÓSÁGI BLOKKDIAGRAM HIERARCHIKUS ÉRZÉKENYSÉGVIZSGÁLATA

HIERARCHICAL SENSITIVITY ANALYSIS OF RELIABILITY BLOCK DIAGRAM

Pokorádi László, CSc, egyetemi tanár, Óbudai Egyetem Mechatronikai és Járműtechnikai Intézet
Bárányi István, PhD, adjunktus, Óbudai Egyetem Gépészeti és Biztonságtudományi Intézet

KIVONAT
A kanonikus rendszerek és azok megbízhatóságának elméleti és gyakorlati vizsgálata számos járműmérnöki területen fontos szerephez jut. Az egyik legfontosabb kérdés a teljes rendszer megbízhatóságának érzékenysége. A tanulmány célja a repülőgépek és a gázturbina motorok matematikai diagnosztikai módszertanának adaptálása a véges kanonikus rendszer megbízhatóságának meghatározására. Tanulmányunk egy egyszerű példán mutatja be a javasolt a megbízhatósági blokkdiagram hierarchikus érzékenységi modellt.

ABSTRACT
Theoretical and practical investigation of canonical systems and their reliability has become important in several fields of vehicle engineering. One of the most important questions is the sensitivity of their reliability. The main aim of this paper is to show adaptation of mathematical diagnostic methodology of aircraft systems and gas turbine engines to determine sensitivity of reliability of finite canonical system. The proposed method is named Hierarchical Sensitivity Model of Reliability Block Diagram (HSMoRBD). The paper shows the proposed method theoretically and its applicability by a simple example.

1. INTRODUCTION

Reliability – that often means dependability –, has a broad meaning in our daily life [7]. Reliability analysis methods are defined by international standard IEC 60300-3-1. The most widely used quantitative analyses are Fault Tree Analysis (FTA) and Analysis of Reliability Block Diagram (RBD) [3].

Scientific work of authors is part of project called *Dynamics and Control of Autonomous Vehicles meeting the Synergy Demands of Automated Transport Systems (EFOP-3.6.2-16-2017-00016)*, in which the following research consortium is taking part: Széchenyi István University, John von Neumann University, University of Dunaújváros and Óbuda University.

During of the project mentioned above Nagy and Tuloki explored [4] a real sensor and commutation network system of fully electric vehicle (Nissan Leaf Z0) and depicted its block diagram. Zentai proposes an algorithm that classifies the vertices of a graph (e.g. vehicles, or road side units) based on their risk value [12].

Szakács introduced a model of a pneumobil vehicle developed at the University of Óbuda [9]. The goal of his modelling is to describe the air pressure and flow, force, and speed behavior of the piston, in order to optimize drive power, and gas consumption. Further goal of the modelling is to develop functional block model of driving system of pneumobil for optimizing its control strategies, in special attention on maximizing vehicle power, and traveling range [10].

In the reliability engineering literature, there are many studies books as well as papers dealing with reliability theory from theoretical and practical points of view.

The aim of Boucerredj's work is to propose a dependability evaluation of system controlled by computer using a new approach based on optimization qualitative and quantitative analysis [1]. This qualitative analysis optimization based on Truth Table method combined with Karnaugh Table used for focus the search of failure on the system study (or parts of the system) that are interesting for dependability analysis, the objective is to determine the causality events between nominal states, degraded state and feared state for deriving Minimal Feared State (MFS).

The paper of Pan investigates a Bayesian approach to system reliability prediction using multilevel incomplete data [5].

In paper of Catelani et.al sensitivity analysis is carried out to assess propagation of uncertainty from nominal values of failure rates taken from reliability data handbooks to system reliability outcome of a generic Safety Instrumented System [2].

In paper [11], the complete process and method of ship reliability analysis are studied. The whole ship is divided into three (equpment; subsystems; system) levels and analysis from bottom to top.

Pokorádi developed a modular approached sensitivity models named as Linear Fault Tree Sensitivity Model (LFTSM) [6][8]; the Linear Sensitivity Model of System Reliability (LSMoSR) and Linear Sensitivity Model of System Unreliability (LSMoSU) [7]. These modular approach tools that use matrix-algebraic method based upon the mathematical diagnostic methodology of gas turbine engines.

Most advantages of the modular approach methods mentioned above are the followings:

- it is an easy-used algorithm;
- elements of coefficient matrices can be easily determined because of they are typical ones;
- sensitivity matrix shows sensitivity coefficients not only for entire system or process but for the subsystems or sub-processes as well;
- sensitivity coefficient's structure is similar, thus substituting parameters makes the whole system typical or typified [8].

The present article follows in the spirit of these works and proposes a new Hierarchical Sensitivity Model of Reliability Block Diagram (HSMoRBD).

The paper is organized as follows; Section 2 represents the Reliability Block Diagram method theoretically and in practice. Section 3 explains the methodology of hierarchical sensitivity analysis of RBD firstly theoretically and then by a case study. Finally, Section 4 concludes the article, summarizes and proposes some future research directions.

2. RELIABILITY BLOCK DIAGRAM

Reliability Block Diagram is easy to evaluate and understand. It has been widely used in reliability engineering for many years Its general methodology is depicted by international standard IEC 60300-3-1 [3]. The RBD has equivalent mathematical characteristics to FTA. The method provides a perspicuous graphical representation of the redundancy inherent within the investigated system.

2.1. Theoretical Solution

The RBD can be used only reliability investigation of simply system. A simply system does not have so-called complex interconnections, therefore it can be represented as a network in which components and subsystems are connected in series, in parallel, or a combination of these.

The serial system means that all of its components must work for the system to be successful (see figure 1). Its reliability can be determined by

$$R_{sys} = \prod_{j=1}^{n} R_j \tag{1}$$

equation, where:
R_j – reliability of j^{th} element;
n – number of elements.

Figure 1 Series System

In case of a parallel system success requires that either one (or more) element must operate successfully. So, the reliability of parallel system:

$$R_{sys} = 1 - \prod_{j=1}^{n} \left(1 - R_j\right) \tag{2}$$

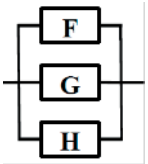

Figure 2 Parallel System

It is important to mention, that serial or parallel system from point of view of reliability do not mean in any case serial or parallel connections from technical, technological points of view.

The combined RBDs can be serially-parallel or in parallel-serial combination. These models include combination of the redundant and no redundant elements or subsystems. In this case we should define different layers of the RBD.

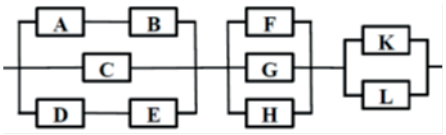

Figure 3 The investigated system

3.2. Case Study

Layer 1: The investigated system (see Figure 3) has been modelled as subsystems X; Y and Z with series connections.

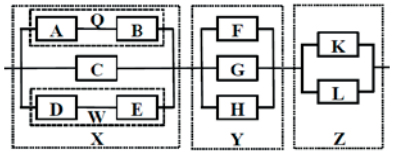

Figure 4 Layers of the Investigated System

The reliability of system can be determined by

$$R_{sys} = R_X R_Y R_Z \tag{3}$$

equation.

Layer 2: The subsystem X has been modelled as

blocks Q; C; W with parallel connection:

$$R_x = 1 - \left\{(1 - R_Q)(1 - R_C)(1 - R_W)\right\} \quad (4)$$

The subsystem Y has been modelled as elements F; G and H with parallel connection:

$$R_Y = 1 - \left\{(1 - R_F)(1 - R_G)(1 - R_H)\right\} \quad (5)$$

The subsystem Y has been modelled as elements K and L with parallel connection:

$$R_Z = 1 - \left\{(1 - R_K)(1 - R_L)\right\} \quad (6)$$

Layer 3: The subsystem Q has been modelled as elements A and B with series connection:

$$R_Q = R_A R_B \quad (7)$$

The subsystem W has been modelled as elements D and E with series connection:

$$R_W = R_D R_E \quad (8)$$

Then – using equations (3) – (8) backwards – the reliabilities of intermediate blocks in the layers and at last reliability of system should be determined.

The Figure 5 shows system reliabilities R_{sys} in case of different reliabilities of all components R_i.

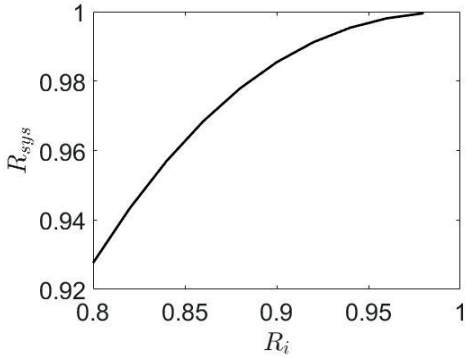

Figure 5 System Reliabilities in Cases of Different Reliabilities of Components

2.3. Simulation-based Sensitivity Analysis

To investigate sensitivities of system reliability the reliabilities of components have been changed severally. During simulation all elements have same r_i = 0.9 reliability, only the reliability of the investigated component is changed from 0.8 to 0.98.

Figures 6 – 9 show the results of simulations, which depict the changing of system reliability and subsystem in layer 1 that comprises the investigated element.

2.4. Discussions

The following conclusions can be drawn from the results of RBD reliability analysis and simulation:

A1: The reliability of system is approaching 1 asymptotically when reliabilities of components increase (see Figure 5)

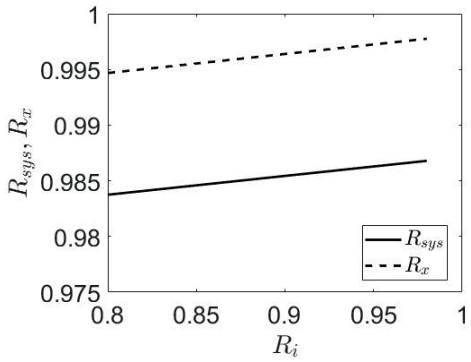

Figure 6 System and Subsystem X Reliabilities in Cases of Different Reliabilities of Components A; B; D and E

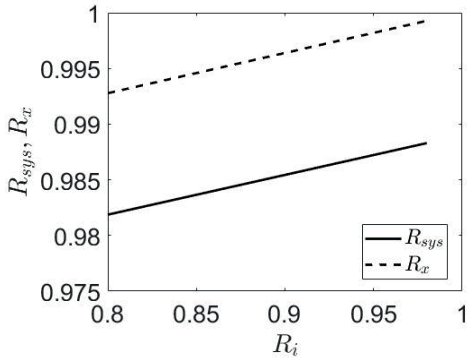

Figure 7 System and Subsystem X Reliabilities in Cases of Different Reliabilities of Component C

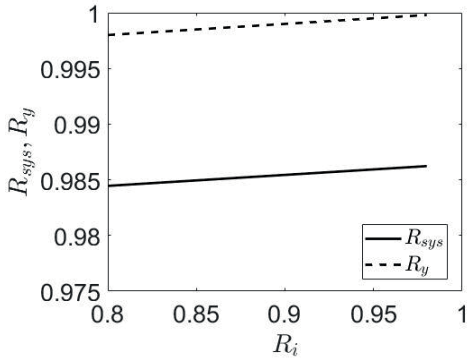

Figure 8 System and Subsystem Y Reliabilities in Cases of Different Reliabilities of Components F; G and H

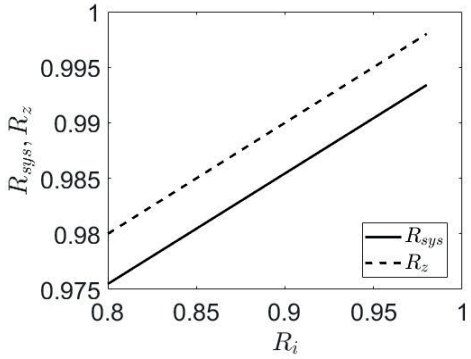

Figure 9 System and Subsystem Z Reliabilities in Cases of Different Reliabilities of Components K and L

B1: The decreasing order of rises of curves is

following:
- K and L (see Figure 9);
- C (see Figure 7);
- A, B, D and E (see Figure 6);
- F, G and H (Figure 8).

B2: The function curves of components K and L have the most rise.

B3: The function curves of components F, G and H have the list rise.

It can be stated that increasing of component reliability K or L results in the biggest increase of system reliability.

3. HIERARCHICAL SENSITIVITY ANALYSIS

For sensitivity investigation, the linear sensitivity model of the discussed RBD should be set-up. In this chapter the method of modular approach sensitivity model setting up will be depicted theoretically and demonstrated practically by the example of the sample RBD mentioned above (Figure 3).

3.1. Theoretical Solution

The sensitivity analysis shows how sensitive the system's output parameter is while changing in any elements of the input parameters. In other words the sensitivity coefficient characterizes measurement of the investigated output system parameter's dependence upon given input one.

Using the mathematical model of investigated system or process relative changing of output parameters can be determined in case of changing of input one (or ones). By literatures [6] and [7], the sensitivity coefficient by input parameter x_i of general function $y = f(x_1, \ldots, x_n)$ can be determined analytically by the coefficients:

$$K_{y,x_i} = \frac{\partial f(x_1;x_2;\ldots x_m)}{\partial x_i}\frac{x_i}{f(x_1;x_2;\ldots x_m)} \qquad (9)$$

a short sign is K_{yi}, and

$$\frac{d\eta}{\eta} \approx \frac{\Delta\eta}{\eta} = \delta\eta \qquad (10)$$

equation, the following linear system can be achieved:

$$\delta y = K_{y1}\delta x_1 + K_{y2}\delta_{x2} + \ldots + K_{ym}\delta x_m \qquad (11)$$

Using equation, mentioned above, how sensitive dependent system output parameters will be to uncertainties of input ones.

The sensitivity coefficients of RBD can be determined by the following ways:

In case of serial systems (or subsystems) – using equation (1)

$$R_{sys} = \prod_{j=1}^{n} R_j \quad \Rightarrow \quad K_i = 1 \qquad (12)$$

In case of parallel systems (or subsystems) – using equation (2):

$$R_{sys} = 1 - \prod_{j=1}^{m}\left(1 - R_j\right) \quad \Rightarrow \quad K_i = \frac{R_i}{R_{sys}}\prod_{\substack{j=1 \\ j\neq i}}^{m}\left(1 - R_j\right) \qquad (13)$$

Next task is to separate events of block diagram into elements and blocks (system and subsystems). Their reliabilities should be arranged into vectors x and y. Then, the connection between reliabilities of elements blocks can be described by

$$\mathbf{A}\delta\mathbf{y} = \mathbf{B}\delta\mathbf{x} \qquad (14)$$

where A and B are coefficient matrices of blocks and elements. If matrix A is invertible, using

$$\mathbf{S} = \mathbf{A}^{-1}\mathbf{B} \qquad (15)$$

relative sensitivity coefficient matrix of investigated RBD, the equation

$$\delta\mathbf{y} = \mathbf{S}\delta\mathbf{x} \qquad (16)$$

can be used for relative sensitivity investigation.

3.2. Case Study

To demonstrate methodology mentioned above, lets' study the RBD shown by figure 3.

The vectors of reliabilities of blocks and elements:

$$\mathbf{y}^T = \begin{bmatrix} R_{sys} & R_Z & R_Y & R_X & R_Q & R_W \end{bmatrix} \qquad (17)$$

$$\mathbf{x} = \begin{bmatrix} R_A \\ R_B \\ R_C \\ R_D \\ R_E \\ R_F \\ R_G \\ R_H \\ R_K \\ R_L \end{bmatrix} \qquad (18)$$

$$\mathbf{A} = \begin{bmatrix} 1 & -1 & -1 & -1 & 0 & 0 \\ 0 & 1 & 0 & 0 & 0 & 0 \\ 0 & 0 & 1 & 0 & 0 & 0 \\ 0 & 0 & 0 & 1 & -K_{XQ} & -K_{XW} \\ 0 & 0 & 0 & 0 & 1 & 0 \\ 0 & 0 & 0 & 0 & 0 & 1 \end{bmatrix} \qquad (19)$$

$$\mathbf{B}^T = \begin{bmatrix} 0 & 0 & 0 & 0 & 1 & 0 \\ 0 & 0 & 0 & 0 & 1 & 0 \\ 0 & 0 & 0 & K_{XC} & 0 & 0 \\ 0 & 0 & 0 & 0 & 0 & 1 \\ 0 & 0 & 0 & 0 & 0 & 1 \\ 0 & 0 & K_{YF} & 0 & 0 & 0 \\ 0 & 0 & K_{YG} & 0 & 0 & 0 \\ 0 & 0 & K_{YH} & 0 & 0 & 0 \\ 0 & K_{ZK} & 0 & 0 & 0 & 0 \\ 0 & K_{ZL} & 0 & 0 & 0 & 0 \end{bmatrix} \qquad (20)$$

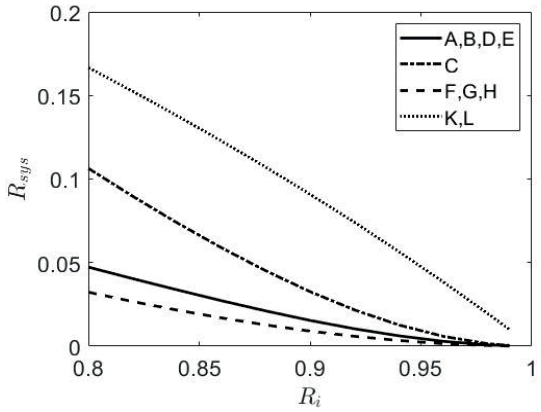

Figure 10 Sensitivities of System Reliability Depends on Reliabilities of Components

The sensitivity coefficients of the investigated RBD can be determined using equations (3) – (8) by equations (12) and (13).

Figure 10 shows sensitivities of system reliability depends on reliabilities of components.

3.3. Discussions

The following conclusions can be drawn from the results of RBD sensitivity analysis:

C1: The relative sensitivity of system reliability decreases if reliabilities of elements increase

C2: Using same reliabilities of components, the relative sensitivity of system reliability to reliability of components are the same in cases of elements A; B; D; E and F; G; H and K ; L..

The conclusions C1 and C2 are in accord with conclusions B1; B2 and B3.

D1: From Conclusions B1; B2; B3 and C2, the authors introduce the terms "***structural sensitivity***" and "***structural sensitivity coefficient***".

The structural sensitivity coefficient characterizes the effect of a given component from constructional point of view. Its value is determined only by localization in the system – not a value – of the given component.

E1: The proposed method can be used to analyze sensitivity of the reliability of the RBD.

E2: Elements of coefficient matrices can be easily determined.

E3: Sensitivity parameters of the possible system states can be used in cases with separate professional meaning (for example road traffic or logistical management).

4. CONCLUSIONS, FUTURE WORK

In this paper a new modular approach method named Hierarchical Sensitivity of Reliability Block Diagram (HSoRBD) was proposed. The Authors' proposed prospective future research direction is the study of sensitivity and uncertainty analysis methodologies of technical systems, such as vehicle sensory network, reliability.

5. ACKNOWLEDGEMENT

The research presented in this paper was carried out as part of the EFOP-3.6.2-16-2017-00016 project in the framework of the New Széchenyi Plan. The completion of this project is funded by the European Union and co-financed by the European Social Fund.

6. REFERENCIES

[1] Boucerredj, L., - Debbache, NE.: Qualitative and Quantitative Optimization for Dependability Analysis, Informatica 42, pp. 439–450 (2018)

[2] Catelani, M., - Ciani, L., - Venzi, M.: Sensitivity analysis with MC simulation for the failure rate evaluation and reliability assessment, Measurement 74 pp. 150–158. (2015)

[3] Dependability management. Part 3-1: Application guide. Analysis techniques for dependability, Guide on methodology (IEC 60300-3-1:2003)

[4] Nagy, I., - Tuloki, Sz. : Fault Analysis and System Modelling in Vehicle Engineering, Proceedings of the CINTI 2018, pp. 313 – 317.

[5] Pan, R.: Reliability Assessment of Hierarchical Systems With Incomplete Mixed Data, IEEE Transactions on Reliability, 6: 4, 1036 – 1047 (2017).

[6] Pokorádi L.: Sensitivity Investigation of Fault Tree Analysis with Matrix-Algebraic Method, Theory and Applications of Mathematics & Computer Sciences 1 : 1 pp. 34-44., (2011)

[7] Pokorádi L.: Sensitivity analysis of reliability of Systems with Complex Interconnections Journal of Loss Prevention in the Process Industries 32 pp. 436-442. , 7 p. (2014)

[8] Pokorádi, L., - Ványi, G.: Analyzing new generation brake system's software development process by LFTSM, Proceenings of the CINTI 2016, pp. 199-202. (2016).

[9] Szakács, T.: Modellierung und Simulation des Zugwinkels zwischen Anhänger und Zugmaschine, LANDTECHNIK 2010 : 3 pp. 178-181, (2010).

[10] Szakács, T.: Pneumatic modelling of a pneumobil. Proceedings of the 2nd Agria Conference on Innovative Pneumatic Vehicles ACIPV 2018, pp. 25-30., (2018).

[11] Zhiwei, Ch. et.al.: Reliability analysis of phased-mission complex systems for warship, Prognostics and System Health Management Conference (PHM-Chengdu), (2016).

[12] Zentai Dániel: Graph Theoretic Risk Classification in Transportation Networks Proceedings of the SISY 2019, pp. 227–230.

TEHERAUTÓ PLATÓ KERESZTTARTÓJÁNAK OPTIMÁLÁSA EVOLÚCIÓS MÓDSZERREL

OPTIMISATION OF CROSS MEMBER OF TRUCK FLOOR WITH EVOLUTIONARY METHOD

Nagy Szilárd PhD hallgató, Dr. Jármai Károly egyetemi tanár

ABSTRACT
Grillage – formally lattice like – structures are built of longitudinal beams, cross-members. Vehicle frames, bus floor frames or complete vehicle can be modeled as grillage. The optimization of cross-member of this structure is shown in this paper. The optimization method is a nature inspired metaheuristic evolutionary method, the flower pollination algorithm. The objective function is the total weight of the optimized cross member. The un-knowns are typical dimensions of cross-sections of cross-member. The design constraints are local buckling and fatigue. Inspection was made with aluminum alloy.

1. BEVEZETÉS

A mesterséges intelligencia heurisztikus ágához tartozó evolúciós algoritmusok kutatása az elmúlt években nagy hangsúlyt kapott. Ez nem meglepő, hiszen jól használhatók nem lineáris, sokváltozós bonyolult keresési, optimálási feladatok megoldására.

Olyan esetekben is képesek eredményesek lenni, amikor a tradicionális gradiens alapú módszerek nehézkesen, vagy egyáltalán nem alkalmazhatók. További nagy előnyük, hogy képesek a célfüggvényt fekete dobozként kezelni. Nem kell ismerni a függvény konkrét belső felépítését elég csak a bemeneteket és az azokra adott választ. Számos előnyük mellet működésükből következően hátrányuk, hogy nem lehet eldönteni a kapott eredményről, hogy az lokális vagy globális minimum. Rengeteg evolúciós algoritmus közül mi a virág beporzási (FPA) algoritmust fogjuk bemutatni és alkalmazni.

Tartórácsot, tartórácsszerű szerkezeteket, sok helyen alkalmaznak a jármű iparban. Ilyen szerkezettel modellezhető például teherautók, buszok alváza vagy akár a hajók cellalemezes kialakítása.

Jelen cikkben egy meglévő háromrétegű teherautó plató optimálását végeztük el, evolúciós algoritmussal. A kereszttartó optimális méretének meghatározására törekedtünk. A plató további részegysége változatlan maradt. Ez azt is jelenti, az új geometriájú kereszt tartó egy az egyben beépíthető a régi helyére.

2. FPA ALGORITMUS

A virág beporzási algoritmust (flower pollination algorithm; röviden: FPA), mint ahogyan a neve is mutatja a növények beporzási folyamata inspirálta. Fiatal evolúciós algoritmusról van szó, amit először Xin-She Yang javasolt 0.

A természetben a növények reprodukciós folyamatára a különböző beporzási módszerek a jellemzőek. Az adott növényre jellemző virágpor, pollen átkerül egy másik növényre, rovarok, madarak, denevérek, egyéb állatok vagy a szél segítségével. Van néhány növény, ami ettől eltérő speciális beporzási módszert választott.
Általánosságban megfogalmazható négy domináns szabály, melyek alapján modellezhető a folyamat, és az algoritmus matematikai alapját képezik:

- **globális-beporzás** (kereszt-beporzás) során a pollen átkerül az egyik egyedről egy másik egyedre. A beporzók mozgása modellezhető Lévy eloszlást követő véletlen számmal.
- **helyi-beporzásnál** a pollen ugyanabból a virágból, vagy ugyanazon növény másik virágából származik.
- adott fajból származó pollen csak az ugyanabba a fajba tartozó növényt tudja beporozni. Az FPA vonatkozásában ez azt jelenti, hogy a beporzás csak akkor történik meg, ha utána a meglévőnél jobb eredmény jön létre.
- helyi- és globális-beporzás bekövetkezésének valószínűségét egy normál eloszlású véletlen valós szám fejezi ki.

A kereszt-beporzás matematikai formája:

$$\bar{x}_i^{(G+1)} = \bar{x}_i^{(G)} + L\left(\bar{g}^* - \bar{x}_i^{(G)}\right) \qquad (1)$$

ahol $\bar{g}^*$ a G generációig megtalált globális minimum, L pedig a Lévy-szám, ami közelíthető az alábbi formulával 00:

$$L \approx \frac{\lambda\Gamma(\lambda)\sin\left(\frac{\pi\lambda}{2}\right)}{\pi}\frac{1}{s^{1+\lambda}} \tag{2}$$

ahol λ egy konstans (ajánlott értéke: $\lambda = 1{,}5$), $\Gamma(\lambda)$ gamma eloszlási függvény, s pedig $s > 0$ véletlen lépés.

A helyi-beporzást pedig a differenciál evolúcióból [9] jól ismert mutációs formulával lehet kifejezni:

$$\bar{x}_i^{(G+1)} = \bar{x}_i^{(G)} + \epsilon\left(\bar{x}_{r_1}^{(G)} - \bar{x}_{r_2}^{(G)}\right) \quad r_1 \neq r_2 \neq i \tag{3}$$

ahol $\epsilon \in [0;1] \cup \mathbb{R}$ normál eloszlású véletlen szám, r_1 és r_2 véletlen egész számok. A teljes algoritmus pszeudokódját a *1. ábra* szemlélteti.

$P^{(0)}$ *populáció inicializálása véletlenszerűen*
$\bar{g}^*$ *legjobb megoldás kiválasztása* $P^{(0)}$*-ból*
$P \in [0;1]$ *valószínűség meghatározása*
ciklus míg $G < maximum\ genráció$
ciklus $i = 1{:}n$ *(összes egyedre)*
ha $rand < P$
L Lévy eloszlású véletlen szám generálása (2)
globális beporzás (1) *alapján*
egyébként
ϵ *véletlen szám generálása*
helyi beporzás (3) *alapján*
ha vége
új függvényérték meghatározás
ha a kapott eredmény jobb, új egyed megtartása
ciklus vége
ciklus vége

---

1. ábra FPA algoritmus pszeudokódja

Az FPA, mint a legtöbb evolúciós algoritmus folytonos problémák megoldására lett kitalálva. A mérnöki gyakorlatban előforduló problémák viszont korlátosak.

$$\text{ha} \quad \begin{matrix} \min \mathcal{F}(\bar{x}) & \bar{x} = [x_1, x_2 \cdots x_i \cdots x_D] \\ g_j(\bar{x}) \leq 0 & 1 \leq j \leq q \\ h_k(\bar{x}) = 0 & q+1 \leq k \leq r \end{matrix} \quad x_A \leq x_i \leq x_F \tag{4}$$

ahol D a probléma változóinak száma, x_A és x_F alsó és felső határok. A korlátos, nem folytonos problémát szükségszerű folytonossá alakítani. A gyakorlatban a leggyakoribb módszer, hogy ha nem teljesül az egyenlőtlenségi vagy egyenlőségi feltétel a minimálandó fitnesz $\mathcal{F}(\bar{x})$ függvényhez hozzá adódik egy büntető paraméter. Célszerű úgy felvenni a büntető függvényt, hogy ha teljesülnek a feltételek a fitnesz értéke ne változzon, illetve elhanyagolható legyen a változás. Ha pedig nem teljesülnek a hozzá adott érték nagyságrendekkel változtassa meg (jelen cikkben ez az érték 10^6).

$$\alpha(x) = \begin{cases} 0 & \text{ha } x \leq 0 \\ 10^6 & \text{egyébként} \end{cases} \tag{5}$$

Ha a programozási, szimulációs környezet támogatja, szokás a végtelent is hozzá adni, de ez a módszer nem a legjobb. Előfordulhat, hogy a kezdeti populáció nem tartalmaz minden korlátot kielégítő egyedet, és ekkor az optimálás nem folytatható. Az egyenlőségi feltételekhez büntető függvényt nem definiálunk, mivel a továbbiakban optimálandó probléma ezt nem igényli.

A büntető függvénnyel kiegészített folytonos optimálási probléma:

$$\min \mathcal{F}(\bar{x}) + \sum_{j=1}^{q} \alpha\left(g_j(\bar{x})\right) \tag{6}$$

3. TEHERAUTÓ PLATÓ

Jelen esetben vizsgált teherautó alváza két hosszirányú acél gerendából áll. Ehhez csatlakozik egy köztes tartón keresztül a három rétegű plató (*2. ábra*). Név szerint a három réteg kereszttartók, hossz irányú tartók és padlólemez. A kereszt- és hossztartók anyaga AlMgSi0.7 [1], a padlólemezé pedig AlMg2.5 [2]. A szerkezetet körbe öleli az oldalsó keret, mely közvetíti a további felépítményekből (tető, oldalfalak, ajtó) adódó terheléseket.

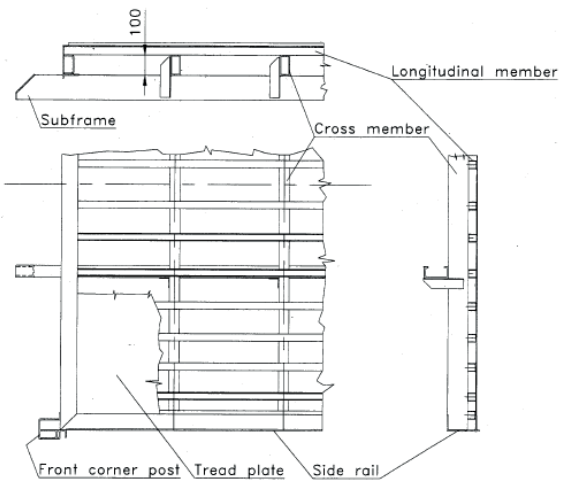

2. ábra Teherautó padlózatának szerkezete [4]

Az optimálás célja a teherautó plató anyag költségének csökkentése, a kereszttartók keresztmetszeti méreteinek változtatásán keresztül. A keresztmetszeti méretek jelölését és magyarázatát a *3. ábra* tartalmazza. A [4] korábbi számításai kimutatták, hogy az eredeti

zártszelvény (RHS szelvény), a vizsgált I és C szelvény közül tömeg szempontjából a legkedvezőbb eredményeket az I-szelvény adja. Ezért a továbbiakban a számításokat az utóbbival végeztük csak el.

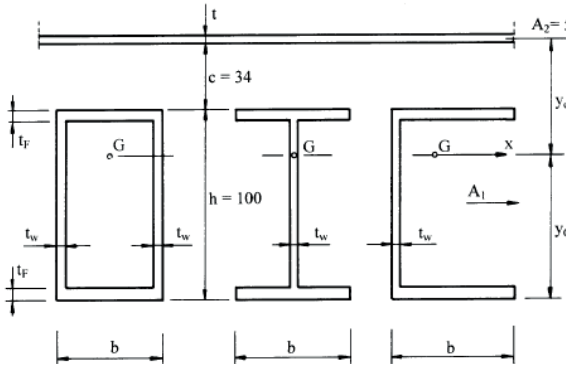

3. ábra Kereszttartók keresztmetszeti méretei [4]

A padlólemez effektív szélessége $50t$, ahol t a lemez vastagsága. A geometriai jellemzők I-szelvény esetén, úgymint keresztmetszeti terület, súlyponti távolságok és másodrendű nyomaték:

$$A = A_1 + A_2 \quad A_1 = ht_w + 2bt_f \quad A_2 = 50t^2 \tag{7}$$

$$y_G = \frac{A_1}{A}\left(\frac{h+t}{2} + c\right) \tag{8}$$

$$y_c = h + c + \frac{t}{2} - y_G$$

$$I_x = \frac{h^3 t_w}{12} + \frac{bt_f h^2}{2} + A_1\left(y_c - \frac{h}{2}\right)^2 + A_2 y_G^2 \tag{9}$$

A (7)-(9) jelöléseivel és korábban megfogalmazott célok alapján az optimálás fitnesz függvénye:

$$\mathcal{F}(\bar{x}) = \rho A_1 L_c n_c; \quad \bar{x} = [b, t_f] \tag{10}$$

ahol $\rho = 2{,}7x10^{-6}\, kg/mm^3$ az alumínium sűrűsége, $L_c = 2440mm$ egy kereszttartó hossza, és n_c a kereszt tartók száma. Látható, hogy csak az övlemez jellemző méretei változnak. A gerinclemez magassága $h = 100mm$ megegyezik az eredeti RHS szelvény magasságával. A $t_w = 3{,}4mm$ vastagság pedig a gyárthatóságot még biztosító minimális érték.

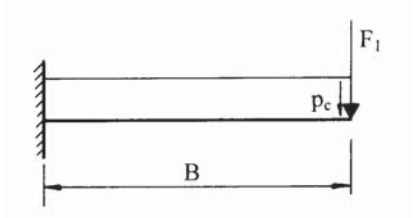

4. ábra Kereszttartók félkonzolos mechanikai modellje [4]

A kereszttartók terhelése, két erőrendszer szuperpozíciójaként értelmezhető hajlító nyomaték és nyíróerő (*4. ábra*). Első erőrendszer hasznos teher súlyából adódó megoszló terhelés.

$$p = \frac{F_p n_p}{BL} \tag{11}$$

ahol F_p=8500N a feltételezett raklapok súlya, $n_p = 5$ a felhelyezett raklapok száma, $B = 720mm$ és L a félkonzolos plató felület jellemző méretei. Az egy kereszt-tartóra jutó vonal mentén megoszló terhelés:

$$p_c = \frac{pL}{n_c - 1} \tag{12}$$

A második erőrendszer a felépítmény súlyából adódó $F_1 = 1946N$ koncentrált erő. Vízszintes helyzetben a hajlító nyomaték

$$M_h = \frac{p_c B^2}{2} + F_1 B = \frac{F_p n_p B}{2(n_c - 1)} + F_1 B \tag{13}$$

a nyíróerő

$$Q = \frac{F_p n_p}{n_c - 1} + F_1 \tag{14}$$

és a feszültségek

$$\sigma = \frac{M_h}{I_x}\max(y_G, y_C) \tag{15}$$

$$\tau = \frac{Q}{ht_w} \tag{16}$$

Az optimálás korlátait a tönkremeneteli határállapotokból lehet származtatni. Az első ilyen korlát a hegesztési varrattok fáradása határból adódik. A [3] és [7] szerint a megengedett feszültség $\sigma_C = 28MPa$, és $\tau_c = 28MPa$ nyírófeszültség $2x10^6$ ciklusszám mellet. Ebből származtatható a tényleges $N = 2x10^5$ ciklusszámhoz tartozó érték.

$$\log\Delta\sigma_N = \frac{1}{3}\log\frac{2x10^6}{N} + \log\sigma_C \tag{17}$$

$$\log\Delta\tau_N = \frac{1}{3}\log\frac{2x10^6}{N} + \log\tau_C \tag{18}$$

a korlátok pedig kifejezve (15)-(18) egyenletekből

$$g_1(\bar{x}) = \frac{\gamma_{Mf}\sigma}{\Delta\sigma_N} - 1 \le 0 \tag{19}$$

$$g_2(\bar{x}) = \frac{\gamma_{Mf}\tau}{\Delta\tau_N} - 1 \le 0 \tag{20}$$

ahol $\gamma_{Mf} = 1.25$ biztonsági tényező.

További korlátok adódnak a stabilitási feltételekből. Gerinclemez horpadási feltételéből adódó

$$g_3(\bar{x}) = \frac{\beta h}{22t_w\varepsilon} - 1 \le 0 \tag{21}$$

ahol β és ε az alábbiak szerint számolható

1. táblázat Optimalizálás eredménye

	Eredeti RHS szelvény [4]			Optimált I-szelvény				
n_c	14	12	10	16	14	12	10	8
b [mm]	55,0	115,0	120,0	73,9	66,1	80,8	78,1	74,3
t_f [mm]	5,4	3,0	3,4	4,6	5,9	5,6	7,0	9,4
A_1 [mm^2]	1274	1370	1496	1019,88	1116,36	1246,57	1437,52	1738,32
Tömeg [kg]	117,50	108,31	98,56	107,50	102,96	98,55	94,70	91,62
Anyag költség [$]	202,10	186,28	169,51	184,90	177,09	169,50	162,89	157,58

$$\beta = \begin{cases} 0{,}65 + 0{,}35\dfrac{y_0}{y_c} & \text{ha } 1 > \dfrac{y_0}{y_C} \geq 0 \\ 0{,}65 + 0{,}30\dfrac{y_0}{y_c} & \text{ha } 0 > \dfrac{y_0}{y_C} \geq -1 \end{cases} \quad (22)$$

$$\varepsilon = \sqrt{\frac{250}{\sigma/\gamma_{M1}}} \quad (23)$$

$$y_0 = y_G - \frac{t}{2} - c \quad (24)$$

az övlemezek horpadási feltétele pedig

$$g_4(\bar{x}) = \frac{b}{14 t_f \varepsilon} - 1 \leq 0 \quad (25)$$

4. OPTIMÁLÁS EREDMÉNYE

Az optimálást $n_c = 8{,}10{,}12{,}14{,}16$ darab kereszttartó mellett végeztük el. Az eredményeket a *1. táblázat* foglalja össze. I-szelvény optimált méretekkel tömeg csökkenést és költségmegtakarítást eredményez az eredeti RHS szelvényhez képest.

A feltüntetett anyagköltség az összes szükséges kereszttartó költségét jelenti.

$$K_m = k_m m_c = k_m \rho A_1 n_c L_c \quad (26)$$

ahol $k_m = 1{,}72\$/kg$ [8] a fajlagos anyag költség. A szerszámozási költség el lett hanyagolva, mert [4][6] korábbi számításai alapján egy tartóra vetítve, az anyagköltséghez viszonyítva elhanyagolható.

A kereszttartók számának növelésével a keresztmetszeti terület csökken az össztömegük pedig nő. Az eredeti $n_c = 10{,}12{,}14$ számhoz képest a tartók számát tovább csökkentve még nagyobb megtakarítás érhető el.

Optimálás során a mértékadó korlát a varratok fáradási feltétele volt.

5. KONKLÚZIÓ

A bemutatott optimálás során egy húzott, alumínium profilokból hegesztett kamion plató kereszttartói keresztmetszeti méreteinek meghatározása történt meg. Korlátnak a varratok fáradási feltétele és helyi horpadási feltételek voltak figyelembevéve. Az eredeti RHS szelvényű szerkezethez képest minden kereszttartó számnál megtakarítást eredményezett mind tömegben, mind költségben. Ez nem csak a gyártási költségeket csökkenti, hanem az üzemeltetési költségeket is.

6. KÖSZÖNETNYILVÁNÍTÁS

A cikkben ismertetett kutató munka az EFOP-3.6.1-16-2016-00011 jelű „Fiatalodó és Megújuló Egyetem – Innovatív Tudásváros – a Miskolci Egyetem intelligens szakosodást szolgáló intézményi fejlesztése” projekt részeként – a Széchenyi 2020 keretében – az Európai Unió támogatásával, az Európai Szociális Alap társfinanszírozásával valósul meg.

7. IRODALOM

[1] DIN 1725-1983: Aluminiumlegierungen. Knetlegierungen, Knetlegierungen 1983

[2] DIN 1748-1983: Strangpressprofile aus Aluminium und Aluminium-Knetlegierungen. Eigenschaften, Zulässige Abweichungen, 1938

[3] Eurocode 3 Part 1.1.: Design of steel structures. General rules and rules for buildings, European Committee for Standardization, Brussels, 2005

[4] Farkas J., Jármai K., Dúl R.: Minimum cost design of a truck floor welded from aluminium-alloy profiles, Welding in the World, Pergamon Press, Vol. 45, No. 9-10, (2001), pp. 19-22, ISSN 0043-2288

[5] Farkas J. Jármai K.: Optimum design of steel structures, Springer Verlag, Heidelberg, 2013

[6] Farkas J., Jármai K.: Truck floor design for minimum mass and cost using different materials, Vehicle and Automotive Engineering, Springer 2017, ISBN 978-3-319-51188-7

[7] Hobbacher A.: IIW Recommendations for fatigue design of welded joints and

components, IIW-doc, IIW-1823-07, ex XIII-2151r3-07/XV-1254r3-07
[8] London Metal Exchange, www.lme.com/metals, megnézve: 2020.03.05
[9] Storn R., Price K.: Differential Evolution – A Simple and Efficient Heuristic for global Optimization over Continous Spaces, Journa of Global Optimization, Vol. 11, (1997), pp 341-359, doi.org/10.1023/A:1008202821328
[10] Xin-She Y.: Flower pollination algorithm for global optimization, Unconventional Computation and Natural Computation, Vol. 7445, (2012), pp. 204-249
[11] Xin-She Y.: Nature-Inspired Metaheuristic Algorithms Second Edition, Luniver Press, Frome, 2010

A FELÜLETVASALÁS FELKEMÉNYEDÉSRE GYAKOROLT HATÁSÁNAK VIZSGÁLATA

EXAMINATION OF THE EFFECT OF SURFACE BURNISHING PROCESS ON HARDENING OF PHENOMENON

Ferencsik Viktória, egyetemi tanársegéd
Dr. Varga Gyula, egyetemi docens

ABSTRACT
This paper deals with the examination of changing of surface micro-hardness caused by diamond burnishing process. We examine how the different technological parameters of burnishing, such as the feed rate, speed and the burnishing force have effect on hardening of phenomenon for a lower (EN AW-2011) and a higher hardness (hardened C60) material. The experiments we designed and executed using full factorial experimental design method.

1. INTRODUCTION

During recent years, considerable attentions are being paid to the post finishing operations, such as burnishing process. The aim of this process is to achieve a surface quality with appropriate roughness, micro-hardness, wear and corrosion resistance [1-2]. Moreover, it improves resistance against fatigue strain by causing residual stress in the subsurface area which can be one of the quality requirements in industrial practice [3].

To design and execute the experiments of burnishing of external cylindrical surfaces, full factorial experimental design method [4-5] was chosen which is an active, effective experimental technique and the purpose of it is to determine function relationship between dependant and independent variables that are called factors, which can take more levels. In the present experiment the examined parameters, so the independent variables were the burnishing force (F), feed rate (f) and burnishing speed (v_b) for two types of material: C60 hardened steel and EN-AW-2011 low alloyed aluminium.

Measuring of the surface micro-hardness of the specimens was realized with Wilson Instruments Tukon 2100B measuring equipment in Vickers hardness.

2. BURNISHING OF EXTERNAL CYLINDRICAL SURFACES

In burnishing, the working part of the tool is pressed under a force onto the workpiece surface and this pressure is generated by the ball exceeds the yield point of the softer piece part surface at the contact area, resulting plastic deformation on the surface structure [2, 6-7]. The range of this deformation and as the hardening layer of the material is quite high, and changes in the structure of the surface layer occur at a significant depth [8].

The operation was performed with PCD spherical burnishing tool with 3.5 mm radius, attached to a CNC lathe produced by firm OPTIMUM type OPTIturn S600. This lathe was installed in the workshop of the Institute of Manufacturing Science at the University of Miskolc. The lubrication was solved by manually and the applied oil's kinematic viscosity was 70 mm^2/s. The practical implementation can be seen in Fig. 1.

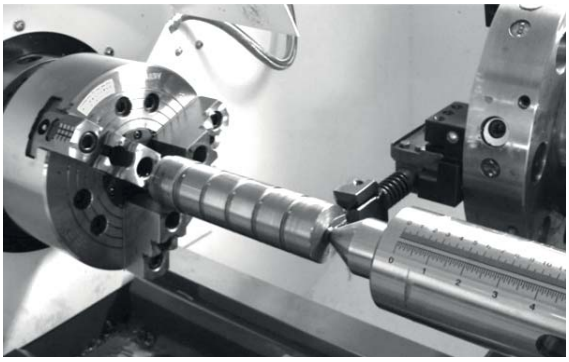

Figure 1. Executing of burnishing process

This process is applied in machine-building, automotive and aircraft industries in machining of various sorts of materials. For the experiments low alloyed aluminium and C60 hardened steel was chosen in order to compare the process applying in a low and higher density material.

3. EXPERIMENTAL CONDITIONS

3.1. Burnishing parameters

The effect of different burnishing parameters (burnishing force, feed rate, burnishing speed) on heat-treated steel [9-13] and on aluminium alloy workpieces [14-18] was investigated by many researchers.

To obtain the optimum value of these parameters for these two kinds of materials, require many experiments.

Based on literature review and preliminary experiments different values were determined for hardened steel than the low alloyed aluminium which was also justified by the difference in density between them.

The matrixes of these are shown in Table 1 that contains the pre-experimental testing parameters for both the natural and transformed dimensions.

Table 1. Applied burnishing parameters

C60

No.	Burnishing parameters			Transformed parameters		
	F [N]	f [mm/rev]	v [m/min]	x_1	x_2	x_3
1	50	0.05	40	-1	-1	-1
2	100	0.05	40	+1	-1	-1
3	50	0.1	40	-1	+1	-1
4	100	0.1	40	+1	+1	-1
5	50	0.05	80	-1	-1	+1
6	100	0.05	80	+1	-1	+1
7	50	0.1	80	-1	+1	+1
8	100	0.1	80	+1	+1	+1

EN AW-2011

No.	Burnishing parameters			Transformed parameters		
	F [N]	f [mm/rev]	v [m/min]	x_1	x_2	x_3
1	10	0.001	15	-1	-1	-1
2	20	0.001	15	+1	-1	-1
3	10	0.005	15	-1	+1	-1
4	20	0.005	15	+1	+1	-1
5	10	0.001	30	-1	-1	+1
6	20	0.001	30	+1	-1	+1
7	10	0.005	30	-1	+1	+1
8	20	0.005	30	+1	+1	+1

3.2. Measuring of surface micro-hardness

The applied measuring equipment - Wilson Instruments Tukon 2100B - has the same measuring principle as all other hardness measurement equipment. It examines how a material is subject to plastic deformation by using a standard force. In this investigation a 136° diamond pulley is pressed with a specific force, 10 N for 10 seconds on the surface for both materials to be measured on 3 points with 120° rotation. Fig. 2. shows a measuring state during measurement.

Figure 2. Executing of measuring process

4. RESULTS

For evaluation of measured data improvement ratios were introduced, which are shown in formula (1) and (2):

$$\rho_{HV} = \frac{HV_{after}}{HV_{before}} \quad (1)$$

$$\rho\% = (\rho - 1) \cdot 100\% \quad (2)$$

, where:

ρ_{HV} Improvement ratio of surface micro-hardness (HV). This is a dimensionless ratio, which textures the changes occurring because of manufacturing,

HV_{after} Surface micro-hardness remain after burnishing,

HV_{before} Surface micro-hardness before burnishing,

$\rho\%$ The percentage value of the improvement ratio.

The higher the values of ρ_{HV}, the greater the improvements due to burnishing.

The measured data and the calculated improvement ratios are summarized in Table 2.

Table 2. Measured values and calculated improvement ratios

No.	HV_{C60}		ρ_{C60} [%]
	Before	After	
1	882.4	985.5	**11.68**
2		914	**3.58**
3		977	**10.72**
4		1059	**20.01**
5		1024	**16.05**
6	883	860	**-2.60**
7		832	**-5.77**
8		854.5	**-3.23**
No.	$HV_{EN\ AW-2011}$		ρ_{EN} [%]
	Before	After	
1	160.7	169.3	**5.35**
2		180.3	**12.19**
3		160	**-0.44**
4		162	**0.81**
5		181	**12.63**
6	162.7	170	**4.49**
7		158	**-2.89**
8		170	**4.48**

Application of Factorial Experiment Design method empirical formulas (3) and (4) were determined from the calculated values. Calculations and axonometric figures (Fig. 3-4) were created by using MathCAD software.

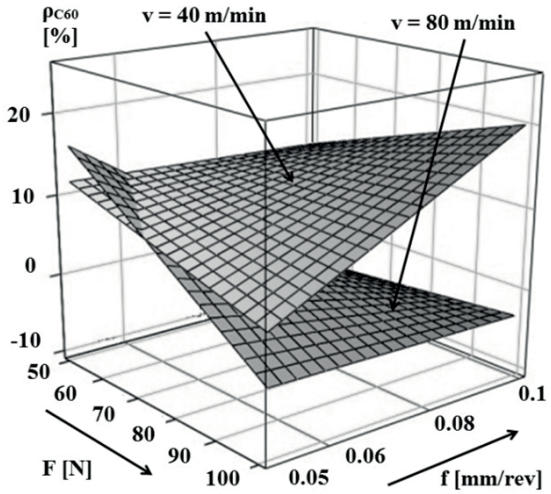

Figure 3. Changing of improvement ratio of C60 surface micro-hardness

$$\rho_{C60} = -1.45 - 0.223 \cdot F + 126.2 \cdot f + \\ +0.989 \cdot v + 5.436 \cdot F \cdot f - 7.175 \cdot 10^{-3} \cdot F \cdot v - \\ - 12.33 \cdot f \cdot v + + 0.038 \cdot F \cdot f \cdot v \qquad (3)$$

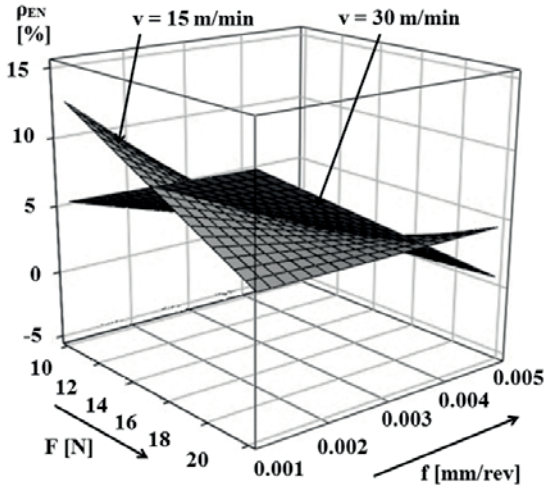

Figure 4. Changing of improvement ratio of EN AW-2011 surface micro-hardness

$$\rho_{EN} = -31.408 + 2.849 \cdot F + 7.657 \cdot 10^{-3} f + \\ +1.998 \cdot v - 667.25 \cdot F \cdot f - \\ -0.135 \cdot F \cdot v - 513.833 \cdot f \cdot v + 35.167 \cdot \\ \cdot F \cdot f \cdot v \qquad (4)$$

5. SUMMARY

The paper deals with the investigation of diamond burnishing process on hardened steel and low alloyed aluminium cylindrical components. The purpose of this study was to determine how the chosen burnishing parameters have effect on the changing of surface micro-hardness. The experiments and the evaluation of the measurement results were performed by using the full factorial experimental design method. According to the measured, calculated and illustrated results the following conclusions can be stated:

- In case of hardened steel among the examined parameters, the effect of feed rate is the most dominant and it has a strong interaction with the burnishing speed; parameters that resulted the most favourable surface micro-hardness were follows:
  F = 100 N
  f = 0.1 mm/rev
  v = 40 m/min
- In case of low alloyed aluminium also the influences of feed rate and force are significant and higher improvement was caused by the application of these burnishing parameters:
  F = 10 N
  f = 0.001 mm/rev
  v = 30 m/min

6. ACKNOWLEDGEMENT
"Project no. NKFI-125117 has been implemented with the support provided from the National Research, Development and Innovation Fund of Hungary, financed under the K_17 funding scheme."

7. REFERNCES

[1] Thamizhamanii S., Hasan S.: An Experimental Work on Multi-Roller Burnishing Process on Difficult to Cut Material – Titanium Alloy. International Journal of Integrated Engineering. Issue on Mechanical, Materials and Manufacturing Engineering (2009) pp: 1-6
[2] Vukelic D., Miljanic D., Randjelovic S., Budak I., Dzunic D., Eric M., Pantic M.: A burnishing process based on the optimal depth of workpiece penetration. MTAEC9, 47 (2013) pp: 43-51
[3] Mertinger V., Sólyom J. Benke M.: MonoCap optics for X-ray diffraction tests. Journal of Materials Testers (2012) pp: 60-64
[4] Taguchi G.: System of experiment design. Experimental design Kraus International Publications, 1 (1984) pp: 143
[5] Fridrik L.: Chosen chapters from the topics of experimental design of production engineering. Műszaki Könyvkiadó, (1987) (In Hungarian)
[6] Borkar A. P., Kamble P. S., Seemikeri C. Y.: Surface Integrity Enhancement of Inconel 718 by using Roller Burnishing process. Int. J. of Current Engineering and Technology 4 (2014) pp: 2595-2598
[7] Posdzich M., Stöckmann R., Morczinek F., Putz M.: Investigation of a plain ball burnishing process on differently machined Aluminium EN 2007 surfaces. MATEC Web of Conferences, 190 (2018) pp: 7
[8] Dzionk S., Scibiorski B., Pryzybylski W.: Surface Texture Analysis of Hardened Shafts after Ceramic Ball Burnishing. Materials 12 (2019) pp: 1-15
[9] Bálint L., Gribovszki L.: The basics of machine engineering technology. (1975) pp: 418-442 (in Hungarian)
[10] Ferencsik V.: Examination of 3D Surface Roughness of diamond Burnished Surfaces. Scientific Student Paper (2013) pp: 37
[11] Brostow W., Czechowski K., Polowski W., Rusek P., Toboła D., Wronska I.: Slide diamond burnishing of tool steels with adhesive coatings and diffusion layers. Material Research Innovations (2013) pp: 269-277
[12] El-Taweel T.A., El-Axir M.H.: Analysis and optimization of the ball burnishing process through the Taguchi technique. International Journel Advertising of Manufacture Technology 41 (2009) pp: 301-310
[13] Varga G: Effects of Technological Parameters on the Surface Texture of Burnished Surfaces. Precision Machining VII, Key Engineering Materials 581 (2013) pp: 403-408
[14] Babu P.R., Ankamma K., Siva Prasad T., Raju A.S., Eswara Prasad N.: Optimization of burnishing parameters and determination of select surface characteristics in engineering materials. Sadhana 37 (2012) pp: 503–520
[15] Luo H., Liu J., Wang L., Zhong Q.: Investigation of the burnishing process with PCD tool on non-ferrous metals. Int J Adv Manuf Technol 25 (2005) pp: 454-459
[16] Majzoobi G. H., Zare Jouneghani F., Khademi E.: Experimental and numerical studies on the effect of deep rolling on bending fretting fatigue resistance of Al7075. Int J Adv Manuf. Technol. 2 (2015) pp:1-12
[17] Stalin John M. R., Suresh P., Raguraman D., Vinayagam B. K.: Surface Characteristics of Low Plasticity Burnishing for Different Materials Using Lathe. Arab J Sci Eng 39 (2014) pp: 3209-3216
[18] Tadic B., Todorovic M., Luzanin O., Miljanic D., Jeremic M., Bogdanovic B., Vukelic D.: Using specially designed high-stiffness burnishing tool to achieve high-quality surface finish. Int J Adv Manuf Technol 67 (2013) pp: 601-611

PNEUMATIKUS HENGER SZABÁLYOZÁSA

CONTROL OF A PNEUMATIC CYLINDER

Tamás Szakács, PhD 1081 Budapest Népszínház u. 8 +3616665406 szakacs.tamas@bgk.uni-obuda.hu

ABSTRACT
A modular design MATLAB/Simulink® model has been created in order to model pneumatic cylinder motion, and cylinder control for speed, and position. A simple control model was developed, which can be realized by PLC, or an Arduino like embedded controller. Simulation results are also presented in this paper.

1. INTRODUCTION

A Matlab/Simulink® pneumatic cylinder model has been developed, validated, and presented in the last years of ACIPV conferences.

The in this paper presented pneumatic system description is based on the air mass-flow between the connecting components. The mass flow is driven by pressure difference, and the consumption of one component, is the supply on the other. The model consists of a compressed air supply, pressure reducing valve, T-joints, directional control valves cylinder, and load. The main part of the model is a double acting pneumatic cylinder, which converts pneumatic energy into mechanical one. There are different types of load, and control systems also modelled.

Pneumatic industrial solutions is a fast-developing area, which has many advantages compared to other solutions, like hydraulics, mechanical systems, or electronic drive, and control.

Pneumatic process control, and drive have great history. Besides industrial manufacturing solution, there are other mainly vehicle industrial technical solutions too [1]. For example the first self-propelled airplane, the first self-propelled U-boat had air-motor, but there were compressed-air engine propelled locomotives, trams, cars bicycles, etc. Since 2008 Bosch firm (and successors, Rexroth, Aventics, and Emerson) are organizing the pneumobile competitions, which is a race for pneumatically driven vehicles [2]

Of course, pneumatic solutions have disadvantages too. The main drawbacks are originated from the fact, that the working medium is compressed air.

Compressed air is a mixture of different gases, mainly oxygen, hydrogen, sometimes moisture, and particles as well, and it can be treated as a single component gas. In certain circumferences air can be treated as ideal gas without phase changes, condensation of moisture, etc.

Even with this simplification air dynamic is a lot more difficult to describe, and model, than fluid mechanics. [11] All the thermodynamic state variables of compressed air, like specific, and absolute volume, density, pressure, and temperature are greatly depend on each other. It is hard to find any parameter, which can be base of the model description. Practically the gas constant is the only parameter, which remains constant.

Modelling of a pneumatic system must therefore be based on mass conservation law, and all the thermodynamic properties must be calculated based on the state changes. If at least the change of density would remain close to constant, like in case of fluid mechanics, modelling and control of pneumatic systems would be as easy as in case of hydraulic systems, but because density and thus specific volume greatly depend on pressure and temperature precise position and force control of pneumatic systems are difficult. This complexity can be seen in work of Ferenc Szlivka: Different Mathematical Solutions on Gas Oscillation [8]. Eszter Sárközi publicated a mathematical model of pneumatic piston using using Stribeck Friction [3]. A completely analytical mathematical modelling is described by Vladislav Blagojević, Miodrag Stojiljković [4], and Spartak Poçari, and Andonaq Londo [10]

In general, pneumatic systems are not force and position controlled technical equipment. Usually pneumatic cylinders are making from-end-to end stoke motions without force and position control, except sensing the and-stroke positions.

Modelling a pneumatic cylinder as if it was a hydraulic one draws many mistakes. First of all, the most popular piston force balance equation is not complete, therefore not exact.

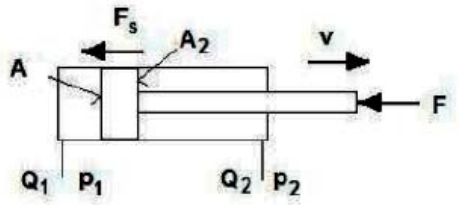

Fig. 1 General representation of a double-acting cylinder [5]

The annotations taken from the original source [5] are the followings: A is the greater, A_2 is the smaller area of the piston. F_s is the friction force, F is the load. p_1, and p_2 are the pressures in the corresponding cylinder chambers, Q_1, and Q_2 are the volume flows. The force balance of the cylinder according to the literature is:

$$F = p_1 \cdot A - p_2 \cdot A_2 - F_s \quad (1)$$

Using D as the piston, and d for the rod diameter, A, and A_2 surfaces are:

$$A = \frac{D^2\pi}{4} \; ; \; A_2 = \frac{(D-d)^2\pi}{4} \quad (2)$$

Because of A_2 is $\frac{d^2\pi}{4}$ smaller than A_1. Putting such a cylinder both lines open to the environmental pressure (p_1, and p_2 both are p_0) it is obvious that such a model will produce an $F=p_0 \cdot \frac{d^2\pi}{4}$ piston force, which having F load =0, would – according to the model – move outwards. It is an obvious modelling mistake.

The corrected force balance equation is:

$$F = p_1 \cdot A - p_2 \cdot A_2 - F_s - p_0(A - A_2) \quad (3)$$

An other often overlooked problem is the pressure in the opposite chamber (p_2), relative to the piston motion direction, especially when a long stroke piston takes a fast forward motion. (Fig 2)

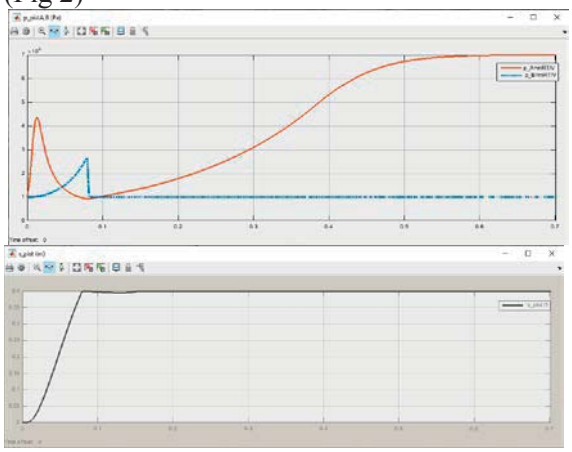

Fig. 2 Pressure, and motion of a fast-moving long-stroke fast moving cylinder

(Description of the simulation to produce the results can be found in the Results chapter.) It can be seen that the dashed line, which represents the p_2 pressure (marked p_B in the picture) reaches about one half of the p pressure (p_A). The longer the way of the exhausted gas from chamber B to the environment, the more the pressure increase is. The pressure increase is also proportional to the piston speed, and the A_1/A_2 ratio.

2. PROBLEM DESCRIPTION

In order to develop a precise control system for pneumatic piston position and force control an adequate model of the pneumatic system has to be derived.

The Matlab/Simulink® model used in this work consist of blocks representing two types of air sources, which are compressed air bottle, or a compressed air pipeline network. In both cases air consumption is calculated, in case of bottle supply the current bottle pressure is calculated as well. Both sources are connected to a pressure reducing valve, which is often called regulator. There are pneumatic pipelines, T-joints, and directional regulating valves also modelled. The main components in the model are the double acting two-chamber linear cylinder, connected to the load-model.

The overall structure of the model shown in Fig. 3.

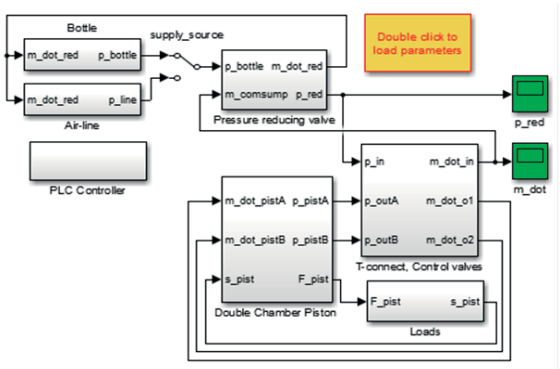

Fig. 3 Overall structure of the model

The compressed air tank is a constant volume, changing mass thermodynamic system. The operation of the model: the filled bottle of V volume contains m kg amount of gas which is characterized by R gas constant. (Fig. 4)

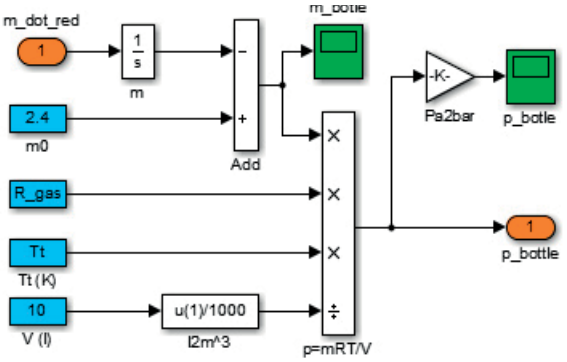

Fig. 4 The bottle model [6]

The pressure in the tank can be calculated as:

$$p = \frac{mRT}{V} \tag{4}$$

The temperature in the tank is considered constant, and equal to the environmental temperature. The $\dot{m}$ gas consumption is calculated in the pressure reducing valve submodel. (Fig. 6). Having the mass flow of the consumption integrated in time, the mass reduction of the enclosed gas is calculated, from which the pressure of the tank is updated in each simulation step.

In this figure the function annotations, and the color codes will be explained. Orange color is used for input, and output signals in the submodels. Light blue blocks are the constants, greens are scopes. Yellow blocks are Goto, and From pairs, mainly used for control signals (See later in Fig. 10), except the reduced gas temperature, which is used by all the systems in the model (See later in Fig. 8)

Using of colors are significantly increasing reading comfort, and lucidity of the model. Naming the blocks after their function equations, or signal names also help the better understanding the components, and their relations.

It can be seen that the inputs, and constants are aligned to the left, and all the output and scopes are lined up on the right side. All the important signals are scoped for better understanding, and validation. there are 40+ scopes in the model currently

The compressed air line model is very simple (Fig. 5)

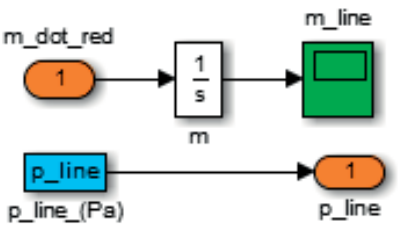

Fig. 5 Compressed air line model

This model calculates comsumpted air from integrating mass flow of consumption and sets line pressure to p_{line}.

The model is fully parametric. There no handtyped constant values, (except 0, 1, and 2) each constant value is handled by global variables from Matlab surface.

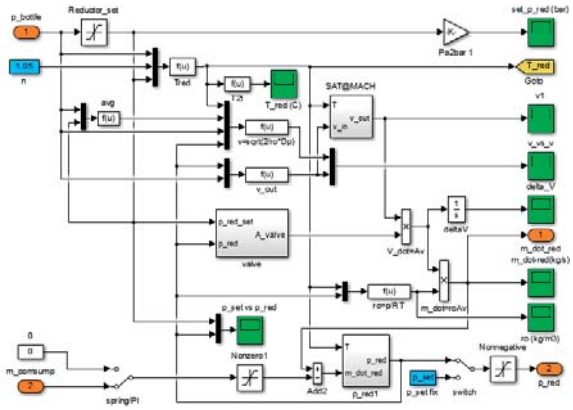

Fig. 6 The pressure reducing valve model [7]

The pressure reducing valve model shown in Fig. 6 has the following tasks to fulfill

- To determine the sound speed corresponding to the gas state
- To determine the reduced pressure gas temperature in the working chamber
- To calculate the pressure in the regulator working chamber
- To model the valve closing element motion in the pressure reducing valve
- To calculate the gas speed, volume-, and mass flow.

The dual chamber piston model consist of two air chambers. Chamber A, and B. Instead of using Fig. 1 it is recommended to use Fig. 7

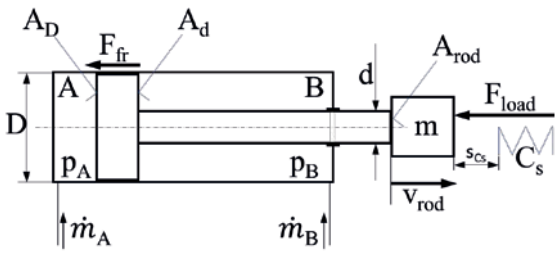

Fig. 7 The dual chamber piston used in the model

The variables used in the modelling are: A is the chamber opposite the piston rod, B is the chamber when the piston rod is A_D is the greater, A_d is the smaller area of the piston. F_{fr} is the friction force, F_{load} is the load. p_A, and p_B are the pressures in the corresponding cylinder chambers, $\dot{m}_A$, and $\dot{m}_B$ are the mass flows, m-is the mass of the load, F_{load} is the external load force, C_s, is the load spring stiffness (if there is any), s_{Cs} is the spring distance.

The force balance equation is described in Eq 3, using the above annotations is:

$$F = p_A \cdot A_D - p_B \cdot A_d - F_{fr} - p_0 \cdot A_{rod} \quad (5)$$

The complete model can be seen in Fig. 8

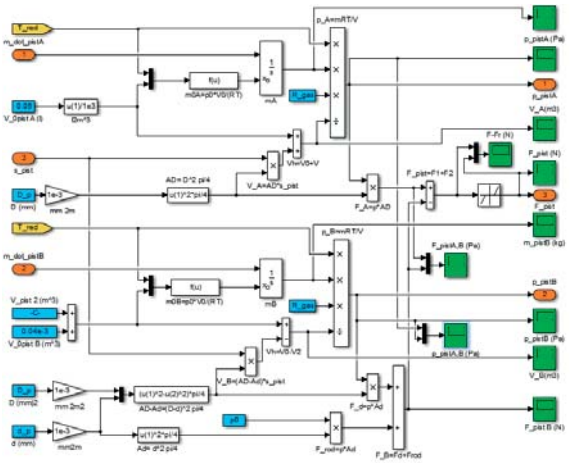

Fig. 8 The dual-chamber piston model

For better understanding model, one half of the piston force model is shown in Fig. 9.

As it can be seen, the initial chamber pressure, which is p_0 is provided by setting the integrator of mass to initial m_0 equivalent mass of air in a V_0 piston chamber volume at p_0 pressure. The corresponding equation is:

$$m_0 = \frac{p_0 V_0}{RT} \quad (6)$$

$$V_h = V_0 + A_D \cdot s_{pist} \quad (7)$$

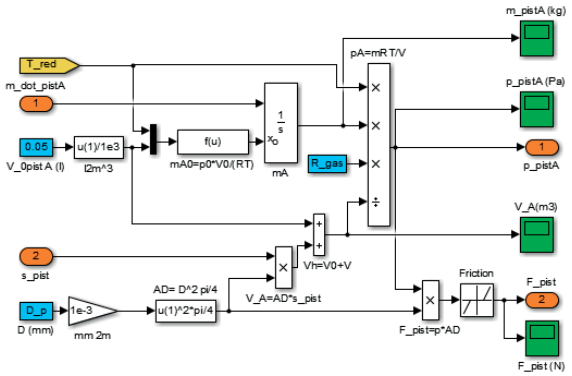

Fig. 9 Chamber A part of the dual-chamber piston model

The piston force is then calculated as pressure times working area:

$$F_{pist} = p \cdot A_D \quad (8)$$

The chamber B force is calculated in the same way, except the working area is smaller, because of the piston rod.

The two-chamber piston required to develop a T-junction model, because the air had to divide in between the chambers. The chambers are alternatively connected to the supplied air-, or the environment pressure, or in case of X/3 type of directional control valve, the gas amount in the chamber can be enclosed. Usually one chamber is filled, the other is exhausting, like when using 4/2, or 5/2 bi-stable directional control valves. In some cases ,4/3, or 5/3 central locked, valves are used, when in middle position all the channels are closed, or two pieces 5/2 type monostable valves are used, which allows individually chamber A, and B to be charged, locked, or exhausted. This modell uses on/off solenoid valves [10]

To control which one is filled and which is exhausting the pressure there was need to develop directional control valves. The T-junction, and the directional control valves are realized for practical reason in one submodel. The total model is shown in Fig. 10.

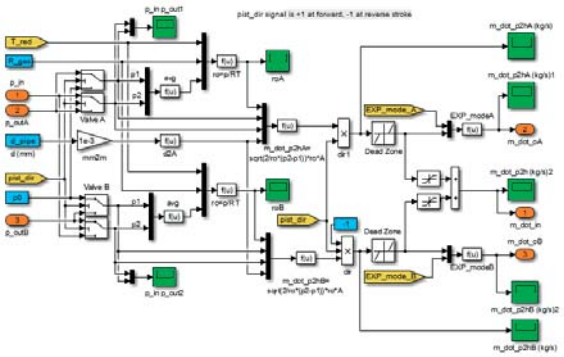

Fig. 10 5/3 Valves, and T-junction model

Fig. 11 shows a 4/2, or 5/2 type of realization of the directional control valve. This figure is a cut from Fig. *10*. This part of the model connecting chamber A with p_{in} (charge), and B with P_0 (exhaust) when piston stroke is forward, and oppositely in reverse stroke.

Fig. 12 shows the solution of T-junction, which connects chamber A, and B consumption $\dot{m}_{oA,B}$ when chambers are filled, and connects consummated mass flow ($\dot{m}_{in}$) to pressure reducing valve block.

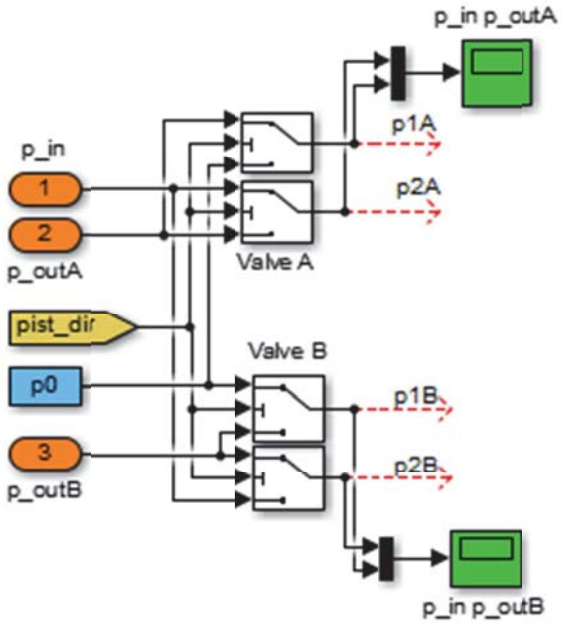

Fig. 11 4/X or 5/X type of directional control valves

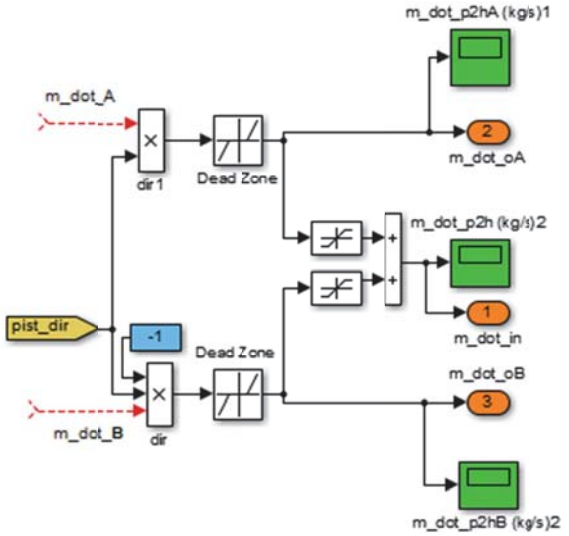

Fig. 12 Check valves, and linearized flow resistance in T-joint, X/2 variant

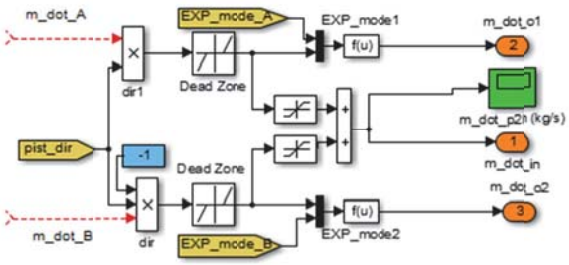

Fig. 13 Check valves, and linearized flow resistance in T-joint, X/3 locked variant

Fig. 13 shows solution, when instead of 4/2 (or 5/2) a 4/3, (or 5/3) valve are used. The X/3 valves have floating, or locked neutral position. The figure shows the locked version, when in middle position gas flows are locked in all channels. In this case EXP mode A, and B values are 0.

The consumption of piston chambers A, and B are calculated inFig. *14*. The input parameter for the calculation is the pressure difference between chamber, and connected pressure ($p_{reductor}$, or p_0). Its relating equations is:

$$\dot{m}_{p\to hA,B} = \sqrt{\frac{2}{\rho}(p_2 - p_1)} \cdot \rho A \qquad (9)$$

The gas average density required by Eq. 9 is calculated from average pressure as follows:

$$\rho = \frac{\bar{p}}{RT} \qquad (10)$$

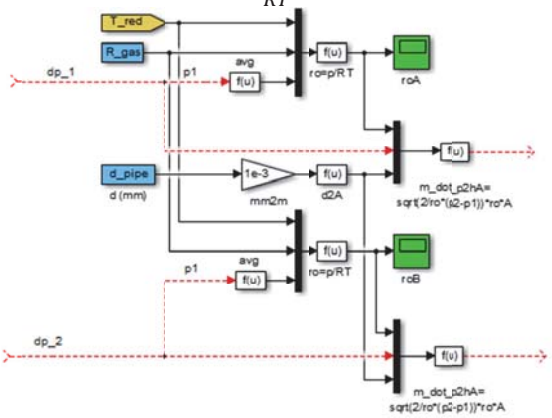

Fig. 14 Calculating mass flows to chamber A, and B from pressure differences

The load model is a simple Newtonian calculation using an M load which is accelerated linearly. Acceleration of the mass is calculated by a=F/m. Acceleration is integrated to have piston speed, and piston travelled distance. The speed integrator is reseted at stroke ends. Stroke end is detected by saturating piston distance at stroke end, and stroke=0. Reaching stroke end can be se to reverse piston motion.

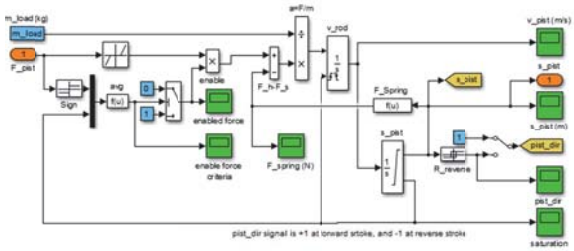

Fig. 15 Load, and piston motion model

Beside inertia load, there is a spring load also developed (see Fig. 7) When piston stroke exceeds s_{Cs}, then spring load force is also calculated.

3. RESULTS

There are 40+ scopes in the model. After simulation run all the important parameters can be investigated and compared. In the results chapter only three scopes will be shown, which are Chamber A, and B pressures, piston motion, and piston force.

The Fig. 2, which is showing the pressure build-up in a fast-moving cylinder is a result of the above described model.

The parameters used to produce the figure are:

```
% ** General properties **
R_gas=287.05; % Gas constant (J/(kgK))
Tt=273.15+20; % Tank air temperature (K)
p0=1e5;       % Environmental temperature p0=
10^5(Pa) = 1 Bar
p_set=7e5;    % Reductor set absolute presure
(Pa)
p_line=9e5;   % Pneumatic line absolute presure
(Pa)
d_pipe=10;    % Pneumatic pipe diameter (mm)

% ** Piston properties **
h_p=0.4;      % Sroke (m)
D_p=80;       % Piston diameter (mm)
d_p=36;       % Piston rod diameret (mm)
F_pr=40;      % Piston friction force (N)

% **  Load properties   **
m_load=5;     % Mass of load (kg)
mu_mech=0.8          % Mechanism friction
coefficient                              (-)
Cs_load=0;    % Load spring coeddicient (N/m)
s_Cs=0;              % load spring distance from
inposition (m)
```

During this simulation the reductor pressure is significantly decreasing, caused by the increasing air consumption. Most of the cases when fast piston movements are required, the reductor is the bottleneck of the system. In such cases using of a puffer tank is recommended.

Fig. 16 Reductor pressure during simulation

Changing the supply pressure to constant pressure, which is possible to switch the source switch to $p_{set\ fix}$ in the reductor model (Fig. 6))the same simulation is providing the following results:

The chamber pressures and piston position shown on Fig. 2, is changed to Fig. 17.

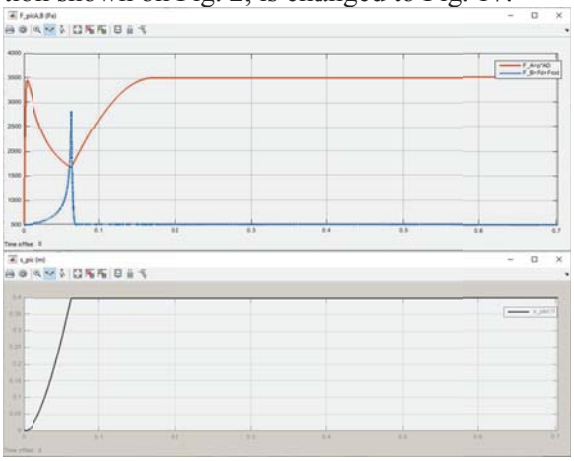

Fig. 17 Pressure, and motion of a fast-moving long-stroke fast moving cylinder

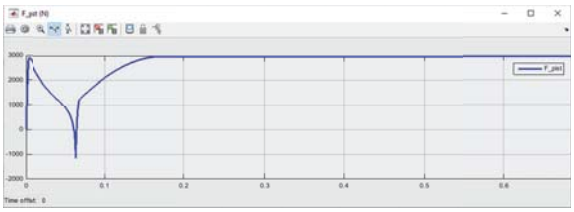

Fig. 18 The piston force during the simulation

4. CONCLUSIONS

Having the model developed, and tested, the net step is to develop a control system, which is able to control the piston force, and position. Instead controlling the pressure in chamber A, to provide force to move the piston to position, it is recommended to control both A, and B chamber pressures, to maintain maximum pressure in chamber B, and a Δp pressure in between the chambers. in this way air pressure, and as a consequence air density is also maximized, reducing the piston position sensitiveness from load change.

The model will be extended by user interface, and animation of piston, and load motion for education purposes.

Cylinder friction will be modified from Coulomb to Coulomb+ Static+ viscous friction or Stribeck friction model [3], [9]

5. SUMMARY

MATLAB/Simulink® model was created in other to simulate mechanic, thermodynamic, and fluid-mechanic behavior of a pneumatic system used in industrial application. Pneumatic system specific modelling aspects has been

described, model has been developed, and introduced.

ACKNOWLEDGEMENT
The research presented in this paper was carried out as part of the EFOP-3.6.2-16-2017-00016 project in the framework of the New Széchenyi Plan. The completion of this project is funded by the European Union and co-financed by the European Social Fund.

REFERENCES
[1] Tóth, István Tibor: Different Compressed Air, as an Alternative Fuel, 1st Agria Conference on Innovative Pneumatic Vehicles ACIPV 2017 pp. 17-19.
[2] XIII. International AVENTICS™ Pneumobile Competition https://en.pneumobil.hu/
[8] Szlivka Ferenc: Different Mathematical Solutions on Gas Oscillation ACTA POLYTECHNICA HUNGARICA 11 : 02 pp. 101-115. , 15 p. (2014)
[3] Sárközi Eszter: Modelling and Simulation of Pneumatic Cylinder using Stribeck Friction SCIENTIFIC BULLETIN, Serie C, Fascicle: Mechanics, Tribology, Machine Manufacturing Technology, ISSN 1224-3264, Volume 2016
[4] Blagojević Vladislav, Stojiljković Miodrag,:Mathematical and simulink model of the pneumatic system with bridging of the dual action cylinder chambers. Facta Universitatis Series: Mechanical Engineering Vol. 5, No 1, 2007, pp. 23 – 31
[5] Szlivka Ferenc: Irányítástechnika Hidraulika, Pneumatika ACTA POLYTECHNICA ÓE-BGK 3058, Budapest, 2014.
[6] Szakács Tamás: Pneumatic modelling of a pneumobil In: Pokorádi, László: Proceedings of the 2nd Agria Conference on Innovative Pneumatic Vehicles ACIPV 2018 Eger, Hungary, (2018) pp. 25-30. , 6 p.
[7] Szakács Tamás: Modelling and Validation of a Pneumobil In: Pokorádi László: Proceedings of the 3th Agria Conference on Innovative Pneumatic Vehicles – ACIPV 2019 Eger, Hungary (2019) pp. 31-35. , 5 p.
[9] Czmerk, A. (2015). Pneumatikus rendszerek dimanikájának és beállási pontosságának a javítása. PhD Thesis. BME Budapest.
[10] Spartak Poçari, and Andonaq Londo, Mathematical modelling, simulation and experimental verification of a pneumatic system. European Journal of Engineering and Technology Vol. 6 No. 1, 2018 ISSN 2056-5860
[11] V. Jouppila, S. A. Gadsden, A. Ellman, Modeling and identification of a pneumatic muscle actuator system controlled by an on/off solenoid valve. Proceedings of 7th International Fluid Power Conference March 22-24, 2010, Aachen, Germany

BEÁGYAZOTT RENDSZER KIEGÉSZÍTŐ KÁRTYÁJÁNAK FEJLESZTÉSE JÁRMŰ KOMMUNIKÁCIÓHOZ

DEVELOPMENT OF EMBEDDED SYSTEM EXTENDER CARD FOR VEHICLE COMMUNICATION

Péter Gulyás, István Kecskeméti

ABSTRACT

The SZEnergy Team have been developing light-weight concept cars since 2005. Our current vehicle communication system is based on different protocols used in the vehicle industry such as CAN, LIN, SPI and UART. As the main control unit of the vehicle we use an embedded controller produced by National Instruments, which sometimes struggles with UART driver loading and incompatibility which makes our communication system unreliable. In this case our car cannot start, and we need to restart the whole system, which is not permissible under competition situations. As a solution we decided to create our own function specific extender card, a special CAN to LIN transceiver, and a CAN to SPI transceiver to bypass all UART related actions. With the designed boards we can cope with cabling issues, analog signal routing and previous incompatibility problems. We designed the boards to be modular, so the two communication transceivers are capable to work as a standalone device as well. With the self-designed boards, we could not only reduce the cost of the communication system but also optimize our signal and power routing.

1. INTRODUCTION

The main goal of our work aims the reliability of our internal communication system and the space saving of the control module. Power line communication [1] and the standard of CAN 2.0 [2] is available since the beginning of the 90s. These communication standards are still in use in the automotive industry and are implemented in our concept car as well. With these communication protocols we can control the motor, read sensor values, and operate all the different peripherals around the car. Our main controller unit is a NI myRIO – 1900 [3] which does not have dedicated CAN[1] or LIN[2] communication connector. Users must implement software and hardware connection on different available ports to be able to use these communication protocols. The current and upcoming communication model of our concept car is shown in *Figure 1*.

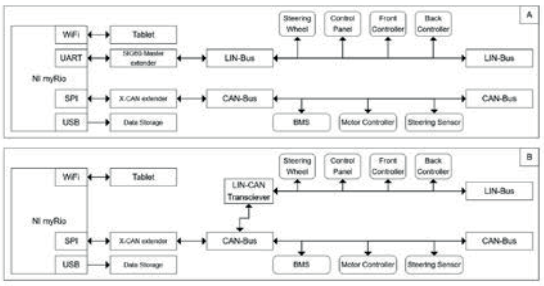

Figure 1
A: SZEmission communication model - 2019
B: SZEmission communication model - 2020

2. CAN-SPI GATEWAY

The default CAN expander card offered by National Instruments is an X-CAN named module [4] which is shown in *Figure 2*. This module is a hardware gateway between the CAN bus and the SPI[3] bus of the NI myRIO. It consists of few parts but takes up a lot of space next to the myRIO, while only a fraction of the outputs is used. Most of the unused connector pins are routed to socket headers, which provide unreliable connection, therefore these are not safe to use in automotive applications.

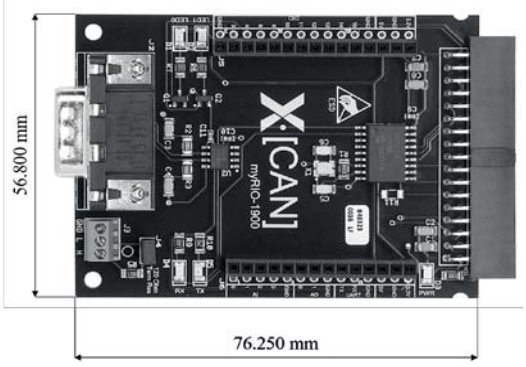

Figure 2. X-CAN module produced by National Instruments

[1] Controller Area Network

[2] Local Interconnect Network
[3] Serial Peripheral Interface

2.1 Schematic design of the CAN-SPI module

The new circuit has the same function as the X-CAN module, but in a smaller package and has the capability to work individually. For the CAN bus controller, a MCP2515 named IC[4], produced by Microchip is used [5]. It works with both high speed and low speed CAN and capable of using the standard and extended CAN message frames as well. The microcontroller also has several modes of operation such as sleep mode and listen-only mode to reduce energy consumption. It has an SPI interface, to communicate with the myRIO, and it is available in small UQFN packaging. The transceiver for the CAN bus is also a Microchip product, a MCP2652 coded IC. The circuit (*Figure 3*) also includes the CAN bus termination, which must be chosen for the actual application. For inline modules 1.5 kohm resistors, for end point modules 120 ohm resistors should be used as termination.

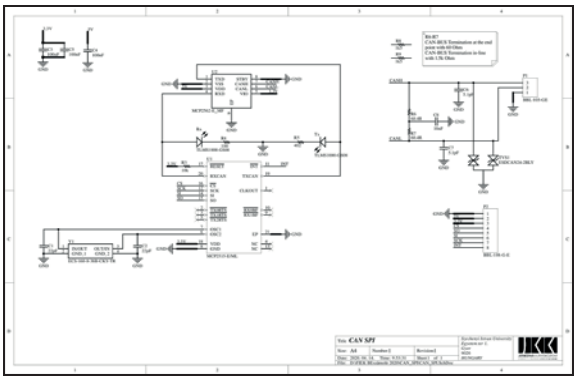

Figure 3 Schematic of the CAN-SPI module

2.2 PCB design of the CAN-SPI module

During the designing of the PCB[5] we focused on size reducing therefore every part is placed as close to each other as possible, considering the ease of manufacturing. To achieve this every component is 0402 size and the IC-s are chosen in the smallest QFN package available. To minimize routing, every component is placed and oriented in the correct way. Because of this communication protocol does not need high current supply, we could design the board with 8 mil routing width, which also helped our design goals. The headers on the edge of the PCB have a pitch of 2.54 mm, hence it is easily implementable not only in our but in other applications as well. The circuit inherits its power supply directly from the myRIO, through the lower extender board. As a result, the final product is 13 times smaller than the original X-CAN module, while keeping the same functionality (*Figure 4*).

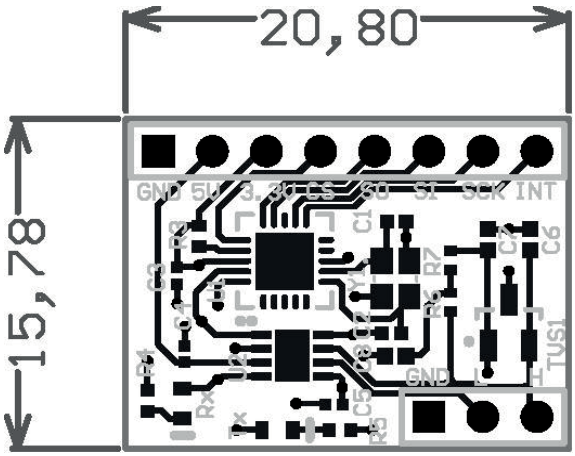

Figure 4 PCB plan of the CAN-SPI module

After the assembly procedure of the CAN-SPI gateway, we could test it via temporary cabling with the myRIO instead of the X-CAN module to check our vehicle communication with the newly designed communication board. On *Figure 5* the myRIO sends necessary data for the motor controller via the new CAN-SPI gateway. The test and therefore the new communication module succeeded.

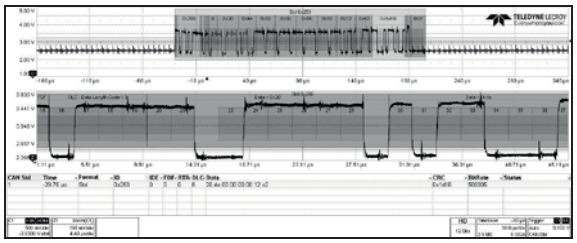

Figure 5 CAN message inspection on the new CAN-SPI gateway

3. CAN-LIN GATEWAY

Since the SIG60 coded integrated circuit, can cope with the coding and decoding of LIN communication as master unit, is only capable of UART[6] communication [6], that gives no choice for developers, they must work with that. Even with dozens of hours invested to optimize UART communication for the NI myRIO and the SIG60, we struggled to create a reliable and robust communication and that is why we decided to design our own module. We solve the UART communication problem via leaving this port unused on the myRIO, and insert a specific microcontroller, which will cooperate with the SIG60 integrated circuit, then translate all the

[4] Integrated Circuit

[5] Printed Circuit Board

[6] Universal Asynchronous Receiver-Transmitter

messages to the CAN bus. In this scenario our main controller does not have to work with UART at all, and a dedicated microcontroller can easily handle this communication translation.

3.1 Schematic design of the CAN-LIN module

The custom circuit is built up by the references of the manufacturer, and some custom added parts, for easier debugging and optional settings. We also made pinout for the "*Command*" pin of the SIG60 IC (*Figure 6*) for future programming options, which are currently not in use, but probably would be useful if we would like to take full advantage of all the features the IC has. All the parts used in the schematics are chosen to save as much space as possible, and to create an easy to assemble board. The controller IC have been chosen to a low power type manufactured by Microchip, which also has the minimal number of pins and functions what is needed. The controller IC powered from 3.3 VDC source, and capable of 100 MIPS[7], although in our case it will only run around 15 MIPS to save power. This complex module will also connect to the custom expander card via two low-profile headers, which card will be described in detail in the 4th section.

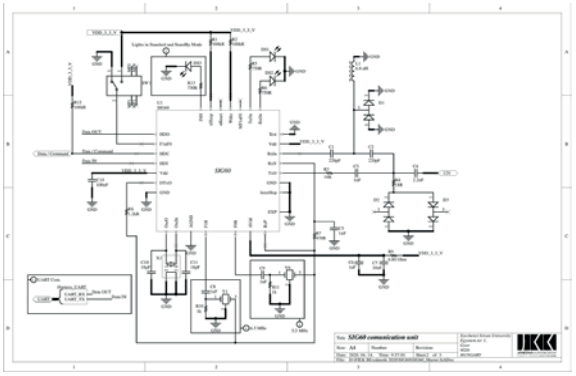

Figure 6 Schematic of the SIG60 IC.

3.2 PCB design of the CAN-LIN module

The biggest challenge during the design of the printed circuit board was the routing [7]. We wanted to organize all the parts to the physical minimum therefore in some cases we had to use 0201 sized capacitors. Even with the difficulties of the manual manufacturing, overall board size was prioritized. Some components were recommended by the manufacturer and caused some extra problem for our design e.g. not having proper PCB footprint for design or being much larger for other components. Exception to this were all the headers we design on the board to ensure the ease of connectivity to the expander card, or any further applications (*Figure 7*).

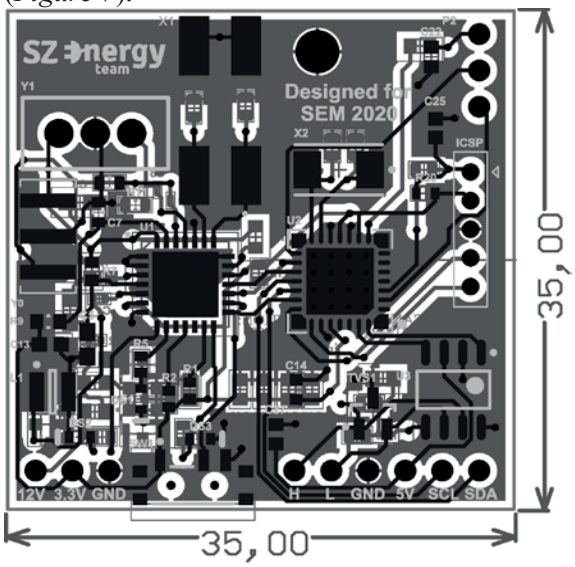

Figure 7 PCB plan of the CAN-LIN module

4. CUSTOM EXTENDER CARD

National Instruments offers extender card for the myRIO, which can be used in any desired application, however it also has the same socket headers as the X-CAN Module, which are not suited for automotive applications. It also lacks the ability to house many custom components on the board due to the small available place.

The new design uses both output ports of the myRIO, offers much more freely available space, and houses the two communication interfaces. Also, in our application a 12V line was implemented for power line communication. The extender card has two standard DSUB-9 connectors for CAN communication, and several plugin terminals for secure connection of analog and digital signals from other electronics. Several output pins from the myRIO are routed to the plugin terminals for easy access. The two-dimensional view of the PCB plan could be seen below, on *Figure 8*.

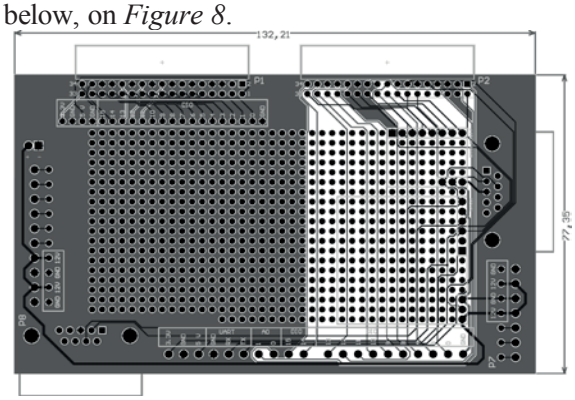

Figure 8. Custom designed Extender Card for myRIO.

[7] Million Instructions Per Second

5. CONCLUSION

We managed to create a complex extender card with two communication gateways for the myRIO embedded system, to solve our previous issues around the power line communication and space utilization. We successfully reduced the size of the X-CAN module by 13 times, and within the original size of the extension card, we added a custom CAN-LIN gateway. This way we created spare place for other electronics on the extender side of the myRIO. Moreover, we designed the Extender Card such way, our cable management needed all the connections for the best fit in our electric vehicle. The assembled and connected PCB-s are shown in *Figure 9*.

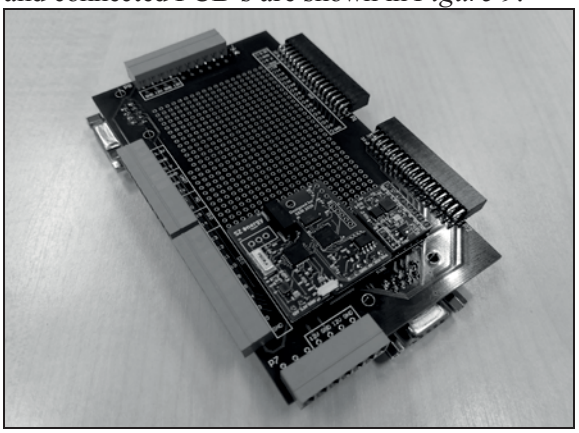

Figure 9 The completed Extender Card for myRIO

6. FUTURE DEVELOPMENT

Currently only two specially designed interfaces are installed on the board. However, with further analysis more communication protocols can be implemented in the same way, even as interchangeable devices. Modularity is a key word here, as every device can work individually. The myRIO itself can be used for many applications, such as motor controlling, data logging etc., therefore there are many possibilities for further development.

7. ACKNOWLEDGMENT

The research presented in this paper was carried out as part of the "Autonomous Vehicle Systems Research related to the Autonomous Vehicle Proving Ground of Zalaegerszeg (EFOP-3.6.2-16-2017-00002)" project in the framework of the New Széchenyi Plan. The completion of this project is funded by the European Union and co-financed by the European Social Fund.

REFERENCES

[1] P. Gulyás, G. Szakállas, Z. Szeli: *Implementation of LIN communication on DC power line in an electric experimental vehicle*, XXVII. International Conference on Mechanical Engineering, Oradea, Romania, 25-28 April 2019

[2] Steve Corrigan: *Introduction to the Controller Area Network (CAN)* Texas Instruments, Dallas, Texas, May 2016

[3] NI myRIO – 1900 documentation: *http://www.ni.com/pdf/manuals/376047c.pdf* (Last opened: 07.03.2020)

[4] X-CAN module documentation: *http://www.ni.com/pdf/products/us/X_CAN_Hardware_User_Guide_and_Specifications.pdf* (Last opened: 07.03.2020)

[5] MCP2515 IC datasheet: *http://ww1.microchip.com/downloads/en/DeviceDoc/MCP2515-Stand-Alone-CAN-Controller-with-SPI-20001801J.pdf* (Last opened: 07.03.2020)

[6] SIG60 IC datasheet: *https://www.yamar.com/datasheet/DS-SIG60.pdf* (Last opened: 07.03.2020)

[7] High Speed Routing Guidelines for Advanced PCBs: *https://resources.altium.com/pcb-design/high-speed-routing-guidelines-for-advanced-pcbs* (Last opened: 07.03.2020)

ALTERNATÍV HAJTÁSLÁNCÚ AUTONÓM JÁRMŰVEK SZABÁLYZÁSI KIHÍVÁSAI

CONTROL CHALLENGES IN AUTOMATED VEHICLES WITH ALTERNATIVE POWERTRAIN SOLUTIONS

Árpád Takács, Tamás D. Nagy, Dániel A. Drexler, Imre J. Rudas and Tamás Haidegger
Antal Bejczy Center for Intelligent Robotics, University Research and Innovation Center (EKIK), Óbuda University, Hungary H-1034 Budapest, Bécsi út 96/b

ABSTRACT: The automotive industry has gone through rapid changes in the past decade, which is partially driven by technological advancement, including the ever-growing palette of alternative powertrain solutions and autonomous features. While the two development areas are seemingly independent of each other, many synergies can be found in the underlying technologies. This paper collects the most important aspects of autonomous vehicle controller design with respect to the powertrain solution employed, primarily focusing on the differences between traditional combustion engines and fully electric driven vehicles. It aims to identify the major trends along which todays automotive industry is evolving.

1. INTRODUCION

The development of Autonomous Vehicle (AV) technology embraces diverse fields of research and applied science. As of today, quite a few car manufacturers (Original Equipment Manufacturers, OEMs) already offer a limited stack of automated driving assistant features in production vehicles, the efficient implementation of higher levels of automation is an actively discussed topic among research communities, automotive suppliers and software companies [1].

In less than 5 years, the number of companies working on self-driving vehicle prototypes grew above 100, yet the diversity of the vehicle platforms is significantly lower. Development history indicates that some platforms/vehicle models are more suitable for prototyping or production purposes than others, which defines a set of criteria that such platforms need to adhere to. These criteria may be affected by the comfort, spaciousness, power(-capacity), powertrain or physical dimensions of the vehicle, which needs to satisfy the basic requirements of the unique hardware and software of automated vehicles [2].

This paper discusses the challenges and requirements of automated vehicle control with respect to the powertrain solution used for development/production.

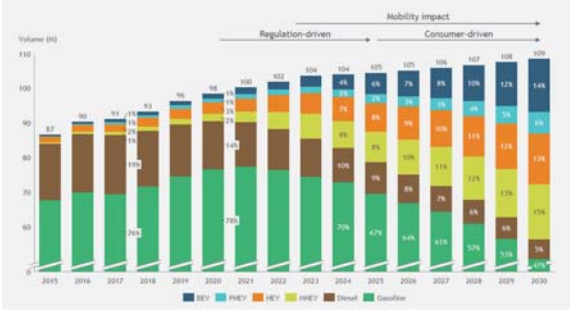

Figure 1 The Boston Consulting Group's market forecast of the share of alternative powertrain vehicles [3]. The tendency suggests that the share of hybrid and electric vehicles will significantly increase in the next decade.

2. POWERTRAIN SOLUTIONS

Today, more than 90% of all production vehicles are equipped with internal combustion engines (ICEs), and the ratio of gasoline and diesel powered engines is 5:1, respectively. Fig. 1 indicates that the share of (plug-in) hybrid vehicles (HEV/PHEV) remains at 5%, although hybrid technologies have evolved a lot in terms of efficiency in the past years, increasing their reliance on electric power. The fully electric or battery powered electric vehicles (BEVs, including hydrogen fuel cell solutions) have gained popularity this decade, however, their global volume percentage has barely reached 1% in 2019.

Autonomous Electric Vehicles (A-EVs) is a commonly misinterpreted umbrella term for future automotive technology. From the technology point of view, an autonomous vehicle does not need to be neither electric, nor hybrid

to ensure safe and efficient operation, while most BEVs lack any form of autonomous features today. There are, however, numerous synergies with the two technologies. However, as algorithm development, computational capacity and safety regulations pose a bottleneck in AV development today, these synergies are less frequently addressed in the literature.

There is no consensus among OEMs and developer communities on the optimal powertrain solution for autonomy. Some OEMs (Tesla: BEV, GM: ICE, Daimler: PHEV) implement autonomous features on mass-produced vehicles, seemingly independent from the powertrain itself. Software companies and automotive suppliers prefer globally available and integration-ready models (Ford Focus, Toyota Prius/Camry) or they are bound by partnerships (Waymo-FCA, Argo.ai-Ford). However, PHEV and BEV solutions are dominantly preferred among OEM-independent developers and suppliers, which, besides the positive marketing impact due to environmental-friendliness, highlights the technological advantages over traditional ICE assemblies.

The next section discusses the potential advantages of using alternative powertrain solutions in self-driving vehicle prototypes from control engineering aspects.

3. CONTROL ASPECTS OF SELF-DRIVING VEHICLES

With the growing number of autonomous vehicle prototypes, the focus of development has shifted from hardware to software, which contradicts with the traditional motor vehicle design. Software algorithms are responsible for perception, prediction, decision making and control. They mostly rely on sensor data from cameras, radars and other automotive sensors, which are later fused together to create an environmental and dynamic model to aid decision making, path planning, and eventually motion control.

Vehicle control relies on a robust trajectory, which consists of parametrized curves defined by a curvature center and radius. Regardless the control paradigm or vehicle dynamics, one can select 3 parameters to define this trajectory:

1. The road curvature center, which the vehicle aims to turns about at a given time instant
2. Kinematic rotation center, which is bound to the vehicle. It is found by taking the intersection of all the lines perpendicular to the wheels
3. Dynamic turning point, which refers to the actual point in space the vehicle turns about.

When designing a trajectory, one needs to consider the geometry of the feasible road surface, the temporal changes in the environment and the kinematic and kinetic constrains of the vehicle. Due to the nonlinear dynamics of motion and rapid trajectory changes, a large number of different control approaches can be found today using linearization, LQ-optimal control or Model Predictive Control / Model Predictive Path Integral Control [4].

For autonomous vehicles there are two dynamically coupled, yet often separately addressed fields of control: longitudinal control and lateral control. The embedded software responsible for signal generation receives data from a high-level prediction and decision making module, using either formal logic, artificial intelligence or both. This module usually defines high level actions to be taken based on the dynamic environment and the current vehicle state.

Longitudinal control utilizes information from various sources in order to correctly function [5]. These are attributes of objects surrounding the ego-vehicle, such as relative position, speed and acceleration. The self-motion or *egomotion* of the controlled vehicle is also used by the software to create efficient predictions on in time. Position, speed and acceleration data can be directly measured by conventional vehicle-mounded sensors (radar, LIDAR, ultrasonic) or indirectly by supporting algorithms (stereo depth, distance estimation from detection size). In longitudinal control, most scenarios are related to automatic cruise control (ACC), where the ego vehicle maintains a cruising speed limited by the presence of potentially slower vehicles. At high speeds, the time delay of gaining information of the preceding vehicles is crucial, the sensor input may become noisy. This affects the performance of the control algorithms, and it is highly dependent on the powertrain method.

Lateral control is responsible for lane keeping, obstacle avoidance and route changing maneuvers. In the case of state machines and formal logic-based systems, the robust functioning of this module strongly depends on the quality of trajectory planning and state predic-

tion. The comfort threshold for humans is considerably lower for lateral motion compared to that of the longitudinal, therefore the smoothness, applied acceleration and jerk (first time-derivative of the acceleration) should be carefully selected and may pose a challenge for vehicles with alternative powertrains.

From the control strategy point of view, lateral control may be treated as a tracking control problem following a temporarily changing spatial trajectory. On the other hand, a unified lateral guidance approach can be used to guide the vehicle by specified yaw and yaw rate values. These values are taken as a reference from predefined motion patterns and high-level maneuvers, all depending on the environmental conditions and the vehicle state.

4. INDIVIDUAL REQUIREMENTS WITH ALTERNATIVE POWERTRAINS

Today, purely internal combustion engines dominate the automotive market, while hybrid and fully electric cars take up most of the remaining market share with respect to unit numbers. From the powertrain design point of view, ICE and BEV vehicles represent the two extremes, while hybrid vehicles soften this boundary by providing a balance between the two significantly different approaches.

With the rising number of limited autonomous features, new design criteria have been defined by automakers to increase cruising comfort, and to address design methods and power efficiency of the vehicles.

4.1. Model-based control

In most autonomous vehicle control designs, both lateral and longitudinal control algorithms rely on a complex dynamic or simple kinematic model of the vehicle. Adaptive control methods and sliding-mode control approaches utilize a coarse system model to achieve robust operation. Model predictive control requires a more general knowledge about the system, including the predicted effect of known inputs (throttle, steering, braking). System identification and proper dimensionality reduction are also popular methods for finding optimal control architectures, which are often aided by AI-based identification methods and neural networks.

The dynamic behavior of ICEs is dominated by their nonlinear power and torque curves, indicating the correlation between engine rotation speed and available engine torque, as shown in Fig. 2. These curves are usually determined by standardized measurements under controlled conditions, but their highly nonlinear behavior and steep slopes, determining the current dynamic state of the vehicle is challenging. Local model linearization partly solves this issue in controller design, however, the uncertainty of the current working point in these curves result in noisy predictions and slow adaptation.

BEV systems on the other hand provide a smooth, virtually (piecewise) linear torque curve, allowing designers to make accurate predictions for the vehicle behavior as response to specific control inputs. Nevertheless, the true kinematic motion of the vehicle remains nonlinear, but from the controller design point of view, the mathematical model of the acting driving force on the wheels simplifies significantly.

4.2. Energy efficiency

ICEs present many idle cycles during the driving task, where fuel is burned only to maintain the continuous operation of the engine and keep the speed of rotation at a dynamically sensitive area of operation. This indicates that the longitudinal maneuverability of an ICE vehicle largely depends on the current state of the powertrain, where an inadequate choice of rotation speed and transmission state may increase response delay in the system.

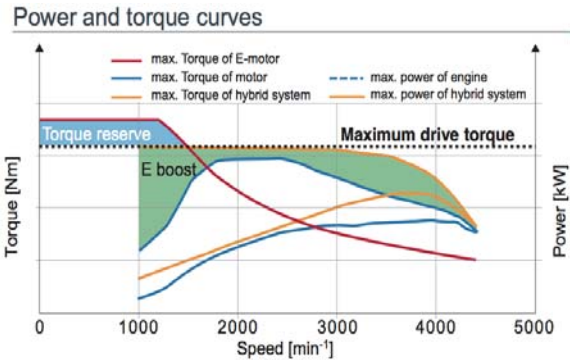

Figure 2: Power and torque curves of conventional ICE engines, hybrid systems and fully electric motors, according to a case study by Volkswagen [6]. Besides the considerably higher torque reserve of fully electric vehicles, the nearly constant torque available at lower speeds is favorable by autonomous vehicle design.

BEVs allow a rapid state change between fuel (battery) discharge and charge, the longitudinal maneuverability does not significantly depend on the current rotation speed and they are free of transmission-related issues. This

makes these systems a preference for efficient trajectory design, where besides comfort and speed efficiency, power or consumption efficiency can also be implemented as a criteria for controller design.

This includes trajectory planning, control signal optimization to avoid saturation, and execution efficiency.

4.3. Control smoothness

Human drivers have various driving styles, ranging from cautious to often daring. Both their lateral and longitudinal control trajectories are smoothed over the course of driving path to increase control. This can be experienced in curved roads, where the width of the lane offers the driver a freedom of trajectory choice rather than restricting the vehicle position to the lane centerline. Similar phenomenon can experienced in longitudinal control situations, where the catching up pace to a vehicle from behind depends on the traffic conditions and the driving style of the human driver, and the resulting differential speed is not only the function of relative distance, like it would be a result of the naïve control law formulation [7].

Today, most autonomous vehicles follow formally defined rules on longitudinal and lateral control, creating strict boundaries for position and speed trajectory planning, where low tracking error is requested. However, it is important to note that these strict boundary conditions may be smoothed by fuzzy control or neural networks-based methods (such as reinforcement learning).

In the case of ICEs, closely following the planned trajectory may result in an often rapidly updated control signal input and thus a heavy oscillation on the fuel intake side. This increases the fuel consumption significantly and ultimately may lead to the early amortization of the engine and transmission units. BEVs, on the other hand, are not sensitive to the rapid changes in the magnetic field responsible for driving the electric motor, and due to the nearly constant torque available at different speeds, their control response is a lot faster than the response of ICEs.

4.4. Cruising stability

Most of today's vehicles are equipped with advanced electronic stability programs (ESP) to monitor the reduction or loss of traction. In the case of stability or traction loss, these systems aid the human driver to regain control of the vehicle. Advanced driver assistance functions (ADAS) also actively contribute to the improved maneuverability of the vehicles in critical situations. When the vehicle is controlled by a human driver, these functions are independently operating in the background and use complex vehicle dynamic models to assess system dynamic behavior. ESP systems collect data and predict values for tire *slip*, the vehicle stability boundaries under given environmental conditions and assess the system state with respect to the friction curve [8].

Due to the long system response time in the case of acceleration, ICE ESPs are operating by applying brake force on the wheels individually. Lateral control, however, remains in the hands of the human driver, therefore stabilization efficiency strongly depends on the driver capabilities and response time. Autonomous vehicles offer the advantage of lateral control applied *simultaneously* with the ESP's longitudinal assistance. However, in higher levels of automation, the combined and coordinated operation of lateral and longitudinal control, individual ESP systems will become obsolete as their functionalities will be included in the global vehicle control.

Many BEV constructions incorporate the electric motors in the wheels rather than distributing the torque through a differential unit. This allows the individual and immediate control of all wheels and thus braking-based stabilization can be enhanced by applying both positive and negative torque values to all wheels. This increases the overall stability of the system, allowing for more dynamic and/or efficient driving behavior.

5. DISCUSSION AND CONCLUSION

As autonomous features and alternative powertrain solutions are simultaneously getting integrated into production vehicles, software developers, control designers and mechanical engineers need to update and improve motor vehicle designs to address a new set of requirements. Autonomous vehicles are gradually taking over the control responsibilities from the human driver, and the previously quasi-independent control systems (longitudinal, lateral control, ESP and transmission) are getting merged in a unified, coordinated vehicle control unit. This paper listed several important design aspects that indicate that engineers are strongly recommended to take the limitations and advantages of different powertrain solutions into considera-

tion when designing new systems. Vehicles with electric powertrain offer several advantages over traditional internal combustion engines from the trajectory control point of view. Most advantages can be derived from the faster response time and less model and construction complexity, although the aspects included in this paper can be discussed in the scope of hybrid, fuel-cell electric or other alternative powertrain solutions as well.

ACKNOWLEDGEMENT
The research presented in this paper was carried out as part of the EFOP-3.6.2-16-2017-00016 project in the framework of the New Széchenyi Plan. The completion of this project is funded by the European Union and co-financed by the European Social Fund. T. Haidegger is a Bolyai Fellow of the Hungarian Academy of Sciences.

6. REFERENCES

[1] T. Lázár-Fülep, "Overview of an Ongoing Scientific Research about Vehicle System Reliability with Complex Interconnections.", *Gradus,* vol. 6, no. 4, 2019. pp: 139–144

[2] D. A. Drexler, A. Takacs, T. D. Nagy and T. Haidegger. "Handover process of autonomous vehicles: Technology and application challenges." *Acta Polytechnica Hungarica* vol. 16, no. 9, 2019. pp. 235–255.

[3] [Online] Green Car Congress: "XL1 dive and drive: Volkswagen aggressively optimizes for efficiency in its sleek diesel plug-in hybrid" 2013, https://www.greencarcongress.com/2013/09/20130911-vw.html (accessed on 2020-02-28)

[4] Y. Rasekhipour et al. "A potential field-based model predictive path-planning controller for autonomous road vehicles." *IEEE Transactions on Intelligent Transportation Systems*, vol. 18 no. 5, 2016. pp: 1255–1267.

[5] P. Tamás, and I. Lakatos. „Vehicle Dynamic-based Approach for the Optimization of Traffic Parameters of the Intelligent Driver Model (IDM) and for the Support of Autonomous Vehicles' Driving Ability." *Acta Polytechnica Hungarica* vol. 16, no. 3, 2019. pp. 121–142.

[6] [Online] X. Mosquet: "The Electric Car Tipping Point" 2017, https://www.bcg.com/en-hu/publications/2018/electric-car-tipping-point.aspx (accessed on 2020-02-28)

[7] A. Khodayari, A. Ghaffari, S. Ameli, and J. Flahatgar. "A historical review on lateral and longitudinal control of autonomous vehicle motions." *in 2010 International Conference on Mechanical and Electrical Technology*, 2010, pp. 421–429.

[8] K. Kritayakirana, and J. Christian Gerdes. "Autonomous vehicle control at the limits of handling." PhD dissertation, Stanford University, 2012.

Szárnyaló fejlődés van.

IPAR NAPJAI
Nemzetközi ipari szakkiállítás

2020. október 19-22.

GL events hungexpo

VILÁGMÁRKÁK, MULTINACIONÁLIS CÉGEK, KIS- ÉS KÖZÉPVÁLLALATOK EGY IDŐBEN, EGY HELYEN:

IPAR NAPJAI – *új időpontban, 2020 októberében*
a HUNGEXPO BUDAPEST Kongresszusi és Kiállítási Központban!

A Hungexpo ipari szakkiállítása a legátfogóbb rendezvény, mely egy időben, egy helyen ad lehetőséget minden ipari szegmens bemutatására, felvonultatva az ipar összes ágazatát.

Magyarország legjelentősebb üzleti eseménye és találkozója az iparban
Az IPAR NAPJAI kiállítás évről évre teret ad az ipari ágazatok, az egyedülálló innovációk bemutatkozására, valamint az üzleti kapcsolatépítésre.

Kiemelt téma: Ipar 4.0 – M2M, IoT, AI, smart solutions, termelési hálózatok és további számos technológiai irányzat

Legfontosabb megjelenő tematikák: elektronika, automatizálás, gépipar, robotika, logisztika, energetika, IT, beszállítóipar és még sok más iparág

Betétkiállítás: Védőháló Budapest
Biztonságos és egészséges környezet otthon és a munkahelyen – munkavédelmi kiállítás

Egyidejű rendezvény: AUTOMOTIVE HUNGARY

Kedvezményes jelentkezési határidő kiállítók részére: 2020. június 30.
Bővebb információ: www.iparnapjai.hu

Szakmai partnerek: SZTAKI

JEGYZET

CONTENTS

GÉP

INFORMATIVE JOURNAL

for Technics, Enterprises, Investments, Sales, Research-Development, Market of the Scientific Society of Mechanical Engineering

DEAR READER,

The fourth Agria Conference on Innovative Pneumatic Vehicles - ACIPV 2020 has took place on 7th of May 2020, following a future forward, online format with regards to the global pandemic.

The initial goal of the Conference, founded in 2017, was to showcase the results of scientific researches conducted by university professors, PhD, Master and BSc students for their projects within the International AVENTICS Pneumobile Competition. By know its scope has been extended to control and automotive engineering researches too.

Business and academic world joined forces to organize the Conference series: Óbuda University's Institute of Mechatronics and Vehicle Engineering is responsible for the academic part while Emerson – representing its AVENTICS brand – is the host of the event. It is of great pleasure, that Ministry for Innovation and Technology is the patron of the Conference – here we would like to express our gratitude for their support.

This year we have welcomed twenty-two speakers during the Conference, whose studies could be read in this issue of the GÉP journal.

István Gödri,
Managing Director
Emerson Automation Fluid Control and Pneumatics
founder of the Conference,

Prof.Dr. László Pokorádi
Full Professor
Óbuda University
director of Mechatronics and Vehicle Engineering
Founder chair of the Conference

Managing Editor: Vesza József. Editor's address: 3534 Miskolc, Szervezet utca 67.
Phone/fax: (+36-46) 379-530, (+36-30) 9-450-270 • e-mail: mail@gepujsag.hu
Published by the Scientific Society of Mechanical Engineering, 1147 Budapest, Czobor u. 68., Postal address: 1371, Bp, Pf. 433
Phone: 202-0656, Fax: 202-0252, E-mail: a.gaby@gteportal.eu, Web: www.gteportal.eu
Web: http://www.gepujsag.hu * Kereskedelmi és Hitelbank: 10200830-32310236-00000000

Publisher: Dr. Igaz Jenő, Managing Director
Gazdász Nyomda Kft. 3534 Miskolc, Szervezet u. 67. Telefon: 06-46/379-530 • e-mail: gazdasz@chello.hu

Distributed to subscribers by Magyar Posta Zrt, Postal address: 1900 Budapest
Subscription: subscription can be ordered at any Hungarian post office, from postmen, from the link: www.posta.hu WEBSHOP (https://eshop.posta.hu/storefront/), via e-mail: hirlapelofizetes@posta.hu, by phone: 06-1-767-8262, or mail to: MP Zrt. 1900 Budapest
Subscription: subscription can be ordered from overseas and to overseas at Magyar Posta Zrt. Visit: www.posta.hu WEBSHOP (https://eshop.posta.hu/storefront/), mail to: 1900 Budapest, 06-1-767-8262, or hirlapelofizetes@posta.hu
Domestic subscription prices are: HUF 1,260 a single copy and HUF 2,520 a double copy.

INDEX: 25 343 ISSN 0016-8572

The published articles have been reviewed.
The publication is supported by the National Cultural Fund of Hungary

Meet safety standards without compromising productivity

Ensuring compliance with changing machine safety standards can affect production line availability and throughput. Emerson's machine safety experts and extensive range of well-proven solutions help keep workers safer, simplify safety systems, improve machine functionality and maximize productivity.

Learn more at: **Emerson.com/Aventics**

AVENTICS™

EMERSON™

CONSIDER IT SOLVED™

Emerson: a pneumatika gyártója Egerben

hu.aventics@emerson.com

EMERSON

CONSIDER IT SOLVED™